Annex 3A: Beamline at the Near Site

Long-Baseline Neutrino Facility (LBNF)/DUNE Conceptual Design Report

May 2015

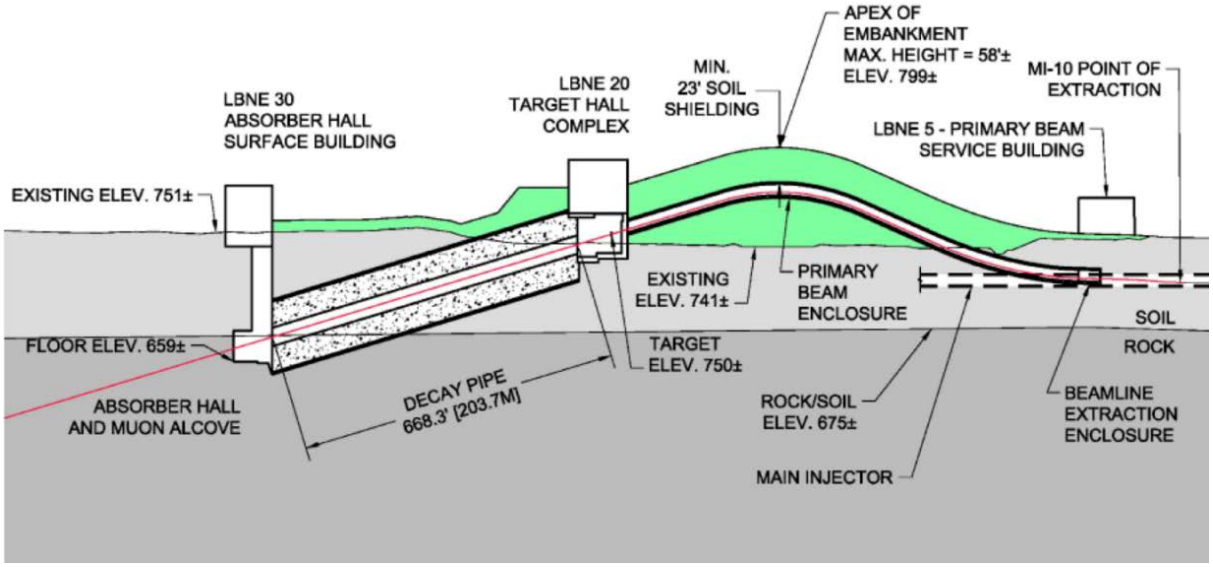

APPROVALS AND SIGNATURES

Include the following personnel:

- *Project Manager and Deputy*
- *Fermilab Director (only if needed)*
- *Other members of Directorate as appropriate, e.g. Chief Project Officer*
- *Division/Sector/Center heads as appropriate (include ESH&Q head)*
- *Representatives from partner laboratories and institutions, if appropriate*

Note: Signatures of DOE staff are not required as per request.

Elaine McClusky/
Project Engineer

_____

Insert Name **Date**
Role/title

James Strait/
Project Manager

_____

Insert Name **Date**
Role/title

_____

Insert Name **Date**
Role/title

_____

Insert Name **Date**
Role/title

CHANGE LOG

This version of the document may not be the most current approved revision. The current revision is maintained in the Project's Document Management system (DocDB), where all internal Project document approvals are managed. The current approved version is always available in the DocDB. This document will be reviewed and updated annually or as needed. The Configuration Manager (or Document Manager) is responsible for maintaining an up-to-date version and obtaining required signatures.

Table of Contents

APPROVALS AND SIGNATURES ..... **II**

CHANGE LOG ..... **III**

LIST OF TABLES ..... **VIII**

LIST OF FIGURES ..... **IX**

ABBREVIATIONS AND ACRONYMS ..... **XV**

1 INTRODUCTION TO THE LBNF BEAMLINE (WBS 130.02) ..... **XVIII**

1.1 Overview and General Layout ..... **xviii**

1.2.2 Primary Beam xix
1.2.3 Neutrino Beam xxi
1.2.4 System Integration xxvi
1.2.5 Estimation of Protons on Target xxviii
1.2.6 Modeling of the Beamline xxix
1.2.7 Near Site Conventional Facilities xxix

1.3 Participants ..... **xxx**

2 PRIMARY BEAM (WBS 130.02.02.05) **33**

2.1 INTRODUCTION **33**

2.2 Design Considerations **33**

2.2.1 Length and Elevation 33
2.2.2 Existing Infrastructure and Shielding 34
2.2.3 Beam Control 34

2.3 Reference Design Overview **35**

2.4 Lattice Optics (WBS 130.02.02.07) **37**

2.4.1 Introduction 37
2.4.1 Design Considerations 38
2.4.2 Reference Design 38
2.4.2 Trajectory Correction 47

2.5 Magnets (WBS 130.02.02.02) **49**

2.5.1 Introduction 49
2.5.2 Design Considerations 49
2.5.3 Reference Design 50

Magnet Power Supplies (WBS 130.02.02.03) 67
Introduction 67
Design Considerations 67
Reference Design 67

2.6 **Primary Water System (WBS 130.02.02.04) 72**
2.6.1 Introduction 72
2.6.2 Design Considerations 72
2.6.3 Reference Design 73

2.7 **Beam Instrumentation (WBS 130.02.02.05) 76**
2.7.1 Introduction 76
2.7.2 Reference Design 77
2.7.3

2.8 **Primary Vacuum (WBS 130.02.02.06) 79**
2.8.1 Introduction 79
2.8.2 Design Considerations 79

2.9 Reference Design 80
2.9.1 Pumps 80
2.9.2
2.9.3
2.9.4

Magnet Installation 81

2.10

3 **BEAM-LOSS CALCULATIONS 85**

3.1 **Introduction 85**

3.2 **Design Considerations 85**
3.12.2 Neutrino Beam Modeling 93

4 **NEUTRINO BEAM (WBS 130.02.03) 96**

4.1 **Introduction 96**
4.1.1 Design Considerations 97

4.2 **Neutrino Beam Modeling 98**
4.2.1 Design Considerations 99
4.2.2 Reference Design 99

4.3 **Targetry (WBS 130.02.03.03) 101**
4.3.1 Introduction 101
4.3.2 Design Considerations 102
4.3.3 Reference Design 104
4.3.4 Target Options: R&D 110
4.3.5 Target and Horns Instrumentation 113
4.3.6 Modules and Carriers 117

4.4 **Horns (WBS 130.02.03.04) 119**
4.4.1 Design Considerations 120
4.4.2 Reference Design 121
4.4.3 Horn Support Modules 135

Support Module Stripline Blocks 139

Horn Power Supplies (WBS 130.02.03.05) 140
Design Considerations 140

4.4.4 **Target Hall Shielding (WBS 130.02.03.08) 145**
4.5 Introduction 145
4.5.1 Design Considerations 145
Reference Design 145

4.6
4.6.1 **Helium-filled Concentric Decay Pipe (WBS 130.02.03.06) 153**
4.6.2 Introduction 153
4.6.3 Design Considerations 154

4.7
4.7.1 **Beam Windows (WBS 130.02.03.02) 162**
4.7.2 Introduction 162
Design Considerations 162
4.8 Reference Design 163
4.8.1
4.8.2
4.8.3 **Hadron Absorber (WBS 130.02.03.07) 174**
4.9 Introduction 174
4.9.1 Energy Deposition Calculations 175
4.9.2 FEA and Analysis 182
4.9.3 Mechanical Design and Remote Handling 190
4.9.4

4.10 **Remote Handling Equipment (WBS 130.02.03.11) 195**
4.10.1 Introduction 195
4.10.2 Design Considerations 195
4.10.3 Reference Design 196

4.11
4.11.1 **RAW Water Systems (WBS 130.02.03.09) 210**
4.11.2 Introduction 210
4.11.3 Design Considerations 211
Reference Design 212

5

5.1 **RADIOLOGICAL CONSIDERATIONS (WBS 130.02.01) 215**

5.2
5.2.1 **Overview 215**
5.2.2

Shielding 216
6 Primary Beamline 216
Other Radiological Design Issues 220

6.1

6.2 **SYSTEM INTEGRATION (WBS 130.02.04) 224**
6.2.1
6.2.2 **Introduction 224**

Controls (WBS 130.02.04.02) 224
Introduction 224
Reference Design 225

Radiation-Safety Interlock Systems (WBS 130.02.04.03) 226
Introduction 226
Methods 227
Reference Design 228

6.3 Alignment (WBS 130.02.04.04) 230
6.3.1 Overview 230
6.3.2 Design Considerations 230
6.3.3 Reference Design 231

6.4 Installation Coordination (WBS 130.02.04.05) 238
6.4.1
6.4.2
6.4.3

6.5

LIST OF TABLES

Table 1-1 : Summary of Principal Beam Design Parameters....xxi
Table 1-2: Beam Stability Requirement xxi
Table 1-3: Partial Set of Relevant Parameters for the Reference Design xxvii
Table 2-1: Magnet Parameters of the LBNE Proton Beamline at 120 GeV/c and β*=86.328 m. 41
Table 2-2: Final Focus gradients for the examples in Figure 2-6 46
Table 2-3: Orbit Offsets and Corrector Kicks for the Trajectories in Figure 2-8 49
Table 2-4: Summary of Primary-beam Magnet Specifications 49
Table 2-5: Properties of IDA Dipoles....51
Table 2-6: Properties of IDD Dipoles....51
Table 2-7: Properties of the MI Lambertson Magnets....56
Table 2-8: ICA Main Injector C-Magnet Properties....58
Table 2-9: QQB: Hollow Conductor 3Q120 Properties 60
Table 2-10: QQC: Quadrupole Magnet Properties 61
Table 2-11: LBNF Trim Dipole Properties (IDS) 64
Table 2-12: Specifications of the LBNF Extraction Kicker Magnet System 66
Table 2-13: Dipole (Bending) Magnet Loops 67
Table 2-14: Quadrupole Magnet Loops 69
Table 2-15: Corrector Magnet Power Supplies....70
Table 2-16: Summary of Heat Loads 73
Table 2-17: Specifications for the Ion Chamber Loss Monitor 77
Table 2-18: List of Major Vacuum Components 80
Table 2-19: Magnet Installation Parameters 82
Table 3-1: Apertures (Half-size of Primary Beamline Elements Used in Simulations)....86
Table 4-1: Material Properties of Graphite and Beryllium 103
Table 4-2: Horn Parameters. The Inner and Outer Conductor Parameters are Abbreviated by IC and OC, Respectively. 121
Table 4-3: Summary of Heating Loads on the Horns. The Results are Separate for the Inner Conductor (IC) and the Outer Conductor (OC). 127
Table 4-4: Horn 1 Operational Safety Factors at Critical Conductor Locations 132
Table 4-5: LBNF Horn PS Circuit Parameters 141
Table 4-6: Shielding Requirements for the Top of the Target Chase....148
Table 4-7: Shielding Requirements for the Walls and the Floor of the Target Chase 149
Table 4-8: Temperature Result for 120 GeV, 80 GeV and 60 GeV on the Decay Pipe Upstream Window with no cooling on the flange and convection cooling on both surfaces of the window foil. Normal beam (not accident) conditions....171
Table 4-9: Steady State Operating Temperatures and Stresses for 120 GeV and 60 GeV. 183
Table 4-10: Steady State Normal Operation Safety Factors 185
Table 4-11: On-axis Accident Temperature and Stress Results 186
Table 4-12: Target Hall Crane Characteristics....202
Table 4-13: Morgue Storage Requirements....204
Table 6-1: Alignment Tolerance Requirements (1σ) 231
Table 6-2: HG Honeywell 2001 INS Sensor Performance Specifications 234

LIST OF FIGURES

Figure 1-1: Schematic View of the Systems Included in the LBNF Beamline. The top of the engineered hill is 18.3 m above grade. xviii
Figure 1-2: Energy Range of the Oscillation Peaks xxiii
Figure 1-3: The First Horn Magnet xxiii
Figure 1-4: Neutrino Fluxes at the Far Detector as a function of energy in the absence of oscillations with the horns focusing positive particles. In addition to the dominant ν_μ $(\bar{\nu}\mu)$ flux, the minor components are also shown. Note the logarithmic scale. xxiv
Figure 1-5: Antineutrino Fluxes at the Far Detector as a function of energy in the absence of oscillations with the horns focusing negative particles. In addition to the dominant $\nu_{\square}$ flux, the minor components are also shown. Note the logarithmic scale. xxv
Figure 1-6: The number of neutrino interactions in the far detector depends on the length and diameter of the decay pipe. Here, the number of events is plotted as a function of length, with two curves for each colored energy range: solid is for a diameter of 2 m and dashed is for a diameter of 4 m. The reference design is a pipe 4 m in diameter and 203.7 m long LBNF xxvii
Figure 1-7: LBNE Overall Project Layout at Fermilab xxix
Figure 1-8: Organization Chart for the Beamline L2 Project (to WBS Level 4) xxxi
Figure 2-1: View showing the concept of elevating the beamline, thereby minimizing the deep excavation and tunnels. The beam comes from the right through the primary beam enclosure and interacts with the target in the Target Hall Complex. Fill used to elevate the beam is shaded in green... 34
Figure 2-2: View of the beamline from near the end of extraction region in the MI through the wall and up and over the apex of the hill. The Main Injector beamline is at the bottom and the Recycler at the top. 36
Figure 2-3: Configuration of the LBNE Extraction Lambertsons and C-magnet Straddling MI Quad Q102 39
Figure 2-4: Horizontal (Solid) and Vertical (Dashed) Lattice Functions of the LBNE Transfer Line. The final focus is tuned to produce a spot size of σ_x=σ_y=1.50 mm at 120 GeV/c and ϵ=30π μm (99%, normalized)] 42
Figure 2-5: Magnet Apertures and Beam Envelopes. The 99% contour (dashed) with nominal MI beam parameters, and the 100% envelope (solid) corresponding to the MI admittance at transition (γ_t = 21.600). 43
Figure 2-6: Tuning Range of the Final Focus. The two examples assume nominal MI beam parameters. These extremes correspond to 60 GeV/c with σ* = 1.0 mm; β* = 19.184 m and βmax = 104 m (lower), and at 120 GeV/c and σ* = 3.20 mm; β* = 393 m and βmax = 483 m (upper). Vertical dispersion, shown across the bottom, rises from zero at the entrance to the dipole string, reaches a maximum of $\eta_y \approx 3$ m, and is completely corrected to (η_y, η_y') = (0,0) by the end of the bends. 45
Figure 2-7: Phase Space Used in Front End Study (From lbne-doc-8420.) 47
Figure 2-8: Uncorrected/Corrected Trajectories with Random Misalignments and Dipole Field Errors. The plot begins at the upstream end of the first extraction Lambertson at MI-Q102. 48
Figure 2-9: MI Dipole Cross Section 52
Figure 2-10: Layout of one IDA and one IDB Dipole in a Half Cell 53
Figure 2-11: Beam Tube Cross Section 54
Figure 2-12: Typical IDA Excitation Curve 55
Figure 2-13: MI Lambertson Magnet End and Cross Section 57
Figure 2-14: Excitation Curve of a MI Lambertson Magnet 57
Figure 2-15: ICA MI C Magnet 59
Figure 2-16: ICA Beam Tube Shown in Horizontal Bending Orientation 59

Figure 2-17ICA integrated Strength as a Function of Current 60
Figure 2-18: Cross-section of QQB and QQC Quadrupoles 62
Figure 2-19: Typical QQB Excitation Curve 62
Figure 2-20: Typical QQC Excitation Curve 63
Figure 2-21: Schematic of LBNF 3-in (76.2-mm) Aperture Gap Trim Dipole (IDS) 65
Figure 2-22: Integrated Strength of NuMI Dipole Corrector 65
Figure 2-23: Magnet Power-Supply Block Diagram 68
Figure 2-24: Ion Chamber Loss Monitor 78
Figure 2-25: SEM Beam Profile Monitor. Left: Rotary Mechanics with Ti Multiwire Frame; Right: Ti Foil Heating Estimation for 708 kW Beam Power 79
Figure 2-26: Overview of the Primary Beamline 82
Figure 2-27: Magnet Installation on Sloped Surfaces 83
Figure 3-1: Horizontal (Left) and Vertical (Right) Beam Distributions at Baffle Entrance as a Function of Dipole (Top) and Quadrupole (Bottom) Power Supply Instability 87
Figure 3-2: The Halo Particle Loss Distribution Along the LBNE Beamline at Dipole Strength Instability of dB/B=±0.002 (left), dB/B=±0.005 (right) and Quadrupole Strength of dG/G=±0.005 with Individual Power supply for Each Magnet (top) and with Common Power Supply for Several Magnets (second line). Beam Loss Population at the Baffle is Shown on the Bottom. 88
Figure 3-3: The 3σ Core Beam Population (Top) and Distributions (Middle and Bottom) at the Baffle (Left), and at the Far Detector (Right) 89
Figure 3-4: An Example of Beam Trajectories Along the Beamline for a Beam Lost Due to Accidental Degradation of Bending Magnet Strength 90
Figure 3-5: The Halo and Core beam loss at 120 GeV along the LBNE Primary Beamline (Top) and at the Baffle (Bottom) as a Function of the Dipole Magnetic Power-supply Instability with Common Power Supply for Several Dipoles 91
Figure 3-6: An Instantaneous Temperature Rise Along and Across the Dipole Magnet Beam Pipe at Accidental Loss of Entire Beam 92
Figure 3-7: Residual Dose Rates along the Beamline and Magnets. Following a loss of 0.3% of the beam for 30 days followed by one day cool-down. The color-coded logarithmic scale has units of m-Sv/h (1 m-Sv/h is equivalent to 100 mrem/h). 93
Figure 4-1: A Cartoon of the neutrino beamline showing the major components of the neutrino beam. From left to right, the beam window, horn-protection baffle, target, the two toroidal focusing horns, decay pipe and absorber. The air volume surrounding the components between the window and the decay pipe is called the target “chase”. The target chase and rooms for ancillary equipment (power supplies, cooling, air recirculation and so on) is included in the area called the target complex (not shown in picture). 97
Figure 4-2: Schematic of the upstream portion of the LBNF neutrino beamline showing the major components of the neutrino beam. The target chase bulk steel shielding is shown mainly in green. Inside the target chase from right to left (the direction of the beam) pointing downwards: the beam window, horn-protection baffle and target mounted on a carrier, the two toroidal focusing horns and the decay pipe. Above the chase and to the right is the work cell for horn and target system repairs. The beige areas around the decay pipe indicate concrete shielding. The yellow and red lines indicate multi-ply geosynthetic barriers, separated by a drainage layer (blue). 98
Figure 4-3: An Example of the MARS Model Detail. The Graphic Shows Upsteam End of the First Horn with the Graphite Target Inserted at Nominal Position. 100

Figure 4-4: A Section of the MARS Model for the Downstream Part of the First Horn. Water Cooling Spray Nozzles are Along the Top of the Outer Conductor and the Drain with Reservoir are Below the Horn. 101
Figure 4-5: Proposed LT Target for LBNF. Beam Enters through the Beryllium Window on the Left, Encounters the Graphite Core, and Exits through the Beryllium Window on the Right. Units are Inches Unless Otherwise Noted. 105
Figure 4-6: Cross-section of LT Target for LBNF. The Alignment Rings do not Run the Full Length of the Target. Units are mm. 106
Figure 4-7: Equivalent Stress Developed in the Maximum Stressed Graphite Fin just after a Beam Pulse when Operating with 120 GeV, 1.2 Second Cycle Time, and 7.5E+13 Protons per pulse. Shown is a Quarter-symmetry Model with Beam Aligned with the z-axis. 108
Figure 4-8: Early Prototype of a Target Graphite Core Bonded to a Titanium Cooling Line 109
Figure 4-9: Baffle Baseline Design for LBNF 110
Figure 4-10: BLIP Test Sample Holder. This Figure Shows Cassettes of Material Samples Irradiated in the BLIP Facility. The Beam Enters from the Right. 112
Figure 4-11: Data from NuMI Running of the Correlation Between the Muon Monitor Response and Protons/Spill 116
Figure 4-12: Decrease of Muon Monitor Response as Proton Beam is Mis-steered off Target. The Data is Bit Noisy as they were Collected with very Low Beam Intensity. 117
Figure 4-13: Target Carrier in Target Pile Shielding. The length of the baffle plus target assembly is shown in the fully inserted downstream position, and also in the furthest out position 2.5 m upstream of that. 5588 mm is taken as the maximum reasonable carrier length to extract between the carriage cross beams that are 5640 mm apart. The extra 1000 mm length of a baffle for 2.4 MW operation is also sketched in, showing that the usable range of target motion may be modestly reduced by that upgrade. 118
Figure 4-14: Horn 1 Section. The Reference “MCZERO” is the Point along the Beam that Sets the Coordinate System origin for Monte Carlo Simulations. Horn 1 Specifications are Listed in Table –3-2. 119
Figure 4-15: Horn 2 Section. Horn 2 Specifications are Listed in Table 3-2 120
Figure 4-16: Idealized Shape of the Horn 1 Inner and Outer Conductors. z=0 is the Beamsheet Location MCZERO 121
Figure 4-17: Idealized Shape of Horn 2 Inner and Outer Conductors. z=0 is the insertion Point of Horn 2, which is 6.6 m Downstream of MCZERO, the z=0 Point of Horn 1. 122
Figure 4-18: Horn 1 Inner Conductor Water Spray Coverage 122
Figure 4-19: Additional Support and Stability for the Thin Inner Conductor are Provided by Welded Struts or Spider" (web) Supports (Thin Red Pieces) 123
Figure 4-20: Horn 1 Stripline Connection at the Downstream End 124
Figure 4-21: NOvA Horn 1 Stripline Analysis at 1.2 MW/120 GeV Operation 125
Figure 4-22: NOvA Horn 1 Stripline Analysis at 1.2 MW/120 GeV Operation with Increased Cooling ... 126
Figure 4-23: Half-symmetry, Axial Cross Sectional View, of Horn 1 Conductor Temperature after Beam Pulse 127
Figure 4-24: Half-symmetry, Axial Cross Sectional View, of Horn 2 Conductor Temperature after Beam Pulse 128
Figure 4-25: Detailed load points for conductor analysis. 1: Start of current Pulse, 2: Start of beam pulse, 3: End of beam pulse, 4: End of current pulse. Temperature profile of the horn neck is represented by the green line. 128
Figure 4-26: Half Symmetry, Axial Cross Sectional View, of Horn 1 Magnetic Pressure Loading 130
Figure 4-27: Half Symmetry, Axial Cross Sectional View, of Horn 2 Magnetic Pressure Loading 130

Figure 4-28: Horn 1 Conductor Stresses 131
Figure 4-29: Horn 2 Conductor Stresses 132
Figure 4-30: Horn Cooling Water Manifolds 133
Figure 4-31: Horn Hanger Structural Analysis with Tri-axial Loading 134
Figure 4-32: Horn Support Module Concept. The Beam comes from the Left, through the Target Carrier Assembly, Followed by the Horn 1 and Horn 2 Module Assemblies 136
Figure 4-33: Adjustment Fixtures for the Horn-support Module Concept. The Modules are Fixed only Horizontally along the Beam Direction 137
Figure 4-34: Cooling Passage Layout and Module Subsections for Analysis 138
Figure 4-35: Preliminary Thermal Expansion Results for Horn 1 Module Mainframe 138
Figure 4-36: Conceptual Horn Stripline Block 139
Figure 4-37: Stripline Block Remote Clamp Assembly 140
Figure 4-38: LBNF Horn PS Simplified Circuit Diagram 140
Figure 4-39: Layer Stripline 143
Figure 4-40: Upper: Connection to Horn-1, End View Looking DS; Lower: Vertical Section, Horn/Stripline Interface 144
Figure 4-41: Beamline Elevation View – Beam direction is Left to Right 147
Figure 4-42: Cross Section of Target Chase Steel Shielding (Cross-hatched Areas). The Secondary Beam is Confined to the Rectangular Opening in the Center. 148
Figure 4-43: View of the Bulk Steel Shielding after the Large Steel Pieces have been Installed and Installation of the Downstream end has Started 150
Figure 4-44: The Flows for the Target Pile and Decay Pipe Air-cooling Concept are Shown Schematically 152
Figure 4-45: Supply and Return Air Ducts for the Target Pile 153
Figure 4-46: Typical Cross section of Concentric Decay Pipe and Shielding Concrete 155
Figure 4-47: Concentric Decay Pipe Snout and Upstream Window 156
Figure 4-48: Cooling Airflow Schematic for the Concentric Decay Pipe and Shielding Concrete 157
Figure 4-49: Downstream Decay Pipe Steel Head and Aluminum Window 159
Figure 4-50: Downstream Decay Pipe: The Three Energy Deposition Cases for Heat Transfer and Stress Analyses 159
Figure 4-51: Supply and Return Air Ducts for the Concentric Decay Pipe 161
Figure 4-52: (a) Shielding Wall with Embedded Stepped Liner. (b): After Cartridge Insertion 164
Figure 4-53: (a) Section View of Replacement Window Assembly. (b): End View of Window Assembly 164
Figure 4-54: Spatial Distribution of Beam Energy Deposition 165
Figure 4-55: Temperature History at the Center of Beam Window 166
Figure 4-56: Temperature Distributions at Valley and Peak 167
Figure 4-57: (a) Section View of 2.4-MW-Capable Beryllium Window. (b): End View of Window Assembly 167
Figure 4-58: Upstream Decay Pipe Window from NX Solid Model 168
Figure 4-59: Finite Element Model to Simulate the Helium Fill of Decay Pipe 172
Figure 4-60: CO2 Mass Fraction at 1358 173
Figure 4-61: CO2 Mass Fraction at 6758 173
Figure 4-62: Maximum CO_2 content during the Decay Pipe Purging Process as a Function of Time in Seconds 174
Figure 4-63: Left, cross section of absorber through beam axis. Right, cross section of absorber core. 175
Figure 4-64: The Distribution of the Incoming Flux at the Downstream End of the Decay Pipe ... 177

Figure 4-65: The calculated incoming flux at the downstream end of the decay pipe in the central region in radius, and the results of fitting with two Gaussians (σ_1=0.9 cm and σ_2=5.3 cm). 177
Figure 4-66: The double grid employed in transverse direction for MARS15 energy deposition calculations in the sculpted core aluminum blocks. In the outer grid, the bin size is 2cmX2cm, and this linear bin size is three times as large as that in the inner grid. 178
Figure 4-67: Distribution of Total Power Deposited in the Central Part of the Absorber (see Figure 1). 179
Figure 4-68: Calculated Two-dimensional Distribution of Power Density over theAbsorber at 120 GeV 180
Figure 4-69: A longitudinal view of the grid employed for MARS15 energy deposition accident calculations in the core aluminum blocks. The yellow regions show the water-cooling channels. 181
Figure 4-70: Calculated two-Dimensional Distribution of Deposited Energy over the Absorber for the Case of "No-target on-axis" Accident at 120 GeV. 182
Figure 4-71: Temperature (°C) and Von-Mises stress (Pa) for 3rd Sculpted Block 184
Figure 4-72: Effect of a Down Water Line on Sculpted Block 3. Left: Temperature (°C). Right: Von-Mises Stress (Pa). 185
Figure 4-73: Locations of Absorber Accident Conditions..... 186
Figure 4-74: Contour Plots after Two off-axis Accident Condition Pulses. Left, Temperature (°C). Right, Plastic Strain..... 187
Figure 4-75: Water Pressure (Pa) in Cooling Channels of Sculpted Al Blocks Right: 2 and Left: 3 During off-axis Accident..... 188
Figure 4-76: Routing Method for Air Cooling of Outer Steel Shielding 189
Figure 4-77: Simplified Model of Absorber Steel Shielding for Air Cooling Calculations..... 189
Figure 4-78: Absorber Shielding Temperatures (°C) with Air Cooling 190
Figure 4-79: NuMI Target Hall Chase with T-block and Lifting Fixture 191
Figure 4-80: Left: Cut-away Cross Section through a Water Line in a Sculpted Absorber Core Bock. Upper Right: Connections to the Aluminum Tubes. Lower Right: Connections to the Manifold..... 192
Figure 4-81: Top, Core Block Assembly with T-block. Bottom, T-blocks Assembled into Absorber Showing Water Line Connections 193
Figure 4-82: Left, thermocouple assembly in T-block. Center, thermocouple tip locations. Right, thermocouple mounting and routing 194
Figure 4-83: Cross Section of the Absorber Showing Morgues 195
Figure 4-84: LBNF Target Hall Enclosure Beamline Elevation Section 197
Figure 4-85: Target Complex Plan View 198
Figure 4-86: Target Complex Plan: Expanded View of Figure 4-83..... 199
Figure 4-87: Target Hall Work Cell Concept..... 200
Figure 4-88: Photo of Cask-to-Morgue Cell Transfer System Used at C-0 Remote Handling Facility..... 205
Figure 4-89: Absorber Hall Section 207
Figure 4-90: Absorber Hall Section Showing Details of the Absorber Core and Shielding Arrangement 208
Figure 4-91: Cross Section of Absorber Hall Beam View Showing Morgue Storage Area 209
Figure 4-92: Cross Section of Absorber Hall Beam View Showing Hadron-monitor Replacement Concept 210
Figure 5-1: Sum of the ratio of radionuclide concentrations (Ci) over the Federal drinking water limits (Ci,max) for tritium and 22Na as a function of decay pipe shield thickness. The dashed red line shows the self-imposed limit on the ratio sum which will result in the radionuclide concentrations in the ground water to be below the detection limits 217
Figure 5-2: Muon isoflux contours (cm-2 s-1) in the rock and steel kern downstream the Absorber Hall; muon plume length is reduced from 170 m in pure rock to 113 m 219

Figure 5-3: Hadron (E > 30 MeV) isoflux contours (cm-2 s-1) in the rock and steel kern downstream the Absorber; hadron fluxes outside the steel kern are below the accepted limit of 400 cm-2 s-1 for groundwater activation 220
Figure 6-1: GPS Network Tying Fermilab and SURF to the CORS System 233
Figure 6-2: Residuals in Latitude/Longitude and Residuals in Height 234
Figure 6-3: Fermilab LBNF Surface Geodetic Network 236
Figure 6-4: Distribution Observation Residuals for the Target and Near Detector Halls in MINOS 238
Figure 6-5: Primary Beamline Areas of Installation 239

ABBREVIATIONS AND ACRONYMS

<<TBF>>

A	
AC	alternating current
ACNET	Accelerator Controls NETwork
ASME	American Society of Mechanical Engineers
atm	atmosphere
AWG	American Wire Gauge
B	
BLM	Beam-loss monitor
BLIP	Brookhaven Linac Isotope Producer
BNB	Booster Neutrino Beam
BNL	Brookhaven National Laboratory
BPM	Beam-position monitor
BuLB	Basic Micro Learning Box
C	
CAMAC	Computer Automated Measurement and Control charge-coupled device
CDC	Critical Device Controller
CDR	Conceptual Design Report
CCD	
CORS	Continuously Observed Reference Station
CP	charge parity
CUB	Central Utilities Building
D	
DAQ	data acquisition
DC	direct current
DCCT	DC current transformers
DI	de-ionization
DOE	Department of Energy
DS	Downstream
DUSEL	Deep Underground Science and Engineering Laboratory
E	
E-Net	Ethernet
ESS	Electrical Safety System
F	
FEA	Finite Element Analysis
FF	final focus
FFT	fast fourier transform
FODO	A repetitive configuration of focusing (F) and defocusing (D) magnetic elements separated by a fixed spacing of non-focusing elements (O)
FPGA	field programmable gate array
FRCM	Fermilab Radiological Control Manual
ft	foot or feet
G	
gpm	gallons per minute
GPS	global positioning system
GRS	Geodetic Reference System
H	

hBN	Hexagonal boron nitride
hp	horsepower
HRM	Hot-link Rack Monitor
HTO	tritiated water molecule
Hx	Heat Exchanger
I	
ID	inner diameter
IHEP	Institute for high energy physics
IMU	Inertial Measuring Unit
INS	Inertial Navigation System
IPM	Ionization Profile Monitor
L	
L	used here to indicate the “level” underground, in feet
LC	inductive/capacitive
LCW	low-conductivity water
LHC	Large Hadron Collider
LOTO	lock-out/tag-out
M	
MAD	Methodical Accelerator Design
MARS	a monte carlo code
MCC	Motor control centers
MECAR	Main Injector Excitation Controller and Regulator
MI	Main Injector
MI-10 (60, 64 etc)	Surface buildings above extraction point on Main
MIBS	Main Injector Beam Synchronous Clock
MPS	machine-protection system
MUX	multiplex
N	
NGS	National Geodetic Survey
NAD	North American Datum
NOvA NuMI	Off-axis “nu sub e” Appearance Experiment
NuMI	Neutrinos at the Main Injector (Beamline facility at Fermilab)
O	
OD	outer diameter
P	
P5	Particle Physics Project Prioritization Panel
PLC	Programmable Logic Controller
POCO	name of graphite supplier (POCO Graphite)
POT	Protons on Target
Ppm	parts per million
psid	pounds per square inch differential
PW	Pond Water
R	
RAL	Rutherford Appleton Laboratory
RAW	Radioactive water
RF	radio frequency
RH	remote handling
RSS	Radiation Safety Interlock Systems
S	
SCR	silicon-controlled rectifier
SEM	secondary emission monitor
SI	Systems Integration

SURF	Sanford Underground Research Facility (in Lead, S.D., the LBNE Far Site)
T	
TCLK	Tevatron Clock
TCV	Temperature control valve
TH	Target Hall
THI	Target Hall instrumentation
THSP	Target Hall shield pile
TLM	Total-loss monitor
U	
UHV	Ultra High Vacuum
US	upstream
V	
VA	Volt-Ampere (also kVA, MVA)
VAC	Volts AC (also mVAC, kVAC, MVAC)
VFD	variable-frequency drive
VME	VMEbus, VERSAmodule Eurocard bus, ANSI/IEEE 1014-1987; a computer bus standard
W	
WBS	Work Breakdown Structure

Introduction to the LBNF Beamline (WBS 130.02)

Overview and General Layout

1 The LBNF beamline at Fermilab will be designed to provide a neutrino beam of sufficient intensity and appropriate energy range to meet the goals of the DUNE experiment with respect to long-baseline neutrino-oscillation physics. The design is a conventional, horn-focused neutrino beamline. The

1.1 components of the beamline will be designed to extract a proton beam from the Fermilab Main Injector (MI) and transport it to a target area where the collisions generate a beam of charged particles. This secondary beam aimed toward the Far Detector is followed by a decay-pipe where the particles of the secondary beam decay to generate the neutrino beam. At the end of the decay pipe, an absorber pile removes the residual hadrons.

The facility is designed for initial operation at a proton-beam power of 1.2 MW, with the capability to support an upgrade to 2.4 MW. In the reference design, extraction of the proton beam occurs at MI-10, a new installation. After extraction, this primary beam establishes a horizontally straight compass heading west-northwest toward the Far Detector, but will be bent upwards to an apex before being bent downwards at the appropriate angle—101 milliradians (5.79°) as shown in **Figure 1-1.**

The primary beam will be above grade for about 550 feet; this design minimizes expensive underground construction and significantly enhances capability for ground-water radiological protection. However, this requires construction of an earthen embankment or hill, whose dimensions are commensurate with the bending strength of the dipole magnets required for the beamline. The embankment will need to be approximately 950 feet long and 60 feet high above grade at its peak.

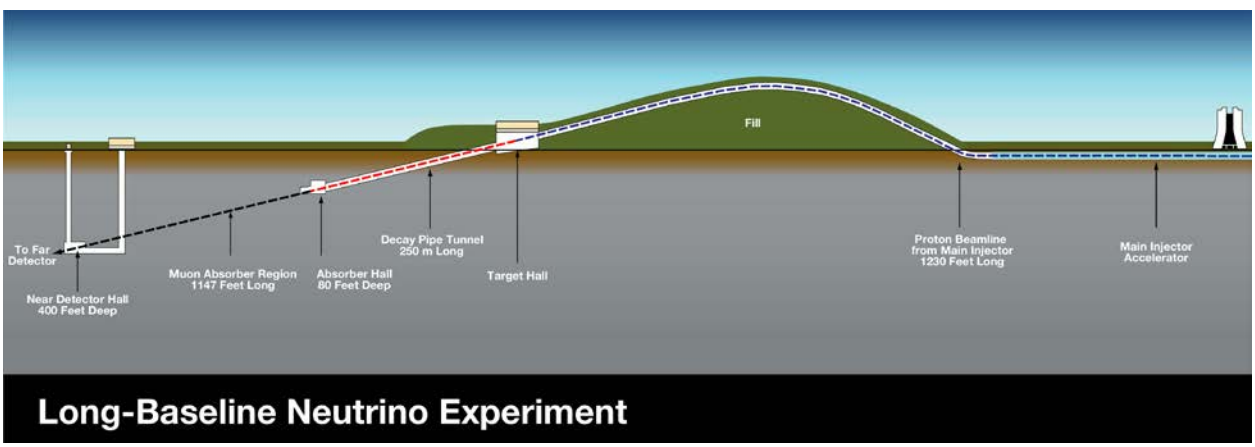

Figure 1-1: Schematic View of the Systems Included in the LBNF Beamline. The top of the engineered hill is 18.3 m above grade.

The target marks the transition from the intense, narrowly directed proton beam to the more diffuse, secondary beam of particles that in turn decay to produce the neutrino beam. The secondary particles are short-lived and most decays generate a muon, which penetrates deep into the surrounding rock, and a neutrino that continues on toward the Far Detector.

After collection and focusing, the pions and kaons that did not initially decay need a long, unobstructed volume in which to decay. This decay volume in the LBNF reference design is a pipe of circular cross

section with its diameter and length optimized such that decays of the pions and kaons result in neutrinos in the energy range useful for the experiment. The decay volume is followed immediately by the absorber, which removes the remaining beam hadrons.

The LBNF Beamline is broken into three principal systems for organizational purposes: the Primary Beam (referring to the components required for the initial, high-intensity proton beam), the Neutrino Beam (for the components used to create a high-intensity neutrino beam from the initial proton beam) and System Integration.

It is important to note that the design and construction of high-intensity neutrino beams has been an integral aspect of Fermilab's program for decades. The experience gained from the various neutrino projects has been employed extensively in the LBNF Beamline conceptual design. In particular, the NuMI beamline serves as the prototype design. Most of the subsystem designs and their integration follow, to a large degree, from previous projects.

Radiological protection is integrated into the LBNF beamline reference design in two important ways. First, shielding is optimized to reduce exposure of personnel to radiation dose and to minimize radioisotope production in ground water within the surrounding rock. Secondly, the handling and control of tritiated ground water produced in or near the beamline drives many aspects of the design. Production of tritium is unavoidable, and it is necessary to minimize its accumulation in the soil or rock in the form of tritiated water (HTO).

The reference design for the primary beam and the neutrino beam is suitable for the initial beam power of 1.2 MW in all respects. Some aspects of the reference design are also appropriate for a beam power of 2.4 MW. These include the radiological shielding and the size of the enclosures as well as the beam absorber, the remote handling, the decay-pipe cooling, the decay pipe downstream window and the RAW system piping in the penetrations, none of which can be upgraded after exposure to a high-intensity beam.

The LBNF Beamline is being designed for twenty years of operation, while we are planning for the lifetime of the Beamline Facility, including the shielding, for thirty years. We are assuming conservatively that for the first five years we will operate at 1.2 MW beam power and for the remaining fifteen years at 2.4 MW.

The LBNF Beamline will become operational after the currently planned six-year run of the NOvA experiment. With the concurrence of the Fermilab Directorate, LBNF assumes components from the NuMI Beamline will be available for removal and reuse [?].

1.2.2 Primary Beam

1.2.2.1 Extraction from Fermilab's Main Injector

The primary proton beam for LBNF will be extracted from the Main Injector (MI) using a method called "single-turn" extraction, in which all the protons accelerated in the MI synchrotron ring will be diverted to the dedicated LBNF beamline within one circuit. Although the NuMI beam operates at 120 GeV, further studies on optimizing the LBNF signal-to-detector backgrounds may indicate desirability of a lower energy. The design proton energy thus ranges from 60 to 120 GeV. Approximately 7.5×10^{13}protons will be extracted every 1.2 seconds at 120 GeV, resulting in a beam power of 1.2 MW.

The extraction point, located near the MI-10 surface building and called simply MI-10, will be a new installation, different from the one used for NuMI.

1.2.2.2 Beam Transport

The design of the primary proton beam transport is driven by both the goals of the LBNF physics program and radiological safety concerns. The beam must first of all be intense enough to create a flux of neutrinos at the Far Detectors sufficient to meet the physics objectives of the experiment. Secondly, the beam energy must be set to optimize the energy spectrum of the neutrinos, yet not produce excess background signals that could compromise the measurements. And the system must be safe. Together these requirements imply that the beam must reach the target with very low losses to ensure both efficient production of neutrinos as well as minimal radiological activation of components in the beamline. Due to accelerator duty-cycles, some reduction of total beam power at lower energies is expected (see Table 1-1). And of course sufficient shielding must be in place in case of any accidental mis-steering of the beam.

The primary beamline elements necessary for transport include dipole (bending) magnets, quadrupole (focusing) magnets, corrector magnets, monitoring instrumentation and vacuum equipment. LBNF will use conventional dipole and quadrupole magnets to guide the beam in the right direction and focus it on the target, respectively. Their optics will closely follow the design of the Main Injector elements. The magnets and their power supplies will be optimized for performance and cost, and will include both new and refurbished elements. The LBNF beam optics will be simulated and analyzed for optimum transport properties. The beam trajectory points to a Far Detector positioned at the 4850L, aligning the beam with the Far Detector location.

The general primary-beam specifications are listed in **Table 1-1**. As discussed later in the chapter, the accelerator complex and the LBNF Beamline are planned to deliver 1.1×10^{21} primary protons to the neutrino target per year at 120 GeV proton beam energy and beam power of 1.2 MW. This number includes allowances for scheduled shutdowns for maintenance and upgrades as well as unscheduled failures estimated from past experience. The fast, “single-turn” extraction technique delivers all the protons in one machine cycle (1.2 seconds for 120 GeV) to the LBNF target in 10 microseconds. When synchronized to the detector electronics, this short spill helps ensure a high rejection of background events at the Far Detector that do not originate from the accelerator beam.

1.2.2.3 Beam Stability

The primary beam needs to be stable in position and direction at the neutrino production target. Deviations in the beam position, for example, affect not only the spatial distribution of the distant neutrino flux, but can also affect the energy spectrum. These systematic effects must be minimized to the extent that they become negligible in the physics analyses. Although the full physics analysis procedures will not be available for some time, guidelines from simple analyses and experience from previous experiments provide a basis for estimating the effects of a poorly positioned beam.

Table 1-1 : Summary of Principal Beam Design Parameters

Parameter	Value
Protons per cycle (120 GeV)	7.5×10^{13}
Spill duration	1.0×10^{-5} sec
Energy	60 to 120 GeV
Protons on target per year	1.9×10^{21} to 1.1×10^{21}
Beam size at target	1.5 to 1.7 mm
Δp/p	11×10^{-4} 99% (28×10^{-4} 100%)
Beam/batch (84 bunches)	8×10^{12} nominal; (3×10^{11} commissioning)
Transverse emittance	30πμm 99% (360πμm 100%)
Cycle time (120 GeV)	0.7 to 1.2 sec
Beam divergence (x,y)	17 to 15 μrad
Beam Power	1.03 to 1.20 MW

Table 1-1 lists the maximum allowable deviations from the design goals of beam position, angle and size. A set of beam-position monitors with control feedback will be installed at points along the primary beamline to ensure stability.

Table 1-2: Beam Stability Requirement

Parameter	Value
Position at target	±0.45 mm
Angle at target	±70 μrad
Size at target, rms	10% of σ(x,y)

1.2.3 Neutrino Beam

The neutrino beam must be optimized for direction and energy to enable the neutrino-oscillation physics at the Far Detector. The neutrino beam will be created from the primary (proton) beam in a three-step process.

1. The primary beam strikes the neutrino production target in the Target Hall.
2. The charged products of these interactions, mostly pions and kaons, are collected in the Target Hall and focused in the direction of the Far Detector.
3. Those pions and kaons that are aimed correctly enter the long pipe of the decay volume, where they decay into neutrinos forming the neutrino beam.

The beamline elements involved in these three steps must be designed to work together to maximize the neutrino flux in the useful energy range for the experiment.

The target, the first element of the neutrino beam system, will be designed to interact with approximately 85% of the primary protons and to minimally absorb the charged pions and kaons created in those interactions. To accomplish this, the target needs to be relatively small in cross section. This requires a tight focus of the primary beam, resulting in a very dense energy deposition in the target material. The challenge is to design a long and narrow piece of material that can be adequately cooled and can survive these demanding conditions for as long as possible before being degraded by radiation and requiring replacement.

The neutrino-beam energy spectrum must be tailored to maximize the signal in the ν_e appearance oscillation experiment, in which muon neutrinos oscillate to electron neutrinos. There are, in effect, two predicted energy intervals of interest in this experiment, referred to as the first and second oscillation maxima. The beam must provide a concentrated neutrino flux at the energies bounded by these oscillation peaks, shown in. The higher-energy regime, 1.5- to 5-GeV neutrino energy ("1" in **Figure 1-2**, corresponds to focused pions of approximately 3.5 to 12 GeV, and is relatively straightforward to reach with toroidal, or horn, magnetic focusing elements. The lower-energy part of the neutrino spectrum ("2" in **Figure 1-2**) is more challenging to produce with high efficiency; it corresponds to pions and kaons of less than a few GeV that are scattered more and emerge at large angles making a sharp focus difficult. LBNF's on-axis design, with the beam pointing directly to the detectors, optimizes the neutrino flux over the broad energy range needed to cover both oscillation maxima. The spectrum optimized for oscillation physics has the target fully inserted into Horn 1, however, it is possible to increase the energy of the spectrum significantly by adjusting the target's position upstream by up to 2.5 m. See **Figure** 1-3.

The focusing of pions and kaons within the broad energy range of 2 to 12 GeV requires at least two horn magnets. The target and horns will be mounted inside a heavily shielded vault (called the "chase") that is open to the decay pipe at the downstream end. Low-energy pions and kaons usually pass through a large section of the magnetic field in the first horn and are focused to a point between the horns. A schematic of the first horn is shown in **Figure** 1-3. The second horn acts to redirect these particles toward the decay pipe. Most of the higher-energy pions and kaons are collected with the second horn, due to the small angles at which they are produced. The reference design for the target and horns has been simulated, and the parameters, listed in **Table 1-3** have been tuned to deliver a neutrino-beam spectrum adequate for the physics goals. The parameters may be further optimized for the physics of LBNF, subject to material and engineering constraints. The neutrino flux at the Far Detector site is shown in Figure **1-4** and **Figure 1-5**, calculated for a 120 GeV proton beam, the NuMI horns at 230 kA, 6.6 m apart and at a distance of 17.3 m from Horn 1 to the decay pipe (4 m in diameter and 203.7 m long). The NuMI target starts -45 cm from Horn 1.

Over the lifetime of the experiment, the target and focusing horns will need to be replaced. Accommodating the safe routine replacement of parts in a radioactive environment is an essential part of the Target Hall design, and remote-handling procedures involving activated targets and horns are being developed.

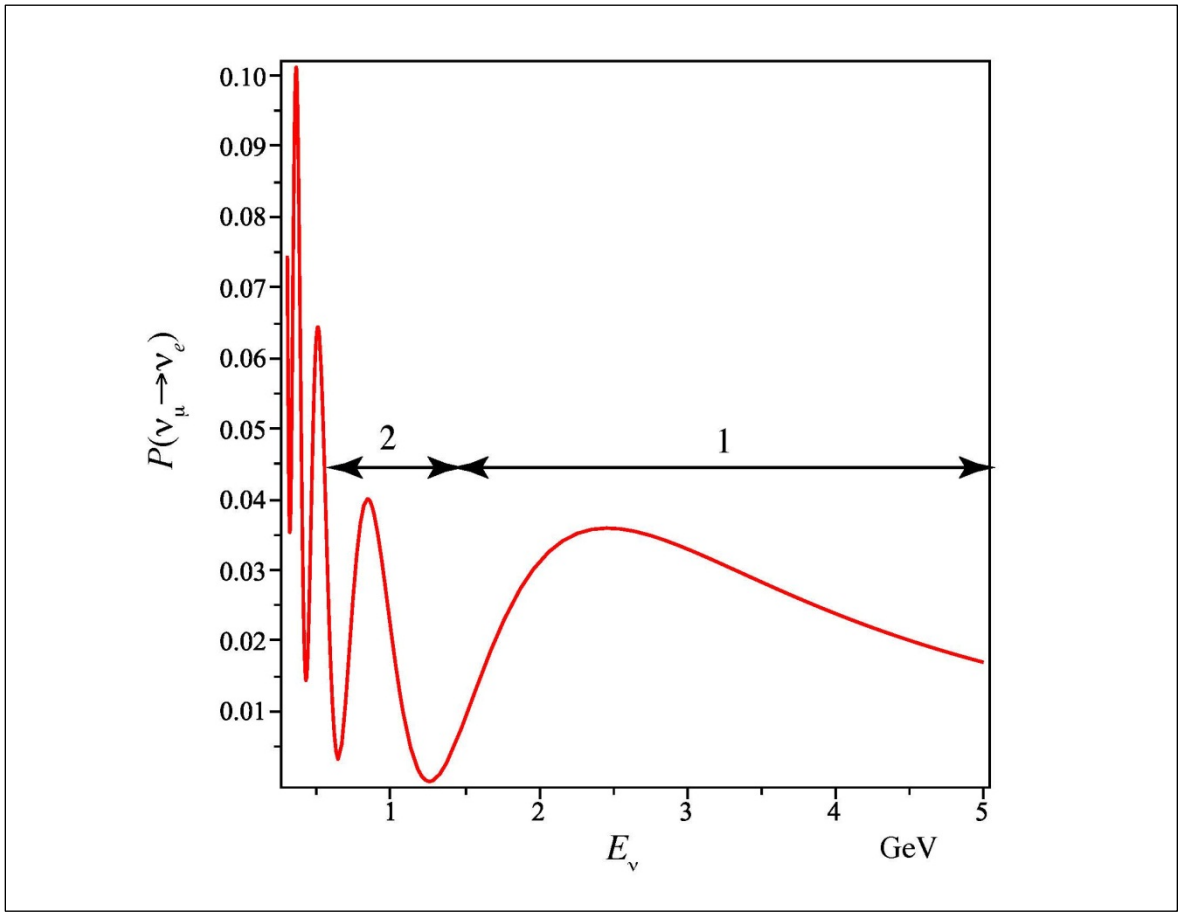

Figure 1-2: Energy Range of the Oscillation Peaks

The energy range of the first and second oscillation peaks are denoted by the respective numerals. The beam design is optimized to produce neutrinos within this range. The true probability depends on a parameter, θ_{13}.

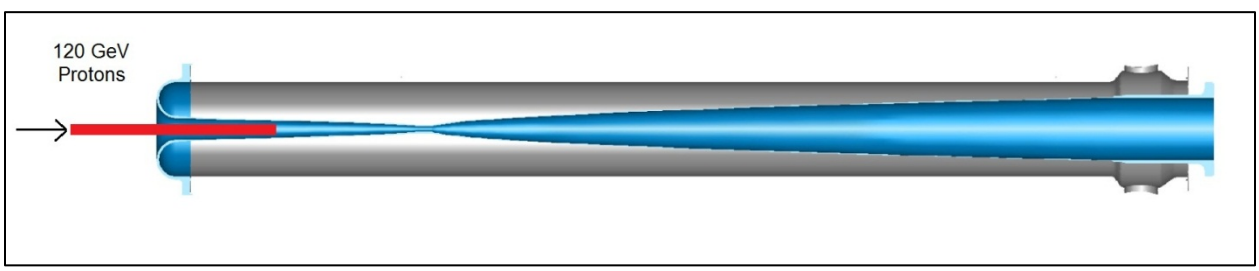

Figure 1-3: The First Horn Magnet

The conductor of the horn is shaded blue, and the graphite target (red) is inserted into the horn. The beam is incident from the left and the magnetic field region is between the shaped inner conductor and the cylindrical outer conductor (gray). Horn 1 is 336 cm long. The target is shown in the fully inserted position.

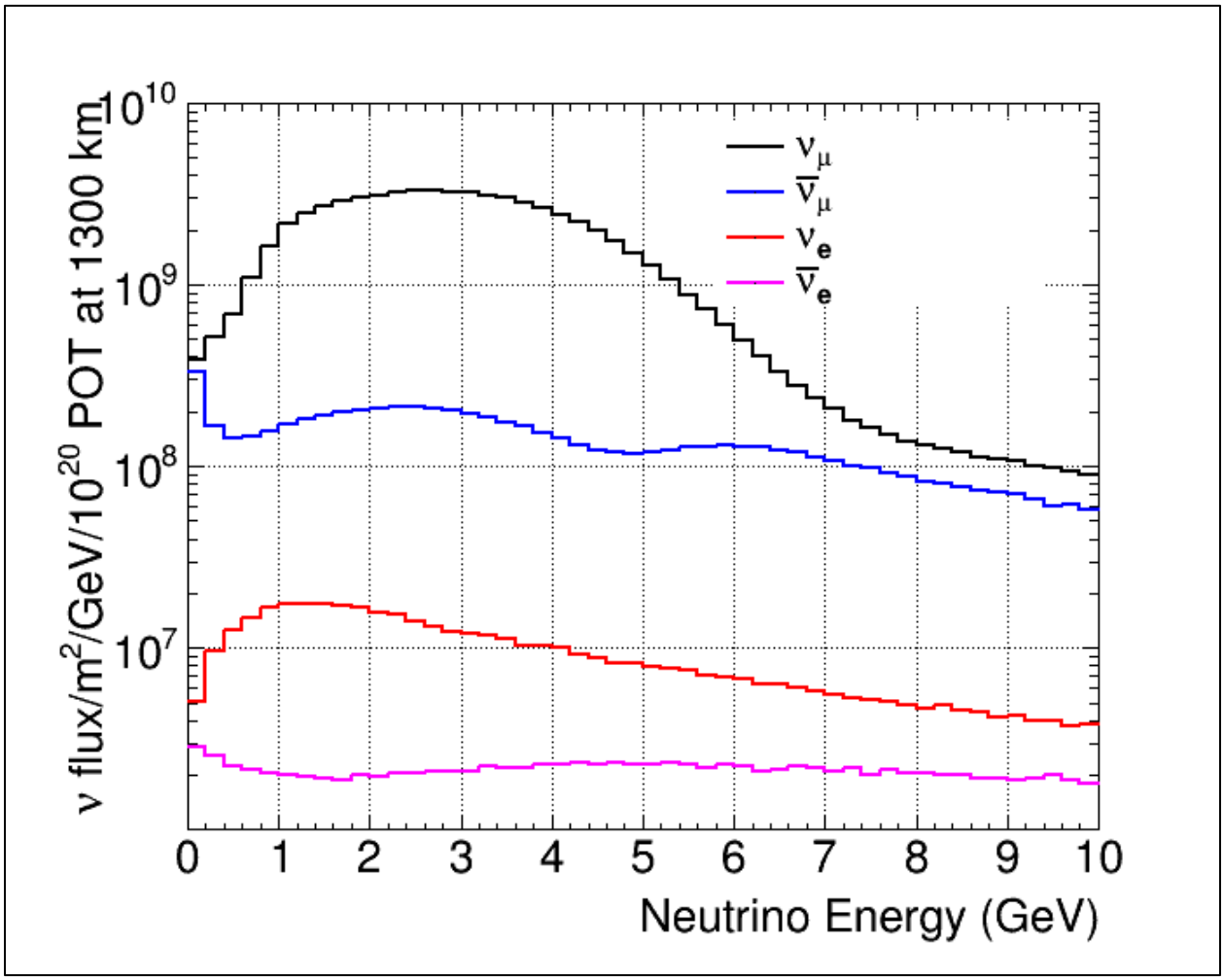

Figure 1-4: Neutrino Fluxes at the Far Detector as a function of energy in the absence of oscillations with the horns focusing positive particles. In addition to the dominant ν_μ ($\bar{\nu}\mu$) flux, the minor components are also shown. Note the logarithmic scale.

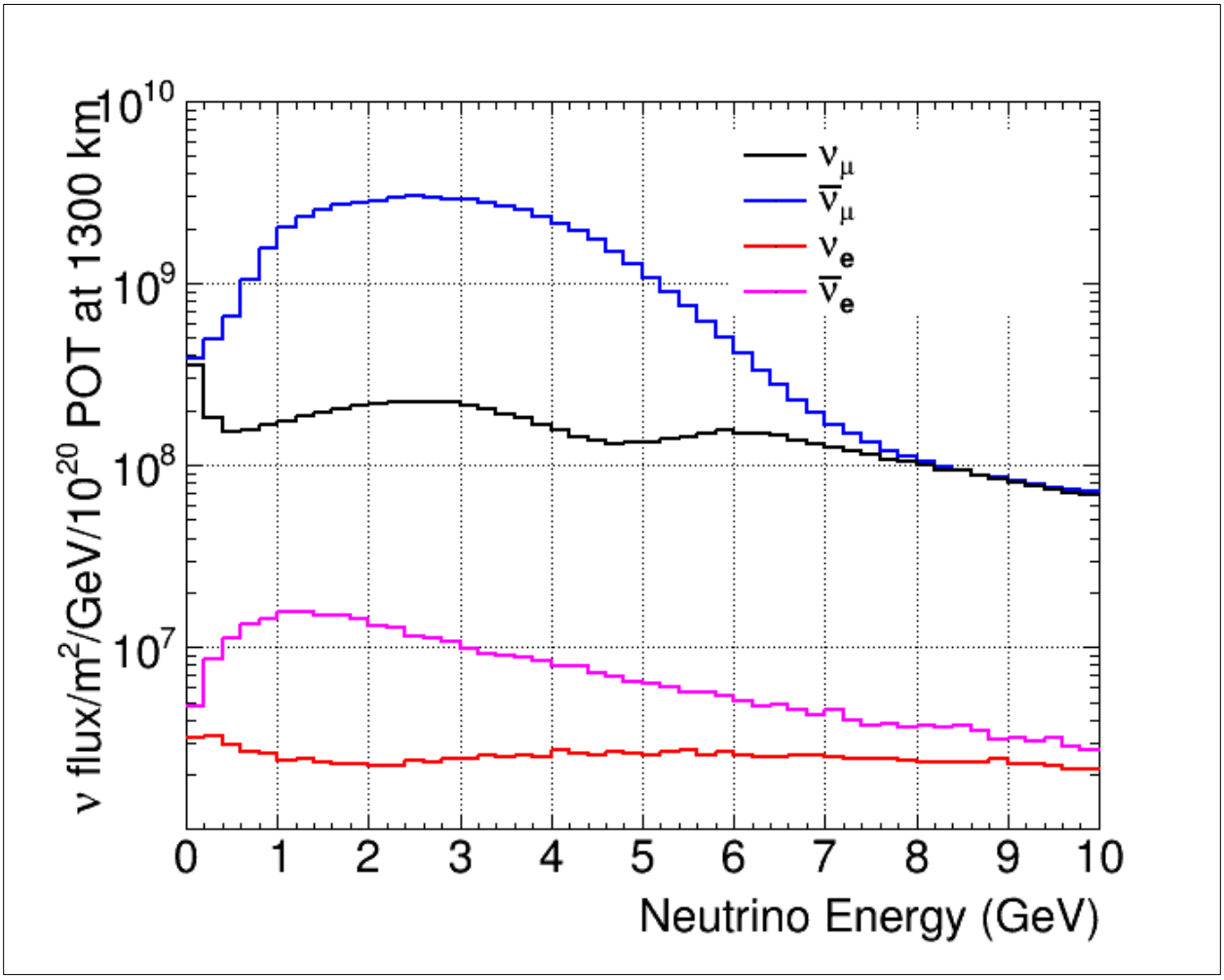

Figure 1-5: Antineutrino Fluxes at the Far Detector as a function of energy in the absence of oscillations with the horns focusing negative particles. In addition to the dominant ν□flux, the minor components are also shown. Note the logarithmic scale.

After collection and focusing, the pions and kaons that did not initially decay are allowed to decay in a long volume. This decay volume in the LBNF reference design is a He-filled pipe of circular cross section, oriented toward the Far Detector. Its diameter and length are optimized to allow decays of pions and kaons such that they produce neutrinos in the useful energy range. In general, a longer pipe allows for the decays of higher-energy particles. These occur naturally at smaller production angles and are thus distributed close to the beam axis. Therefore longer pipes with smaller diameters are desirable for higher-energy beams. Lower-energy pions and kaons are not as well collimated and hence require a larger-diameter pipe. The two extrema in energy, as required by the physics measurements, provide the basis for optimization of the decay pipe geometry. The reference design calls for a 203.7 m long decay pipe of diameter 4 m; this represents an acceptable balance between obtaining the desired neutrino energies and cost. See **Figure 1-6**.

A considerable fraction of beam power, 23%, is deposited within the decay region. This heat energy will be removed by air convection with a system of blowers and heat exchangers. The beam power deposited in the decay region implies creation of radioisotopes within the walls surrounding the pipe,

requiring shielding and sealing from the surrounding ground water. The reference design uses a minimum of 5.6 m of concrete between the pipe and the native rock or soil (engineered fill or glacial till).

The roughly 15% of protons that do not interact with the target, along with the residual pions and kaons, must be absorbed to prevent them from inducing radioactivity in the surrounding rock or soil. This is accomplished with a specially designed aluminum and steel pile, called the absorber that transforms the beam's kinetic energy into heat, thus protecting the rock or soil from beam-activated nuclides. The absorber occupies an excavated enclosure at the end of the decay pipe. The neutrino beam specifications are listed in **Table 1-3**.

1.2.4 System Integration

Integration of installation plans and procedures across the Beamline sub-project is an essential task given the complexity and interconnectedness of the beam systems. The System Integration group is responsible for a variety of control, monitoring, alignment, installation coordination and other elements that must ensure safe and proper operation of the beam. Control systems, in particular, will be built specifically for the LBNE Beamline, but will be based on and must integrate into Fermilab's present accelerator-controls system. Section 6, System Integration (WBS 130.02.04) is dedicated to System Integration.

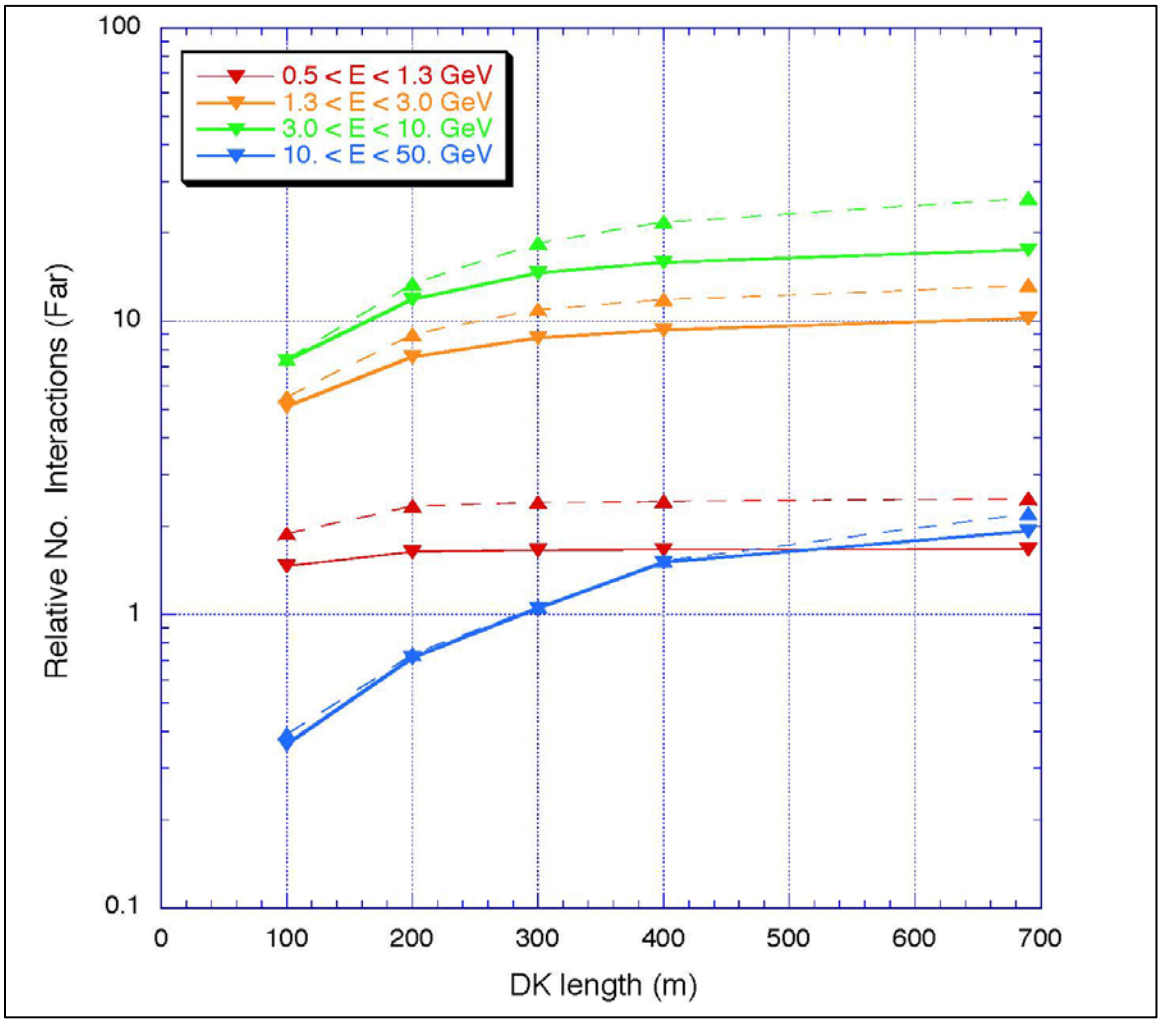

Figure 1-6: The number of neutrino interactions in the far detector depends on the length and diameter of the decay pipe. Here, the number of events is plotted as a function of length, with two curves for each colored energy range: solid is for a diameter of 2 m and dashed is for a diameter of 4 m. The reference design is a pipe 4 m in diameter and 203.7 m long LBNF

Table 1-3 presents the partial set of the relevant parameters for the elements of the reference design. Other important details such horn shapes are found in the subsystem sections herein. The third column lists the range of a parameter that has been studied for both physics or engineering considerations.

Table 1-3: Partial Set of Relevant Parameters for the Reference Design

Element	Parameter	Range	Reference design value
Target	material	graphite, Be	graphite
	transverse size	5 to 16 mm	10 mm
	length	2 interaction lengths	951 mm
Focusing Horn 1	length	2500 to 5500 mm	3360 mm
	current	180 to 300 kA	230 kA
Focusing Horn 2	length	3000 to 5000 mm	3630 mm
	current	180 to 300 kA	230 kA
	dist. from Horn 1 (front)	6000 to 14500 mm	6600 mm

Element	Parameter	Range	Reference design value
Decay Pipe	length	200 to 250 m	203.7 m
	radius	1.0 to 3.0 m	2 m
	atmosphere	Air, He, vacuum	99% He (1 – 1.1 bar)

1.2.5 Estimation of Protons on Target

The goal for accumulating 120-GeV protons at the neutrino target with beam power of 1.2 MW is 1.1×10^{21} protons-on-target (POT) per year. This assumes 7.5×10^{13} protons per MI cycle of 1.2 sec [1-POT-new]. The total LBNF efficiency used in the POT calculation and discussed below includes the total expected efficiency and up-time of the accelerator complex as well as the expected up-time of the LBNF Beamline.

The total accelerator operational efficiency is the product of efficiencies of the Proton Source, Linac, Booster and MI. The product of the first three stages (Proton Source, Linac and Booster) is expected to have average efficiency of 0.85 [2-POT-new]. The number of protons delivered from the MI to NuMI has been limited by delivery to other programs (anti-protons source for collider operations and test beams). The MI efficiency is expected to be approximately 0.93 in the PIP-II era [3-POT-new]. The annual scheduled maintenance, a facility shutdown, averaged 2 months (60 days) on the basis of historical data (annual fraction of 0.84).

The estimated unscheduled down time, using data from the operation of NuMI, including power failures and down-time for chillers, dehumidifiers and tritium mitigation systems, is small; the efficiency is 0.98. Assuming that LBNF target and horn replacements take 29 days per year in addition to the facility shutdown, the LBNF efficiency/up-time due to component replacement is estimated to be 0.91. This efficiency takes into account two and a half target replacements per year and 0.67 horn replacements per year where the target/horn replacement takes 14/24 days respectively per changeout including the cool down period. It is assumed that one of the two and a half target replacements will take place within the scheduled annual shutdown and that the horn replacement has 50% probability to take place within the scheduled shutdown. An additional 0.95 efficiency is assumed due to programmatic issues and very short downtimes (less than a few minutes). Thus, the total efficiency for LBNF is estimated to be approximately $0.85\times0.93\times0.84\times0.98\times0.91\times0.95=0.56$. It is also assumed this overall efficiency can be maintained from beam startup to completion of the oscillation physics goals.

The total expected POT per year, given above, is thus the product of the total efficiency (0.56), the number of protons per second (6.25×10^{13}) and the number seconds in a (perfect) year (3.15×10^{7}).

The reliable delivery of higher than NuMI/MINOS beam to the target should be aided greatly by the operation of NuMI/NOvA, which will test the proton slip-stacking in the Recycler Ring. The reliability of very low-loss transport through the LBNF section will be enhanced from the one for NuMI by state-of-the-art beam monitors and an active control-feedback system. With deliberate beam commissioning and start-up, the efficiency in the LBNF primary beam should be very high taking into account that the

corresponding operating efficiency for the NuMI primary beam over a nine-year period has been greater than 0.99.

1.2.6 Modeling of the Beamline

An essential aspect to beam design work is numerical simulation of the primary and secondary neutrino beams. These Monte Carlo type simulations provide input to detailed engineering calculations for beam heating effects for all components in or near the beams. Also, the same software package give radiological estimates for prompt and residual doses that dictate the amount of shielding needed along and traverse to the beamline. At Fermilab, the MARS [1-Intro-MARS] code is used for all these estimates, with a sufficiently detailed model of the entire beam system.

1.2.7 Near Site Conventional Facilities

The Near Site Conventional Facilities not only provide the support buildings for the underground facilities, but also provide the infrastructure to direct the beamline from the below-grade extraction point to the above-grade target. The layout is shown in **Figure 1-1**. Following the beam from east to west, or from right to left in this figure, is the underground Primary Beamline Extraction Enclosure, the in-the-berm Primary Beamline Enclosure and its accompanying surface based Service Building (LBNE 5), the in-the-berm Target Complex (LBNE 20), the Decay Pipe and the underground Absorber Hall and its surface Service Building (LBNE 30).The Project limits are bounded by Giese Road to the north, Kautz Road to the east, Main Injector Road to the south, and Kirk Road to the west.

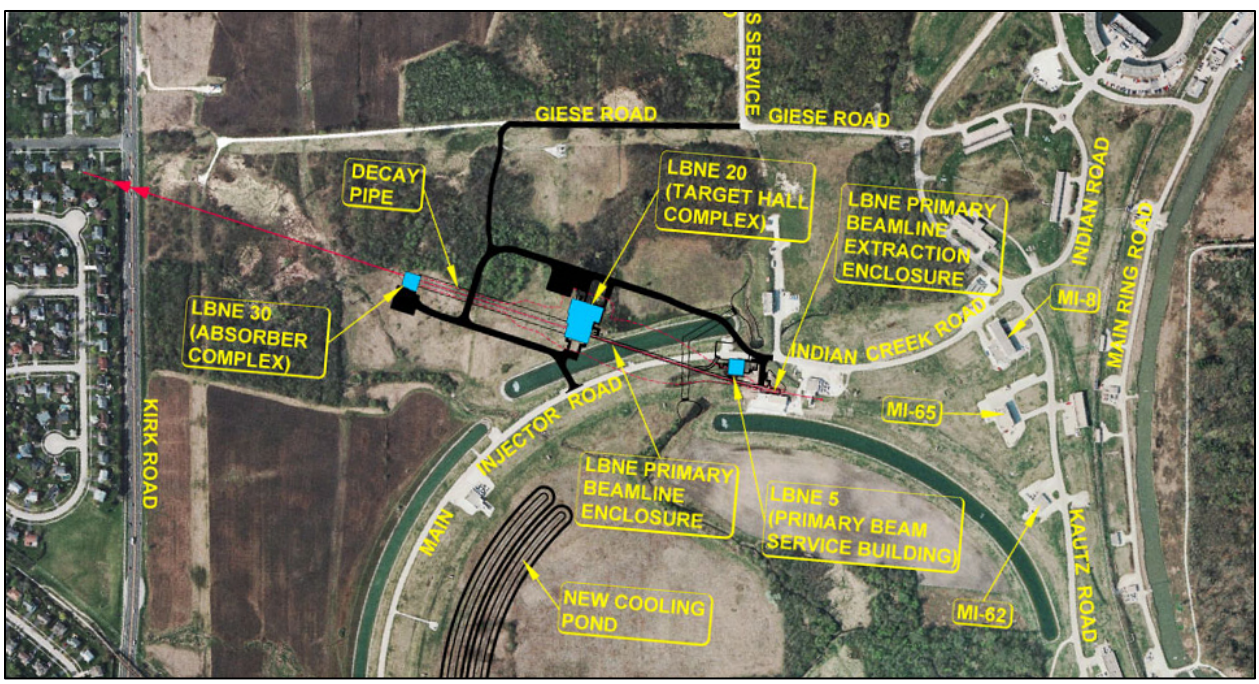

Figure 1-7: LBNE Overall Project Layout at Fermilab

These facilities are described in detail in Volume 5?? of this CDR. (TBF)

Following is a list of references to text about conventional??-facilities design choices in LBNF CDR Volume 5???: Facilities at the Near Site that relates to the following Beamline L2 Project elements. (All elements are also addressed in Volume 5 Section 1.2.)

- Primary beam enclosures: Section 5.1
- Service buildings LBNE 5, LBNE 20, LBNE 30: Sections 4.1, 4.2 and 4.3
- Target Hall target chase: Section 4.2
- Target Hall support rooms: Section 4.2
- Near-surface storage and morgue: Section 4.2
- Decay pipe: Section 5.2
- Absorber Hall: Section 5.3

1.3 Participants

The conceptual design for the LBNF Beamline has been carried out by an LBNF L2 Project team, managed at Fermilab and to date made up of physicists, engineers, designers and technicians mainly from Fermilab as well as a few additional institutions. In addition, several contracts with other institutions and consultants have been completed for conceptual design work on particular beamline systems or components:

- Argonne National Laboratory (MOU, target)
- Brookhaven National Laboratory (MOU, target)
- Institute of High Energy Physics, Protvino, Russia (Accord, target)
- Oak Ridge National Laboratory (contract, remote handling)
- Rutherford Appleton Laboratory (Accord, target)
- Bartoszek Engineering (contract, Horn support structures)

Collaborations continue with Rutherford Appleton Laboratory and CERN on Target R&D, with University of Texas at Arlington on the Hadron Monitor and with IHEP/China on beam simulations and the design of the downstream decay pipe window. We also collaborate with several University colleagues on beam simulation efforts. The Beamline management coordinates the design activities of the consultants and collaborators to assure that the efforts remain on track. The beamline is planned for construction at the Fermilab site, which is managed by the Fermi Research Alliance (FRA).

The LBNF Beamline effort is managed by the Work Breakdown Structure (WBS) Level 2 Manager for the Beamline Project. The supporting team includes a WBS Level 3 Manager for the Beamline's two principal systems, Primary Beam and Neutrino Beam, as well as for System Integration. WBS Level 4 Managers manage the design of the components in these beamline systems and the interfaces between them.

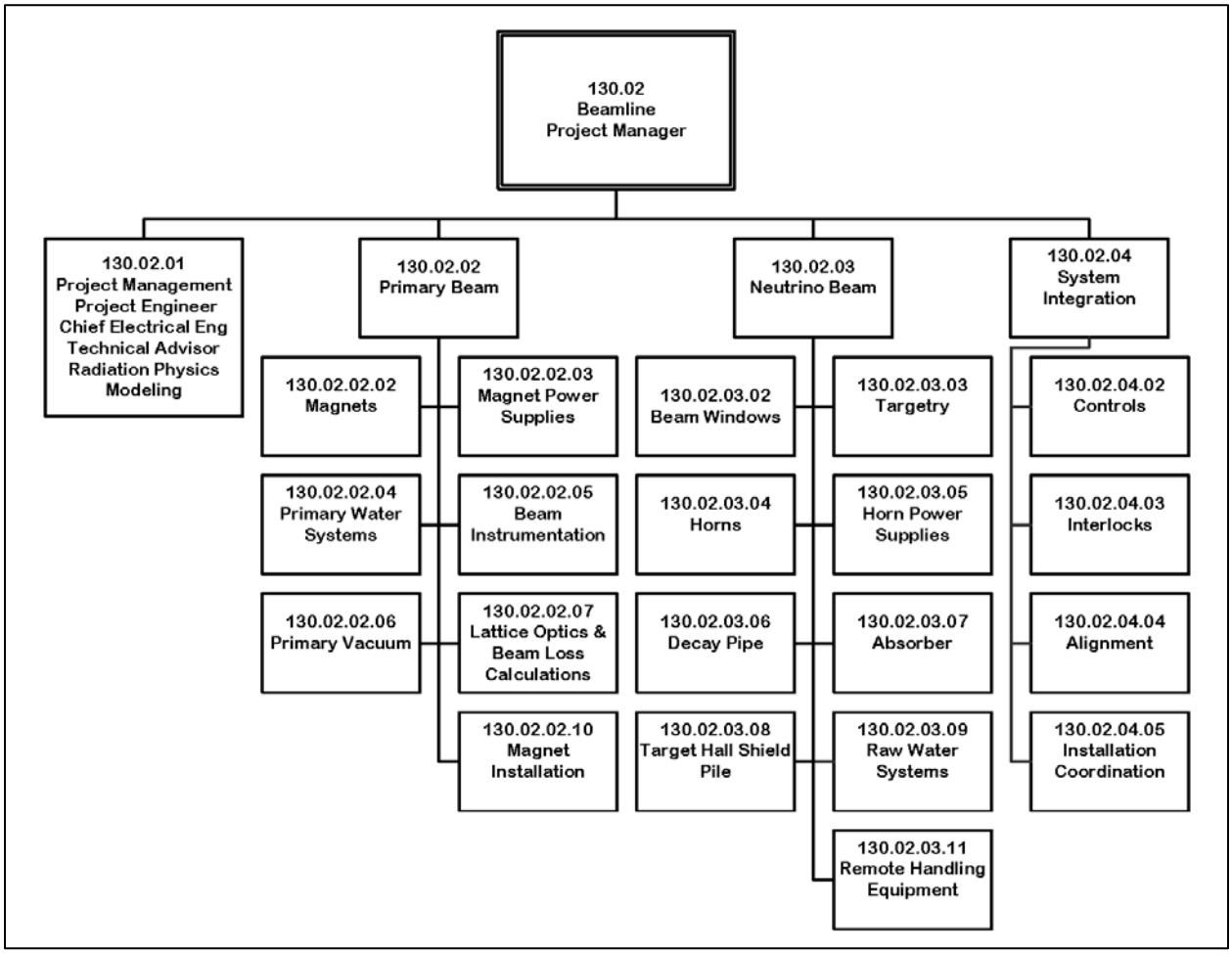

Figure 1-8: Organization Chart for the Beamline L2 Project (to WBS Level 4)

Assisting and advising the Beamline L2 Project is an ES&H Coordinator, two Radiation Physicists and a Project Controls specialist.

Interaction amongst the Beamline team, and between this team and the design consultants as well as the LBNE Near Site design team, has been done via weekly meetings, periodic design interface workshops, and electronic mail.

References:

[1-POT-new] Proton Improvement Plan II, http://projectx-docdb.fnal.gov/cgi-bin/RetrieveFile?docid=1232

[2-POT-new] Proton Improvement Plan I, B. Pellico

[3-POT-new] Historical Accelerator data and I. Kourbanis, private communication

[1-Intro-MARS] N.Mokhov, “The Mars Code System User’s Guide,” tech. rep., 2009. Fermilab-FN-628.

PRIMARY BEAM (WBS 130.02.02.05)

2 INTRODUCTION

This chapter describes the reference design for the LBNF primary (proton) beamline. This system will extract protons from Fermilab's Main Injector (MI) synchrotron, using a single-turn extraction method, and transport them to the target in the LBNF Target Hall. The nominal range of operation will be from 60 to 120 GeV.

2.1

The principal components of the primary beamline include specialized magnets at the MI-10 extraction point to capture all of the protons in the synchrotron and redirect them to the LBNF beamline, a series of dipole and quadrupole magnets to transport the proton beam to the target, power supplies for all the magnets, a cooling system, beamline instrumentation and a beam-vacuum system for the beam tube.

All of the LBNF primary-beam technical systems are being designed to support sustained, robust and precise beam operation. Careful lattice optics design (described in Section 4) and detailed beam-loss calculations (described in Section 14) are essential for the proper operation of the primary-beam system, as are a detailed understanding and monitoring of component alignment and development of the comprehensive beam-permit and control systems, described in Chapter 27.

2.2 Design Considerations

2.2.1 Length and Elevation

As discussed in the Alternatives Analysis document [?], primary-beam extraction using the "MI-10 Shallow" design was chosen after a thorough value-engineering process evaluating shallow and deep configurations at both MI-10 and other locations. It offers several advantages over the other designs.

The shallow beam design offers a significant cost savings for the neutrino beam facility, plus significant advantages with tritium mitigation for the near-grade Target Hall. Also, given the limited available site footprint, a deep Target Hall, as exists for NuMI/ NOvA, would require the primary-beam transport to be considerably longer to reach the depth at which sufficient structural rock cover exists above the hall. This added distance is neither necessary nor available with MI-10 extraction for a 120-GeV beam.

The target elevation of a few feet above natural grade elevation is chosen to optimize overall facility-construction technical and resource requirements [?]. It was selected as the best balance between minimizing Absorber Hall depth in the rock and the extent of the primary beam transport line above natural grade level. Additional constraints include limiting the maximum primary-beam enclosure elevation angles to 150 milliradians, and achieving the required trajectory for transport of the neutrino beam to the Far Detector site. A profile-view schematic of the target lineup for the primary-beam transport with Target Hall and decay region is shown in **Figure 2-1**. Colors in the figure illustrate the height of earth fill needed, including shielding for the primary-beam enclosure, along with the location of the Target Hall and decay region with respect to the underlying glacial till and rock strata.

Existing Infrastructure and Shielding

The choice of a shallow beam extracted at MI-10 avoids beamline crossings, and allows for a simpler extraction enclosure, enabling a cost-effective facility design of the entire extraction region. It interferes minimally with existing beam systems in this region, reduces magnet count, and also provides some shielding separation from accelerator-tunnel beam losses at the beginning of the LBNF primary-beam transport enclosure.

The MI-10 primary-beam layout on the Fermilab site is shown in **Figure 2-1**

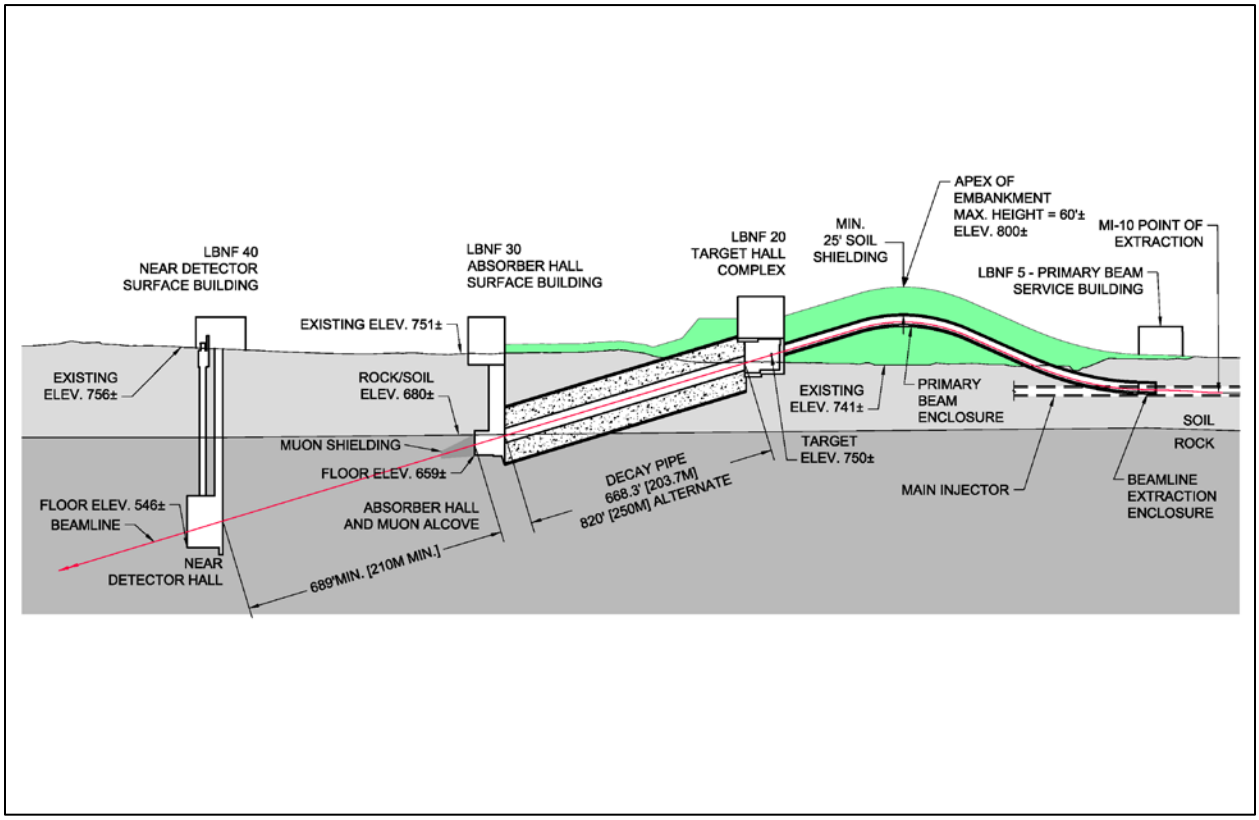

Figure 2-1: View showing the concept of elevating the beamline, thereby minimizing the deep excavation and tunnels. The beam comes from the right through the primary beam enclosure and interacts with the target in the Target Hall Complex. Fill used to elevate the beam is shaded in green.

Beam Control

Techniques, hardware and control applications for accomplishing primary-beam control at the required level were developed for the NuMI proton beamline. These features have been demonstrated to perform very well during the nearly decade long operation of the NuMI beamline and are therefore being used in the design for the LBNF primary beam. Included are

- A comprehensive beam-permit system (described in Section 29) with more than 250 parameters that are to be verified prior to each beam extraction,
- Open-extraction channel and primary-transport magnet apertures capable of accepting a range of extracted beam energies,
- Primary-extraction channel and LBNF beam-transport component apertures sized to accept a beam envelope larger than the MI dynamic aperture of 360 π mm-mrad, without beam loss,
- Excellent magnetic-field uniformity to match the beam-envelope apertures,
- Major power-supply regulation to a few parts per million to achieve good beam-transport stability,
- A strong focusing beam optics design with excellent control of beam size and dispersion,
- Fully automated beam position control, with no manual adjustment of beam positions required during operation, and
- Robust beam instrumentation to enable maintenance of beam-targeting accuracy to approximately 100 µm.

2.3 Reference Design Overview

The LBNF primary beamline is extracted using single-turn, or “fast” extraction, in which all the protons accelerated in the MI synchrotron ring will be diverted to the LBNF beamline within one revolution after each acceleration cycle. The train of bunches of protons in the MI extends most of the way around the ring. After extraction, the beam is controlled by a series of dipole (bending) and quadrupole (focusing) magnets collectively called the “lattice optics.” This term refers to the overall design of the system, i.e., the magnet types, strengths, order, relative placement and other characteristics. The LBNF primary-beamline lattice optics is designed to direct the proton beam toward the target and resulting neutrinos toward the downstream Far Detector, with a beam spot size appropriate for maximizing the physics potential of LBNF.

LBNF will implement a modular optics design comprised of three distinct lattice configurations in series: the specialized MI-to-LBNF matching section, the transport section and the final focus of the beam on the production target. The layout of the beamline is shown in **Figure 2-2.** (For another view, see **Figure 2-26** in sub-subsection 2.10, **Magnet Installation**)

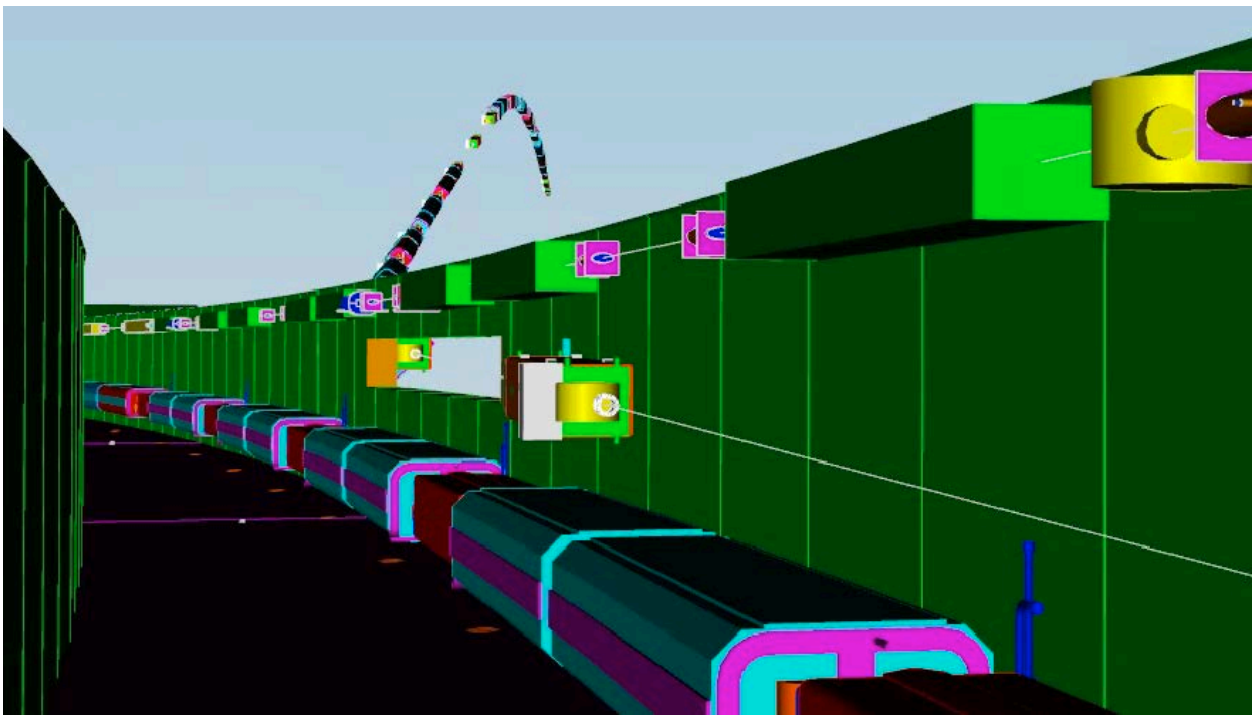

Figure 2-2: View of the beamline from near the end of extraction region in the MI through the wall and up and over the apex of the hill. The Main Injector beamline is at the bottom and the Recycler at the top.

After the kicker magnets in the MI apply a horizontal kick to the beam, the beam passes through a set of three special purpose magnets, called Lambertsons, that vertically extract the beam from the MI. The Lambertsons sit in the path of the beam, both when it circulates and when it is extracted, accommodating both paths. The circulating beam passes through a field-free hole in the magnet yoke, while the extracted beam instead passes through the (separate) magnetic aperture, is bent upward and away from the MI trajectory. Each Lambertson in the line bends the beam more, such that after passing through all three (and one focusing quadrupole, a component of the MI lattice that sits between the first and second Lambertsons), the extracted beam is sufficiently separated from the MI orbit to pass through the first bending magnet external to the MI line, a C-magnet. The C magnet clears the MI beam tube downstream of the third Lambertson and provides an additional upward bend, enough so that the extracted beam can pass above the outside of the next quadrupole in the MI lattice. The C-magnet is the last element of the specialized extraction channel.

The transport section includes a series of rolled dipole magnets (tilted about the beam axis to vary the direction of bend) interspersed with regularly spaced quadrupole magnets to ensure that transverse beam size does not exceed that in the MI. The first dipole bends the beam horizontally further from the MI and reduces the rate of vertical rise. Several quadrupoles maintain the beam size as the beam tube passes through the wall between the MI tunnel and the LBNF primary-beam enclosure. The beam is then bent to the right and up, and back down from the apex at an angle of 101 milliradians (5.79 deg.) toward the target, thus establishing the needed trajectory for the neutrino beam.

In the last section of the primary beamline, the beam size and its angular spread are tailored to the desired distribution for hitting the production target. This is accomplished by eight independently tunable quadrupoles in the final-focus section, which can be tuned to produce a wide range of beam spot sizes while maintaining a narrow angular spread.

Some magnets will be grouped ito a single “magnet loop” and powered by a single power supply, whereas others will be powered individually, according to the lattice optics design. In order to maintain the lowest possible power consumption, all of the larger magnet loops will be ramped. A primary water system will feed cooling water to the magnets and power supplies. Beam instrumentation will characterize and monitor important beam parameters, for example, beam positions, stability, losses, intensity and transverse emittance. A vacuum system will maintain a vacuum of better than 10^{-7} torr residual gas pressure in the beam tube in order to reduce the beam loss due to proton-gas interaction.

Utilities (power, water, cabling), crates, etc.) for the beamline elements in the extraction region come from the existing MI-10 service building. Those in the primary beam enclosure are serviced from the new LBNF-5 building via the magnet access tunnel. (See Figure xx, installation coordination section.) Magnet in the extraction region will be installed from the main injector; those in the primary beam enclosure are moved from to the primary beam enclosure via the magnet access tunnel for installation.

The remainder of the chapter is organized as follows. First we describe the lattice optics design and performance, and the component magnets. This is followed by a discussion of the magnet power supplies, the cooling water system, beam instrumentation, and the vacuum system. Installation of the magnets in the beamline enclosure is the most difficult of the installations, and we discuss this in the last section.

2.4 Lattice Optics (WBS 130.02.02.07)

2.4.1 Introduction

LBNF will implement a modular optics design comprised of three distinct lattice configurations in series: the specialized MI-to-LBNF matching section, the transport section and the final focus of the beam on the production target.

A series of six fast-pulsed kicker magnets in the MI ring (Section 9.3.6) extract the beam. The kicker magnets have a fast ramp-up to the required current followed by a ramp-down; the ramps occur during gaps in the circulating MI beam. The kickers are followed by the set of three Lambertson magnets that bend the extracted beam away further (upward) from the MI trajectory. To match the MI optics to the optics of the transport section, a string of individually controlled quadrupole and dipole magnets is used.

The transport section steers the beam from extraction/matching section up to and over the hill toward the Target Hall. The matching section is followed by an optical lattice consisting of a series of six periodic focusing units, “FODO” cells, which terminates 119 m upstream of the target. A set of eight independently tunable quadrupoles form the achromatic final-focus (FF) optics to obtain the desired

beam size on the target. This final focus is tunable to produce a spot-size (σ) from 1.00 to 4.00 mm over the entire momentum range 60 to 120 GeV/c.

2.4.1 Design Considerations

The design of the lattice for LBNE, as detailed in the next section, is constrained by the experimental needs, civil construction requirements and operational factors in transporting an intense beam over long periods of time. These include:

- large changes in elevation in order to keep the Target Hall above grade
- extraction and transport over a range of beam momenta (60 to 120 GeV/c)
- beam position and focus at target which is finely adjustable
- transport of beam with very low average losses

These constraints drive most of the fundamental aspects of the technical design. The optics presented here were computed using Methodical Accelerator Design (MAD) and the design reflects the large amount of experience of the designers.

2.4.2 Reference Design

Protons are extracted from the MI-10 straight section. The extraction magnets are of the standard MI design with six kicker modules at the upstream end of the MI-10 straight section to kick the beam horizontally into three vertically-bending Lambertsons plus a C-magnet straddling the MI quad Q102 located 90° in betatron phase downstream; see **Figure 2-3**.

A single, rolled, long (6 m) MI-style IDA dipole (Section 9.3.1) steers the beam horizontally towards the MI enclosure wall between MI quads Q105 and Q106, while leveling the beam off somewhat to a gentle vertical slope of +0.60°, thereby bisecting the space separating the MI and Recycler Ring magnets. A 15.6-m-long carrier pipe transports the beam through the MI tunnel wall into the new primary beam extraction enclosure that houses the main body of the line.

From that point the protons are transported a further 257.9 m to the target, located 10 ft above grade (750 ft above sea level) and aimed towards the Far Detector. In the main body of the beamline, 12 IDA dipoles plus 12 short (4-m) MI-style IDD dipoles together bend the beam -7.180° horizontally and -5.789° net vertically. Bends are grouped into twelve 4+6 meter pairs. The first three cells accomplish the horizontal alignment to the Far Detector while generating a +143-mrad vertical trajectory. This upwards trajectory continues through the subsequent empty FODO cell, reaching maximum beam elevation 30 ft above grade. This is followed by three full cells that create the 244 mrad of downward bend necessary to obtain the final -101 mrad trajectory to the Far Detector.

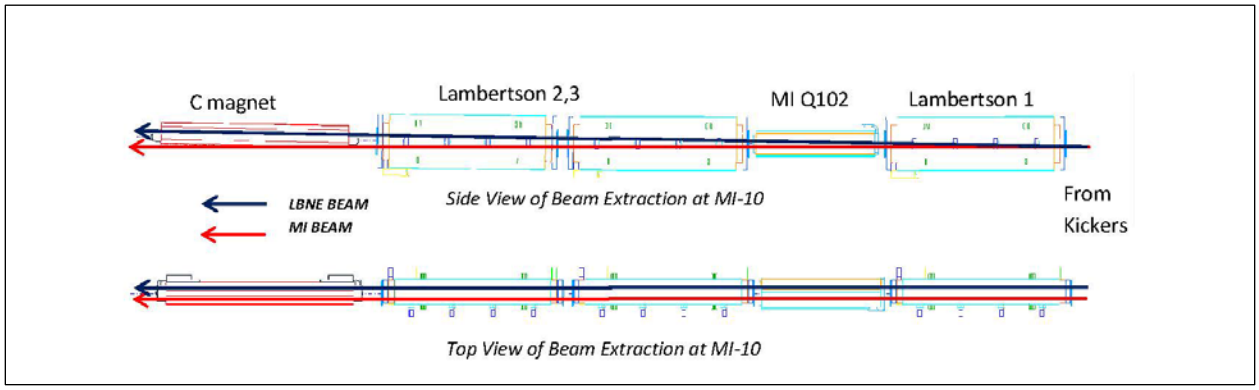

Figure 2-3: Configuration of the LBNE Extraction Lambertsons and C-magnet Straddling MI Quad Q102

Optical properties are defined by 21 quadrupoles (grouped as 20 focusing centers) of the proven MI-beamline-style modernized 3Q60/3Q120 series (QQC/QQB) (Sections 9.3.4 and 9.3.5). All focusing centers are equipped with redesigned MI-style IDS orbit correctors (Section 9.3.5) and dual-plane beam-position monitors (BPMs) (Section 8). Ample space is available in each cell to accommodate ion pumps and diagnostic instrumentation. Parameters for the main magnets are listed in **Table 2-1**.

2.4.2.1 Optics

This 60-120 GeV/c transfer line design comprises distinct optical modules, as illustrated in **Figure 2-4** extraction/matching section, transport section and a widely tunable quadrupole triplet module to control beam size on target.

The first six quadrupoles in the beamline are powered individually to perform the optical match between lattice functions of the MI and those of the LBNE transfer line; the roll angles of dipoles in the first three half-cells are selected specifically to contribute to the dispersion matching of (η_x,η_x') and (η_y, η_y'). This matching section is followed by six 120° FODO half-cells characterized by quadrupoles Q207 through Q212. Cell length and phase advance are chosen such that beam size does not exceed that of the MI 90° lattice cell structure, while also optimizing efficient use of space for the achromatic insertions. Dispersion generated by variations in the beam trajectory is corrected locally and cannot bleed out to corrupt the optics elsewhere in the line. Quadrupoles Q214 through Q221 form the tunable final-focus optics capable of producing a spot-size of σ = 1.00 to 4.00 mm over the entire momentum range 60 to 120 GeV/c. (The quadrupole numbering scheme is chosen to match the MI convention, in which even numbers are horizontally focusing and odd numbers are defocusing. This results in quad Q218 being absent).

Magnet apertures (including the impact of rolls) and beam envelopes are shown in **Figure 2-5**. One contour corresponds to nominal MI beam parameters of $\epsilon = 30\pi$ µm (99%, normalized) and Δp_99/p = 11×10^{-4}. The larger envelope shown is calculated for $\epsilon = 360\pi$ µm (100%, normalized) and Δp_100/p = 28×10^{-4}. The latter values reflect the admittance of the MI at transition (γ_t = 21.600), and the transfer of such a beam to LBNE could only result from a catastrophic failure of the MI and LBNE safety and

regulatory systems. The maximum transverse emittance of 360π μm is determined by the restricted horizontal aperture in the Lambertson magnets seen by the circulating MI beam. The momentum spread is the maximum value that can be contained in a radio frequency bucket through acceleration. The ϵ = 360π μm and Δp_100/p = 28×10^{-4} envelopes, therefore, demonstrate that the LBNE primary beamline should be able to transport, without losses, the worst quality beam that the MI could transmit.

Table 2-1: Magnet Parameters of the LBNE Proton Beamline at 120 GeV/c and β*=86.328 m.

DIPOLE NAME	TYPE	L (m)	B (T)	TILT (deg)		QUAD NAME	TYPE	L (m)	G (T/m)
MI-10 EXTRACTION → LBNE									
						Q100	3Q100	2.540	+16.16016
KICKER (6)	RKB	1.2954	0.05890						
						Q101	3Q84	2.134	-15.81326
LAM1	ILA	2.8000	0.53242	−90.000					
						Q102	3Q84	2.134	+16.16016
LAM12 (2)	ILA	2.8000	1.00000	−90.000					
V100	ICA	3.3528	1.00284	−90.000					
MATCH FROM MI → LBNE FODO LATTICE & 143 mr UP BEND									
						Q201A→201B	3Q60	1.524	−11.13509
HV201	IDA	6.09981	1.22335	+62.844					
						Q202	3Q120	3.048	+12.48756
						Q203	3Q120	3.048	−9.18907
						Q204	3Q120	3.048	+13.06221
HV204A	IDD	4.06654	1.38347	−44.126					
HV204B	IDA	6.09981	1.38347	−44.126					
						Q205	3Q120	3.048	−13.52413
HV205A	IDA	6.09981	1.38347	−44.126					
HV205B	IDD	4.06654	1.38347	−44.126					
						Q206	3Q120	3.048	+16.16931
HV206A	IDD	4.06654	1.10813	−48.179					
HV206B	IDA	6.09981	1.10813	−48.179					
FODO CELLS									
						Q207	3Q120	3.048	−15.83240
HV207A	IDA	6.09981	1.10813	−48.179					
HV207B	IDD	4.06654	1.10813	−48.179					
						Q208	3Q120	3.048	+15.83240
HV208A	IDD	4.06654	1.00297	−56.109					
HV208B	IDA	6.09981	1.00297	−56.109					
						Q209	3Q120	3.048	−15.83240
HV209A	IDA	6.09981	1.00297	−56.109					
HV209B	IDD	4.06654	1.00297	−56.109					
						Q210→212	3Q120	3.048	±15.83240
244 mr ACHROMATIC DOWN BEND & FINAL FOCUS ON TARGET									
V212A	IDD	4.06654	1.60431	+90.000					
V212B	IDA	6.09981	1.60431	+90.000					
						Q213	3Q120	3.048	−13.96520
V213A	IDA	6.09981	1.60431	+90.000					
V213B	IDD	4.06654	1.60431	+90.000					
						Q214	3Q120	3.048	+16.54570
V214A	IDD	4.06654	1.60431	+90.000					
V214B	IDA	6.09981	1.60431	+90.000					
						Q215	3Q120	3.048	−15.26976
V215A	IDA	6.09981	1.60431	+90.000					
V215B	IDD	4.06654	1.60431	+90.000					
						Q216	3Q120	3.048	+13.81046
V216	IDD	4.06654	1.60431	+90.000					
						Q217	3Q60	1.524	−17.08214
V217A	IDA	6.09981	1.60431	+90.000					
V217B	IDA	6.09981	1.60431	+90.000					
V217C	IDD	4.06654	1.60431	+90.000					
						Q219	3Q120	3.048	−10.53138
						Q220	3Q120	3.048	+15.80329
						Q221	3Q60	1.524	−13.39482

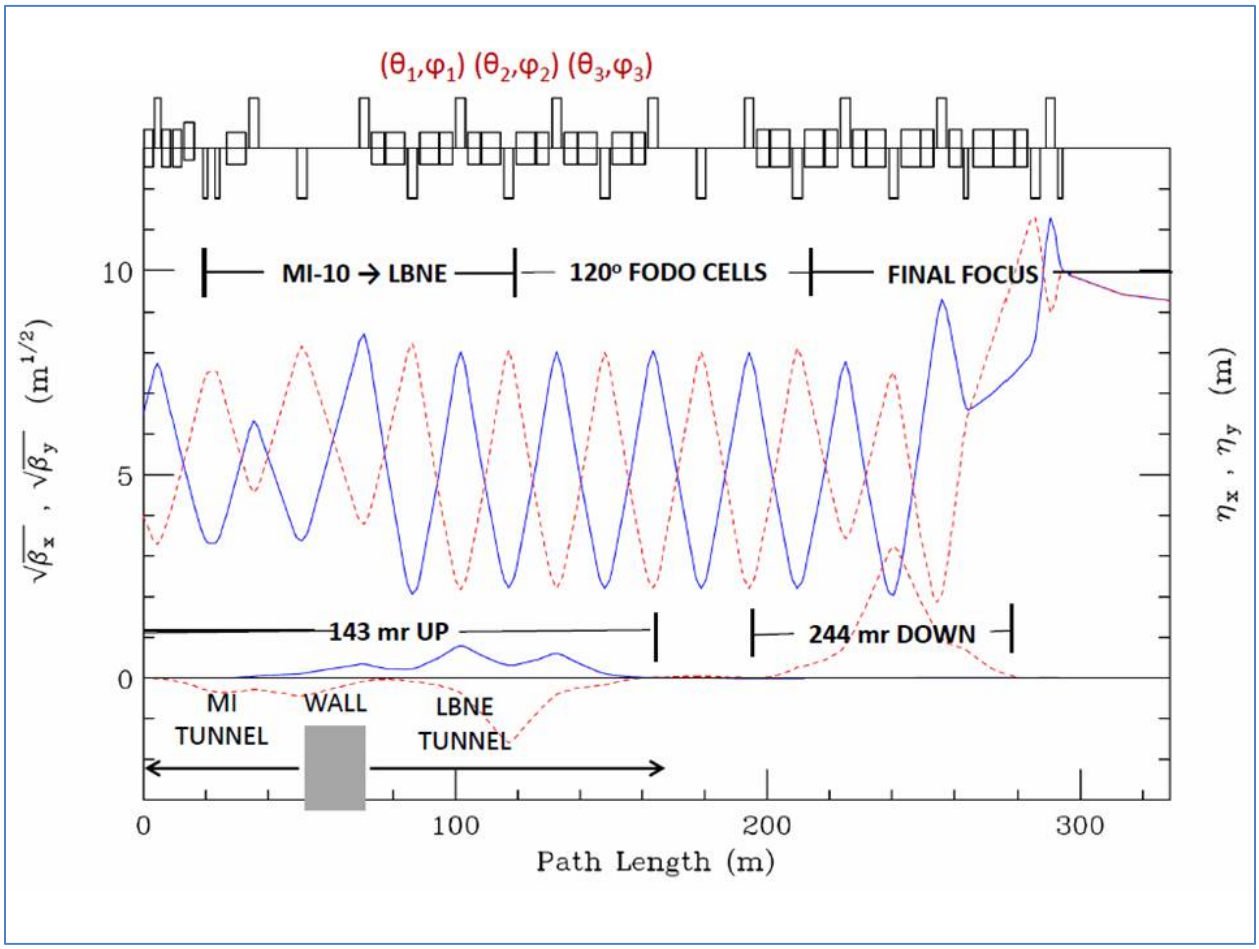

Figure 2-4: Horizontal (Solid) and Vertical (Dashed) Lattice Functions of the LBNE Transfer Line. The final focus is tuned to produce a spot size of $\sigma_x=\sigma_y=1.50$ mm at 120 GeV/c and $\epsilon=30\pi$ μm (99%, normalized)]

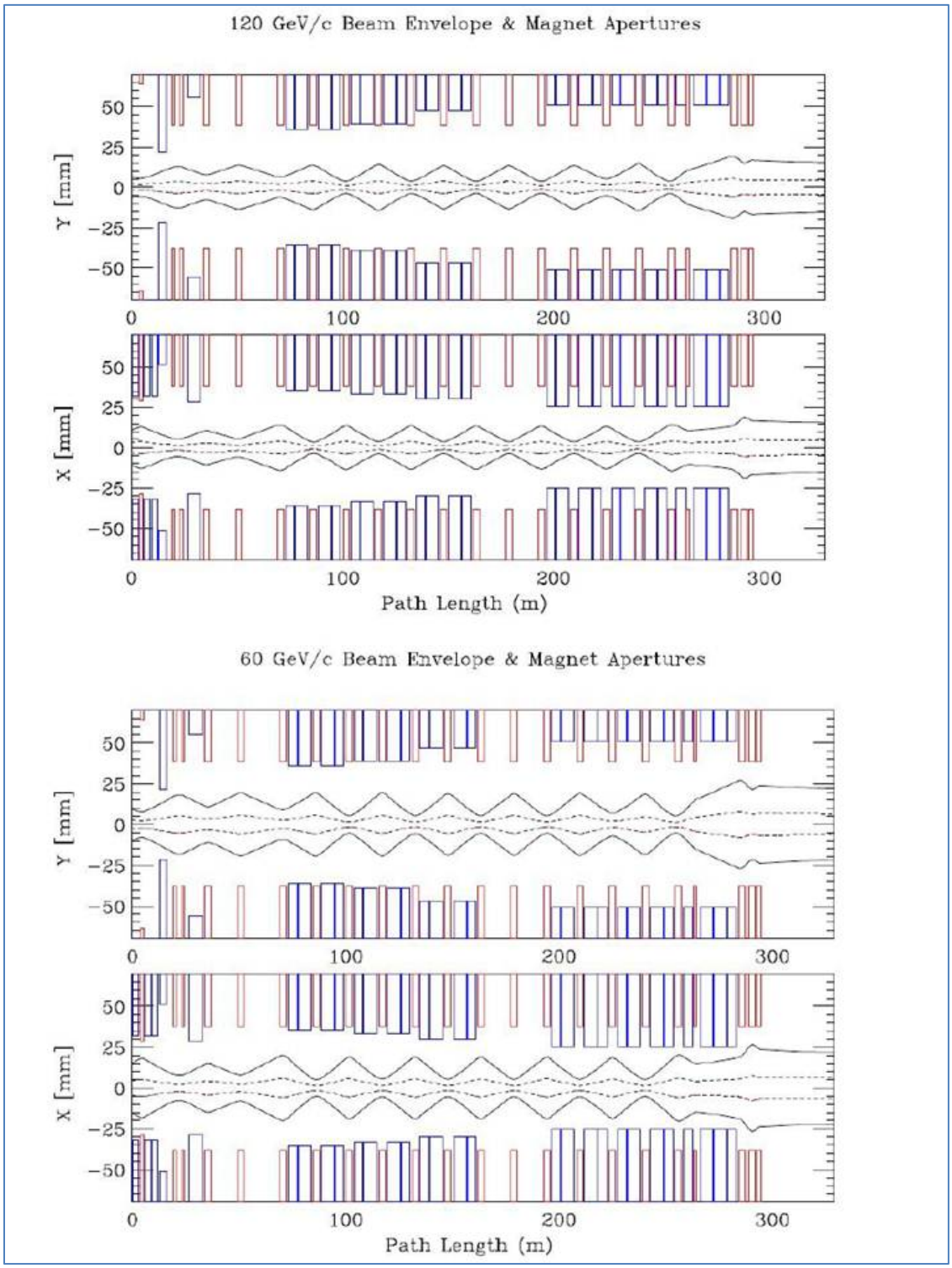

Figure 2-5: Magnet Apertures and Beam Envelopes. The 99% contour (dashed) with nominal MI beam parameters, and the 100% envelope (solid) corresponding to the MI admittance at transition (γ_t = 21.600).

2.4.1.1 Sensitivity to Gradient Errors

It is assumed that the optical integrity of the primary beamline will not be compromised by magnet-to-magnet variations in the integrated quadrupole fields. Experience with the MI-style 3Q120 magnets has shown that these magnets are very high quality, with a spread in gradient errors on the order of $\sigma(\Delta G/G) \sim 0.08\%$ or less. Such a narrow error distribution cannot appreciably impact the beam characteristics or transport capabilities. Implementing even the most rudimentary strategy for sorting production quadrupoles, such as selecting those from the middle of the distribution for installation in the FODO cells, will reduce the spread even further. For nominal beam parameters at 120 GeV/c, a simple thin-lens calculation predicts that the largest error-wave expected in the 99% beam envelope (±3.89 mm nominal at β = 64.5 m) would be less than 75 microns.

2.4.1.2 Beam Size at Target

An essential design requirement of the final focusing section is the ability to tune the spot size σ over a wide range. The optimum spot size at 1.1-MW is thought to fall in the range $\sigma \sim$1.5-2.0 mm, which would grow to ~2.5-3.0 mm for a 2.4-MW upgrade. Spot size is still an evolving parameter. Ultimately, the choice will be driven to a large extent by details of the final target design, but other factors must also be considered. In addition to the 40% difference in beam size between 60 and 120 GeV/c, under real operational conditions the beam parameters (ϵ,$\Delta p/p$) will certainly be different from the ideal nominal values assumed here. Currently, the MI 99% normalized emittance at 120 GeV/c is ~20-22π µm, but it is not clear how this value might change in the future. It is essential that the FF design be sufficiently robust and versatile to anticipate these possibilities.

Figure 2-6 illustrates the wide tuning range of the FF. In principle, spot-size can be tuned to a maximum of σ^* = 4.00 mm before magnet powering limitations take over. In practice, though, the maximum attainable σ^* is ~ 3.20 mm. This limit is imposed by the restricted horizontal aperture (1.90 in) seen by the beam in the last 4-m vertical dipole. Results are shown for the two extremes of operational requirements. Calculations were performed assuming nominal beam parameters but the plot demonstrates that the FF is clearly adaptable to any reasonable set of beam parameters. To meet the two extremes of spot-size criteria considered here, β^* at the target must be continuously tunable by a factor of 21 between its minimum and maximum values. The corresponding quadrupole gradients are listed in **Table 2-2.** The advantages of a modular optics design are evident – variations in the extracted MI beam parameters can be accommodated solely within the FF and do not involve tuning adjustments elsewhere in the line.

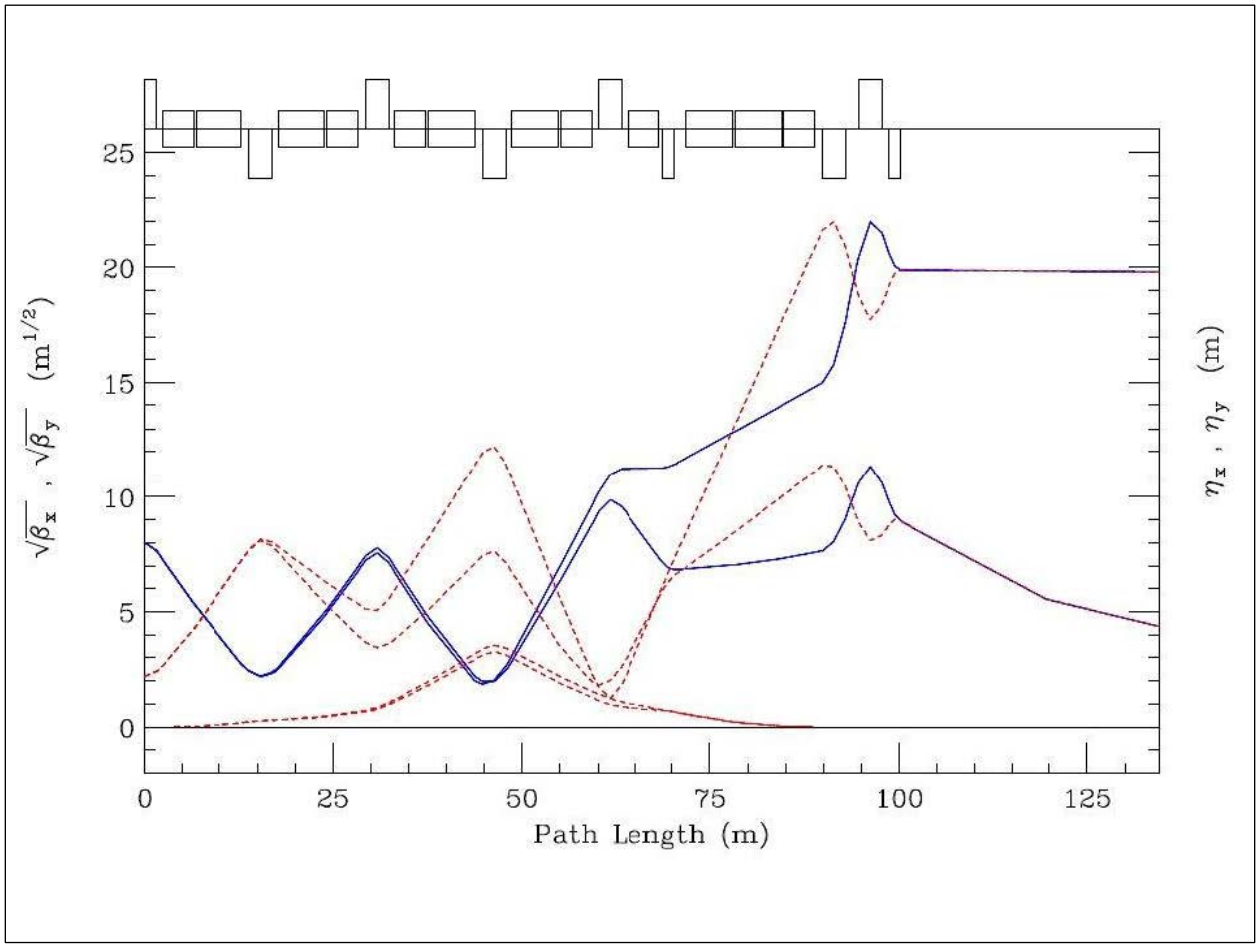

Figure 2-6: Tuning Range of the Final Focus. The two examples assume nominal MI beam parameters. These extremes correspond to 60 GeV/c with σ* = 1.0 mm; β* = 19.184 m and βmax = 104 m (lower), and at 120 GeV/c and σ* = 3.20 mm; β* = 393 m and βmax = 483 m (upper). Vertical dispersion, shown across the bottom, rises from zero at the entrance to the dipole string, reaches a maximum of $\eta_y \approx 3$ m, and is completely corrected to (η_y, η_y') = (0,0) by the end of the bends.

Table 2-2: Final Focus gradients for the examples in Figure 2-6

			σ = 1.00mm @ 60 GeV/c β* = 19.184 m	σ = 3.20mm @ 120 GeV/c β* = 392.89 m
QUAD	TYPE	L (m)	G (T/m)	G (T/m)
Q213	3Q120	3.048	−6.97624	−12.01223
Q214	3Q120	3.048	+8.40581	+17.38185
Q215	3Q120	3.048	−7.64787	−14.48899
Q216	3Q120	3.048	+7.03514	+7.68385
Q217	3Q60	1.524	−8.56034	−3.99561
Q219	3Q120	3.048	−6.66201	−11.74485
Q220	3Q120	3.048	+10.76572	+15.68461
Q221	3Q60	1.524	−10.11021	−12.62987

2.4.2.2 Beam Loss and Transport

As shown in section 2.4.3.1, a 360π mm·mrad (100%, normalized) emittance with 28.0×10^{-4} (100%) momentum spread can be transmitted cleanly through the beamline. This corresponds to the Main Injector admittance at transition. This admittance, in turn, is determined by the aperture of the Lambertson magnets as seen by the circulating MI beam. Thus, the Main Injector acts as a collimator for the LBNF primary beam.

Although a rigorous argument can be made that the beamline will accept anything the Main Injector can send, an additional study was performed. The front end of the extraction was modeled in MARS to allow a ray-tracing study. In the study, the boundary of a 360π mm·mrad phase space was populated in both horizontal and vertical planes (see **Figure 2-7**). 10,000 rays were tracked through the front end. No tracks were lost on any aperture. Details of this study can be found in lbne-doc-8420.

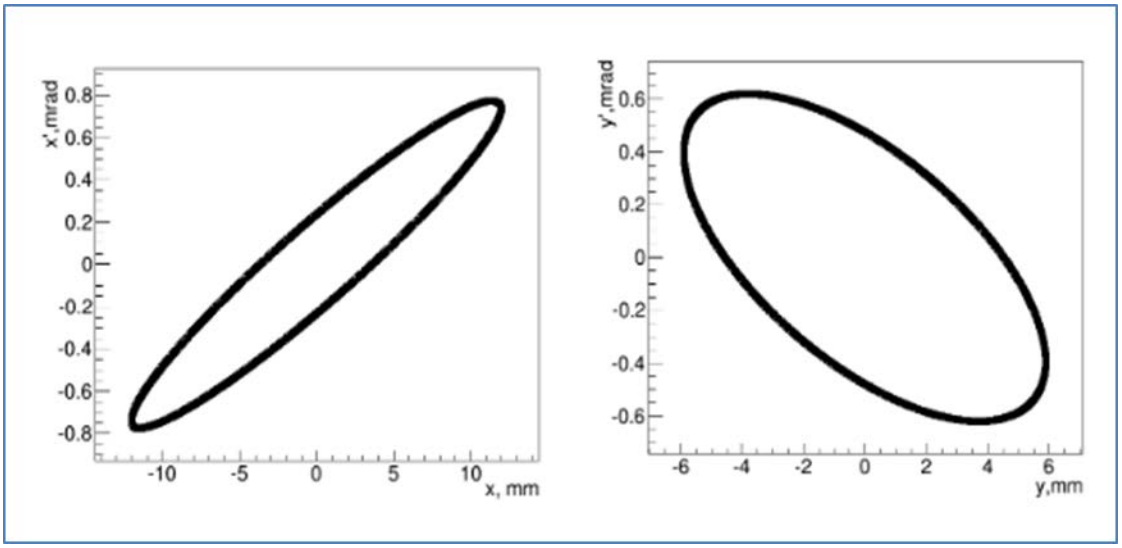

Figure 2-7: Phase Space Used in Front End Study (From lbne-doc-8420.)

2.4.2 Trajectory Correction

Trajectory correction is an issue which, of course, must be addressed in the design of any transfer line, but for the ultra-clean transport requirements of LBNE it is critical that precise position control be available throughout the primary beamline.

Correction of central trajectory errors have been simulated for dipole field errors and random misalignments assigned to all beamline elements (including BPMs). Realistic error values are on the order of $\sigma(\Delta x,\Delta y)$ = 0.25 mm, and $\sigma(\psi_{roll})$ = 0.50 mrad. **Figure** 2-8 shows the trajectory deviations resulting from randomly generated Gaussian error distributions (dashed). After correction using the LBNE trim dipoles the new orbits are also shown (solid), emphasizing the dramatic reduction in offset errors. Results of the tracking are summarized in **Table 2-3**. All corrector strengths are well within the 225 μrad (60% of peak) design specification for the new IDS trims. That orbit deviations are approximately twice as large in the vertical plane reflects the fact that dipole bending is predominantly vertical throughout the line. Dipole angular errors generated by $\Delta B/B = 10^{-3}$ are as significant as the contributions from quadrupole misalignment.

Beam position on the target is accurate to a few microns – far below the 150-μm tolerance set by horn focusing. The worst angular error found is ~0.7 μrad which, 1,300 km away at the Far Detector, translates into ~3 ft of position error, which is clearly negligible.

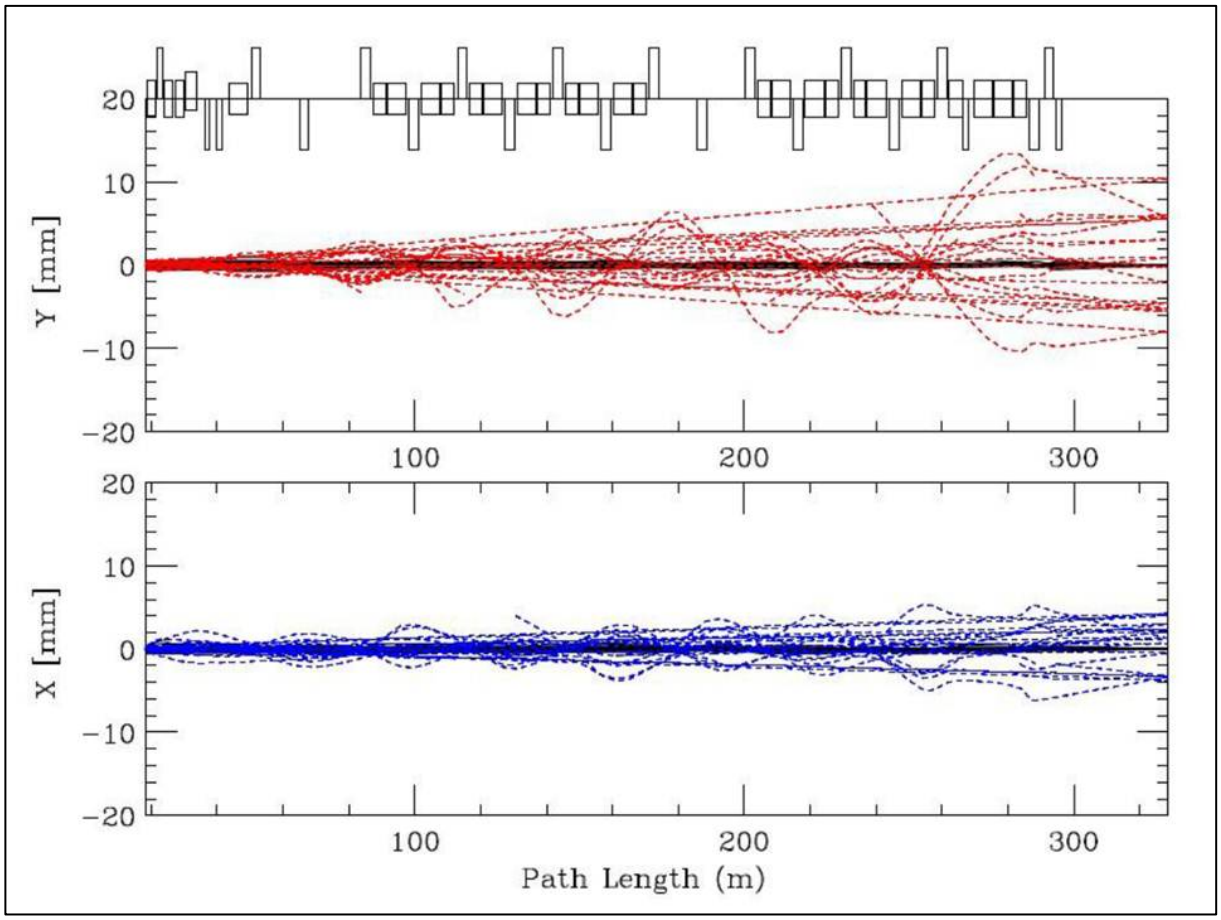

Figure 2-8: Uncorrected/Corrected Trajectories with Random Misalignments and Dipole Field Errors. The plot begins at the upstream end of the first extraction Lambertson at MI-Q102.

Table 2-3: Orbit Offsets and Corrector Kicks for the Trajectories in Figure 2-8

	ORBIT (mm)		CORRECTORS (μr)		ORBIT (mm)		CORRECTORS (μr)	
	X_{max}	X_{RMS}	θ_{max}	θ_{RMS}	Y_{max}	Y_{RMS}	φ_{max}	φ_{RMS}
UNCORRECTED	6.200	1.614	–	–	14.732	3.414	–	–
CORRECTED	0.996	0.285	110.670	26.653	1.101	0.281	114.430	37.901
	BEAM JITTER ON TARGET							
	X (μm)		X' (μr)		Y (μm)		Y' (μr)	
	X_{max}	X_{RMS}	X'_{max}	X'_{RMS}	Y_{max}	Y_{RMS}	Y'_{max}	Y'_{RMS}
CORRECTED	1.079	0.400	0.694	0.230	0.437	0.139	0.330	0.110

2.5 Magnets (WBS 130.02.02.02)

2.5.1 Introduction

This section discusses the magnets that will be used in the primary beamline to steer and focus the beam. The set of magnets includes six extraction kickers, three Lambertson magnets, one current septum C-magnet (the first magnet that is external to the MI ring), 25 main dipole magnets, 21 quadrupole magnets and 23 dipole corrector magnets for fine-tuning. From the extraction point, the lattice optics have to transport the primary beam to the target with the highest possible intensity. The magnet counts are summarized in **Table 2-4**.

2.5.2 Design Considerations

Table 2-4: Summary of Primary-beam Magnet Specifications

Magnet	Common Name	Steel Length	Nom. Strength at 120 GeV	Count
RKB Kicker	NOvA extraction	1.720 m	0.0237 T	6
ILA	MI Lambertson	2.800 m	0.532 / 1.000 T	3
ICA	MI C Magnet	3.353 m	1.003 T	1
IDA/IDB	MI Dipole 6 m	6.100 m	1.003 - 1.604 T	13
IDC/IDD	MI Dipole 4 m	4.067 m	1.003 - 1.604 T	12

Magnet	Common Name	Steel Length	Nom. Strength at 120 GeV	Count
QQB	3Q120 quadrupole	3.048 m	9.189 - 16.546 T/m	17
QQC	3Q60 quadrupole	1.524 m	11.135 - 17.082 T/m	4
IDS	LBNF trim dipoles	0.305 m	Up to 0.365 T	23

There are two technical considerations for the beamline magnets beyond providing the integrated dipole field and quadrupole gradient to establish the design lattice. First, the magnet apertures must be large enough to allow for an upgrade of beam power to 2.4 MW and alignment of the magnets should be sufficiently precise so as to not require any further enlargement due to the relative placement of the apertures. Secondly, the magnets must support rapid ramping of excitation. Beam only passes through the magnets for 10 μs of spill time out of each approximately 1 s beam acceleration cycle, so the current between spills can be turned down to save power. This reduces the cost of the magnets (by reducing the amount of conductor needed), the cost of the power supplies, and the cost of the cooling systems, though the ramping does impose additional requirements. The rates at which the magnets can be ramped affect the average power consumption, which, in turn, affects the heat load and operating cost of the beamline.

The intention is to make use of existing magnets and designs as much as possible for both cost containment and a general commitment to recycling. For each magnet function, the existing uncommitted magnets available at Fermilab and elsewhere have been reviewed. Suitable candidates have been identified for the Lambertsons, C-magnet, QQB and QQC quadrupoles; they will be refurbished or rebuilt as needed for use in the primary beamline. Existing designs to which additional magnets can be built will be used without any design changes except to the mechanical-support system. The main dipoles and quadrupoles fall into this category. The trim dipole magnets will be constructed according to a new design based heavily on current magnets. The kickers will be a minor modification to existing NOvA kicker design. Existing tooling will be used to the extent possible for all magnets.

2.5.3 Reference Design

2.5.3.1 Main Dipole Magnets

The dipole magnets are responsible for directing the primary beam to the target. As the biggest magnets in the beamline, they must be reliable and energy-efficient. They must also provide sufficient strength and aperture to cleanly transport the beam at any energy in the range of 60–120 GeV.

The same type of magnets as used for the MI dipoles are the logical choice for this function, in particular a combination of the 6-m IDA magnet and the 4-m IDD magnet designs. They have performed successfully since the MI's commissioning in 1998. The LBNF magnets will be newly constructed to the existing designs, as mentioned above. The basic properties of these magnets are listed in **Table 2-5** and **Table 2-6**. The magnet cross section is shown in **Figure 2-9** and the layout of an IDA/IDB pair of dipoles, as used in the MI, is shown in **Figure 2-10.** An IDA/IDD pair has the same interconnection.

The MI dipoles are slightly curved to match the path of the bending particles. The sagitta (the distance between that curve and a straight line) in the 6-m dipoles is about 16 mm.

The beam-tube cross section used in the MI dipoles is shown in **Figure 2-11**. The beam-tube cross section is oval, wider in the magnet's horizontal dimension, to accommodate the width of the beam due to protons of(slightly) different momenta bending differently in the magnetic field. (Note that the magnets may be oriented at different angles depending on their locations in the beamline, so "magnet's horizontal" may not necessarily mean horizontal in an absolute sense. "Width" refers to the bending direction, perpendicular to the gap dimension between the poles.) Under vacuum, the beam tube's smaller dimension decreases to enough under 2.000 inches to allow its insertion into a magnet aperture and then to allow bending to match the beam sagitta. The MI tubes were cold-drawn through successive dies to produce the required shape. LBNF plans to take the less costly approach, employed in the Fermilab Recycler, of squashing round tubes to a roughly oval shape. The initial tube size will be selected based on aperture requirements. For example, a squashed 3-in (76 mm) outside diameter (OD) tube would yield an aperture width of about ±47 mm and a 3.5-in OD tube would yield a width of about ±58 mm.

Table 2-5: Properties of IDA Dipoles

Property	Value
Steel length	6.100 m
Magnetic field (nominal at 120 GeV)	1.003 to 1.604 T
Integrated field (nominal at 120 GeV)	6.76 to 10.03 T-m
Gap	50.80 mm
Number of turns	8
Aperture height (with beam tube)	47 mm
Aperture width (with beam tube)	120 mm
Current (nominal at 120 GeV)	5106 to 8748 A
Resistance (at 20°C)	0.8 mΩ
Inductance (at 100 Hz)	2.0 mH
Power dissipation (max, I_{rms} = 0.5 Imax)	16.4 kW
Water flow (at 100 psid)	0.93 l/s
Temperature rise (max at 100 psid)	4.2^{o}C
Weight	18,180 kg
Fermilab drawing numbers	5520-ME-274896, 5520-ME-274897
Color	Light blue

Table 2-6: Properties of IDD Dipoles

Property	Value
Steel length	4.065 m
Magnetic field (nominal at 120 GeV)	1.003 to 1.604 T
Integrated field (nominal at 120 GeV)	4.51 to 6.68 T-m
Gap	50.80 mm
Number of turns	8

Property	Value
Aperture height (with beam tube)	47 mm
Aperture width (with beam tube)	120 mm
Current (nominal at 120 GeV)	5108 to 8748 A
Resistance (at 20°C)	0.52 mΩ
Inductance (at 100 Hz)	1.3 mH
Power dissipation (max, Irms = 0.5 Imax)	10.6 kW
Water flow (at 100 psid)	1.10 l/s
Temperature rise (max at 100 psid)	2.3^{o}C
Weight	12,300 kg
Fermilab drawing numbers	5520-ME-274910
Color	Light blue

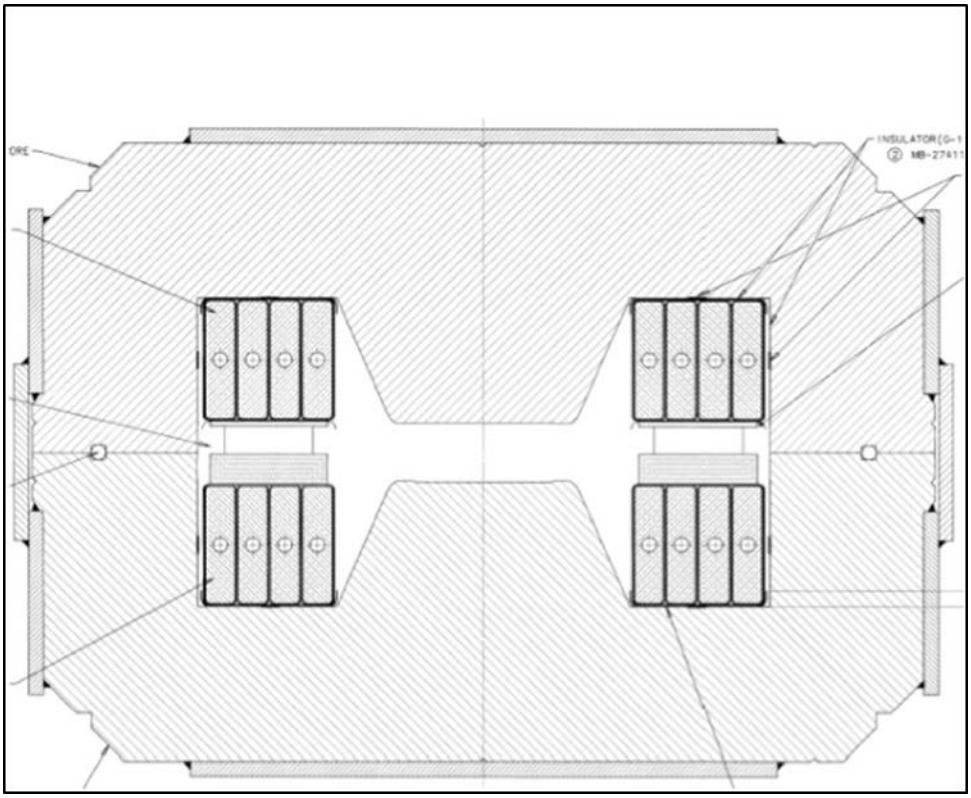

Figure 2-9: MI Dipole Cross Section

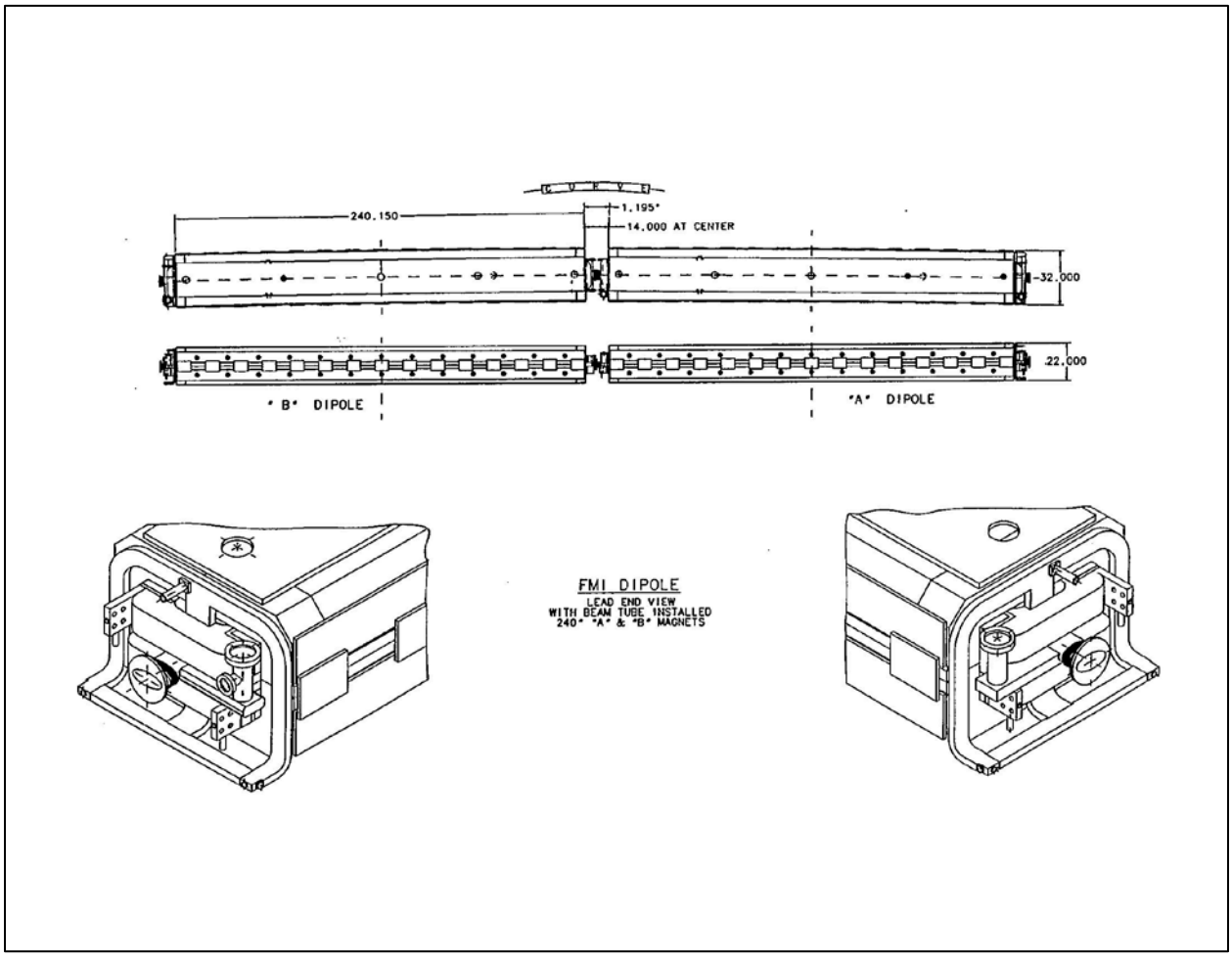

Figure 2-10: Layout of one IDA and one IDB Dipole in a Half Cell

The excitation curve of a typical IDA magnet, in Tesla-meters versus Amperes, measured during production is shown in **Figure 2-12**. The integrated strength of IDD dipoles was measured to be 2/3 the strength of IDA dipoles to better than 0.1%.

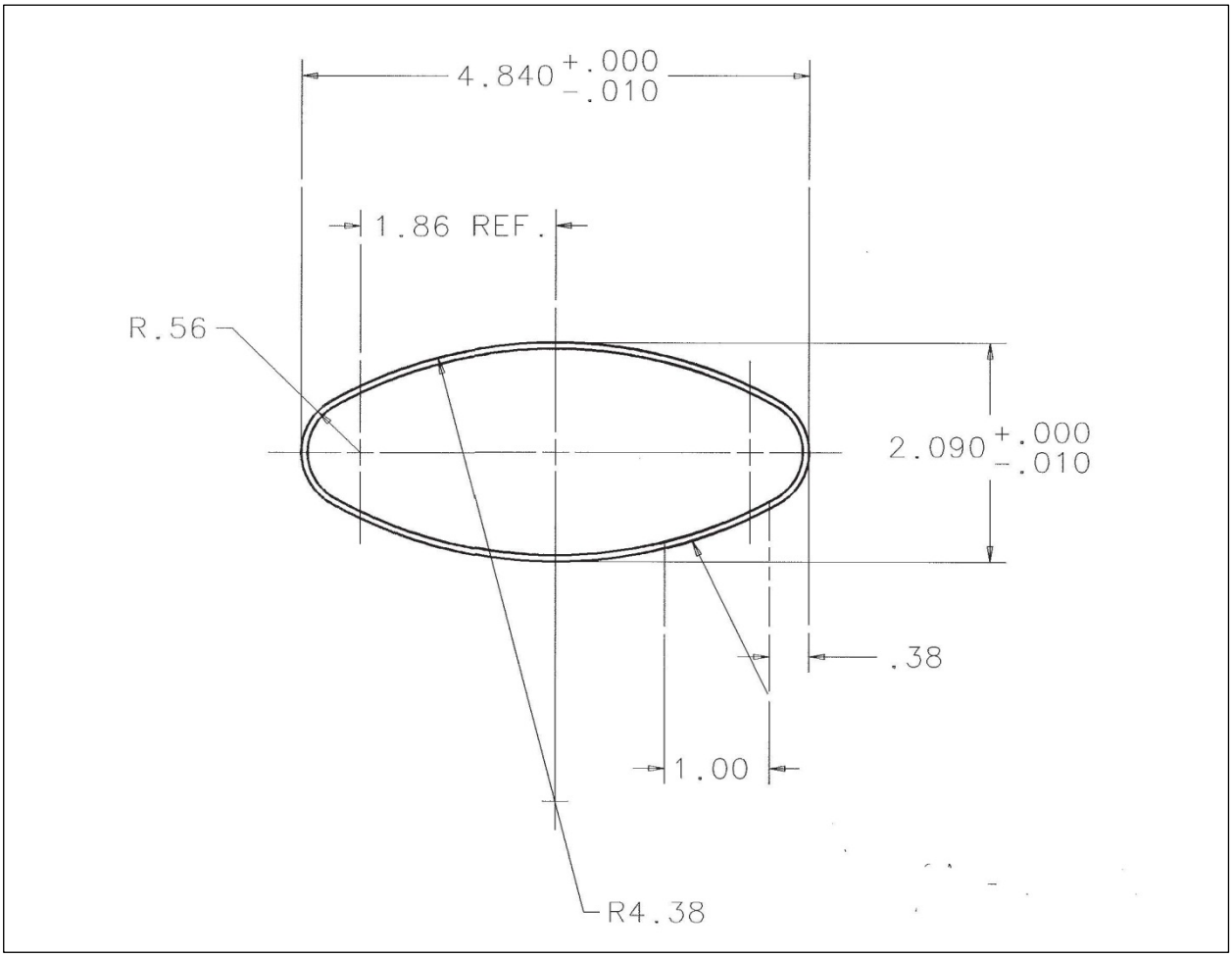

Figure 2-11: Beam Tube Cross Section

The dipole magnets have four terminals, significantly reducing the length of inter-magnet bus work in the main arc; see the center portion of the top image in **Figure 2-10**. Each length of magnet (6 m and 4 m) comes in two variants that differ only in the placement of the through-bus in the magnet and in the end of the magnet that has the more complicated bus and manifolding. The 6-m magnet variants are designated IDA and IDB; the 4-m magnet variants are designated IDC and IDD. In the MI, one IDA and one IDB (or one IDC and one IDD) magnets are compactly placed back-to-back, with their yokes approximately 0.35 m apart, leaving just enough room for the electrical jumpers between magnets and an ion vacuum pump where the beam tubes are welded together. An IDA can be just as well mated with an IDD. This pairing of a 6-m magnet with a 4-m magnet prevails in the LBNF primary beamline. The water connections and the power connections for the bus around the quadrupoles are made at the outside ends of the pair of magnets.

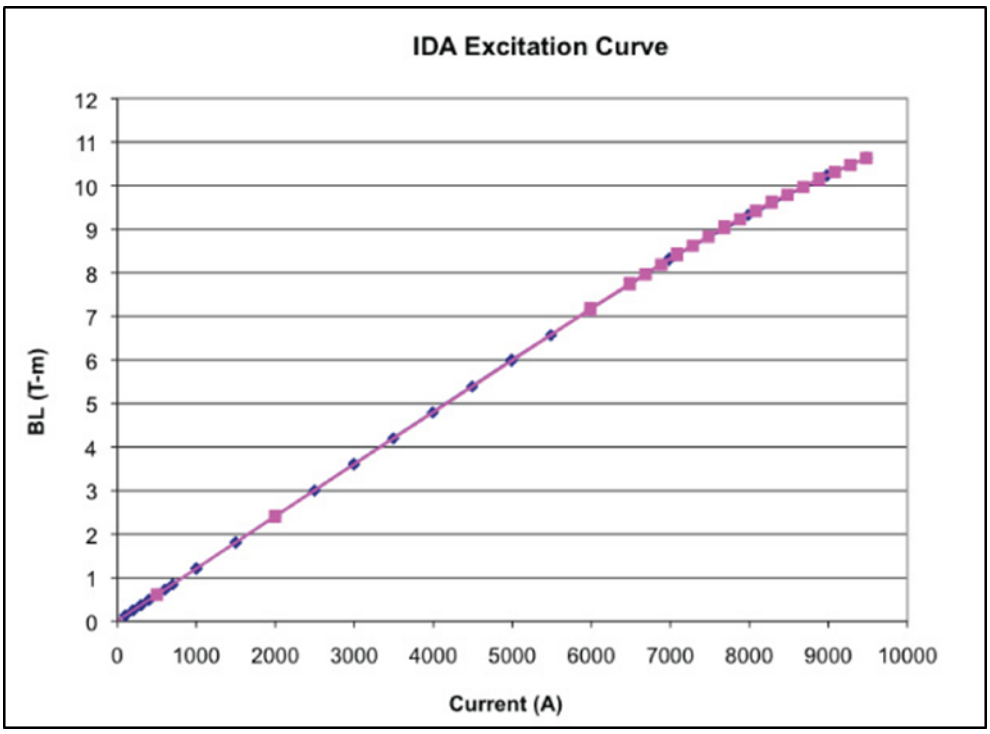

Figure 2-12: Typical IDA Excitation Curve

LBNF plans to follow the procurement strategy used during construction of the MI, developed to minimize the cost and maximize the magnet quality while making extensive use of outside vendors. The major components and subassemblies were fabricated in industry, with all contracts build-to-print (except the steel, which was based on performance) and awarded through a mix of straight bids and a source evaluation board. The cores, coils and beam tubes were assembled into complete magnets at Fermilab. This approach allows Fermilab to control the critical steps in the magnet fabrication and to assume the responsibility for the final performance with confidence, rather than trusting the vendors and paying for the vendors' potential liabilities. By taking ownership of the LBNF components, Fermilab will readily be able to make thorough inspections of the components before assembly and ensure that the final magnets meet the needs of the project.

For the MI, Fermilab purchased the coils of coated sheet steel, as that is a critical component whose magnetic properties need close control. Fermilab contracted for the stamping of the steel into laminations for the core and exercised tight oversight and monitoring of the critical lamination dimensions. Fermilab contracted with a fabrication shop to build the magnet half cores using Fermilab-provided stacking equipment, with Fermilab specifying which boxes of laminations were used in each half core based on steel and lamination data. Fermilab contracted with two specialized vendors to produce the coils, one to fabricate the bare coils and another to insulate them, though for LBNF the coil procurements may be combined. As in the Fermilab Recycler, it is expected that the beam tube will be formed from stock dimension tubes, and Fermilab welders will attach the various bellows, flanges, pump-out ports and other features.

Note: For quality control purposes, all magnets will be subjected to magnetic tests.

During operation, the circuits must be ramped between beam pulses to maintain a conservative temperature rise in the magnets and avoid overheating. It is assumed that an *RMS* current of half the peak current can be achieved.

Table 2-7: Properties of the MI Lambertson Magnets

Property	Value
Steel length	2.800 m
Magnetic field (nominal at 120 GeV)	0.532 / 1.000 T
Integrated field (nominal at 120 GeV)	1.49 / 2.80 T-m
Gap	50.80 mm
Number of turns	24
Aperture height (with beam tube)	50.80 mm
Aperture width (with beam tube)	406 mm
Current (nominal at 120 GeV)	922 - 1815 A
Resistance (at 20°C)	12.9 m □
Inductance (at 100 Hz)	3.9 mH
Power dissipation (Irms = 0.5 Imax)	11.3 kW
Water flow (at 100 psid)	0.96 l/s
Temperature rise (at 100 psid)	2.8^{o}C
Weight	23,500 lb
Fermilab drawing number	5520-ME-331492
Color	Silver

2.5.3.2 Main Injector Lambertson Magnets

LBNF will use three existing MI Lambertson magnets (ILA) for extraction from the MI and injection into the LBNF primary beamline. The magnets were built by Fermilab staff for the MI and NuMI projects. Due to the decommissioning of the Tevatron, a suitable pool of spares will become available, including the four ILA magnets in the Tevatron injection system. They will be inspected, with particular attention to the high-voltage insulation and the water circuits, and refurbished as necessary in preparation for long-term service in the LBNF primary beamline. The basic properties of the Lambertson magnets are listed in **Table 2-7** and a sketch of the magnet is shown in **Figure 2-13**. A typical ILA excitation curve is shown in **Figure 2-14.**

To minimize the thickness of the septum between the hole for the circulating beam and the aperture for the extracted beam, no beam tube is used. Rather, vacuum in the aperture is maintained by a stainless-steel skin that encases the inner core. The large surface area of the laminations inside the evacuable volume necessitates an in situ bake after installation, using the attached electrical heating elements.

To maintain a conservative temperature rise in the magnet and to minimize the impact of any leakage field on the low-energy injected beam, the magnets will be ramped. It is assumed that an *RMS* current of half the peak current can be achieved.

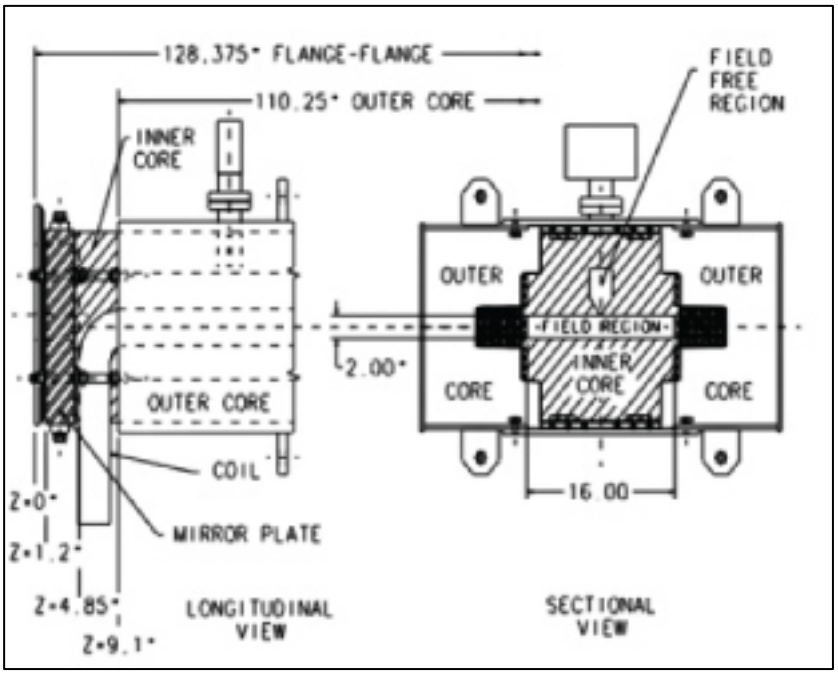

Figure 2-13: MI Lambertson Magnet End and Cross Section

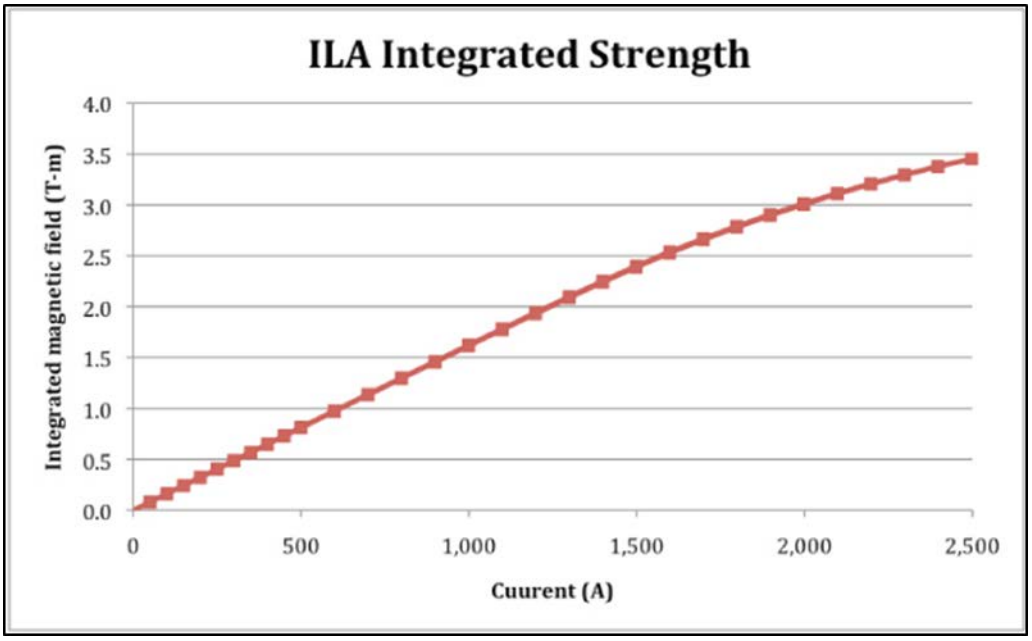

Figure 2-14: Excitation Curve of a MI Lambertson Magnet

Table 2-8: ICA Main Injector C-Magnet Properties

Property	Value
Steel length	3.353 m
Magnetic field (nominal at 120 GeV)	1.003 T
Integrated field (nominal at 120 GeV)	3.36 T-m
Gap	40.61 mm
Number of turns	12
Aperture height (with beam tube)	37.5 mm
Aperture width (with beam tube)	98.3 mm
Current (nominal at 120 GeV)	2679 A
Resistance (at 20°C)	2.11 m □
Inductance (at 100 Hz)	14 mH
Power dissipation (Irms = 0.5 Imax)	12.6 kW
Water flow (at 100 psid)	0.57 l/s
Temperature rise (at 100 psid)	5.3^{o}C
Weight	8,500 lbs
Color	Light blue

2.5.3.3 Main Injector C-Magnets

As at the other high-energy extraction points in the MI, the Lambertson magnets are followed by a current septum C-magnet. The MI C-Magnet, the ICA, was based on the F17 C-Magnet design for the Tevatron I project. Several C-magnets were used in the A150 anti-proton beamline from the MI to the Tevatron and will be available for use in the LBNF beamline. The basic properties of these magnets are listed in **Table 2-8**, and a sketch of the magnet is shown in **Figure 2-15**. The beam tube cross section is shown in Figure 2-16. The excitation curve of a typical ICA magnet is shown in **Figure 2-17.**

In preparation for use in LBNF, the C-magnets will be inspected, and refurbished as necessary, with particular attention to the high-voltage insulation and the water circuits. To maintain a viable temperature rise and avoid overheating, the magnets must be ramped between beam pulses. It is assumed that an *RMS* current of half the peak current can be achieved.

2.5.3.4 Quadrupole Magnets

The LBNF primary beam will be focused with 3Q120 and 3Q60 quadrupole magnets of the specific styles QQB and QQC. These styles of quadrupoles are reliable, compact, energy-efficient and suitably strong. The basic properties of the magnets are listed in **Table 2-9** and **Table 2-10**. The magnet cross section is shown in **Figure 2-18** and the excitation curves are shown is **Figure 2-19** and **Figure 2-20**. The beam tube is round, with a 71.9-mm (2.82-in) minimum inner diameter.

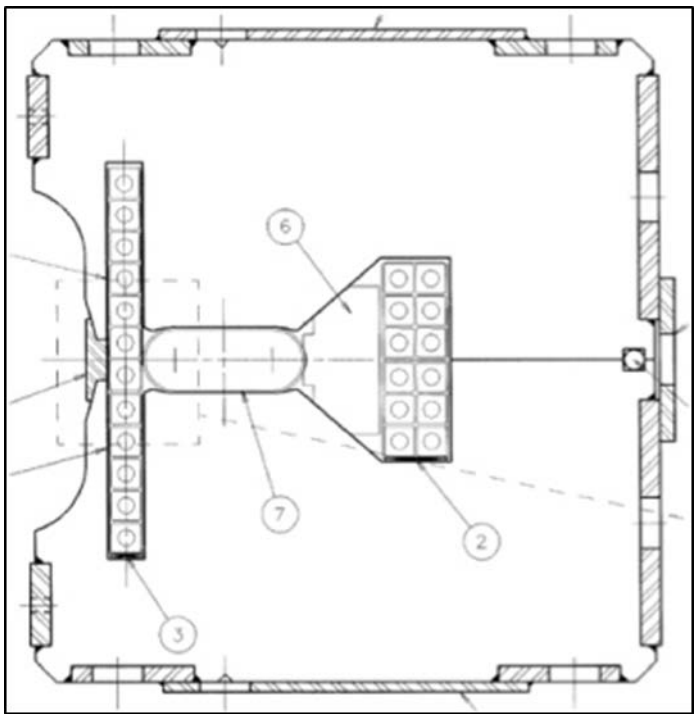

Figure 2-15: ICA MI C Magnet

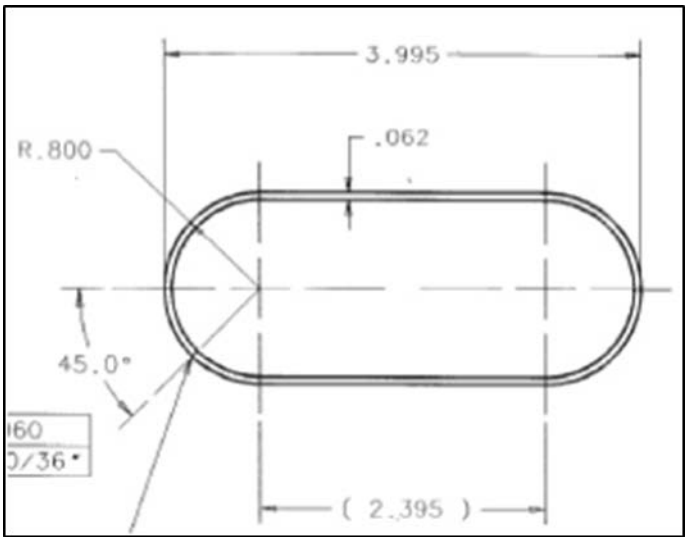

Figure 2-16: ICA Beam Tube Shown in Horizontal Bending Orientation

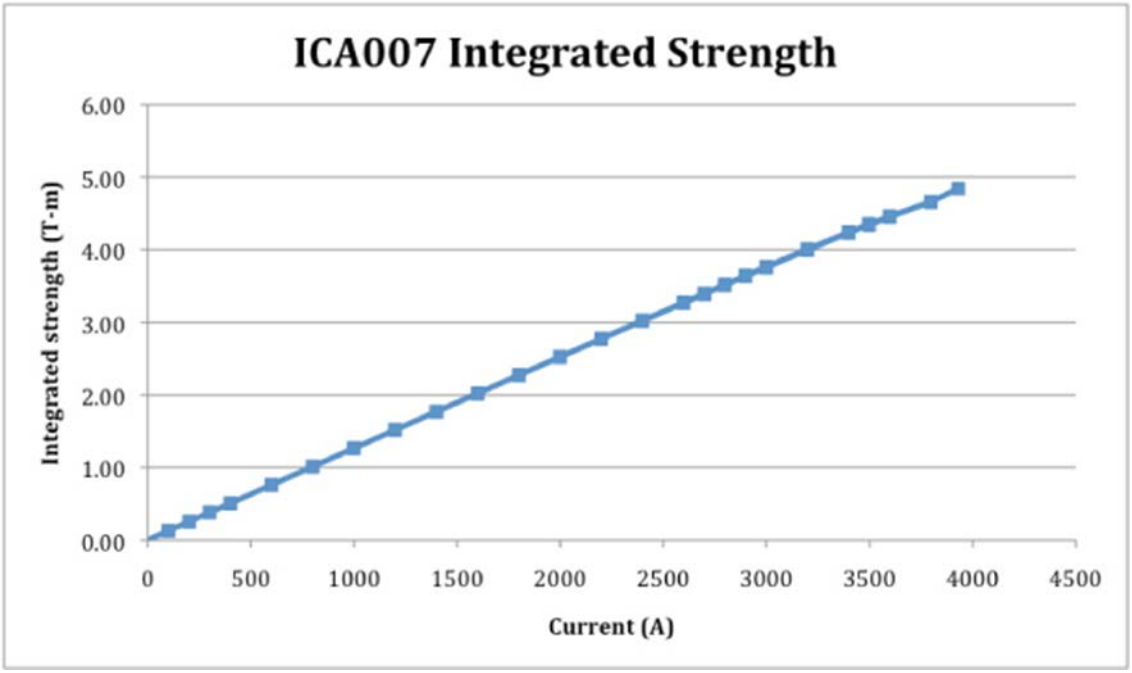

Figure 2-17ICA integrated Strength as a Function of Current

The 3-m QQB magnets are the main focusing quadrupoles of the primary beamline. Shorter QQC quadrupoles are used at four locations because of spacing. At the upstream end of the beamline, just following the C-magnet, the functionality of a single 3-m quadrupole is implemented with two 1.5-m quadrupoles; this avoids interference with a quadrupole in the MI ring. At the other end of the line, two of the five quadrupoles in the final focus are sufficiently weak to suggest a shorter magnet. The basic design of the 3Q120 and 3Q60 dates from the 1970s, when they were first used extensively in the external beamlines of the Fermilab fixed-target program. They are still commonly used, although the yoke and coil configuration have evolved over the years. The QQB and QQC magnets have a slightly larger yoke than the earliest versions (15 in x 17 in rather than 13 in x 17 in), providing more mechanical stability. They also use hollow, water-cooled coils, which allow a higher current density than the original indirectly cooled, solid-conductor models. The water manifolds will be of the same style as designed for the MI. The coil will be vacuum-impregnated in the core.

For quality-control purposes all magnets will be subjected to magnetic measurements.

The circuits will be ramped between beam pulses to maintain a conservative temperature rise in the magnets. It is assumed that an *RMS* current of 53% of the peak current can be achieved.

Table 2-9: QQB: Hollow Conductor 3Q120 Properties

Property	Value
Steel length	3.048 m
Magnetic gradient (nominal at 120 GeV)	9.189 to 16.546 T/m
Integrated gradient (nominal at 120 GeV)	28.01 to 50.43 T-m/m
Pole diameter	76.02 mm

Property	Value
Number of turns	28 per pole
Aperture (with round beam tube)	72 mm
Current (nominal at 120 GeV)	192 to 353 A
Resistance (at 20°C)	156 m □
Inductance (at 100 Hz)	82 mH
Power dissipation (Irms = 0.533 Imax)	5.9 kW
Water flow (at 100 psid)	0.35 l/s
Temperature rise (at 100 psid)	4.0°C
Weight	7,400 lbs
Color	Orange

Table 2-10: QQC: Quadrupole Magnet Properties

Property	Value
Steel length	3.048 m
Magnetic gradient (nominal at 120 GeV)	13.39 to 17.08 T/m
Integrated gradient (nominal at 120 GeV)	20.41 to 26.03 T-m/m
Pole diameter	76.02 mm
Number of turns	28 per pole
Aperture (with round beam tube)	72 mm
Current (nominal at 120 GeV)	233 to 369 A
Resistance (at 20°C)	156 m □
Inductance (at 100 Hz)	82 mH
Power dissipation (Irms = 0.533 Imax)	4.4 kW
Water flow (at 100 psid)	0.35 l/s
Temperature rise (at 100 psid)	2.1°C
Weight	7,400 lbs
Color	Orange

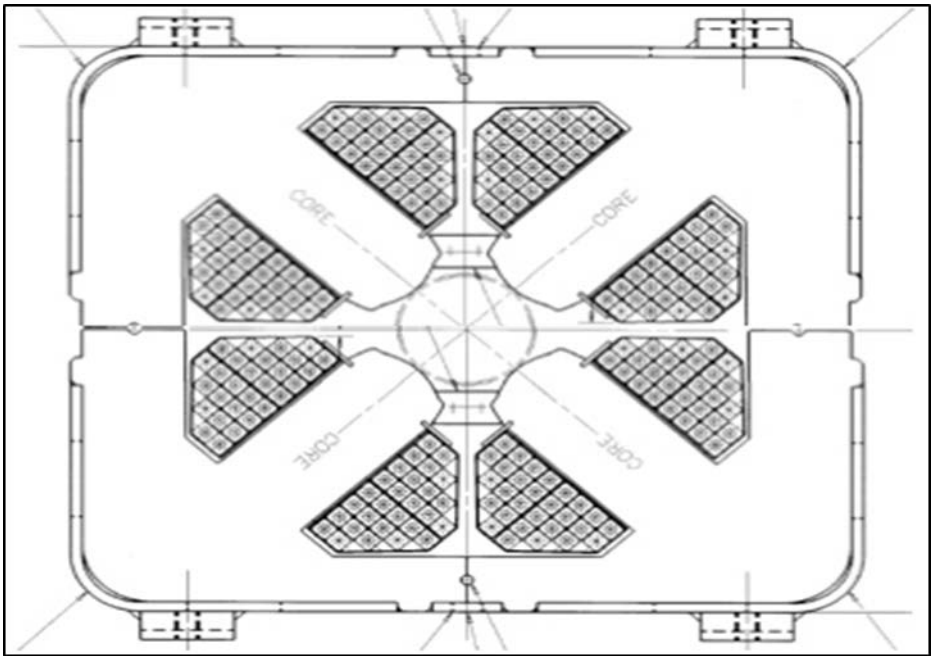

Figure 2-18: Cross-section of QQB and QQC Quadrupoles

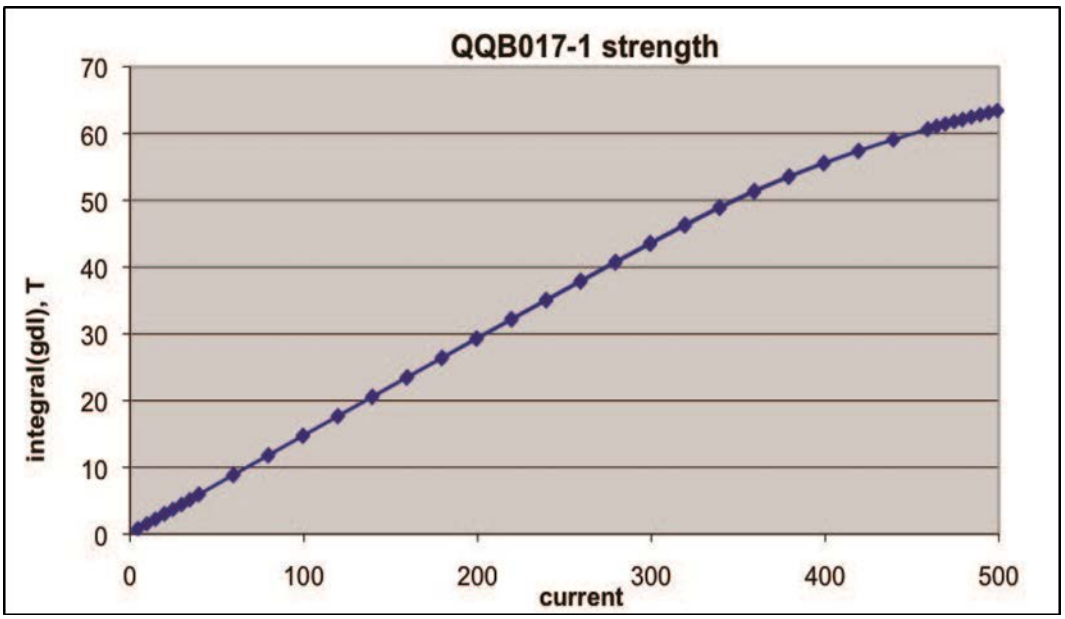

Figure 2-19: Typical QQB Excitation Curve

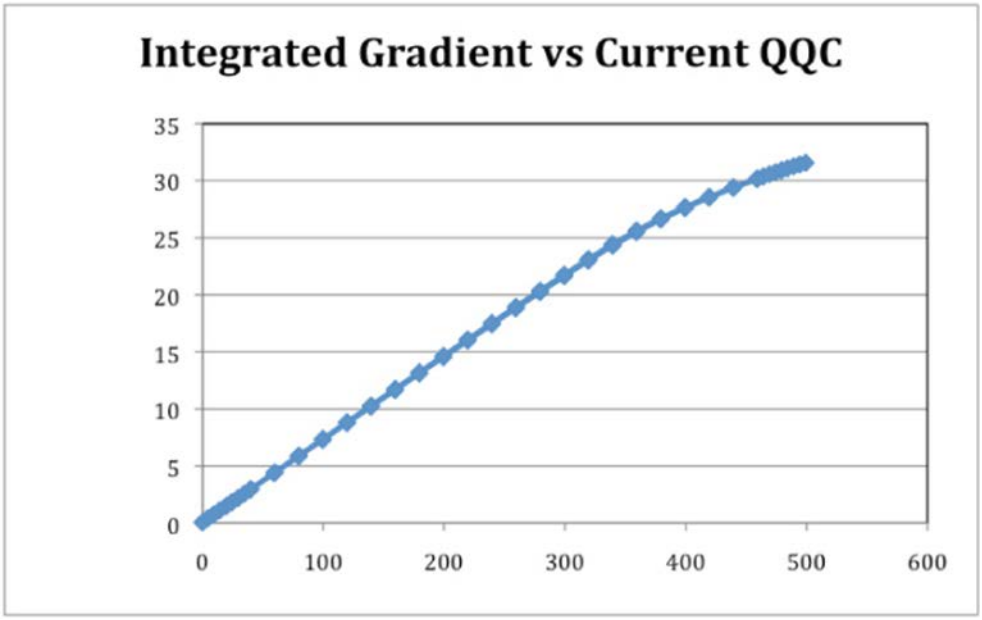

Figure 2-20: Typical QQC Excitation Curve

2.5.3.5 Corrector Magnets

A trim dipole (fine-tuning) magnet, called an IDS, is located at every focusing location. One of these locations has two quadrupoles functioning as one element and two locations are sufficiently sensitive to require steering in both planes, so the trim magnet count does not exactly match the quadrupole count.

This is a new design based on the IDH horizontal trim dipole correctors built for the MI and subsequently used, with modifications, in the NuMI beamline. To allow operation over a wider range of excitations without overheating, the conductor size will be increased from 10-gauge square copper to 8-gauge square copper. To maintain better linearity over the extended operating range, the back leg thickness will be increased.

The corrector magnets have the same pole width at the MI horizontal correctors, but a gap increased from 50.8 mm to 76.2 mm gap to accommodate a round beam tube matching the quadrupole aperture at any rotational angle around the beam. MI correctors with an increased gap are used in the NuMI beam. In NuMI, the increased current needed to reach the desired field strengths required attaching indirect water cooling channels to the core. In the MI, the linear range of the excitation curve has been successfully extended by strapping extra steel plates onto a few magnets to increase the flux return path. Because the water-cooling and added steel plates are cumbersome and labor-intensive to install, it was decided to address both of these issues with a new design. The basic properties of the magnets are listed **Table 2-11** and a conceptual drawing of a trim dipole is shown in **Figure 2-21** Initial design work has been done assuming both a 50.8 mm to 76.2 mm gap, adjustable with back leg spacers. **Figure 2-21** reflects the 76.2 mm configuration.

The measured excitation curve of a MI trim dipole magnet with the increased gap used in NuMi is shown in **Figure 2-22**. Since the pole shape, length, and number of turns in the coil are the same, and the yoke is comparable, this closely matches the expected performance of the LBNF IDS.

Table 2-11: LBNF Trim Dipole Properties (IDS)

Property	Value
Steel length	0.305 m
Magnetic field (maximum peak)	0.365 T
Integrated field (maximum peak)	0.150 T-m
Pole gap	76.2 mm
Number of turns	812
Aperture height (with beam tube)	72 mm
Aperture width (with beam tube)	120 mm
Current (maximum peak)	30 A
Resistance (at 20°C)	~1.4 Ohm
Inductance (at 100 Hz)	1.1 H
Power dissipation (maximum)	315 W
Cooling	Air cooled
Temperature rise (internal)	32 C
Weight	< 500 kg
Color	To be determined

To maintain a conservative temperature rise in the magnets during operation, the stronger circuits must be ramped between beam pulses. It is assumed that an *RMS* current of half the peak current can be achieved. Because heat dissipation is a primary motivation of the new design, the thermal performance has been modeled in detail. To validate the modeling, a prototype magnet will be subjected to extensive thermal tests. The prototype will also be thoroughly measured magnetically to ensure conformance with the design requirements, as will at least a quarter of the production magnets, for quality assurance purposes.

2.5.3.6 Kicker Magnets

To extract the beam at the MI-10 straight section, a six-kicker-magnet system is needed. This system uses more and shorter kicker elements than the 3 2.2 m-long NuMI kicker system. The decision to use shorter kickers is dominated by the available NOvA ceramic tubes. These magnets will be similar to the recently built RTV-potted NOvA extraction kickers (“RKB” type). **Table 2-12** summarizes the parameters of these kickers.

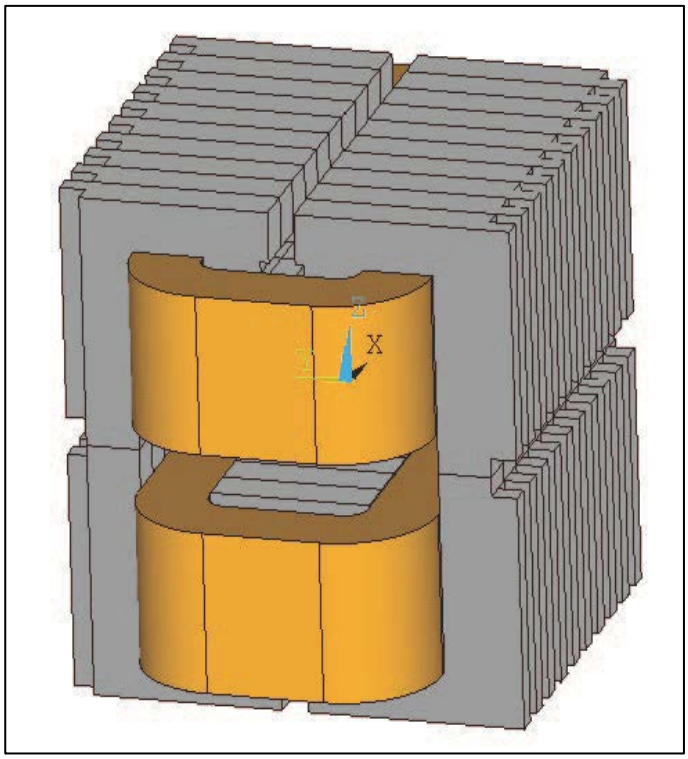

Figure 2-21: Schematic of LBNF 3-in (76.2-mm) Aperture Gap Trim Dipole (IDS)

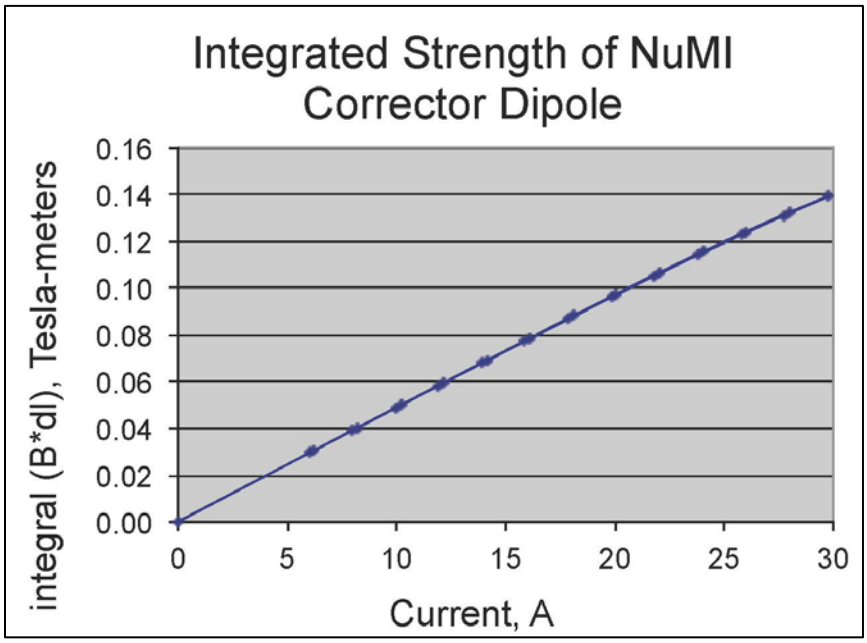

Figure 2-22: Integrated Strength of NuMI Dipole Corrector

Table 2-12: Specifications of the LBNF Extraction Kicker Magnet System

Property	Value
Length (Physical beamline space)	10.58 m
Integrated gradient (maximum peak)	0.491 T-m
Number of turns	1
Aperture height	38 mm
Aperture width	86 mm
Current (maximum peak)	2750 A
Kick Angle (@120 GeV)	1144 □rad
Field rise time (1% to 99%)	1.64 □s
Field flattop time	9.44 □s
Power dissipation (maximum)	1600 W (800 W per magnet string/400 in the load)
Flattop stability	<1%
Cooling	Air cooled
Drawing number	N/A
Color	Silver
Number of kickers	6

2.5.3.7 Kicker Fluorinert System

A temperature-regulation system is needed for the loads of the kicker magnets to meet the stability requirement on kicker amplitude and to remove heat from the loads. A regulation of ±0.5^{o}C is needed on the fluid to meet the stability requirement. Fluorinert is used because it has good high-voltage insulation and thermal conduction, and low viscosity.

The LBNF Fluorinert recirculation system will be very similar to the one currently located in MI-10, which is used for the MI Injection kickers. It will replace that Fluorinert system, once the Mi injection kickers are removed. The current skid at MI-10 will be replaced with one similar to that being designed for the Muon Campus 30, sized for 12 gpm and only 4 kicker loads. It will terminate at the LBNF kicker loads just downstream of MI Q-100. The skid will be cooled by LCW with a temperature-control valve as if it were simply another power supply load. The skid will also have a heater for fine-tuning of the load temperature.

System schematics will be created and should include a piping and instrumentation diagram (P&ID). Piping installation drawings and specifications will be created from this, with sufficient documentation to provide for outside bidding practices. (It may be more cost-effective to use T&M labor rather than bidded contract.) Both piping and vessels will adhere to FESHM Chapter 5031, as well as the Fermilab Engineering Manual. Piping will be designed and installed in accordance with ASME B31.3 Code for Process Piping. Pressure vessels shall be designed in accordance with ASME Boiler and Pressure Vessel Code Section VIII Division 1.

Magnet Power Supplies (WBS 130.02.02.03)

Introduction

2.6

This section describes the power supply system for the magnets that comprise the lattice optics of the primary beamline. Fermilab has a long history of developing and procuring power supplies for large magnet systems and this experience will guide the design of the LBNF magnet power systems. Some magnets will be grouped and powered by a single "magnet loop" (many magnets powered with one set of supplies), the rest will be powered individually, according to the lattice optics design. The power supply system design seeks to minimize power consumption, and reuse existing supplies from the Tevatron and the NuMI beamline, whenever possible, to better manage the cost.

2.6.1

Table 2-13: Dipole (Bending) Magnet Loops

Magnet Loop Name	Number of Magnets	Power Supply Location	Power Supply Type	Power Supply Voltage	Peak Magnet Current	RMS Current	Average Power
E:LAM1	1	MI-10	500 kW	50	922	432	8,259 kW
E:LAM12	2	MI-10	500 kW	200	1,815	882	64,702 kW
E:V1001	1	MI-10	500 kW	50	2,649	1,212	16,587 kW
E:H202	1	LBNF 5	375 kW	50	7,339	3,601	24,256 kW
E:H204	2	LBNF 5	2x375 kW	100	5,878	4,640	72,473 kW
E:H206	6	LBNF 5	2x375 kW	100	5,320	3,724	72,473 kW
E:H208	4	LBNF 5	500 kW	200	5,320	2,975	35,368 kW
E:H214	12	LBNF 5	2.8 MW	420	8,510	4,406	124,735 kW

2.6.2

Design Considerations

Power consumption is a cost driver during operation, and thus a design driver. In order to maintain the low power consumption, all of the magnet currents will be ramped. Each power-supply design will be selected to provide the best balance between the voltage stresses on the magnet and average power consumption. Also, each power supply will be constructed to use the maximum voltage necessary to reach the peak current and settle into regulation before the beam is extracted from the MI.

2.6.3

Reference Design

2.6.3.1 Power-supply Loops

The primary beamline will contain a kicker supply, three extraction power-supply loops, five major bending-magnet loops, one large quadrupole loop, eleven minor quadrupole loops and a series of corrector-magnet power supplies. A simplified diagram for a power supply loop is shown in **Figure 2-23**. **Table 2-13** shows a complete listing of the dipole magnet loops, and **Table 2-14** lists the quadrupole-magnet loops and the assumed locationof the equipment. **Table 2-15** shows the corrector-magnet system, which will use "Booster-style" corrector supplies.

A kicker system, two extraction Lambertson magnet loops and a C-magnet will be placed at the beginning of the beamline. The power supplies for these magnets will need to be powered from the MI-

10 service building and will be part of the MI electrical safety system. This ensures that during access to the MI that these supplies are de-energized using the normal MI procedures. The magnets and the power supplies will be removed from the NuMI beam line extraction and installed at MI-10. The large magnet supplies will be located in the MI-10 service building and will be powered using a relocated, existing transformer from the MI pulse power feeders.

Magnets located in the LBNF Primary Beam Enclosure will be powered from the LBNF-5 Service Building.

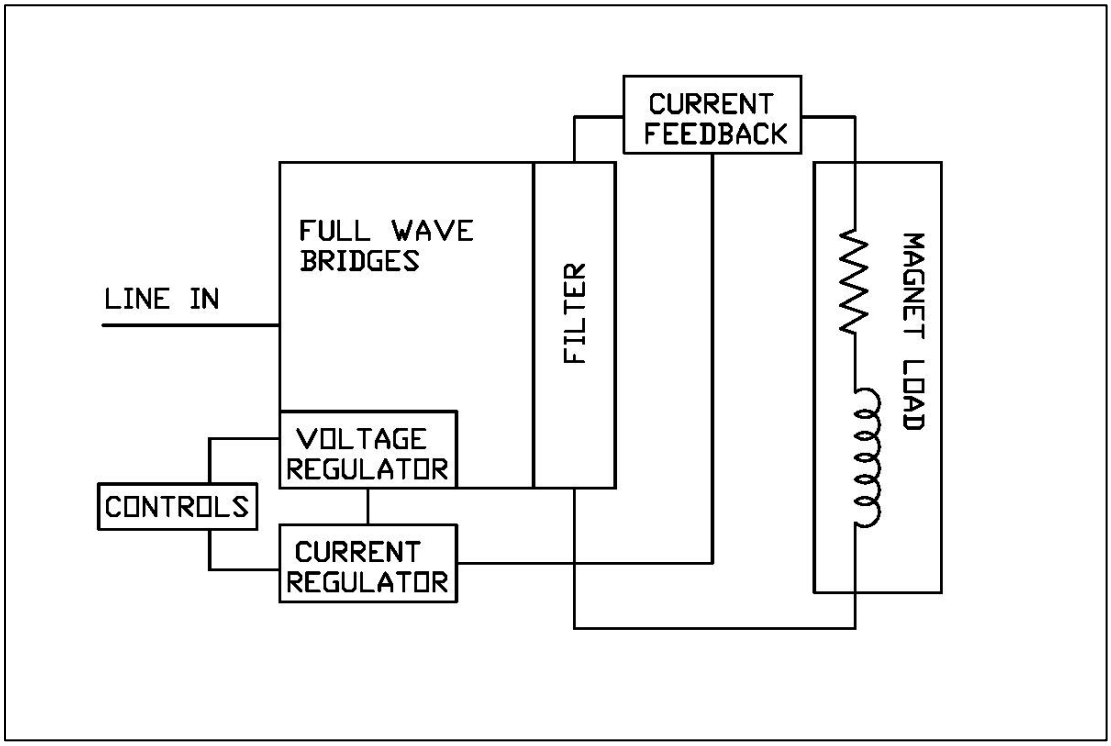

Figure 2-23: Magnet Power-Supply Block Diagram

2.6.3.2 Power Supply Topology

The ramped power supplies will be constructed using 12-pulse rectifiers with a passive filter connected to the output. Only supplies using 12-pulse rectifiers will be connected to the pulse power feeder because a tuned harmonic filter is installed on the feeder to reduce the voltage stress on the 13.8-kVAC components. The feeder will be extended to connect to the MI beamline feeder system (under the Conventional Facilities scope), which has a harmonic filter with the capacity to power the LBNF beamline. The feeder will need to be extended from MI-10 to the new LBNF-5 service building. The details of the feeder and filter construction are given in Volume 5 of this CDR. The on/off switch for the 13.8-kVAC feeder system will be controlled locally at the LBNF-5 Service Building using a motor-driven disconnect to make access to the MI and LBNF easier for the operation crews. This will allow for access into the LBNF enclosure without turning off the MI.

Table 2-14: Quadrupole Magnet Loops

Magnet Loop Name	Number of Magnets	Power Supply Location	Power Supply Type	Power Supply Voltage	Peak Magnet Current	RMS Current	RMS Power
E:Q201/2	1	MI-10	75 kW	150	234	110	2.6 kW
E:Q203	1	LBNF 5	75 kW	150	263	125	3.3 kW
E:Q204	1	LBNF-5	75 kW	150	194	96	1.9 kW
E:Q205	1	LBNF-5	75 kW	150	275	132	3.7 kW
E:Q206	1	LBNF-5	75 kW	150	285	138	4.0 kW
E:Q207	1	LBNF-5	75 kW	150	340	173	6.3 kW
E:Q208	1	LBNF-5	400 kW	800	333	190	48.5 kW
E:Q216	11	LBNF-5	75 kW	150	341	186	8.2 kW
E:Q217	1	LBNF-5	75 kW	150	283	140	4.7 kW
E:Q218	1	LBNF-5	75 kW	150	361	153	1.9 kW
E:Q219	1	LBNF-5	75 kW	150	224	178	7.5 kW
E:Q220	1	LBNF-5	75 kW	150	339	172	6.2 kW
E:Q221	1	LBNF-5	75 kW	150	288	109	1.6 kW

2.6.3.3 Dipole Power Supplies

The dipole power supplies will all be re-used Tevatron and NuMI existing equipment, relocated to LBNF. Most of the equipment being moved from either the Tevatron or NuMI will be usable as is, however the large Tevatron dipole supply will operate at a higher current than in the Tevatron so it will need a new current-regulation system.

2.6.3.4 Quadrupole Power Supplies

None of the Quadrupole power-supply equipment has an equivalent component in the Tevatron, but NuMI has just installed five new quadrupole supplies. LBNF will relocate and use these supplies and procure six new copies for the Quad magnet loops. A single current-regulator card will be installed in the voltage regulator, just as in the present system for the magnet loops. These supplies have proven to be reliable and will continue to be used.

2.6.3.5 Corrector-Magnet Power Supplies

The LBNF primary beamline will utilize upgraded MI-type correction-element magnets. These magnets will all be IDS style, oriented horizontally or vertically, and placed at one end of each Quadrupole magnet in the beamline. The power supplies will use the newly designed Booster correction elements regulator board to provide the fastest ramping operation. These are individual switch-mode units that utilize a common bulk supply similar to those used in the present MI installations. A single bulk power supply installation is capable of driving all of the proposed 23 individual magnets. The power supply is intended to be used as a ramping supply and will provide full four-quadrant operation. The magnets will be ramped to the 40-A peak as needed to achieve the longest life in the magnets, and to minimize high-current DC operation and system heating.

Table 2-15: Corrector Magnet Power Supplies

Magnet Loop Name	Number of Magnets	Power Supply Location	Power Supply Type	Power Supply Voltage	Power Supply Current
E:xT201 thru E:xT221	23	LBNF-5	FNAL Booster 40 A Trim	180	40

2.6.3.6 Kicker Power Supplies

New kicker magnets and a kicker-magnet power supply will be needed to extract the beam from the MI. The present NuMI extraction kicker magnets at MI-60 use three long magnets, but six shorter magnets are planned for the MI-10 extraction (see Section 9.3.6). This change has little effect on the power supply, but it affects the number of cable terminations on/at the loads. This power supply system will be copied from the NuMI extraction kicker, a proven and reliable design, with few changes. The power-supply design consists of a pulse-forming network (PFN), charging supply, resonant charger, switch tube in an oil tank and terminated transmission-line loads. To maintain regulation, high-resistance cooling liquid is circulated through the loads, requiring a heat exchanger to maintain load temperature. All of the controls for this system will be identical to the latest design installed for the NoVA upgrade to the MI and any usable equipment from the NuMI extraction will be relocatedto the MI-10 service building.

2.6.3.7 Power Supply Control

The power-supply control system will use the latest design of the controls interface from the Electrical Engineering Support department of the Fermilab Accelerator Division (AD E/E Support). This controller includes a built-in transient recorder and a single E-Net connection that provides the status and control back to the front-end computers. The current reference design is similar to the ramp generator series commonly used today and referred to as a C46x card. However in the future LBNF will be moving to a VME-based control system that will provide a ramp generator that emulates the present system. The current regulation and controls can support either system without any changes.

2.6.3.7.1 Voltage Regulator

A standard voltage-regulator chassis was developed to improve maintenance and operation of power supplies in the accelerator complex. This Fermilab voltage regulator is specified in 12-pulse supply procurements. This has reduced the maintenance load on Fermilab's engineering staff because, having over 150 copies, the lab is not subject to unique designs supplied by different vendors. The primary beamline will continue to use this chassis design in all of the 12-pulse high-current supplies in the line as well as in the Fermilab high-stability current-regulation system. All of the regulators will come with the Tevatron and NuMI supplies, and LBNF will procure additional units for the seven new quad supplies.

2.6.3.7.2 Current Regulator

The ramps for the beamline magnets move very quickly to high currents, so for the magnet loops with two supplies, both must be programmed to operate at the same voltage. This is in contrast to the MI

where, instead, a controller MECAR (the Main Injector Excitation Controller and Regulator) removes supplies from the magnet loop to reduce feeder-loading during the ramp. MECAR regulation and control is currently installed in the NuMI beamline for HV101 (two supplies) and V118 (three supplies).

The current-regulation system for the large supplies will use the latest version of the BuLB v2.0 current regulator that is a subset of the MECAR regulator and will have a response in current regulation comparable to the MI. These regulators have been installed in the present NuMI beamline high-current supplies to improve the accuracy from pulse to pulse. This regulator is used to provide the highest pulse-to-pulse stability in the LBNF current-regulation system design. It is constructed with a built-in learning system that is used to correct the systematic errors in the current. The power supplies will have filters; the fast changing voltage will ring during the step-down and affect flattop current. It will be impossible to “learn out” the effect of the ring, so the shorter the flattop is, the more structure will be seen in the current. The learning system will make this repeatable ramp-to-ramp and should not affect beam transfer any more than the changes in MI bend-magnet current do. This regulation limit is not unique to LBNF but is fundamental to ramped-power systems, including that of the MI. In addition to providing the current regulation, this system has a built-in transient recorder to capture single-event trips, allowing for faster analysis of random events.

2.6.3.7.3 Series Power Supply Controller

Connection of multiple power supplies in series or parallel increases the risk of back-feed from the other devices. A system of knife switches and disconnect switches will be used to isolate the supplies from the load and the beamline for maintenance of the H214 magnet loop. The knife switches, taken from the Tevatron, will be installed in the large dipole-magnet systems to improve the maintainability of the supply and magnet load.

For the series-connected supplies, a new, custom controller will provide the voltage drive to both supplies and manage their ON/OFF status as a single supply. Controllers of this type, used on three magnet loops in NuMI with up to three 500-kW supplies in series, use a commercial controller (based on a Programmable Logic Controller, PLC) during operation. This controller will also manage the magnet-loop monitors, temperature, voltage-to-ground, bus-water differential pressure and ground current.

All of the high-current power supplies will use a distributed ground system to check for excessive ground current (ground fault) in the power supplies and magnet, and if detected will trip off the supplies. The ground-fault system is built into the smaller supplies but will be part of a separate controller in the series-connected supplies. All of the support hardware in the existing power supplies will be relocated with the supplies and used with the new controller.

2.6.3.8 Power Feeder Loading

The feeder system that provides power to the primary beamline supplies will be routed from the Kautz Road substation, via an extension of the MI beamline feeder 96/97 to both of the LBNF service buildings (as part of the Conventional Facilities scope). This feeder system already incorporates a harmonic filter to reduce the voltage stress on the 13.8-kVAC devices. The peak loading on the feeder is expected to be

6.8 MVA and the harmonic filter has 5 MVARS of correction to the beamline-feeder system. Beam will not be sent through the NuMI or F-sector beamlines during LBNF pulses, so the supplies in the MI beamline will be at 'idle' and not drawing high power. This will allow the needed pulse power to be drawn from the existing capacity of the MI, and continued running with a mix of beamline choices on a time-line generator mix, as is done now, without changes to the feeder system.

2.6.3.9 Power Supply Large Equipment Installation

The large power supplies consist of multiple sub-assemblies that will need final assembly in place in the service buildings. The outdoor equipment is large and will be put in place by a local rigging company. As equipment is taken from the Tevatron and NuMI it will be disassembled using a combination of Fermilab labor and local contractors. All electrical work will be performed by local contractors. Fermilab will locate and assemble the large subsystems and perform all testing and integration into thecontrols system. Fermilab will act as the general contractor to have the large sub-assemblies constructed and complete the final assembly work on site for only the large supplies, new and MR/Tevatron size equipment. The smaller, high-current supplies will be constructed off-site and come in fully operational. They will be installed by Fermilab personnel and the power connections will be made by local contractors. The final testing and integration to the controls will be done by Fermilab staff.

2.7 Primary Water System (WBS 130.02.02.04)

2.7.1 Introduction

The primary water system will feed cooling water to the magnets, power supplies and other equipment of the primary beamline. The system will include a heat exchanger, filtration systems, pumps, expansion tank, instrumentation, buswork, and piping, valves, fittings and other hardware.

This system will supply low-conductivity water (LCW) of a resistivity in the range of 16 to 18 MΩ*cm, at a nominal supply temperature of 95°F. (Operationally, when conditions allow most of the year, the system will be operated at 90F, due to the savings in lower electrical resistive losses caused by heat.) The majority of the system's components will be located in the pump room at ground-level in LBNE 5. From there, LCW will be fed to components in LBNE 5, as well as into and throughout the beamline enclosure, and finally to LBNE 20 Service Building and Target Hall horn power supplies. This system may be used to supply the make-up water to the Target Hall radioactive water (RAW) systems. Beamline
2.7.2 components at the extraction point in the Q-100 area of the MI will be fed from the MI Global LCW System, and are covered under MI Extraction, section XXXX.

Design Considerations

Full system modeling needs to be accomplished once all component requirements are well understood and all configuration options are decided. System schematics will be created in parallel and should include a piping and instrumentation diagram (P&ID). Piping-installation drawings and specifications will be created from this, with sufficient documentation to provide for outside bidding practices. Both piping and vessels will adhere to FESHM Chapter5031, as well as the Fermilab Engineering Manual. Piping will

be designed and installed in accordance with ASME B31.3 Code for Process Piping. Pressure vessels shall be designed in accordance with ASME Boiler and Pressure Vessel Code Section VIII Division 1.

Reference Design

2.7.3.1 Heat Loads and Heat Exchanger

2.7.3

Total heat loads for the system due to components (magnets, power supplies, bus runs) will be about 800kW. Add to that, the heat loads from the LCW pumps, and a margin for efficiency, and final heat exchanger sizing will be for 1.2MW. Final removal of this heat will be through transference to pond water via an LCW – to – pond water heat exchanger, to be located at LBNE 5. This will be a tube-and-shell style exchanger, with pond water on the tube side and LCW on the shell side, to facilitate the cleaning of the pond-water side. The Hx size of 1.2MW gives room for inefficiency due to plating / blockage over time, caused by pond water scum and debris. Heat loads for the LCW are not expected to change significantly with the future upgrade from 1.2 to 2.4MW beam. The LCW heat loads are as in **Table 2-16.**

Table 2-16: Summary of Heat Loads

Component	Heat Load, kW	Location
Dipole / Quad magnet Power Supplies	108	LBNE-5
Magnets	452	PBE
Bus from LBNE to PBE Dipoles	198	LBNE-5 & PBE
TH Horn Power Supplies	60	TH
LCW Pumps	108	LBNE-5
20% Hx Extra, Cushion for Efficiency	185	LBNE-5
Total	**1111**	**LBNE-5**

2.7.3.2 Pumps

LCW will be supplied to the magnets in the enclosure with a pressure differential of 100 psid or greater. This will require pump output at 170 psid to compensate for losses along the route and equates to a dynamic head of 395 ft. Flow will be determined by the final system configuration, but is estimated at this time to be about 950 gpm. LCW pumps will be located in LBNE 5. The tentative arrangement will be for four 50-hp pumps to be piped in parallel, with normal configuration as three pumps in operation and one offline in standby mode. It may be possible to reuse pumps from the Tevatron LCW system, although this is not included in the current scope. In case the TeV pumps would be sufficient, a request has been made to have 6 reserved from the TeV decommissioning. However, further design study may suggest a preference for two 125Hp pumps instead, 1 on line with 1 hot spare.

2.7.3.3 Piping, Valves, Fittings and Hardware

Piping for LCW will be schedule 10 304/304L stainless steel, with full penetration welds. Because the total run length in the direction of the beamline will be about 750 ft, as well as runs to and from the service buildings of roughly 230 ft additional, thermal stresses and the need for expansion should be

addressed in the design. At this time, it appears that a 6” iron pipe size (IPS) will be adequate for enclosure flows, requiring 8” from the LBNE 5 pump room to the tunnel connection.

Piping for the pond water lines to and from the heat exchanger within the LBNE 5 pump room are to be schedule 40 carbon steel. These will have a strainer upstream of the heat exchanger (Hx) and a bypass around the strainer. In addition, building isolation valves will be necessary. Ponds, pond water pump vaults, and piping from the pond vaults to the pump room are to be supplied by Conventional Facilities.

Individual magnet and power-supply component connections will have ball valves on both supply and return taps wherever possible. Where standard FODO cells provide magnets in a dipole-quad-dipole string, secondary manifolds such as used in the MI would be a very good consideration, and are included in the estimate. When this is not possible, such as for the bus lines feeding the dipoles, suitable valving to ensure local isolation will be implemented. At this time, all LCW connections to all magnets are planned to be hosed connections, and will be separate from the electrical connections of the bus.

Hangers and brackets will be stock, such as Unistrut or B-Line, where possible. Custom 3-in-a-row vertical brackets may make the best use of enclosure space, and have been costed for the enclosure run. All nut-bolt-washer hardware is to be 304 stainless steel. All brackets not stainless steel will have a rust-preventing finish such as paint or plating.

2.7.3.4 De-ionizer / Filter Loop

Cooling water will require filtration and deionization polishing to maintain the “low-conductivity” status. This filtration will be located in LBNE 5 and will include pre- and post-filters, as well as several 3.6 cu.ft. bottles of mixed-bed de-ionizing (DI) resins in parallel between the filters.

This system will require a fill line to make up water using LCW supplied from the MI. This water will come into the system through the filtration loop. This system will also require a storage and expansion tank, of around 1,000 gal, that will be an ASME U-stamped coded vessel, supplied with a level indicator and a pressure-relief device. LCW is cycled by passing a small part of the pump discharge stream through the filtration loop and into the expansion tank. This flow then exits the tank as a mix and returns to the main system on the suction side of the pumps. This ensures that the LCW in the tank remains as polished as it is in the remainder of the system.

2.7.3.5 Instrumentation and Control

A three-way valve setup will be used to control the LCW temperature, by directing LCW flow either to the heat exchanger or to bypass the heat exchanger. This will regulate the temperature of the LCW supply leaving the pump room. Flow on the pond water side will remain at full throughput.

The pumps will require Motor Control Centers (MCCs) in the LBNE 5 pump room. Variable-frequency drives (VFDs) will be investigated for this purpose. These, and the Temperature Control Valve (TCV) power, are high-voltage devices, requiring panels similar to what is used in the MI pump rooms.

Both LCW and pond-water systems should have suitable pressure, temperature and flow-measuring instruments, and LCW will require at least two inputs for DI status. All readings should feed to ACNET (described in Section 2.9?) for remote reading and data-logging.

In late 2013, due to feedback from the ANU Lessons Learned panel, it was found that instrumentation had been inadequately estimated for NOvA RAW and LCW Systems. Therefore, a thorough study was completed for all of LBNE LCW and RAW instrumentation. The information was presented to project leadership, and suggested to be implemented as a Change Request. Although agreed upon by Project Management to do this, timing left it out of project action until now. It is hereby included as part of the CD1 Refresh estimate.

2.7.3.6 Buswork

The primary purpose of electrical bus is to carry current to the magnets. However, since buswork must be leak-tight and is installed similar to piping, its installation is included within the scope of the LCW systems. This will include the acquisition and installation of the bus that runs from the power supplies into the enclosure and to the magnets, as well as the end connections and flex flags that connect to the dipoles. Final connections between the bus and magnets are addressed in Section 2.6.3.

Dipoles will require 5 circuits of bus, and be fed from power supplies at LBNE 5. This is made up of an average run in LBNE 5 of 60’, and 135’ through the penetration and Vehicle Access Enclosure, to the alcove in the PBE. From there, one pair turns downstream, and 4 pair head upstream. The total length of bus required is just under 4000’ for the runs, and should include an additional 20% for connections, waste, custom fit-up, etc.

At this time, 5000 feet of 2” square bus is slated to be reclaimed from the TeV, via the TeV Decommissioning Efforts. The repurposing of the TeV bus saves the project about $300k in material.

This bus should be water-cooled as well, using LCW. In addition, all exposed bus between the power supplies in LBNE 5 and the enclosure must be contained in aluminum shielding panels such as those used in the MI Service Buildings. Once into the enclosure, it will be behind the Controlled Access point, requiring LOTO to enter, and shielding will no longer be a necessity. Since the shielding and enclosed bus will weigh around 5000 pounds, it should be subjected to a separate Engineering Review.

Where standard FODO cells provide magnets in a dipole-quad-dipole string, 1-in X 4-in rectangular bypass bus lengths such as used in the MI will be required. Existing MI designs may be sufficient to clear the quads. Since many of the sets of dipoles are rotated, either special mounts and/or end adaptions will be required to match the dipoles. These details cannot be dealt with until far later in the design process. Bus discard from the magnet-building process could be used as material.

2.7.3.7 Other Considerations

Because of the large vertical hump in the beamline trajectory, significant fluid-dynamics modeling of the entire system will need to be done, representing all the components as completely as possible, before committing to a final design.

Because the installation in the enclosure is on a slope, carts for transporting pipe, bus, and gear are to be used. Current designs include these uses in the carts being designed for magnet installation, and will include safeguards to secure loads, and to prevent against run-away conditions. Additionally, argon will be used to purge lines for welding and brazing. Argon dewers for purging will need to be located in or before the Vehicle Access Enclosure. Hard-piped lines for compressed air, nitrogen, and argon are included in Vacuum, section 2.9, Primary Vacuum (WBS 130.02.02.06). The argon line will need installed in advance of the welding.

2.8 Beam Instrumentation (WBS 130.02.02.05)

2.8.1 Introduction

The LBNF primary beamline includes instrumentation and diagnostics to characterize important beam parameters, for example, beam positions, stability, losses, and intensity. It also continuously monitors the operation of all the beamline elements under operating conditions, i.e., with a high-power beam. During the first commissioning and machine studies, the diagnostics systems also have to operate with a low-intensity beam (approximately 3 x 10^{11} protons per batch).

The four core instrumentation systems for the primary beamline are as follows:

1. Beam-Position Monitors (BPM): 26 dual-plane BPMs for beam-trajectory measurement, based on button-style pickups and digital-receiver read-out electronics

2. Beam-Loss Monitors (BLM): 30 ion-chamber BLMs for local beam-loss monitoring, and four long (approx. 250-ft) total-loss monitors (TLM)

3. Beam-Intensity Monitors: two toroidal transformer-based beam-intensity monitors

4. Transverse-Beam Profile Monitors: six dual-plane secondary emission monitors (SEM) to measure the transverse beam profile (effectively a 2D intensity plot of the beam at a given location), from which the beam emittance can be calculated.

BPMs and BLMs are part of an integrated machine-protection system (MPS), where a beam-based technical interlock is used to prevent damage from a mis-steered or out-of-control, high-power beam.

Possible additions (not part of the current design) to this set of beam instruments include, for example:

- A broadband wall-current monitor for beam-timing measurements

- An imaging system to monitor the 2D beam profile at the exit window

- Non-invasive transverse beam-profile monitors, for example, IPMs or e-beam scanners, as required

Reference Design

Table NNN summarizes important beam parameters, to which all installed beam diagnostics must be sensitive. All read-out hardware (signal processing, data acquisition, timing, triggers, power supplies, and so on) will be located outside the enclosure and wired using low-insertion-loss, high-shielding cables for the detection elements in the tunnel. Housing these electronics systems in service buildings MI-10 and LBNF-5 will minimize the cable length. Wherever feasible, components from existing NuMI instrumentation will be re-purposed for LBNF to reduce costs.

2.8.2

2.8.2.1 Beam-Position Monitors

The BPM system will be based on simple electrostatic "button-style" pickup detectors. The measurement of integration time will be a few 100 nsec, which allows for observation of beam displacements within the batch. The anticipated resolution is 25 to 30 μm in a beam pipe with a 3 inch circular cross section. The read-out system is based on digital downconverter and signal-processing technologies very similar to the existing installations at other Fermilab accelerators, for example, the Tevatron, MI, Recycler, transport beamlines and experimental beamlines (e.g., NuMI, BNB). An automatic gain-correction system will continuously monitor and calibrate the electronics, and correct slow drifts due to temperature and aging effects of electronics components.

2.8.2.2 Beam-Loss Monitors

The BLM system will be very similar to the installation in the NuMI beamline. **Figure 2-24** shows an ion-chamber beam-loss detector, the basic element for the 30 BLMs in the primary beamline for detecting local beam losses. These sensors will be placed on the dipole and quadrupole magnets. They offer a 10^6 dynamic range, and will be operated in a window between 10^{-8} fractional beam loss (lower limit) and 10^{-2} fractional beam loss (saturation). The current plan is to re-purpose the existing ion chambers from the NuMI beamline. A digital FPGA-based read-out system may also be considered, similar to the one in the Large Hadron Collider (LHC) at CERN. **Table 2-17** lists the specifications for the loss monitors.

A set of four TLMs, based on argon-filled Heliax cables, will complement the BLMs and monitor the integrated beam loss along the beamline. The readout and gas-monitoring systems for the NuMI TLMs will be re-purposed for LBNF.

Table 2-17: Specifications for the Ion Chamber Loss Monitor

Materials	**Glass, Nickel**
Volume	110 cm^3 Argon gas at 1 Atm
Calibration	70 nC / rad
Response time	1-2 μsec
Leakage current	< 10 pA
Operating range	1 mrad -100 rad

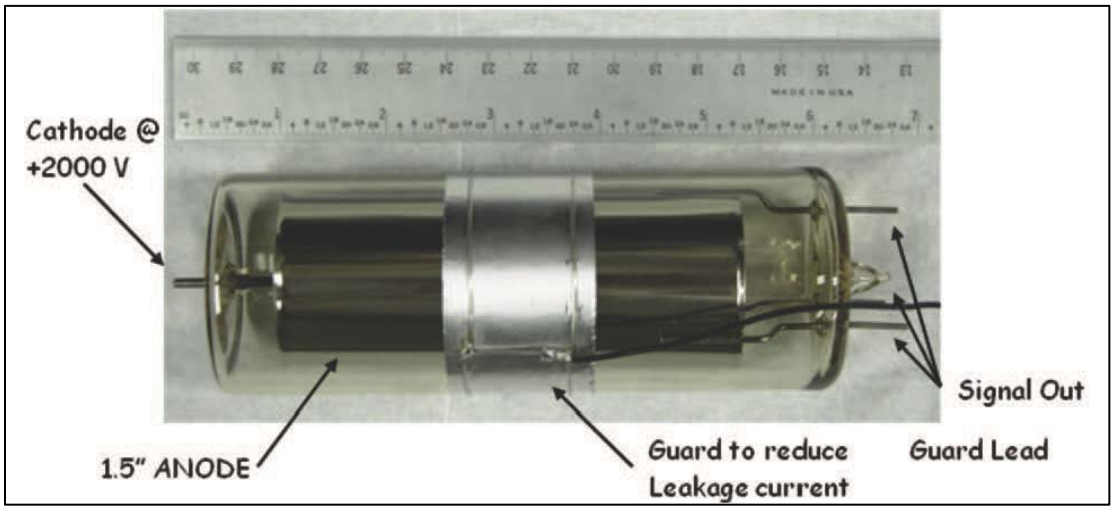

Figure 2-24: Ion Chamber Loss Monitor

2.8.2.3 Beam-Intensity Monitors

Two beam-intensity monitors are needed for the primary beamline and will be based on 3.5-in Pearson toroidal transformers. Monitors used for NuMI will be re-purposed for LBNF. The analog gain and filter stages may need to be located in the enclosure and the digital signal-processing and calibration systems will be located in the service building.

2.8.2.4 Beam-Profile Monitors

The beam-profile monitors are based on the secondary-emission principle. Two orthogonal arrangements of 48 thin titanium wires or foils are used, spaced 0.5-1 mm apart, mounted on a fork-like ceramic carrier substrate, as shown in Figure 2-29 (left). A rotary-motion system sweeps the SEM wire or foil frame into the beam and performs a pulse-by-pulse measurement of the transverse beam profile. **Figure 2-25** [right] shows an estimation of the heating using thin, 5 μm by 150 μm titanium foils with 1 mm pitch as target for a 708-kW beam. With the inserted SEM foil, the maximum tolerable fractional beam loss is limited to 2.5 x 10^{-6}. Monitors used for NuMI will be reused in LBNF. For operation at a higher beam power, carbon filaments may need to be used as the SEM target or non-invasive monitoring techniques may be necessary.

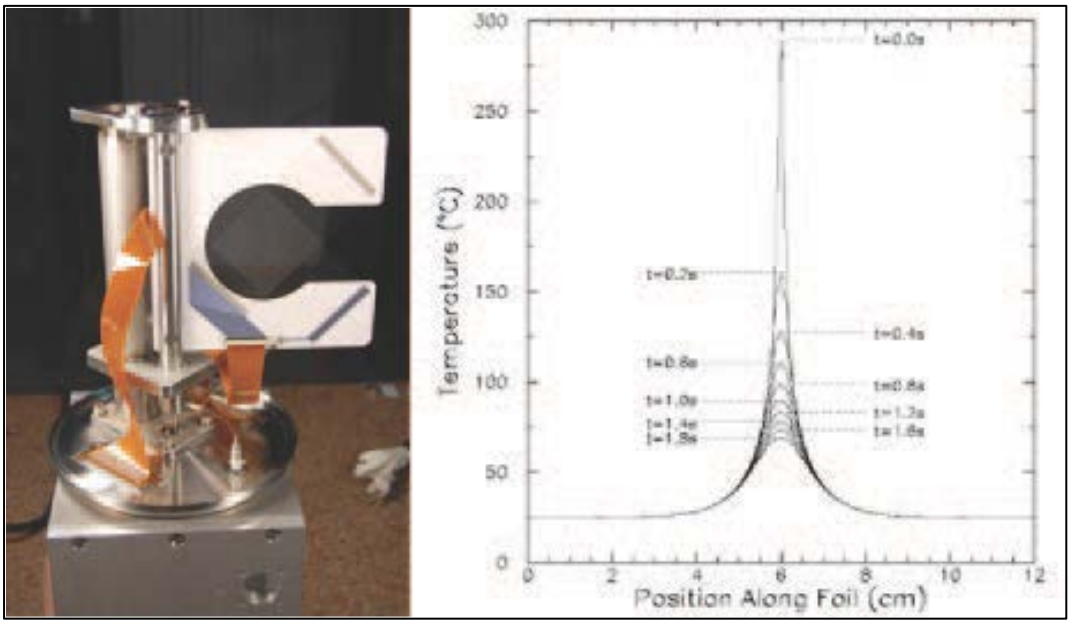

Figure 2-25: SEM Beam Profile Monitor. Left**: Rotary Mechanics with Ti Multiwire Frame;** Right**: Ti Foil Heating Estimation for 708 kW Beam Power**

2.9 Primary Vacuum (WBS 130.02.02.06)

2.9.1 Introduction

The Primary Beamline vacuum system will maintain better than 1 x 10^{-7} Torr residual gas pressure in the beam tube in order to reduce beam losses from proton-gas interaction. The entire system is approximately 1,200 feet long from the extraction at MI-10 to the Target Hall, and it will be divided into several independently evacuated sections to accommodate the physics requirements, civil structures, and the overall pumping scheme. No section shall exceed 400-ft, and each will have about 20 ion pumps to achieve and maintain the required pressure level. The downstream end of this system concludes with a beam window inside the Target Hall, which is covered by the Neutrino Beam WBS.

2.9.2 Design Considerations

LBNF's vacuum system design is typical for a single-pass beamline. The specified residual gas pressure for the beam tube is not technically challenging to achieve, and the design will be similar to existing systems installed for the Main Injector transfer lines and NuMI. Experience from operating and maintaining these vacuum systems validates that a highly reliable, low-maintenance vacuum system is critical for minimizing outgassing and the potential for leaks, and thus for improving the overall operational efficiency of the beamline.

2.9.3 Reference Design

The system will consist of more than 70 45-L/s ion pumps; five section valves and eight gauges will be used for for separation and safety interlocks (see **Table 2-18**). All beamline devices to be installed in the vacuum system must comply with standard UHV practice regarding material choices, cleaning, and handling in order to minimize out-gassing and contamination. Although there is no plan to bake the entire Primary Beamline, pre-baking may be required for some devices. The following pumping scheme will be applied at each section: (1) pump down to 10^{-6} Torr solely by turbo stations at two pumping ports within the section, and perform a leak check with a minimum sensitivity of 2 x 10^{-10} Torr-L/s, (2) start all ion pumps, and (3) valve out turbo stations (i.e., close the valves and remove the temporary turbo pumps) when 10^{-7} Torr average pressure is achieved.

Welding is the preferred method for making vacuum connections and will be used wherever possible, especially where the expected frequency of beamline device maintenance is low. Beam instrumentation devices such as BPM's and multi-wires will be connected using conflat flanges. Vacuum valves, pumps, and gauges will also be attached using conflat flanges.

Table 2-18: List of Major Vacuum Components

Ion Pumps	Section Valves	Instrumentation and Access Ports	Bellows	Beam Tube
~70	5	8	~65	550 feet
Distributed pumping, distance should not exceed 20 feet.	Interlocked gate valves. Section length should not exceed 400 feet.	Pirani pressure gauges and pumping/venting ports.	Mostly elliptical and 3" round.	Mostly 3" round stainless steel. Also six ceramic tubes for kicker magnets.

2.9.4 Pumps

There will be more than 70 ion pumps distributed along the beamline with spacing of 20 feet or less. Once a section is evacuated to 10^{-6} Torr by two portable turbo pump carts, and the section is thoroughly leak-checked, the ion pumps in that section will be turned on.

2.9.4.1 Beam Tubes

The shape and size of beam tubes will vary along the beamline. The vacuum interface between dipoles, between dipoles and quadrupoles, and between adjacent beam tube sections will be welded. The interfaces for beam diagnosis instrumentation will use conflat flanges with a copper gasket. There is approximately 650 feet of beam tubes that reside in the dipole and quadrupole magnets, which will be supplied as part of the magnet. Dipole beam tubes have an elliptical cross section of 2 inches by 4.8 inches, and quadrupole beam tubes have an outer diameter of 3 inches. To accommodate the beam optics and corrector magnet design, most of the connecting beam tubes will have an outer diameter of 3 inches. Ceramic beam tubes with a resistive coating will be developed for use in the six kicker magnets. Various quantities of bellows, flanges, tees, crosses, stands, vacuum-grade bolts, nuts and gaskets are also needed.

2.9.4.2 Valves and Gauges

Five 4-inch, pneumatic gate valves will be used to protect adjacent sectors from failures as well as to assist installation and maintenance. They will be interlocked with beam operation and triggered by Pirani gauges in each segment. A compressed air system will be installed for operating the pneumatic valves. About eight all-metal right-angle UHV manual valves will be used for pumping ports.

2.9.4.3 Instrumentation and Control

Standard 8-ft racks for the controllers of ion pumps, gauges, and valves will be located in service buildings MI-10 and LBNF-5. All the ion pumps, gauges and valves will be remotely controlled, and their outputs will be logged via ACNET. For diagnosis and maintenance, a leak detector, a residual gas analyzer, and local controllers for ion pumps, gauges and valves will be used.

2.9.4.4 Baking and Cleaning

In-situ vacuum baking for the whole beamline is not required, but pre-baking some components may be necessary, especially for beam instrumentation components. All components must follow UHV cleaning procedures before installation. Equipment includes heat tapes, sheets, foils, UHV gloves, lint-free wipes, cleaning fluids, etc. Additionally, the Lambertson magnets require a bake after installation to drive out the large volume of gas trapped in the laminations; a special electrical system will be installed in the tunnel at that location to accommodate the necessary equipment.

2.10 Magnet Installation

The lattice design specifies installation of 56 major magnets (listed in **Table 2-1**), six kicker magnets, and 23 corrector magnets. The total length of the Primary Beamline is approximately 1,200 feet from the extraction at MI-10 to the Target Hall. An image from the preliminary 3-D model is shown in **Figure 2-16** and depicts an overview of the Primary Beamline. Based on experience with NuMI and other MI projects, LBNF will use a combination of magnet installation methods. Although the methods for transporting and positioning magnets will vary by location, the scheme for supporting and adjusting them will be the same. Each magnet will have a stand that provides three-point support and six degrees of freedom for precise adjustment. The magnet installation parameters are shown in **Table 2-19.**

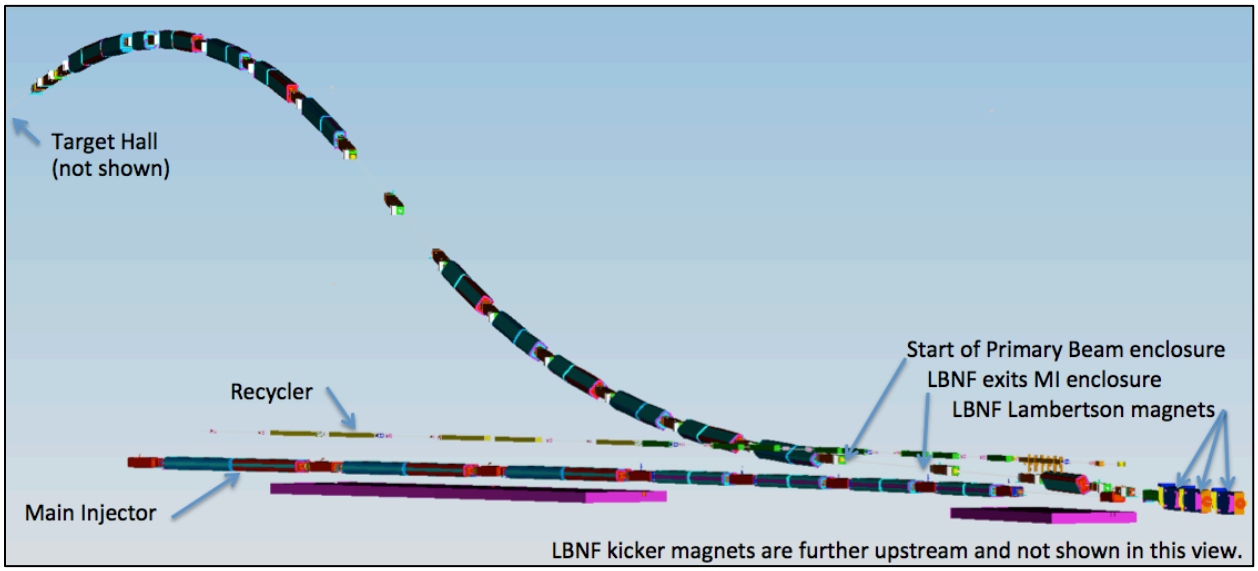

Figure 2-26: Overview of the Primary Beamline

Table 2-19: Magnet Installation Parameters

	Main Injector Enclosure	Primary Beam Enclosure
Section Length	~300 ft	~900 ft
Enclosure Notes	Co-existing with other beamlines.	New enclosure with sloped floor up to 150 mrad.
Major Magnets	15	41
Support/Adjustment	Mixture of new and modified designs.	Modified MI designs.
Transportation Method	Tugger and dolly via MI.	Winch and dolly via LBNF access tunnel.
Positioning Method	Existing MI equipment.	MI hydraulic carriage with modification.

This section focuses on the technical aspects of installation. **6, System Integration,** explains how to best sequence the installation steps relative to each other and all related tasks. Because magnet installation is a significant part of the beamline installation, it must be integrated into the overall plan to ensure it is done safely and efficiently, but the detailed process of magnet installation is developed within its own WBS.

In the Main Injector enclosure, the magnets will be lowered into the tunnel by the crane at MI-60, and then a tugger and dolly will move each magnet to its designated tunnel location. For the Primay Beam enclosure, flatbed trucks will transport the magnets to the magnet installation tunnel just downstream of LBNF-5, and then they will then be moved into the primary beam enclosure. There is currently no tugger that can be used on the sloped floors, so each magnet and its loading dollies will be moved by a winch system in the new enclosure.

The winch system will have a similar line speed (35 feet per minute) as the one that was used in NuMI for a similar installation. The LBNF system will have a larger capacity (exceeding 40,000 lbs), a longer range (1,100 ft), and new features such as variable speed control, self-guidance, and dual-directionality. After installation is finished, the winch system will be removed from the tunnel and will be reinstalled only as necessary for future use. The existing MI dollies require redesign so they are able to work with the winch system on the sloped floors in addition to retaining their current functionality.

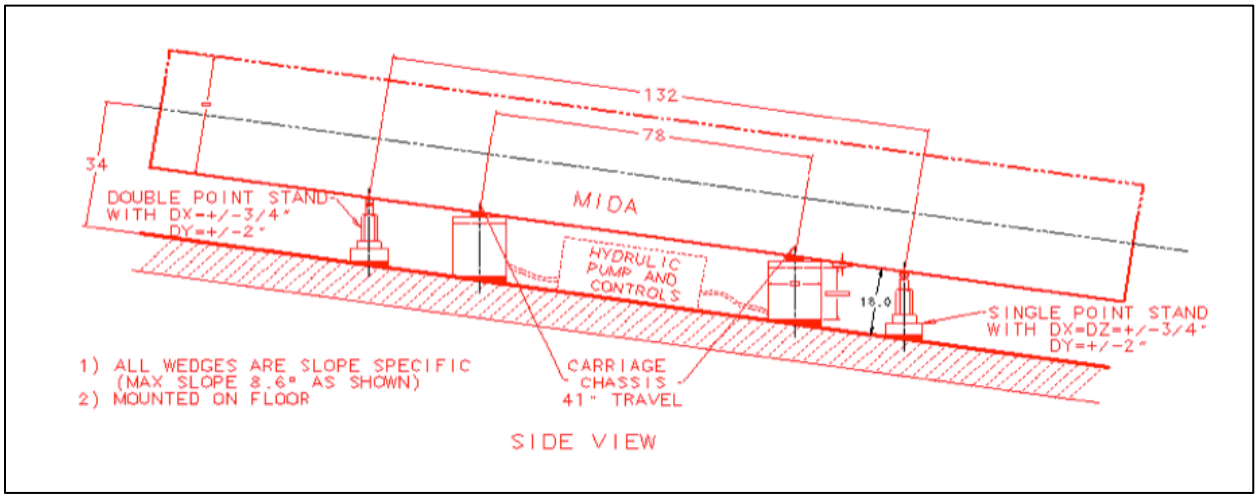

Figure 2-27: Magnet Installation on Sloped Surfaces

Before transporting a magnet to its specified location, the positions of the beamline and magnets will be marked on the floor with direction from a survey crew. Each stand or hanger will be installed within ±0.25 inch of its ideal position; a mounting template may be necessary to achieve this. The stands will be set to the proper position to receive the magnets. Each magnet will then be transported to its location along the beamline and secured in the aisle while the hydraulic carrier is set and secured in the beamline position. The carrier will extend its carriage underneath the magnet waiting in the aisle and transfer the magnet transversely to its beamline location. The stands will be adjusted to engage with the magnet and remove the load from the carrier. At that point, the magnet dollies and the carrier can be removed. Then the stands will be adjusted to coarsely position the magnet, and a survey crew will perform the final precise adjustment. A schematic for this method is shown in Figure 2-27.

In general, MI magnet stands will be used. Their features include a thrust bearing for heavy magnets (up to 40,000 lbs), a low-friction insert for controlled sliding, and a bronze bearing for easy adjustment. The stands have a transverse axial adjustment of ±0.75 inch and a longitudinal axial adjustment of±2 inch to offset any deviation of the tunnel floor from its nominal elevation due to construction tolerances and settlement. Cradles will be designed to restrain magnets in their rotated positions.

Wedges will be used under the base plates for all supports installed on sloped floors to coarsely ensure that the vertical adjustors are upright. Fine shims will also be used to level the wedges due to imperfections in the floor. This method will ensure the forces from gravity will remain vertical despite the slope and removes concern about lateral forces in the adjustors. However, the addition of cradles at

the bottom of the magnets and wedges at the bottom of the stands requires seven more inches than the nominal MI distance between the beamline and the floor.

3 BEAM-LOSS CALCULATIONS

3.1 Introduction

This section provides an overview and important examples for simulations that give information about the mechanisms and results of an improperly controlled primary beam. The high-intensity beam needs to modeled and understood to a very high precision to ensure that beamline components are kept to low activation levels and to be confident that accidental losses are rare and not damaging. The model is as complete as possible, from extraction through the Target Hall, where beam particles (protons) and their interactions are tracked individually and in full detail. Simulated magnets are controlled in groups appropriate to the designed power-supply bus configuration. Errors in magnetic fields for individual magnets can be inserted as random manufacturing errors and as simulated current fluctuations from power-supply errors. Beam loss studies provide one key input in the requirements for the magnet power-supply stabilities.

In addition to providing validation of operational beam-loss control for environmental and component protection, the simulations can provide a level of confirmation for the design of the beam-interlock systems (Sec. 4.3).

Additional studies are needed to determine criteria appropriate for LBNE enclosure and building construction, as well as equipment installation during the MI operation.

Calculations that provide distributions of losses along the primary beamline are obtained with STRUCT code [37_old]. The STRUCT output goes into calculations, done by MARS, of energy deposition and groundwater and component activation.

3.2 Design Considerations

The main design criteria for the primary beamline are (1) the transmission of high-intensity beam with minimum losses, (2) precision of targeting and (3) minimization of component activation. Mitigation of groundwater activation is relatively straightforward for the above-grade beam, however protection from prompt radiation, such as muon plumes, requires mitigation.

Serious consideration must also be given to accidental beam losses that, within just a few beam pulses, can cause beamline-component damage. Significant sources of beam-position instability on the target as well as increased beam loss along the beam line include the power supplies for the extraction kicker, and the quadrupoles and dipole magnets. Variations in the element strength that occur over a period of minutes or hours can be corrected. However, for variations on shorter time scales, such as pulse-to-pulse jitter, the specification on beam instability would have to be met directly at the power supply.

3.12.1.1 Reference Design

The proton beam extracted from the MI-10 straight section is transported 329 m to the LBNE target located 11.4 m above the MI elevation. The design is based on a 708 kW beam with intensity of 4.9 x

10^{13} for a 1.33-second MI cycle. The design must be compatible with an upgraded capability of 2.3 MW beam power with intensity of 1.6 x 10^{14} per cycle.

The worst-case conditions are simulated using a 3σ emittance of 30π mm-mrad for the beam core, with halo cut-off at 360π mm-mrad or 10.4σ, and momentum spread (1σ) of dp/p = 0.0004 with cut-off at dp/p = 0.0028. In the simulations, 1% of the beam in halo is distributed with horizontal and vertical amplitudes in a range from A_{min} = 3σ to A_{max} = 10.4σ as $F=1/A_{x,y}$. The beam intensity is assumed to be 1.6 x 10^{14} per 1.33-s MI cycle (2.3 MW case), that is a factor of six higher compared to the NuMI design. The effects of magnet power-supply instabilities to beam distributions at the target and baffle are calculated for nominal emittance of 30π mm-mrad.

Table 3-1: Apertures (Half-size of Primary Beamline Elements Used in Simulations)

Element	L (m)	Hor. (mm)	Vert. (mm)	Aperture
LAM10	2.80	32.0	25.4	rectangular
Q102 quadrupole	2.1336	63.0	29.0	special
beam line quads (3Q120)	3.048	36.6	36.6	round
beam line quads (3Q60)	1.524	36.6	36.6	round
V100 (vertical dipole)	3.3528	51.6	21.7	rectangular
MI dipole (IDA/IDB)	6.09981	60.0	23.5	elliptical
MI dipole (IDC/IDD)	4.06654	60.0	23.5	elliptical
H-corrector	0.3048	60.0	23.5	elliptical
V-corrector	0.3048	36.6	36.6	round
Long drift sections	-	36.6	36.6	round
Baffle	2.50	7.5	7.5	round
Horn 1 entrance	-	12.0	12.0	round
Target (round target)	0.966	7.5	7.5	round
Horn 1 exit (conical, 10mr, round)	2.00	23.0	23.0	10mr, conical
drift Horn 1 to Horn 2	3.20	50.0	50.0	round
Horn 2	3.00	39.0	39.0	round

3.12.1.2 Primary-Beam Loss

Beam distributions representing a sum of 100 distributions have been produced for independent random values of magnet strengths in the beamline. The calculations are done assuming a common power supply for several magnets, with instabilities as follows: LBNE quadrupole, dG/G=±0.001; extraction kicker, dB/B=±0.005; Lambertson magnet, dB/B=±0.002; MI quadrupoles, dG/G=±0.001; and

MI closed orbit, dA=±1$\sigma_{x,y}$ or ±1.3mm. The effect of quadrupole strength instability to the resulting beam size is much less significant than that for the dipole magnets.

The halo particle-loss distributions along the beamline as a function of dipole and quadrupole strength instability with (1) an individual power supply for each magnet and with (2) a common power supply for several magnets are shown in **Figure 3-2**. The resulting distribution is a sum of 100 distributions for independent random values of magnet strengths in the line. The 360π mm-mrad amplitude corresponds to 10.4σ=13.2 mm at the baffle. For an aperture radius of 7.5 mm, the baffle intercepts ~15 kW of power from beam halo.

Figure 3-3 shows a 3σ beam population and distributions at the baffle (left), and at the Far Detector located 1,300 km distant from the target (right) for a dipole power-supply instability of dB/B=±0.0001, ±0.0003, ±0.001 and ±0.002. Calculations are done for assuming a common power supply for several magnets with instabilities as follows: LBNE quadrupole, dG/G=±0.001; extraction kicker, dB/B=±0.005; Lambertson magnet, dB/B=±0.002; MI quadrupoles, dG/G=±0.001; and MI closed-orbit, dA=±1$\sigma_{x,y}$ or ±1.3mm. It is assumed in these calculations that there is no proton-beam interaction with matter in the target and in the ground downstream of it. Beam distributions are shown for 100 independent, random distributions of magnet strength deviations. The beam spot size is $\sigma_{x,y}$ > 30m in the far detector at dB/B=±0.0004.

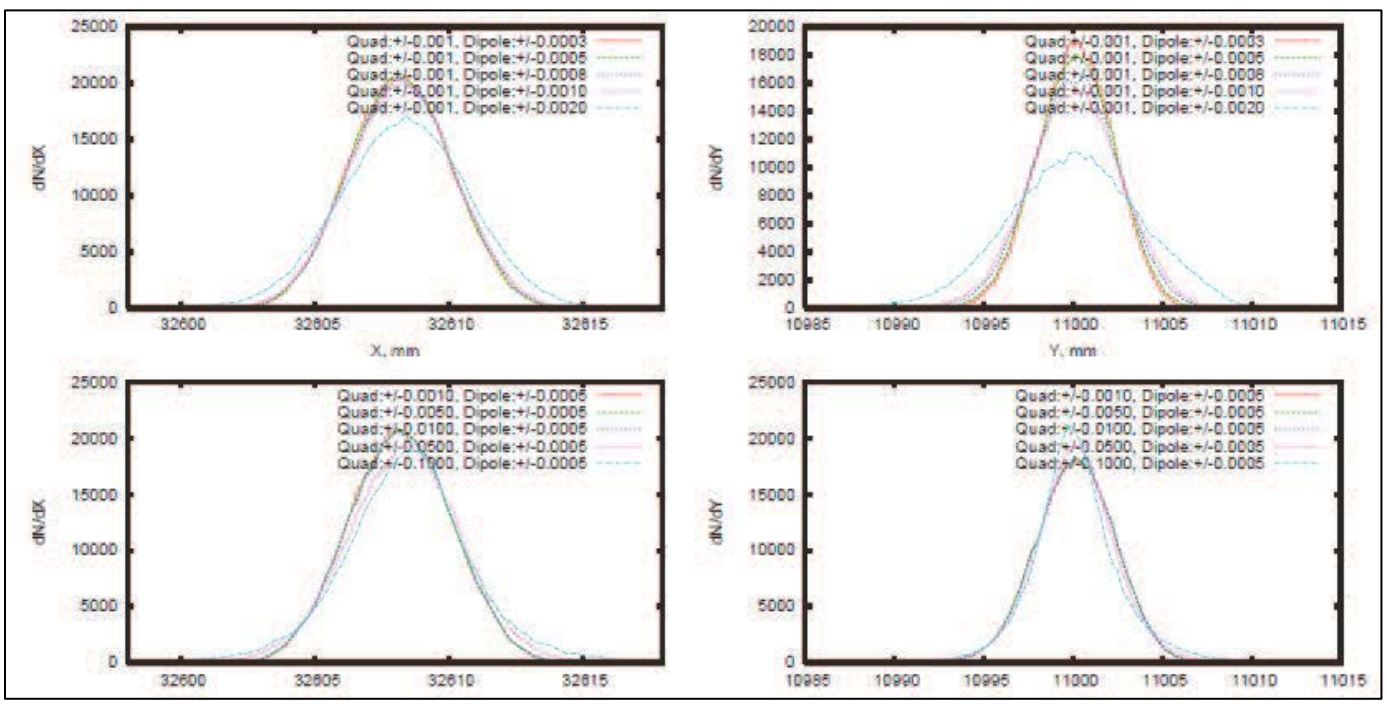

Figure 3-1: Horizontal (Left) and Vertical (Right) Beam Distributions at Baffle Entrance as a Function of Dipole (Top) and Quadrupole (Bottom) Power Supply Instability

The halo and core beam losses along the primary beamline and at the baffle as a function of dipole magnet power-supply instability with a common power supply for several magnets are presented in

Figure 3-5. NuMI operates now at 0.4 MW with maximum allowed fractional beam loss of 10^{-5} from the total intensity. For LBNE's 0.7 MW, the safety level will be 5 x 10^{-6}, and for 2.3 MW it will be 1.5 x 10^{-6}. To have a viable operational margin, the goal is to keep normal beam loss an order of magnitude better than this, or 5 x 10^{-7} for 0.7 MW and 1.5 x 10^{-7} for 2.3 MW, that is ~0.4W. From this point of view, the dipole instability should be less than dB/B<±0.0025, which keeps losses below 1 W/m.

3.12.1.3 Accidental Total Beam Loss

An accidental total beam loss will likely cause component heating and damage, may induce groundwater activation and cause radiation concerns outside the tunnel. The lost-beam trajectories along the beamline due to an accidental degradation of bending-magnet strength have been calculated and are shown in **Figure 3-5**.

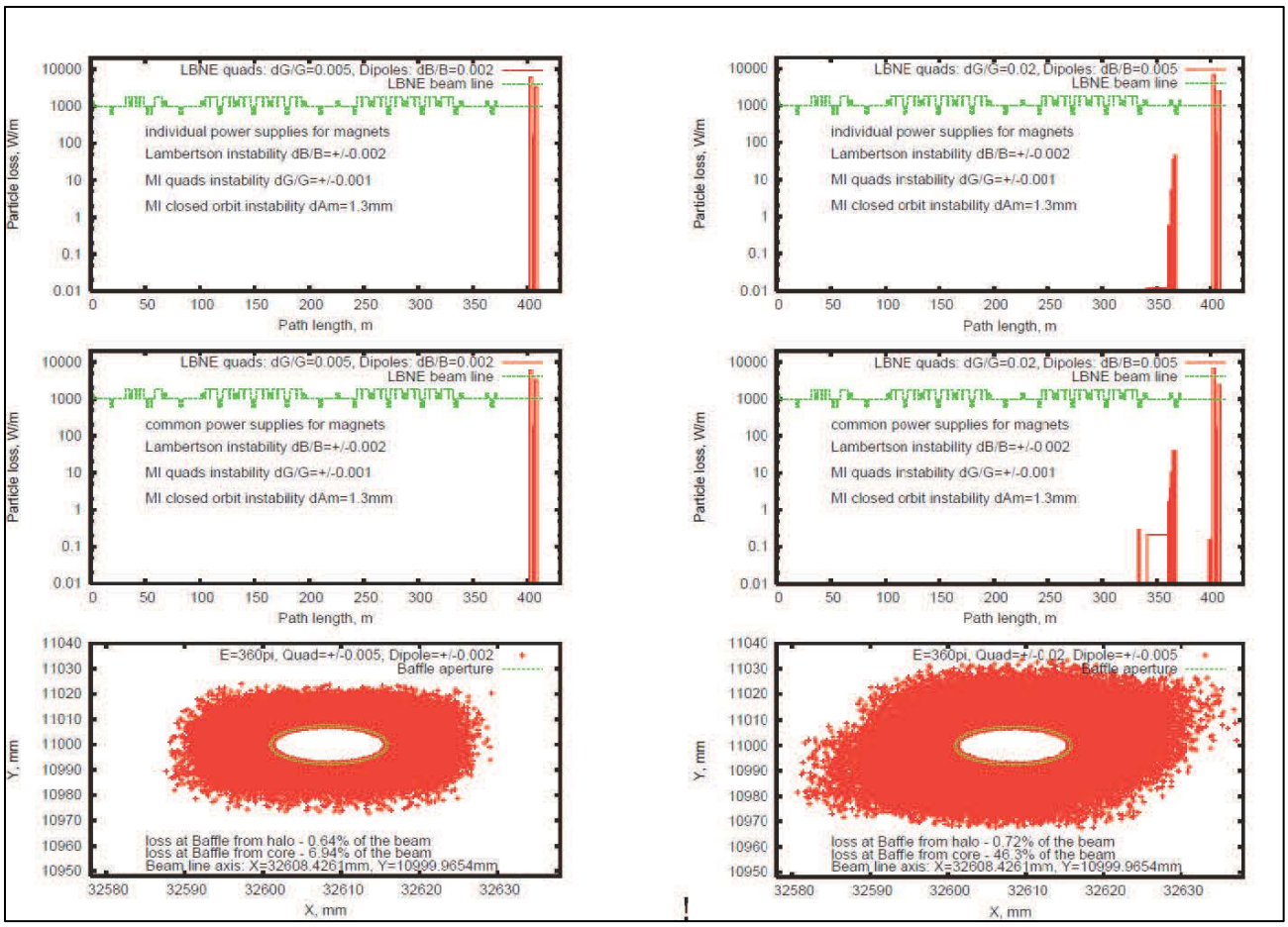

Figure 3-2: The Halo Particle Loss Distribution Along the LBNE Beamline at Dipole Strength Instability of dB/B=±0.002 (left), dB/B=±0.005 (right) and Quadrupole Strength of dG/G=±0.005 with Individual Power supply for Each Magnet (top) and with Common Power Supply for Several Magnets (second line). Beam Loss Population at the Baffle is Shown on the Bottom.

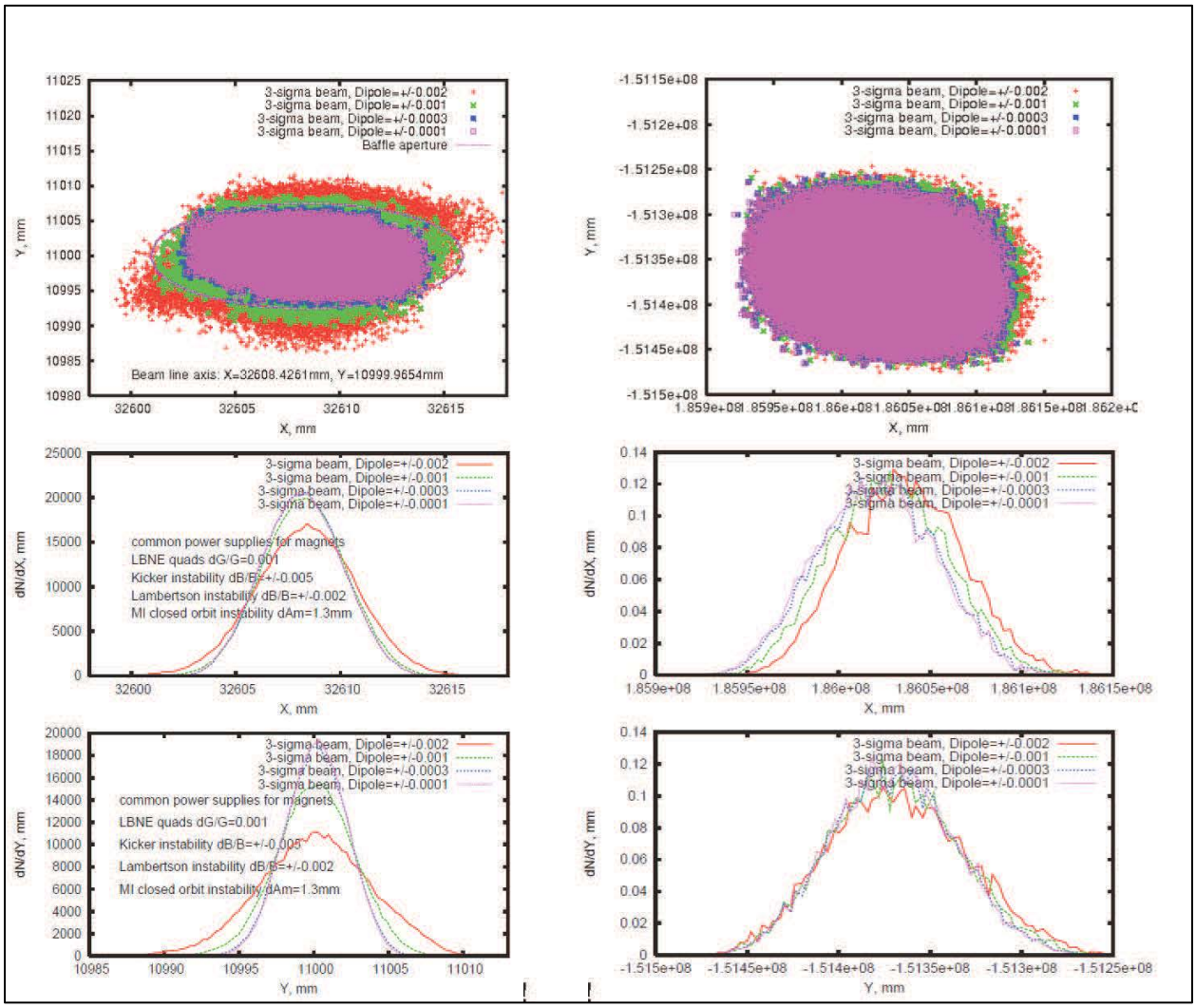

Figure 3-3: The 3*σ* Core Beam Population (Top) and Distributions (Middle and Bottom) at the Baffle (Left), and at the Far Detector (Right)

The instantaneous temperature rise in a dipole-magnet beam pipe (see **Figure 3-6),** following the loss of the entire beam (2.3 MW), is ~ 2500 K, which is a factor of two higher than the melting point of stainless steel. The beam vacuum pipe or a magnet would be effectively destroyed in one beam pulse (or a few pulses at 708 kW). This possibility must be eliminated by analyzing all parameters of the system just before extraction, and then abort the beam to the MI beam dump if any critical parameter is out of the safety region (for details of the LBNE beam-permit system see Section 4.3).

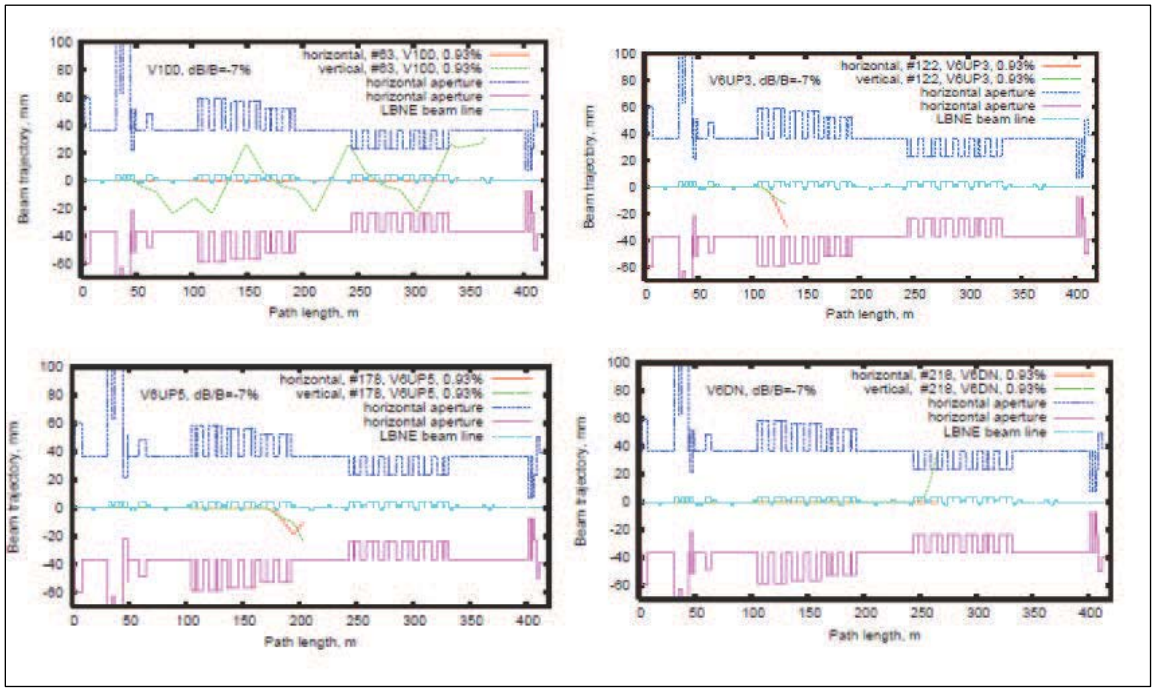

Figure 3-4: An Example of Beam Trajectories Along the Beamline for a Beam Lost Due to Accidental Degradation of Bending Magnet Strength

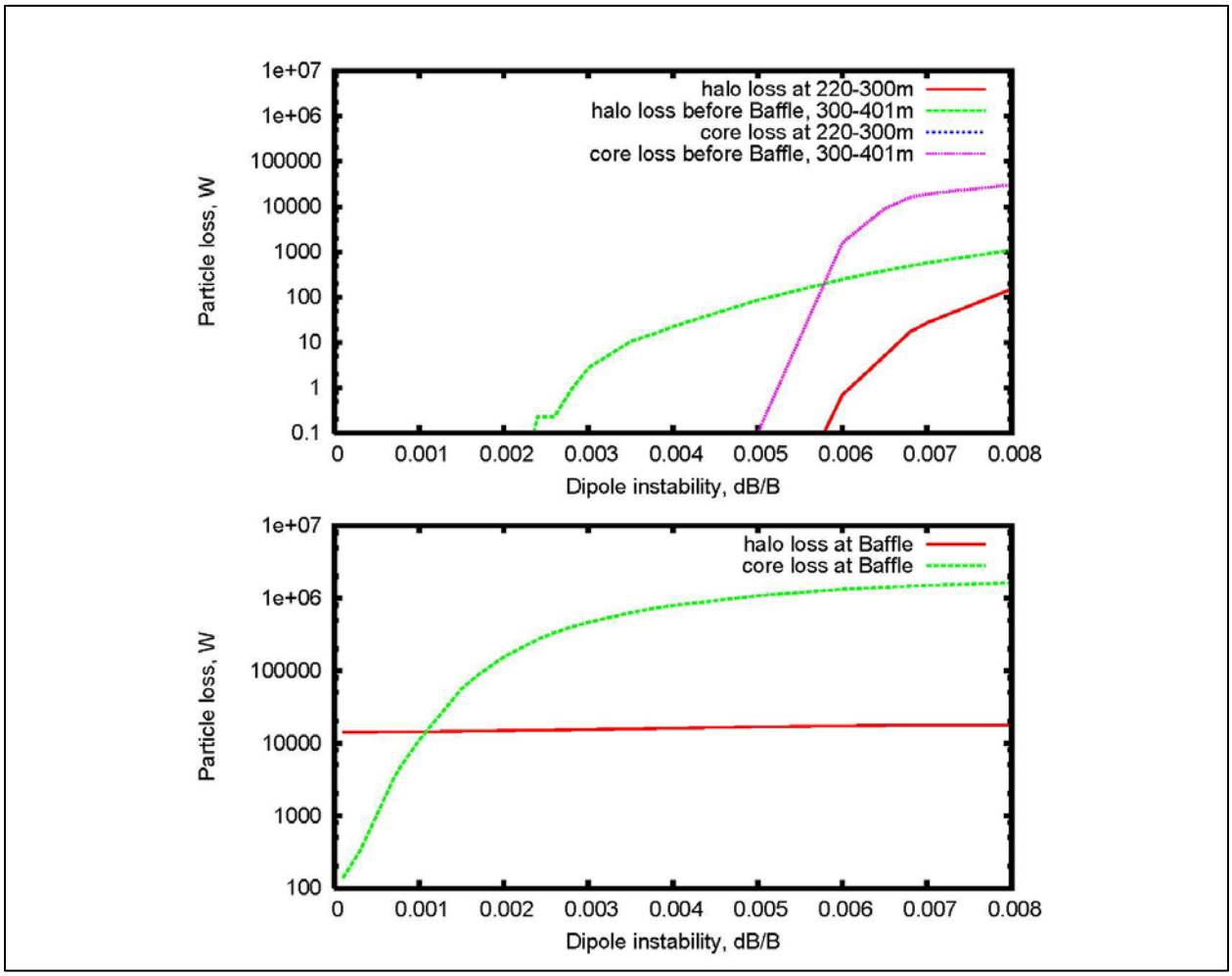

Figure 3-5: The Halo and Core beam loss at 120 GeV along the LBNE Primary Beamline (Top) and at the Baffle (Bottom) as a Function of the Dipole Magnetic Power-supply Instability with Common Power Supply for Several Dipoles

3.12.1.4 Activation of Components

Beamline-component activation is a critical issue in a high-intensity beamline whose operational life is measured in decades. A sample case is presented here, where 0.3% of a 2.3 MW beam is lost continuously, as the outer-most part of the beam envelope interacts with the vacuum pipe, magnets and other installed components. The magnitude of this loss is chosen to be typical of what one might have anticipated in lower-intensity beamlines of the past. Of course for LBNE, this value is unacceptably high, but results from this study can be scaled to estimate tolerable losses. Residual dose rates for losses of 0.003 of total intensity for 30 days, followed by one day cool-down, is shown in **Figure 3-7.** Residual dose rates on the surfaces of bending and quadrupole magnets reach 50 rem/hr, which is three orders of magnitude higher than the goal of less than 50 mrem/hr. Scaling these results to acceptable limits implies that losses need to be no greater than order 10^{-6}. The methods proposed to achieve this are listed in Section 6.4.

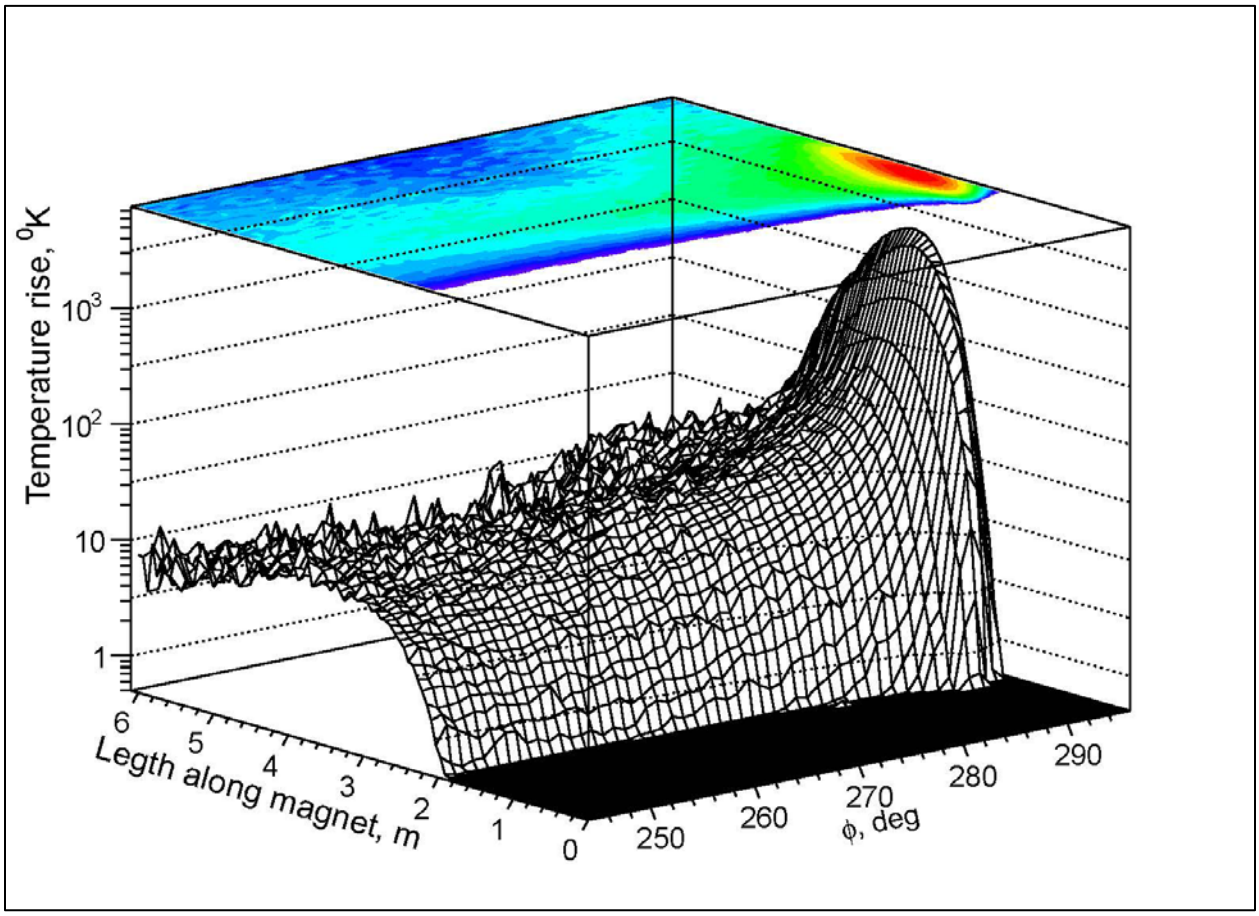

Figure 3-6: An Instantaneous Temperature Rise Along and Across the Dipole Magnet Beam Pipe at Accidental Loss of Entire Beam

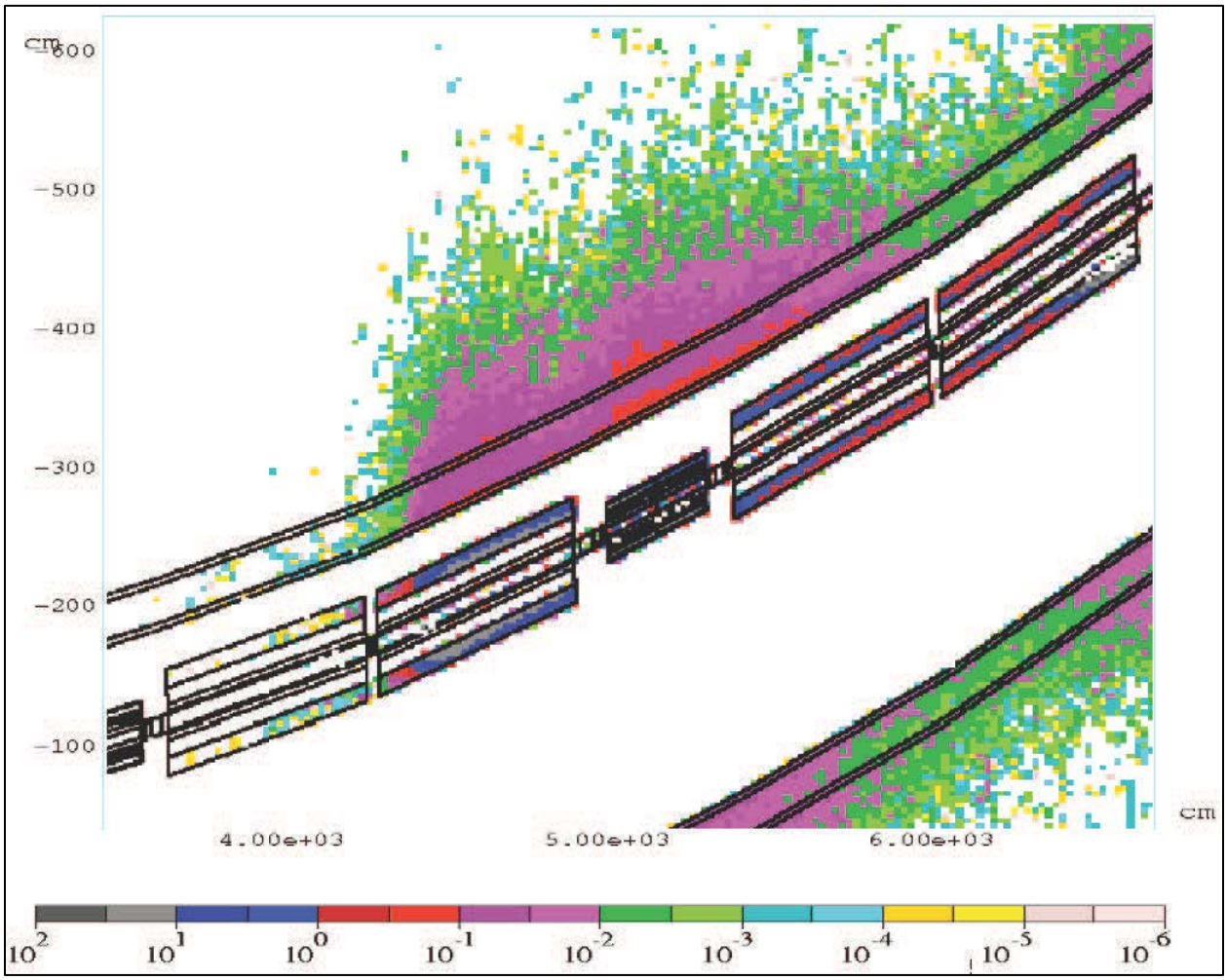

Figure 3-7: Residual Dose Rates along the Beamline and Magnets. Following a loss of 0.3% of the beam for 30 days followed by one day cool-down. The color-coded logarithmic scale has units of m-Sv/h (1 m-Sv/h is equivalent to 100 mrem/h).

3.12.2 Neutrino Beam Modeling

3.2.1.1 Introduction

This section describes the simulation of the neutrino beam and its effects on nearby materials using software models. All simulations of activation, dose rates and beam energy deposition use the MARS package. The MARS model of the reference design will describe the target, horns, decay pipe and absorber, as well as all of the shielding. In particular, MARS will be used for estimating:

- Beam-energy deposition in components, required for engineering considerations and estimating cooling capacities
- Prompt (beam-on) dose rates within halls outside of shields

- Residual dose rates from components within or outside shielding
- Radionuclide production in components, shielding and rock

3.2.1.2 3.12.2.2 Design Considerations

The level of detail in the model will follow the reference design as it evolves. The model already provides a basis for estimating the total thickness of shielding needed. Later, for example, as the block size and stacking pattern become set in the design, these details will be incorporated into the model. Thus, the effect of voids or cracks, which are small in a good design, will be studied at a later time. An estimate for the locations of excavated rock boundaries is needed for estimating tritium production and groundwater concentrations.

The composition of materials used in the MARS model needs to match that of the design materials to the known accuracy. The atomic mass fractions are usually sufficient for the simulations. Items to be modeled include rock, shielding materials and the materials incorporated into technical components. Components present in an engineering design or plan whose effect is negligible, e.g., bolts, will not be included.

3.2.1.3 3.12.2.3 Reference Design

A realistic MARS model has been built for the LBNE target, horns, target station and its shielding, decay pipe and tunnel shielding, and the hadron-absorber system. In the model as in the conceptual design, the proton beam is tilted down by 101 mrad, and the target station and decay channel follow this tilt while the hadron-absorber system is arranged horizontally. The hadron-absorber system includes an aluminum mask that protects the water cooling pipes, a 2.4-m long aluminum core followed by a 2.7-m long iron core surrounded by massive iron shielding in a concrete shell, all in an 18-m long service building. Horn magnetic fields and all details of geometry and materials distributions are included in the model.

In the reference model, a 120-GeV proton beam hits a 0.95-m long cylindrical graphite target at an intensity of 8.0×10^{13} protons per pulse (1.2 MW). 60-GeV and 80-GeV cases are also being considered. We model in great detail both 1.2-MW and 2.4-MW normal operation 1.33-s repetition rate, 8.1×10^{13} and 1.7×10^{14} sec^{-1}, respectively) as well as an accident scenario. The latter is a 3.07-MJ beam accident ("target destroyed"), in which a proton beam interacts with 1-atm helium in the decay pipe and hits the absorber. Substantial modeling efforts are being conducted in the primary-beamline and baffle areas.

MARS is used to calculate energy deposition (peak values and total dynamic heat loads), integrated absorbed dose and residual activation in all the system components (target, horns, decay pipe, shielding, all the components of the hadron absorber, etc.), prompt-dose-equivalent distributions in and out of the service buildings, and radiation load on groundwater and air outside the shielding. These calculations will help in the design of optimal subsystems (target station, decay channel and hadron absorber) and will aid in the evaluation and minimization wherever possible of residual dose levels. They

will also help optimize hands-on maintenance conditions, keep impact on the environment below the regulatory limits, and estimate and maximize wherever possible the component lifetime.

4 NEUTRINO BEAM (WBS 130.02.03)

4.1 Introduction

This chapter discusses the conceptual design of the second main system within the LBNF Beamline, the Neutrino Beamline, which refers to the set of components and enclosures designed to efficiently convert the initial proton beam into a high-intensity neutrino beam aimed at the far detector, 1,300 km away.

The LBNF neutrino beam would be the fourth large neutrino beam facility designed and built at Fermilab. Its design is very similar to the NuMI beam constructed in 2004 [?]. All major elements of the LBNF design have their analogs in the NuMI beamline. Thus, the experience gained in constructing and operating the current facility can be incorporated into LBNF design as improvements. The LBNF neutrino beam must necessarily be of even more robust design since the beam power is expected to be 1.2 MW at start-up, and increasing after some years of operation to 2.4 MW. For most elements, the increased capacity will be met by incremental improvements and replacement strategies.

A proton-beam pulse from the primary-beam system enters the neutrino beamline system (from the left in **Figure 4-1** and **Figure 1-2**.) through a beryllium “window.” This window seals off the evacuated beam pipe of the primary beamline, and the protons enter the air-filled target chase (the volume surrounding the target and focusing mechanisms). Initially they pass through a small aperture in a 1.5-m-long graphite cylinder, called a baffle, which protects equipment downstream from mis-steered beam. Sixty-eight cm past the end of the baffle, they reach the target, a long, thin set of graphite segments in which about 85% of the protons interact and produce secondary particles. The target is surrounded by the first horn, a magnetized structure which provides initial focusing for the secondary particles, predominantly pions and kaons. A second horn, a few feet downstream, provides additional focusing for the secondary particles before they enter a He-filled decay pipe, where a large fraction of the pions will decay to neutrinos, forming the neutrino beam. The final portion of the neutrino beamline is the absorber, downstream of the decay pipe. The absorber is intended to stop the protons that failed to interact in the target and the secondary particles that failed to decay to neutrinos; it must be designed to sustain the beam energy deposition under expected normal operational conditions as well as under accident situations.
Section 2.3 presents a more thorough introduction to the Neutrino Beamline.

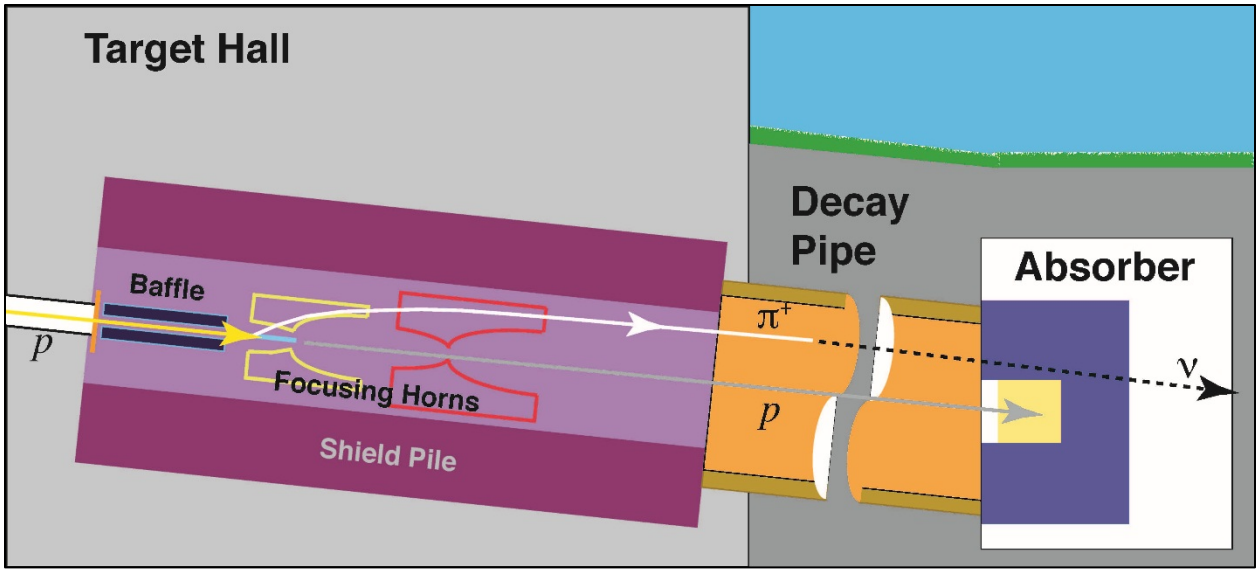

Figure 4-1: A Cartoon of the neutrino beamline showing the major components of the neutrino beam. From left to right, the beam window, horn-protection baffle, target, the two toroidal focusing horns, decay pipe and absorber. The air volume surrounding the components between the window and the decay pipe is called the target "chase". The target chase and rooms for ancillary equipment (power supplies, cooling, air recirculation and so on) is included in the area called the target complex (not shown in picture).

4.1.1 Design Considerations

Primary design considerations include the need to provide a wide-band beam to cover the first and second neutrino-oscillation maxima and the need to plan for an eventual upgrade in incident primary beam power from 1.2 MW to 2.4 MW without retrofitting.

The designs for the neutrino beam components detailed in this Chapter are appropriate for a primary beam energy range from 120 GeV down to 80 GeV/c. Most of the components have already been shown to be viable for a primary beam energy down to 60 GeV, and the analysis is ongoing for the remaining ones.

All neutrino beam subsystems have been designed for 1.2 MW beam power. Subsystems which are difficult or impossible to upgrade to a higher beam power have already been designed for the potential beam power upgrade to 2.4 MW. These include the target pile, the decay pipe and the absorber as well as the main elements of the associated cooling systems.

Radiological concerns, such as prompt dose, residual dose, air activation and tritium production are also important considerations. They have been extensively modeled, and these issues have been addressed in the system design.

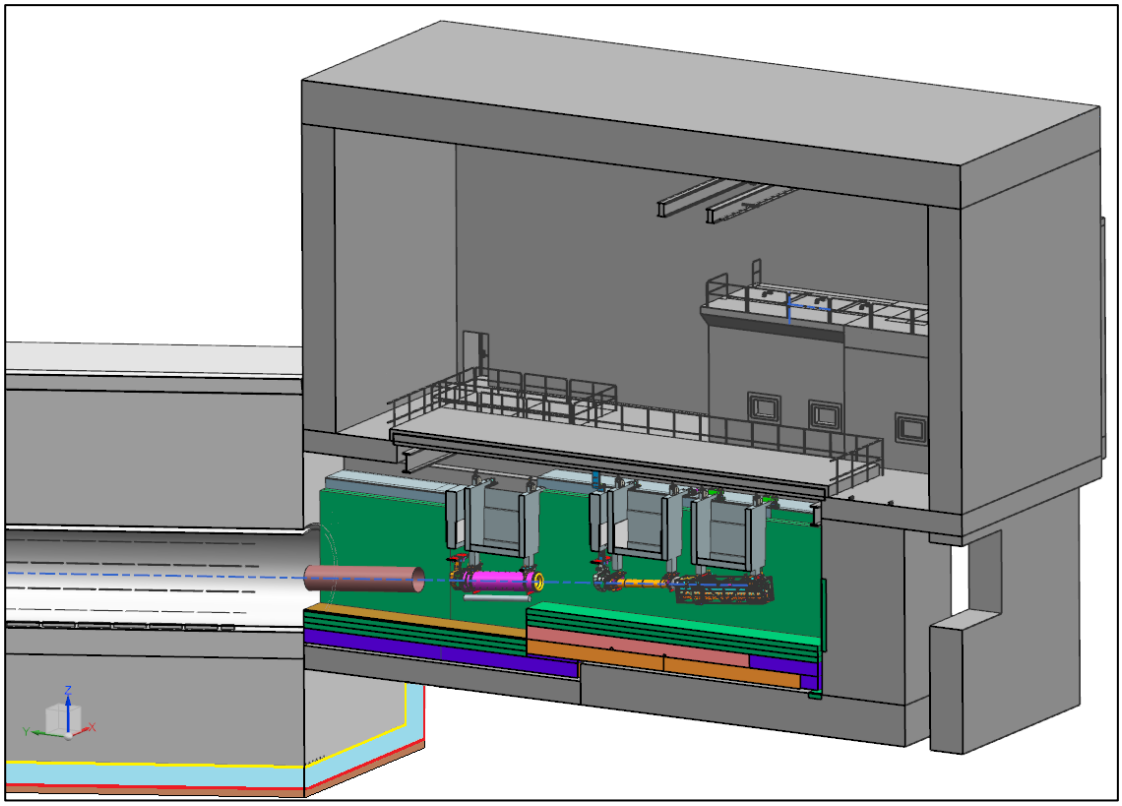

Figure 4-2: Schematic of the upstream portion of the LBNF neutrino beamline showing the major components of the neutrino beam. The target chase bulk steel shielding is shown mainly in green. Inside the target chase from right to left (the direction of the beam) pointing downwards: the beam window, horn-protection baffle and target mounted on a carrier, the two toroidal focusing horns and the decay pipe. Above the chase and to the right is the work cell for horn and target system repairs. The beige areas around the decay pipe indicate concrete shielding. The yellow and red lines indicate multi-ply geosynthetic barriers, separated by a drainage layer (blue).

4.2 Neutrino Beam Modeling

This section describes the simulation of the neutrino beam and its effects on nearby materials using software models. All simulations of activation, dose rates and beam energy deposition use the MARS package. The MARS model of the reference design will describe the target, horns, decay pipe and absorber, as well as all of the shielding. In particular, MARS will be used for estimating:

- Beam-energy deposition in components, required for engineering considerations and estimating cooling capacities
- Prompt (beam-on) dose rates within halls outside of shields
- Residual dose rates from components within or outside shielding
- Radionuclide production in components, shielding and rock

4.2.1 Design Considerations

The level of detail in the model will follow the reference design as it evolves. The model already provides a basis for estimating the total thickness of shielding needed. Later, for example, as the block size and stacking pattern become set in the design, these details will be incorporated into the model. Thus, the effect of voids or cracks, which are small in a good design, will be studied at a later time. An estimate for the locations of excavated rock boundaries is needed for estimating tritium production and groundwater concentrations.

The composition of materials used in the MARS model needs to match that of the design materials to the known accuracy. The atomic mass fractions are usually sufficient for the simulations. Items to be modeled include rock, shielding materials and the materials incorporated into technical components. Components present in an engineering design or plan whose effect is negligible, e.g., bolts, will not be included.

4.2.2 Reference Design

A realistic MARS model has been built for the LBNE target, horns, target station and its shielding, decay pipe and tunnel shielding, and the hadron-absorber system. In the model as in the conceptual design, the proton beam is tilted down by 101 mrad, and the target station and decay channel follow this tilt while the hadron-absorber system is arranged horizontally. The hadron-absorber system includes an aluminum mask that protects the water cooling pipes, a 2.4-m long aluminum core followed by a 2.7-m long iron core surrounded by massive iron shielding in a concrete shell, all in an 18-m long service building. Horn magnetic fields and all details of geometry and materials distributions are included in the model. Two examples of the level of detail in the model of the first horn are shown in Figure XXX3 and Figure XXX4.

In the reference model, a proton beam hits a 0.95-m long cylindrical graphite target at an intensity of 7.5×10^{13} [1.5×10^{14} future high-power operation] protons per pulse for all energies from 60 to 120 GeV, with repetition rates of 0.7, 0.9 and 1.2s for 60, 80 and 120 GeV, respectively. The corresponding power levels of the proton beam are 1.03 [2.06], 1.07 [2.14] and 1.20MW [2.40 MW]. Accident scenarios are also simulated with a 2.4MW beam. This includes a 5.8-MJ beam accident ("target destroyed"), in which a proton beam interacts with 1-atm helium in the decay pipe and hits the absorber (Sec. 3.9). Substantial modeling efforts are being conducted in the primary-beamline and baffle areas.

MARS is used to calculate energy deposition (peak values and total dynamic heat loads), integrated absorbed dose and residual activation in all the system components (target, horns, decay pipe,

shielding, all the components of the hadron absorber, etc.), prompt-dose-equivalent distributions in and out of the service buildings, and radiation load on groundwater and air outside the shielding. These calculations will help in the design of optimal subsystems (target station, decay channel and hadron absorber) and will aid in the evaluation and minimization wherever possible of residual dose levels. They will also help optimize hands-on maintenance conditions, keep impact on the environment below the regulatory limits, and estimate and maximize wherever possible the component lifetime.

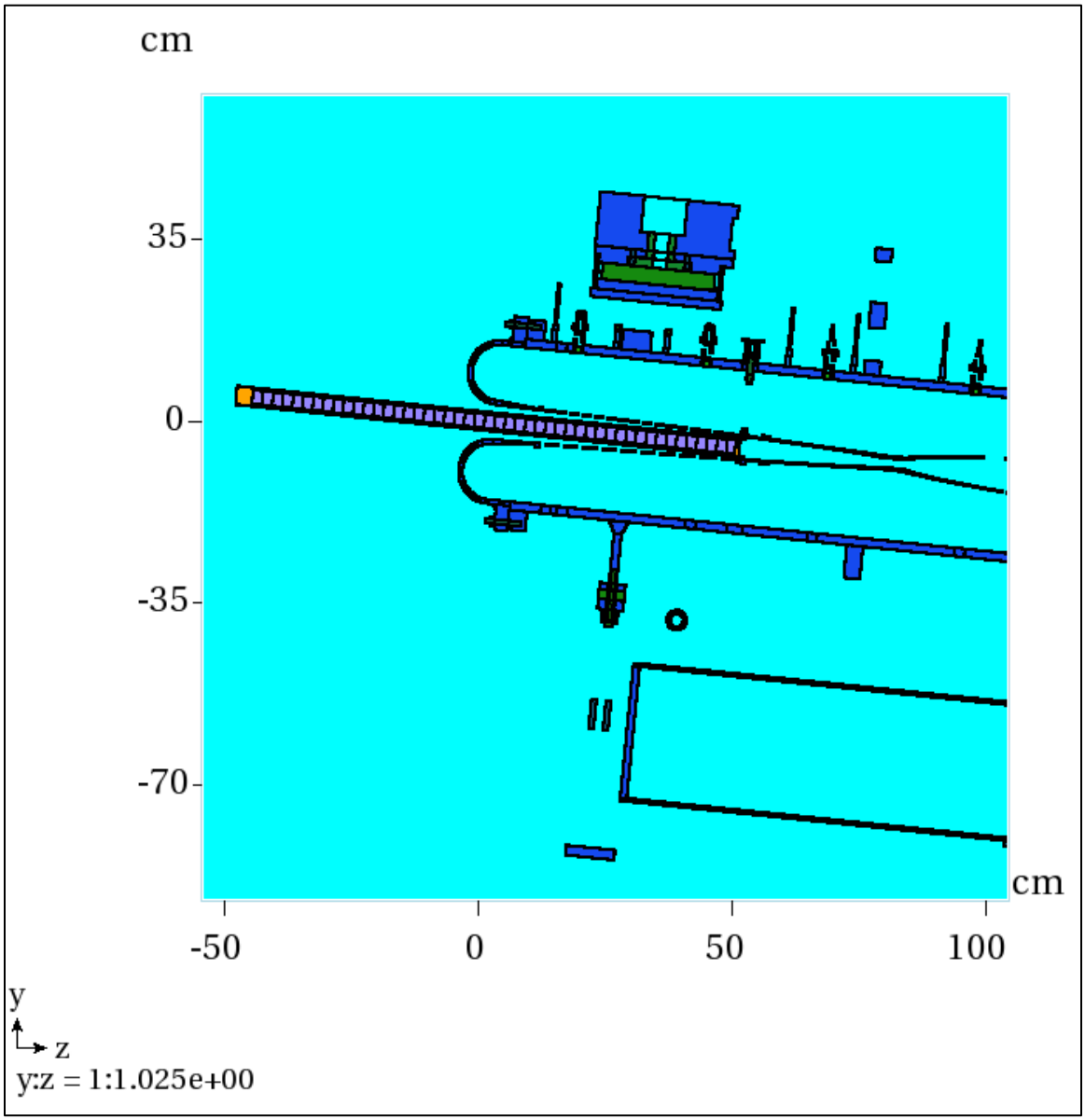

Figure 4-3: An Example of the MARS Model Detail. The Graphic Shows Upsteam End of the First Horn with the Graphite Target Inserted at Nominal Position.

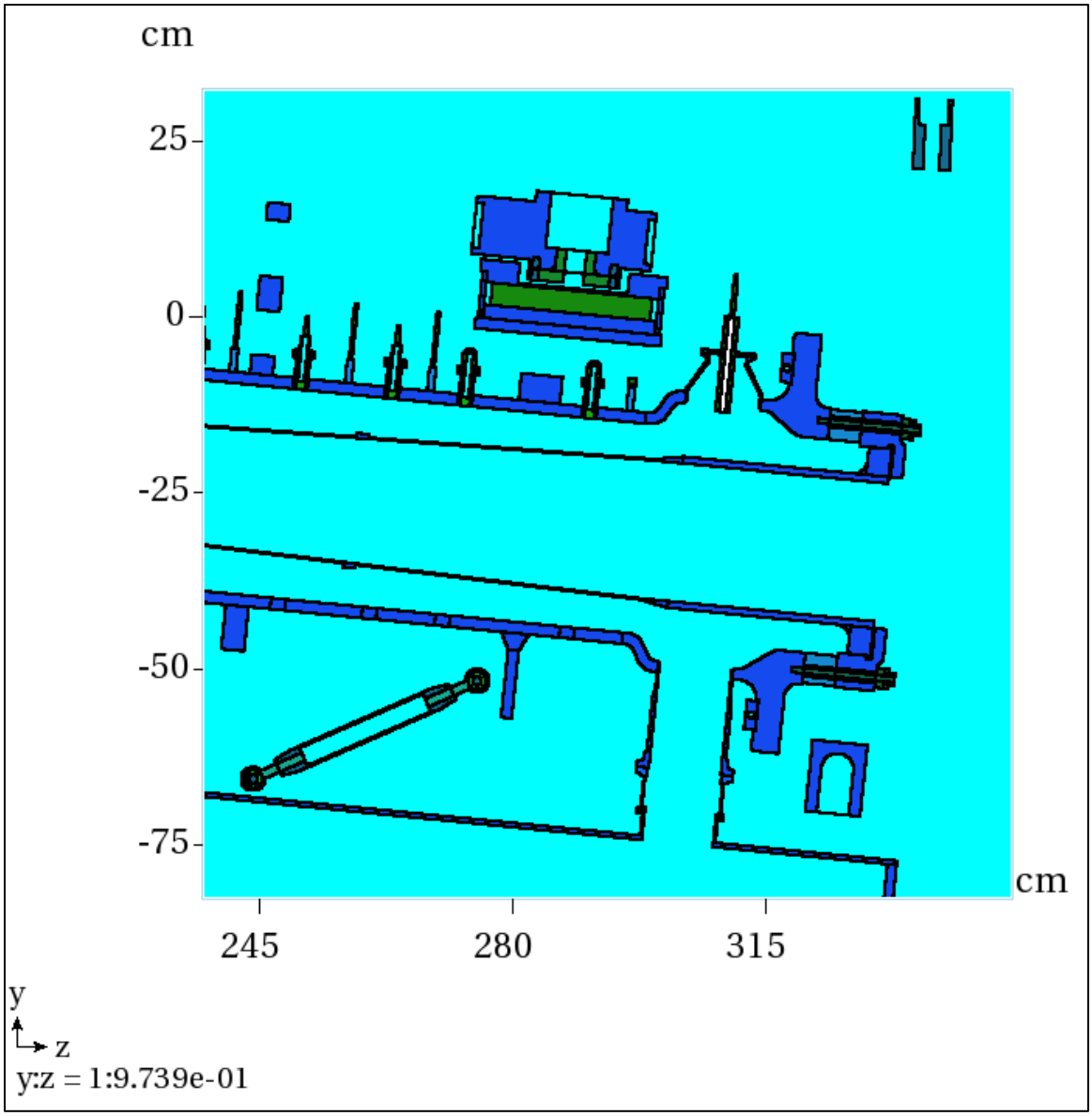

Figure 4-4: A Section of the MARS Model for the Downstream Part of the First Horn. Water Cooling Spray Nozzles are Along the Top of the Outer Conductor and the Drain with Reservoir are Below the Horn.

4.3

4.3.1

Targetry (WBS 130.02.03.03)

Introduction

This section details the neutrino-production target and the accompanying instrumentation for commissioning, alignment and monitoring of the target and focusing system in the beam. Also, the support structures and horn protection baffle are detailed here. The target is the source for the pions and kaons which later decay to produce neutrinos. Although the production of these particles may be

increased with more beam power, engineering and material properties place a limit on beam power for a practical target. These practical concerns include removing beam heating, withstanding thermal shock, and resisting radiation damage. Target replacement strategies also play a role in design. For LBNF, a conceptual design for a target operating at 1.2MW is given, which has adequate margins for reliability in this regime. Research and development of target designs is also pursued, with the goal of greater longevity and reliability.

The LBNF target is substantially based on the NuMI target design which has operated since 2005, with some modifications to accommodate higher beam power. The target core is graphite segmented into short rectangular segments oriented vertically, with the short dimension horizontal to the beam. The heat from the core is removed by dual titanium water lines brazed to the top and bottom of the graphite. The entire assembly is encased within a titanium containment tube. The segments are 10 mm in width and 20 mm in length. A total of 47 segments, spaced 0.2 mm apart, result in a total target core length of 95 cm, corresponding to two interaction lengths. Drawings of the target are shown in Figure 3-3 and Figure 3-4. The target will be cantilevered into the horn and inserted via a carrier similar to that used in NuMI which also carries the baffle.

During the initial commissioning of the beam, the Target and Horns Instrumentation (THI) discussed in Section 3.3.5, will be used to establish that the components and systems are working and will allow a beam-based alignment of their positions. Later, the instrumentation will be used to re-commission the beam whenever major components (e.g., targets, horns) are replaced. The instrumentation will also perform long-term monitoring of the beam properties to provide signs of degradation or failure.

4.3.2 Design Considerations

The neutrino-production target design is determined by balancing the ideal production of mesons for neutrino production and the survivability of the device for tens of millions of beam pulses. The target must have the following features:

- Adequate material to convert the protons into mesons, while not absorbing too many of the produced particles
- The ability to withstand the instantaneous thermal and mechanical shocks due to the beam
- The ability to withstand the sustained thermo-mechanical stresses and temperatures
- A cooling system to remove the heat deposited by the beam interaction (approximately 40 kW, or 3% of the beam energy)
- Resistance to the effects of radiation damage so as not to encounter substantial change in mechanical properties during the run

These considerations lead to a long, thin target design, for which the exact length must be determined by optimization of the entire beamline, but is approximately two nuclear-interaction lengths (1 m for materials with density ~2 g/cm^3. The target width must be sufficient to cover the beam spot, but is otherwise minimized, except for the practical concerns of heat removal and mechanical integrity. The primary target material must have high mechanical strength, high specific heat, high thermal conductivity, a low coefficient of thermal expansion, and good radiation properties. Although a number

of single-element materials generally fit the above requirements, the two materials best fitting those parameters for neutrino beams are beryllium and graphite. Their properties are listed in Table 3-1.

Target longevity is a major issue for the performance of the LBNF facility. Graphite, the material used in the NuMI target, has been adopted as the LBNF reference-design target material, but alternatives are under study. Whereas the NuMI target performance has been on-the-whole successful, a total of six targets have failed or shown deterioration in the neutrino-production rate over a span of months.

Each of these incidents caused operational and experimental complications, required beam downtime for repairs or replacements, or led to a slow decrease in production efficiency.

Table 4-1: Material Properties of Graphite and Beryllium

	Graphite (POCO ZXF-5Q)	Beryllium (S-65C)
Apparent density	1.81 g/cc	1.82 g/cc
Compressive Strength	195 MPa	260 MPa
Tensile Strength	90 MPa	370 MPa
Modulus of Elasticity	12.5 GPa	310 GPa
Thermal Conductivity	70 W/m/K	200 W/m/K
Coefficient of Thermal Expansion	8.1 um/m/K	10.7 um/m/K
Specific Heat	710 J/kg/K	1770 J/kg/K

Features of the NuMI target were changed in later-series targets to improve lifetime. These improvements were in the cooling lines or other parts of the target assembly that were identified as potential weak points. Further features of the LBNF target are under study to reduce the failure and degradation rates. The primary target material, however, has not yet been modified and is the subject of R&D within LBNF.

Regarding the target's mechanical properties, deviations in size, shape or density of a few percent will impact the experiment's measurement capabilities. The source of these changes can be structural damage (change in material strength leading to disintegration), direct decomposition of the material (radiolysis), oxidation of the material, swelling, contraction, and other changes.

The primary target material must be integrated into a structure that provides cooling, structural integrity and environmental isolation. For LBNF, the target is positioned within the upstream portion of the horn to preferentially focus low-energy pions; this configuration has been used in NuMI and other neutrino beams. A position within the horn adds two complications: 1) the horn focuses some secondaries back into the target, increasing the heat load; and 2) the target must be supported either

through cantilevering or contact with the horn conductor. The outer target structure provides either the stiffness for the cantilever or the interface with the horn inner conductor. Typically, the simplest solution is cantilevering the target.

Reference Design

The reference target design for LBNF is an upgraded version of the NuMI-LE target that was used for seven years of beam delivery to the MINOS experiment. The NuMI-LE target (NT series) was designed for
4.3.8 400-kW beam power. This new LBNF design takes advantage of some of the work done for the 700 kW ANU-NOvA target (MET series) that has been used in NuMI since 2013, as well as R&D done towards making the NuMI-LE target more robust. We are designating this target series LT. Figure 3-3 and Figure3-4 show the new target design.

The target material is POCO graphite ZXF-5Q. The target consists of 47 segments, each 2 cm long. Including the space between segments, the total length of the graphite core is 95 cm. The segmentation is to prevent buildup of stress that would be found in a single long segment. The graphite segments are 10 mm wide in the horizontal (transverse to the beam) plane. They are brazed to water cooling tubes at the top and bottom of each segment; the distance between the edges of the water cooling tubes. The cooling tubes have two parallel loops that run side-by-side across the top and bottom of the target to accommodate the increased heat deposition (as composed to the single loop for NuMI). The top and bottom of the graphite segments are sculpted to the radius of the cooling tubes; the vertical edges of the graphite are rounded to prevent stress buildup in corners. The graphite is in helium gas, slightly above atmospheric pressure. The inert atmosphere prevents oxidation of the graphite. Helium helps to cool the outer containment tube, transporting heat to the water cooling tubes.

The NUMI LE target was designed for 4×10^{13} protons per pulse; this will increase to 7.5×10^{13} for LBNF 1.2 MW beam power. Design studies calculated the stress in the graphite segments at these intensities. The results of this study indicate that increasing the beam spot size from the 1.0 mm RMS used in the original NUMI calculations to 1.7 mm RMS is adequate to address the issue of stress in the graphite for the more intense beam. Figure 3-XXX5 shows the equivalent stress developed in the graphite fin with the highest energy deposition density for 120 GeV beam energy (maximum stress is 10.5 MPa). This predicted peak stress is lower than the ultimate tensile strength of the graphite (80 MPa) by a safety factor of 7.6. For the case of the 80 GeV beam and a cycle time of 0.9 seconds, MARS energy deposition studies predict lower peak energy deposition density (about 14% lower) but a higher overall time averaged energy deposition per fin for about the first 17 upstream graphite fins (about 15% higher). Since the location of highest stress during a beam pulse is different from that of the steady state heating, the effect of the higher time averaged heating on the peak stress is actually quite low (estimated conservatively to be less than 5%). The net effect is that maximum stress in the worst fin is predicted to be about 10% lower for the 80 GeV beam case than for the 120 GeV beam case. Therefore the target design for 120 GeV beam is also safe for use at beam energies as low as 80 GeV, and most likely much lower.

The water tubes are 6 mm O.D. 0.4 mm wall titanium. The two tube loops inside the target can are made from single pieces of tubing; there are no joints or welds inside the helium vessel. The lack of

joints reduces the risk of water leaking into the helium vessel, which would be fatal to the target. The water tube bends to the side of the containment tube at the downstream end for water-turn-around, so that it is not directly in the path of the remnant proton beam.

The helium-containment tube around the target segments is 36 mm O.D. 0.4 mm wall titanium. The upstream and downstream windows are beryllium. The upstream window has a stainless steel flange. The rest of the upstream vessel is aluminum. Beryllium has been investigated as an alternative material for the containment tube. Fabrication difficulties and cost prefer a titanium tube, but some additional measures will be required to provide conduction to the cooling pipes. Furthermore, active cooling may be required for the downstream window.

The base plate of the helium containment tube provides the fixed mechanical reference for the target and is flanged to connect to the upstream portion of the target can. The base plate is stainless steel, and helium containment where the water-lines penetrate this plate is supplied by a compression fitting. The base plate also holds the helium supply tube. The target vessel will be evacuated before being filled with helium.

There are five aluminum rings spaced out along the graphite-plus-cooling-tube core to keep it aligned within the helium containment tube.

The target will be inserted into the horn by carrier system, described in Section 3.3.6. The carrier is supported by a module upstream of the horn module. Both the baffle and target are firmly fixed to the carrier. As a unit, the target and baffle can be moved into the horn and transversely moved for alignment and beam tests.

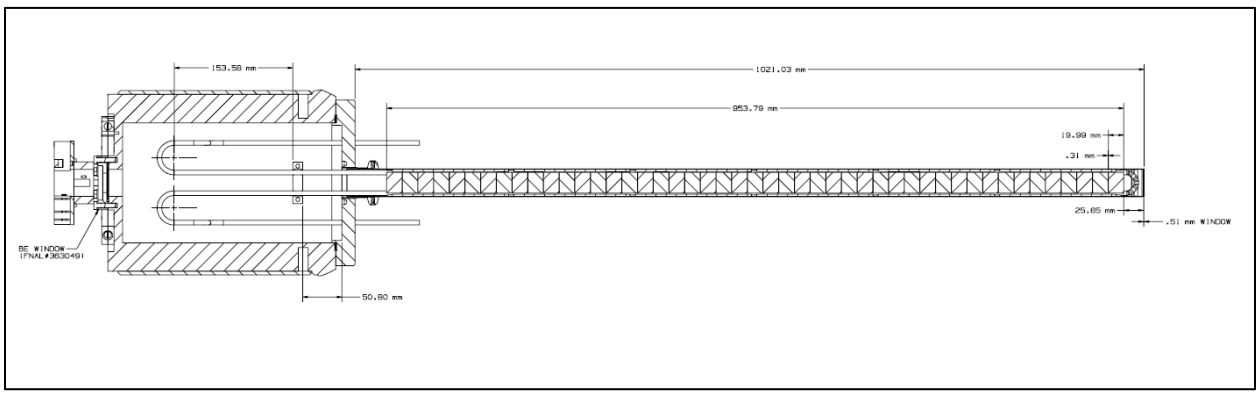

Figure 4-5: Proposed LT Target for LBNF. Beam Enters through the Beryllium Window on the Left, Encounters the Graphite Core, and Exits through the Beryllium Window on the Right. Units are Inches Unless Otherwise Noted.

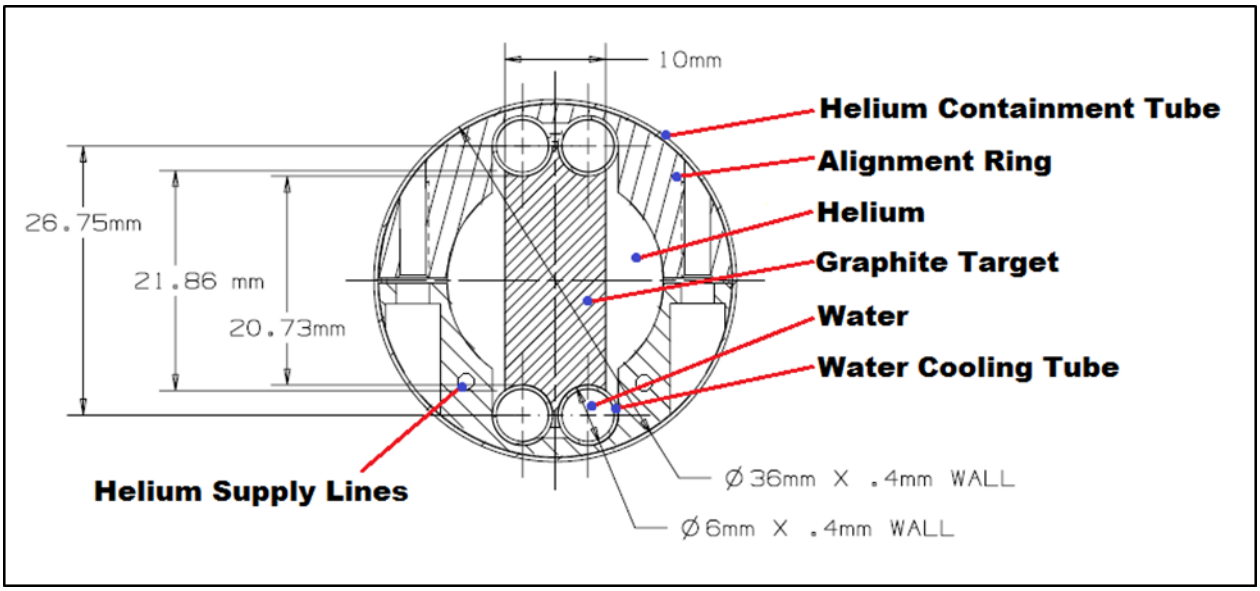

Figure 4-6: Cross-section of LT Target for LBNF. The Alignment Rings do not Run the Full Length of the Target. Units are mm.

One issue with water cooling is the near-instantaneous heating of the water. Water, being relatively incompressible, can produce large pressures when heated in a confined area. This is known as the "water hammer" effect. A straightforward calculation at 30° C suggests the pressure increase could be as much as 50 atm, although further study has indicated that the flexibility of the walls will reduce this factor substantially. While the pressure level itself is not of concern, the cyclic loading is. To ameliorate this problem, the plan is to introduce bubbles of a gas (probably helium) to dissipate the shock. Additionally, lowering the temperature of the water can reduce the water hammer effect, as water's coefficient of thermal expansion decreases at lower temperatures (zero at 4° C).

The LBNF target can be compared to the targets used or planned for the NuMI beamline. The MINOS target was inserted into the NuMI horn, but designed for a beam power of 400 kW. The MINOS target would be problematic in two ways at 1.2 MW beam power. (i) The downstream part of the outer aluminum tube that contains the helium atmosphere and holds the downstream beryllium window would overheat. (ii) At the current water flow rate, the increased differential temperature between the top and bottom water lines would increase the bending of the target between cool and operating conditions. To address these issues:

- The outer tube will be made from titanium instead of aluminum. The titanium can withstand much higher temperatures than the aluminum. Beryllium has also been investigated as an alternative.
- The water cooling lines will be made from titanium instead of the steel used for MINOS targets. Titanium has a lower coefficient of thermal expansion, so the allowable temperature rise of the cooling water is higher. The balance of the compensation is achieved by increasing the water

flow rate via increasing the water pressure differential and including two cooling lines.

Six out of seven MINOS targets have failed. The actual causes of failure are not understood in detail because the targets cannot be easily inspected due to residual radiation. At least five failures seem to result from weak points in the device itself: in the cooling lines or the exterior vessel. The other relevant failure is in the second MINOS target (NT-02). NT-02 had the greatest run period and showed a gradual degradation of neutrino production during its 6×10^{20} proton run. The degradation was not uniform in neutrino energy (consistent with various models) but amounted to 15% at the peak. NOvA has indicated that a 10% degradation would be an upper bound, and that 5% would be preferable. As such, target lifetimes of $4\text{-}5\times10^{20}$ protons or less must be considered, if the degradation mode cannot be addressed.

Although the larger beam spot size on target planned for LBNF may reduce the rate of degradation, the fact that the cause of degradation has not yet been identified motivates the need for some conservancy. Since the improvements identified to overcome the mechanical failures experienced in the MINOS targets are untried in service (titanium cooling lines brazed to the graphite fins; titanium outer tube cooling), assuming similar mechanical failure rates for the LBNF targets as for the MINOS targets is considered reasonably conservative. For MINOS, seven targets serviced $18\text{x}10^{20}$ protons. However, three of the targets suffered infant mortality due to poor water cooling tube welding and insufficient quality assurance. Subsequent improvements in both were demonstrated to be successful. Therefore, the expected lifetime based upon MINOS experiences is $4.5\text{x}10^{20}$ protons on target. For LBNF, taking into account both graphite degradation and mechanical failures, this implies approximately 2.5 targets per year will need to be replaced, and these replacements must be considered as part of the normal operation of the beam.

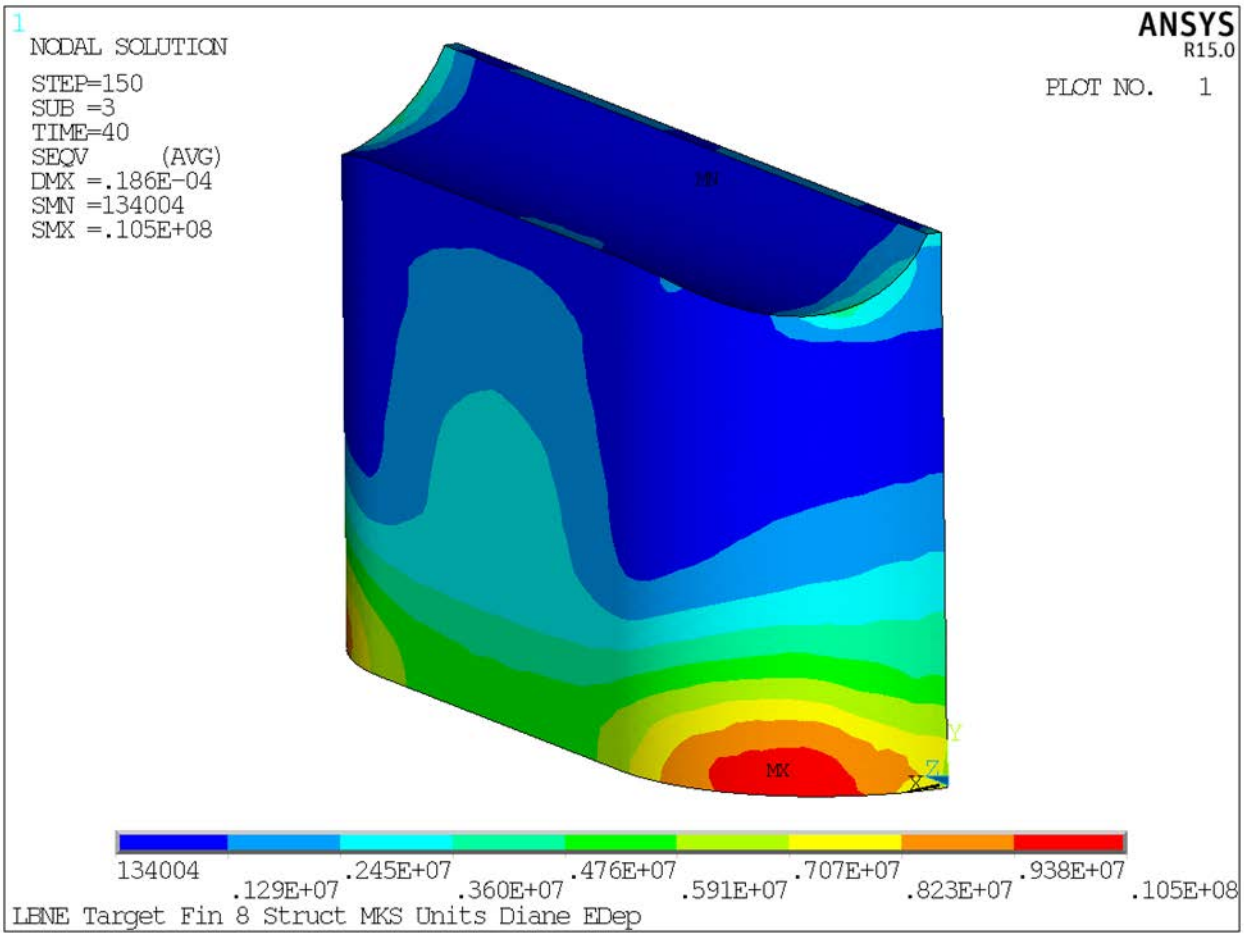

Figure 4-7: Equivalent Stress Developed in the Maximum Stressed Graphite Fin just after a Beam Pulse when Operating with 120 GeV, 1.2 Second Cycle Time, and 7.5E+13 Protons per pulse. Shown is a Quarter-symmetry Model with Beam Aligned with the z-axis.

The NOvA target was developed from a design for the MINOS medium-energy target. It is designed for 708 kW, but does not fit inside the horn, thus widening the design options. The NOvA 708-kW target makes use of long (70 mm) segments that connect to a cooling plate that is well outside the baffle aperture. This longer cooling path simplifies construction and improves the thermal characteristics of the target, thus allowing target segments to handle much higher temperatures (up to as much as 800°C). The mechanical and radiation resistance of graphite is known to improve at higher temperatures (with the exception of oxidation). Additionally, the temperature gradients within the graphite are reduced.

The LBNF target cannot make use of all the improvements that the NOvA target includes, as it must fit inside the LBNF horn. As a result, the LBNF target is much more similar to the MINOS target, with only the above modifications of fin/beam width, dual titanium cooling lines, and a titanium containment vessel.

Prototype titanium-water-cooling-tube-plus-graphite cores were built during the investigation of NuMI target water leaks. The second one was considered entirely successful and ready to be assembled into a target can for a production target (see Figure 3-5). The key development issues were brazing of the graphite to the tubes, bending of the tubes, and precise alignment tolerances. The LBNF-LT target core is practically identical to this.

Figure 4-8: Early Prototype of a Target Graphite Core Bonded to a Titanium Cooling Line

4.3.3.1 Baffle

The baffle, just downstream from the primary proton window, is a passive device that works similar to a collimator. It is a graphite structure intended to prevent any mis-steered beam pulse from causing damage. In particular, it protects the inner conductors of the horns from the primary beam directly striking the aluminum. The baffle design depends on the geometry of the parts it protects as well as beam size, so the reference baffle design follows from the beam, horn and target specifications.

The goal for overall baffle position accuracy is 0.5 mm, including thermal effects, survey tolerance, and carrier instability. The construction and alignment tolerance of the hole through the baffle must be 0.5 mm or better. In general, the baffle design must withstand two thermal conditions induced by the proton beam: normal operation under ~2% continuous beam loss (DC) and a one-pulse accidental event. To accommodate both these conditions, the baffle design relies on heat transfer to the existing airflow through 18-pin radiator sections clamped along the baffle's length. In addition, conductive filler will be used to bridge the thermal-resistance gap between each radiator pin section surface and the 61-mm-diameter aluminum tube outer surface. These thermal conditions increase for both normal operation and one-pulse accidental event going from 1.2 MW to 2.4 MW, as well, and the conductive filler may require further investigation. The baffle's lifetime is not a concern since it will be changed out along with the target (and target carrier).

Early detection of a beam mis-steering event and beam termination through the upstream Beam Position Monitor (BPM), described in Section 12.2.1, and baffle thermocouple instrumentation, described in Section 16.3, limit the amount of errant pulses received. The baffle will need to be replaced for 2.4 MW beam operation.

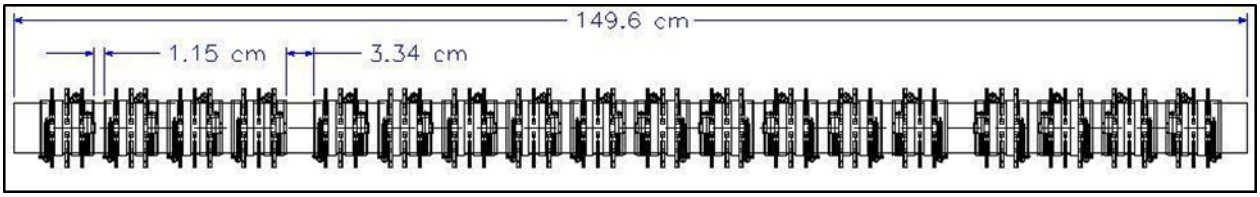

Figure 4-9: Baffle Baseline Design for LBNF

The baffle baseline design consists of ten 57 mm O.D., 17 mm I.D., 150 mm long graphite R7650 grade cores which are enclosed by a 61 mm, 3 mm thick , 150 cm long aluminum tube after annealing. Eighteen 66-mm long radiator pin sections are evenly placed along its length at 11.5 mm intervals with a provision for two 33.4 mm openings supporting the baffle ~22% of the length from each end, as shown in Figure 3-6.

Performing horizontal and vertical beam scans across the baffle and using the hadron monitor for primary instrumentation will provide an accurate check on the baffle centroid position with respect to the beam axis. However, this technique has limited sensitivity to the baffle angle. We will mount the target and baffle together as a rigid unit, so that scanning the target and aligning it on the beam center assures that the baffle angle (and target angle) will be set correctly as well. (Such a scheme was used for the NuMI target). The beam should be able to scan to at least 12 mm at low intensity. At NuMI, these scans are done with 8×10^{11} protons per pulse, which is 2% of full intensity; a similar intensity should also work for LBNF beam scans.

4.3.4 Target Options: R&D

Target longevity is a major issue for the performance of the LBNF facility. A target R&D program will explore options of target material, geometry, cooling, and other design issues.

As mentioned in the previous section, at 1.2 MW primary beam power, a target replacement rate of 2.5 per year is likely based on experience with the NuMI target. The logistics of target replacement in NuMI cost 2 weeks of runtime per target; the LBNF duration may be similar. 2.5 target replacements per year compromises the facility performance by 10-15%. Additionally, there is substantial additional cost in the storage facilities and radioactive handling required for that volume of targets. Reducing the frequency of target replacement could reduce the cost of the project, reduce the cost of operations and produce a more capable facility.

At the ultimate 2.4 MW beam power that is envisaged for the facility, the primary proton beam window, target and magnetic horn systems are expected to be limiting technologies. A program of R&D is planned to identify, design and optimize a target in combination with the horn system to maximize the integrated neutrino yield, taking into account predicted lifetimes of components and shutdown

requirements in addition to instantaneous neutrino flux. This will involve selection and optimization of the preferred material or combination of materials, coolant, target/horn geometry, and limitations on operating conditions and beam parameters. This will help identify infrastructure and utilities requirements of the target station. This work is necessary early in the project to ensure that all components and systems that cannot easily be modified or upgraded after construction or activation are designed to accommodate the full beam power.

The goal of the target R&D program is to be able to produce targets of greater longevity through design choices that negligibly impact neutrino production, however, the choices are somewhat limited. The R&D program of work has three major components:

- Material studies through the Radiation Damage In Accelerator Target Environments (RaDIATE) collaboration (including radiation testing of potential target materials at the BLIP facility at Brookhaven).
- Single pulse thermal shock testing in the HiRadMat facility at CERN.
- Physics and engineering optimization studies to evaluate alternative target concepts

A first round of radiation testing has been performed at the Brookhaven Linac Isotope Producer (BLIP). A series of materials were tested, including different grades of graphite, a carbon-carbon composite and hexagonal boron nitride (hBN): a graphitic form of Boron Nitride that theoretically has superior mechanical properties. These materials have been irradiated to a fraction of the NuMI irradiation of NT-02, well into the range that mechanical properties should be affected. Material studies have been performed in which the samples were gauged for integrity, tensile strength, thermal conductivity, density and other mechanical properties. Figure 3.7 is a picture of the sample holder for the BLIP test.

Initial results from the irradiated samples give support to the historical use of a small grain size, anisotropic grade of graphite from POCO (ZXF-5Q). Additionally the results invalidated previous tests that had shown quite severe radiation damage. Those sample had been irradiated directly in water. The present BLIP test demonstrated that identical samples experienced much greater degradation when irradiated in water instead of an inert environment (argon). The alternative material hBN fared poorly, seemingly ablating in the radiation. Among graphites, POCO (ZXF-5Q) was among the best in terms of its retained strength and ductility. Another grade of graphite and a 3D carbon-carbon composite also appeared attractive. The carbon-carbon composite has a very low coefficient of thermal expansion, minimizing the effects of thermal shock. However, the CTE of the carbon-carbon changes substantially upon irradiation. This change can be reversed with annealing at moderate irradiation, but it is unclear whether the changes can be withstood in a target where bulk annealing may be unachievable. Further investigations will study temperature-dependent effects, particularly annealing.

Additional radiation testing is warranted, though few facilities can provide comparable irradiation. Reactor irradiation is available, but the effects of neutron irradiation can depart widely from that of high-energy protons. The BLIP facility was a good compromise, except for its limited exposure.

Figure 4-10: BLIP Test Sample Holder. This Figure Shows Cassettes of Material Samples Irradiated in the BLIP Facility. The Beam Enters from the Right.

In addition to graphite, R&D activities are also underway to investigate alternative materials for the target and its support assembly. A particular aim is to consider beryllium as an alternative target material to graphite. Beryllium has some history as a target material, notably as the Fermilab MiniBooNE target, which has been exposed to in excess of $6x10^{20}$ protons at 8 GeV. A naive examination of beryllium's basic materials properties suggests that its single-pulse resistance to damage will be much lower than graphite. However, the precise modeling of beryllium damage is somewhat more involved. Particularly, the radiation damage threshold of metals such as beryllium is substantially higher than the crystalline forms of graphite (the data are imprecise, but the difference is about an order of magnitude). Also, beryllium as a metal has substantially greater tensile strength and ductility than graphite and thus may be more immune to fracture.

While beryllium has several known advantages over graphite, it has the overwhelming disadvantage of not being the target material that has operated in the NuMI beam or other high-power neutrino beams (CNGS, T2K). Although thin beryllium beam windows have proven to be quite robust in the NuMI beam, an invaluable test would be to include thick beryllium pieces as an operational neutrino production target in NuMI and verify its performance over an appreciable run period. A NOvA target has been modified to test beryllium as a target material. The beryllium containing NOvA Target is expected to be

installed in the beam later in FY2016. If successful, this material would have all the listed advantages to the LBNF Project and facility, as well as potentially being implemented for the NOvA experiment.

The Radiation Damage In Accelerator Target Environments (RaDIATE) collaboration is a program to investigate various materials of interest in the high energy proton irradiation regime primarily using the Materials for Fission and Fusion Power group at Oxford University. This group has the capability to fully analyze small, highly irradiated samples for mechanical changes due to irradiation. In addition to Oxford and Fermilab, nine other institutions actively participate in collaborative activities. Several samples specifically chosen for LBNF are being investigated at Oxford.

Single pulse thermal shock testing will be performed in the HiRadMat facility at CERN. The response of solid materials to short pulses of proton beam (or quickly moving targets in CW beam) is often simulated. The results of which are used to predict failure. However anecdotal evidence suggests that failure predictions are significantly conservative for certain materials (such as beryllium). Particularly, the strength and other properties of beryllium are substantially different at high strain rate, that is: at the very short duration strains caused by beam irradiation, beryllium's mechanical properties depart from their static values such that it is more resistant to thermal shock. Testing materials in the high intensity pulsed beam available at HiRadMat at CERN will validate simulations and failure criteria, potentially proving beryllium as a valid alternative to graphite.

The physics and engineering optimization studies will take place in parallel with the fundamental material studies described above. Studies are planned to be primarily performed by collaborating institutions, with guidance from LBNF staff, with a work program anticipated to include:

- Assessment and comparison of physics performance as function of target geometry and material, such as comparison of the current reference target design (water cooled segmented fins) with a helium cooled segmented spheres concept.
- Assessment of various coolant mediums, e.g. water or helium, taking all necessary physics, engineering and activation issues into account.
- Investigation of hybrid options that incorporate higher Z-materials to maximize ratio of low-to-high energy pions.
- Optimization of the proton beam dimensions for maximum integrated yield, balancing particle production with target lifetime.
- Optimization of the relative position between the target and the first electromagnetic horn.
- Extension of target simulations to include necessary target support structures, such as the container and support spacers, and evaluating their effects on the neutrino flux.
- Initial physics and engineering optimization studies will investigate the performance and limits of the current reference design (water cooled segmented graphite target, including the outer can). This will then be extended to consideration of other water and helium cooled graphite and/or beryllium target design concepts.

4.3.5

Target and Horns Instrumentation

The Target and Horns Instrumentation (THI) is a set of detectors that provide measurements of the secondary beam for commissioning, alignment, monitoring, and hardware protection. It supplements the primary beam instrumentation and the neutrino detectors. The THI's role is to provide experimental

and operational information to aid in the maximization of neutrino production and to limit the experiment's systematic uncertainties due to imperfect beam modeling and variation in the physical characteristics of the components. Furthermore, the data from the THI can also be used to switch the beam off in case of non-normal operation. The major roles can be broken down as follows:

- **Commissioning:** on initial operation of the beam, the commissioning team will perform a series of tasks to demonstrate that the beam can be delivered to the absorber, target, horn and baffle. The THI will be able to provide live verification of these tasks. For example, the primary beam will be delivered to the beam absorber before installation of the target, and the THI will measure the beam distribution at the absorber. Additionally, this instrumentation will be used to recommission the beam whenever major components are replaced.
- **Alignment:** many of the neutrino beam components will have tight tolerance on their alignment at the start of and during the run. The THI measures the locations of the devices through beam-based alignment, which entails determination of the positions of the devices with respect to the primary proton beam. This alignment is particularly relevant for evaluating the uncertainties on neutrino production without propagating the uncertainties of several optical surveys.
- **Monitoring:** long-term monitoring of the beam characteristics will give indications or measurements of slow variations in the beam. The most significant variation will likely be target degradation. The NuMI NT-02 target was known to degrade up to the point where 15% of the peak flux had been depleted. Monitoring this depletion is necessary for modeling the neutrino beam.
- **Hardware protection:** The intense proton beam may damage equipment downstream such as the absorber if the target is compromised or beam is mis-steered off the target. These off-normal conditions can be detected by measurement of the muons from decay of the mesons produced by protons hitting the target. Live, automated analysis of these measurements can then switch off the beam to prevent damage to the machine.
- **Investigation:** the THI can be used to investigate the failure or malfunction of beam production components. In NuMI, the THI system was invaluable in several such investigations where, on separate occasions, the target containment vessel was breeched and was infiltrated by coolant water.

4.3.5.1 Design Considerations

The detailed tolerances for components, and thus the measurement requirements, must be derived from a physics-based analysis of the effects of misalignments, target degradation and other deviations. The treatment of systematic errors in the MINOS experiment provides guidance, but the nature of the measurements is not precisely the same (MINOS was primarily a muon-neutrino disappearance experiment, while LBNF/DUNE is an electron-neutrino appearance experiment; additionally, the detectors are substantially different in composition and modality). Another requirement for the Target and Horns Instrumentation is that results must be readily apparent and available. A package of software integrating the instrumentation must be available to personnel performing the above analyses online. This software must also be able to interface to primary beam instrumentation and (ideally) the neutrino beam detectors. Correlation of the various data is necessary for the THI measurements.

4.3.5.2 Reference Design

The model for LBNF Target and Horns Instrumentation are the comparable NuMI systems. The suite of instrumentation planned for LBNF are as follows:

- Crosshair monitors which detect the shower of secondary particles produced through interaction of the primary beam together with crosshair-alignment features on the horns.
- A hadron monitor at the end of the decay pipe to measure the remaining secondary particles.
- A muon beam permit to prevent damage to the absorber by measuring the flux of charged particles within or downstream of the absorber.
- Also, the functionality of a target decay monitor is within the scope of the tertiary beam detectors of the Near Detector.

The crosshair monitors are the primary tools for horn alignment and are similar to primary-beamline loss monitors. They will be integrated into the horn modules. During horn alignment, the target will be removed, allowing the primary beam to pass through the horn apertures. The beam is translated across crosshair features fixed to the horn's upstream and downstream ends, producing a modest shower of particles that is detected by these loss monitors.

The hadron monitor resides at the end of the decay pipe, upstream of the hadron absorber and within the secondary beam. It measures the intensity, location and shape of the hadron beam just upstream of the absorber. In NuMI, the hadron monitor was used extensively for alignment by analyzing the change in the remnant beam as the primary beam was scanned transversely across the target, baffle, and horn features. It was used for commissioning, alignment, monitoring and for diagnosing failures. The NuMI hadron monitor was a 1 m^2, 7 × 7 array of parallel-plate ionization chambers. The ionization medium was helium at atmospheric pressure. The NuMI hadron monitor design cannot be simply reused for LBNF, however, as LBNF will have a more intense beam and shorter decay region, producing a smaller and more intense beam spot at the hadron monitor. The hadron monitor must withstand the heating and irradiation of this more intense radiation. Additionally, it must be able to produce measurements at the higher particle fluxes. The NuMI hadron monitor was known to show saturation effects at high intensity; it also was known to show variability with temperature, pressure and impurity level in the helium supply. An evolved concept for the LBNF hadron monitor is to use argon at low pressure (~ 1 torr) to reduce the ionization intensities, and to reduce the variation with gas supply quality. A higher channel count is necessary as the pixel size will need to be at least a factor of 3-5 smaller. Alternative technologies for robust detection of the high particle fluxes will be an area of investigation, particularly by members of the experimental collaboration.

Long-term degradation of the target material under beam irradiation can be monitored by comparing the ratio of muon fluxes of different energies. This system is vital for monitoring the detailed health of the target while not waiting for the analysis of neutrino or other tertiary beam monitors. The functionality of a target decay monitor can be realized through appropriate use of the muon monitors planned as part of the Near Detector scope. The system will consist of two arrays of ionization chambers at different locations within the shielding downstream of the hadron absorber. These devices will be configured in such a way as to produce a live measurement of target degradation through the ratio

technique, wherein the ratios of muon-monitor signals provide an immediate indication of target degradation, after compensating for other detector effects.

The muon-beam-permit system will be a dedicated, simplified set of detectors specifically for machine protection. It will consist of at least two small sealed ionization chambers in the muon monitor area downstream of the absorber (or within the absorber). For each beam pulse, the hardware protection system will compare the ionization from the muon monitor with the proton beam intensity sent to the target as measured by the beam toroid. Figure XXX1 shows data from NuMI of the correlation between the muon monitor response and protons per spill. It also indicates signal correlations outside of the normal region which would pull the beam permit. Figure XXX2 shows data from NuMI at low beam intensity of how the muon monitor response falls off as beam is mis-steered off target. The principle of operation is that muon signal per proton will be changed (generally reduced) as protons which interact in the absorber instead of the target cannot produce mesons with enough potential decay length to produce muons.

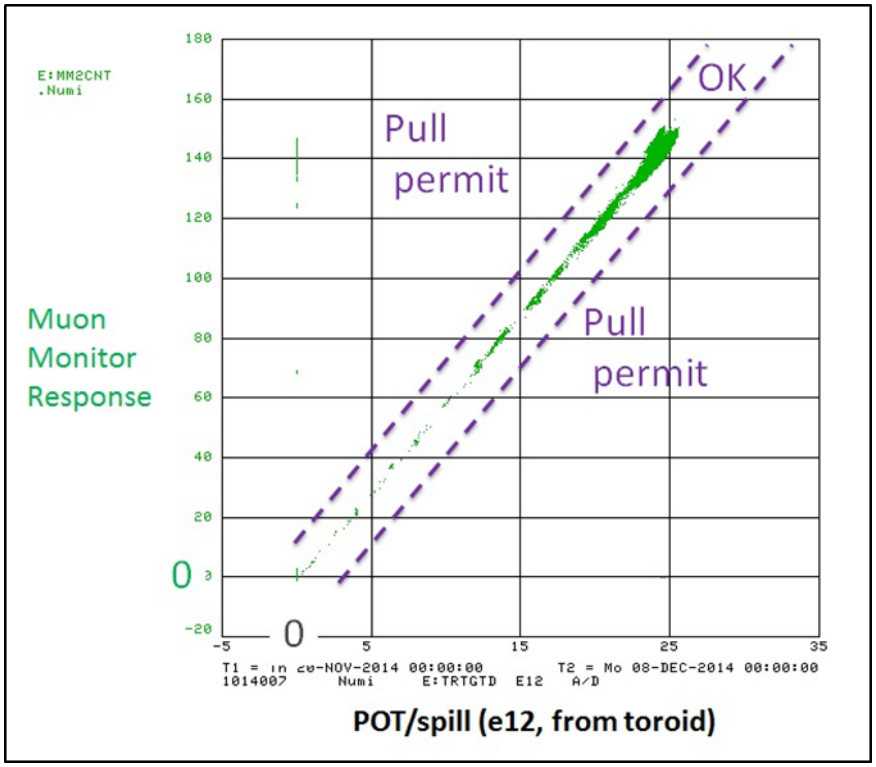

Figure 4-11: Data from NuMI Running of the Correlation Between the Muon Monitor Response and Protons/Spill

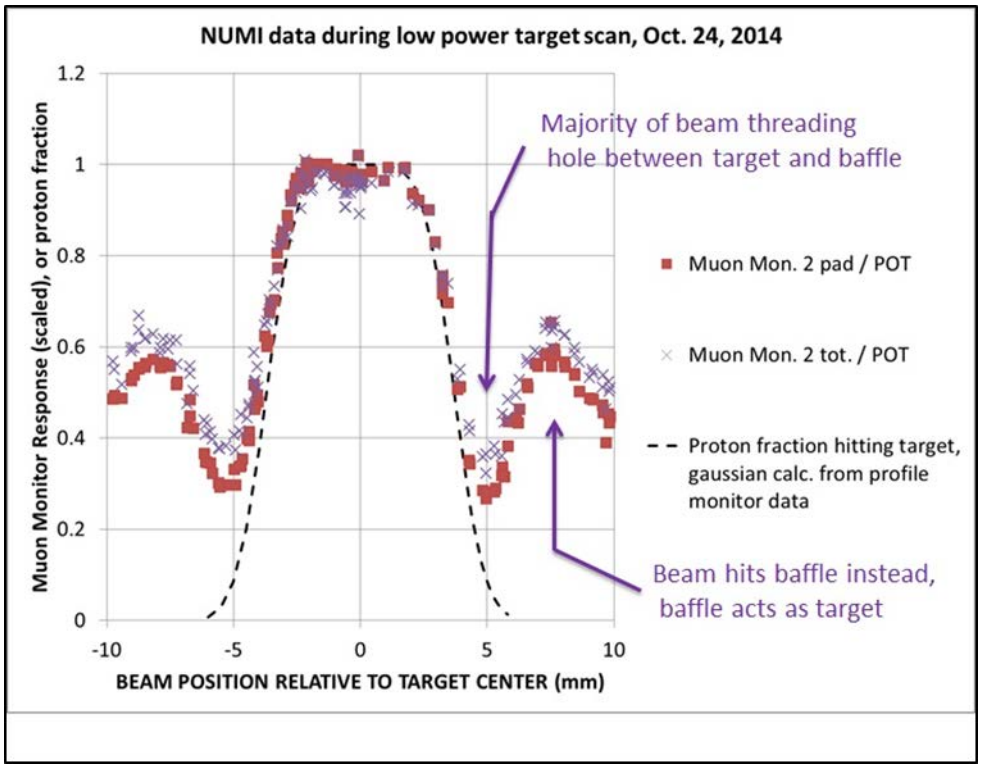

Figure 4-12: Decrease of Muon Monitor Response as Proton Beam is Mis-steered off Target. The Data is Bit Noisy as they were Collected with very Low Beam Intensity.

The whole system of the above devices will be integrated with data from primary-beam devices and neutrino devices, if available. The software to integrate these devices will be readily available as a live accelerator-controls application, as well as recording all these data into the appropriate accelerator and experimental databases.

4.3.6 Modules and Carriers

A "module" refers to the heavy shielding module that supports beam components below it. The module has motor drives to provide vertical and transverse horizontal motion for precise alignment of the component/carrier below it. Modules are described in section 3.4.3. (The target/baffle module design is basically the same as a horn module, except it does not need the stripline block). The module is expected to last the life of the facility, and its shielding thickness is designed for 2.4 MW operation. Another, much simplified module, supports the hadron monitor just upstream of the absorber.

The target and baffle are mounted on a carrier that hangs off of shafts extending through the module. The carrier supplies motion of the target along the beam direction that allows (i) insertion of the target into the horn for standard running and (ii) the flexibility to move the target up to 2.5 m upstream of its standard location for special runs. The baffle is mounted rigidly to the target, and moves with it, relative to the outside carrier frame. When a target is replaced, the carrier and baffle are replaced with it as a unit. This conceptual design copies exactly the NuMI target/baffle carrier design.

Attachment/removal of the target+baffle+carrier unit to/from the module is done in the target hall work cell.

For 2.4 MW operation, it is expected that the baffle will have to be ~ 1 m longer. This will impact the possible range of motion of the target, which may be reduced to ~ 2 m. The limitation comes from the worry that the carrier drive could freeze up with the baffle fully extended, and could not be extracted past the carriage beams when in the 2.5 m position, see Figure 3-8.

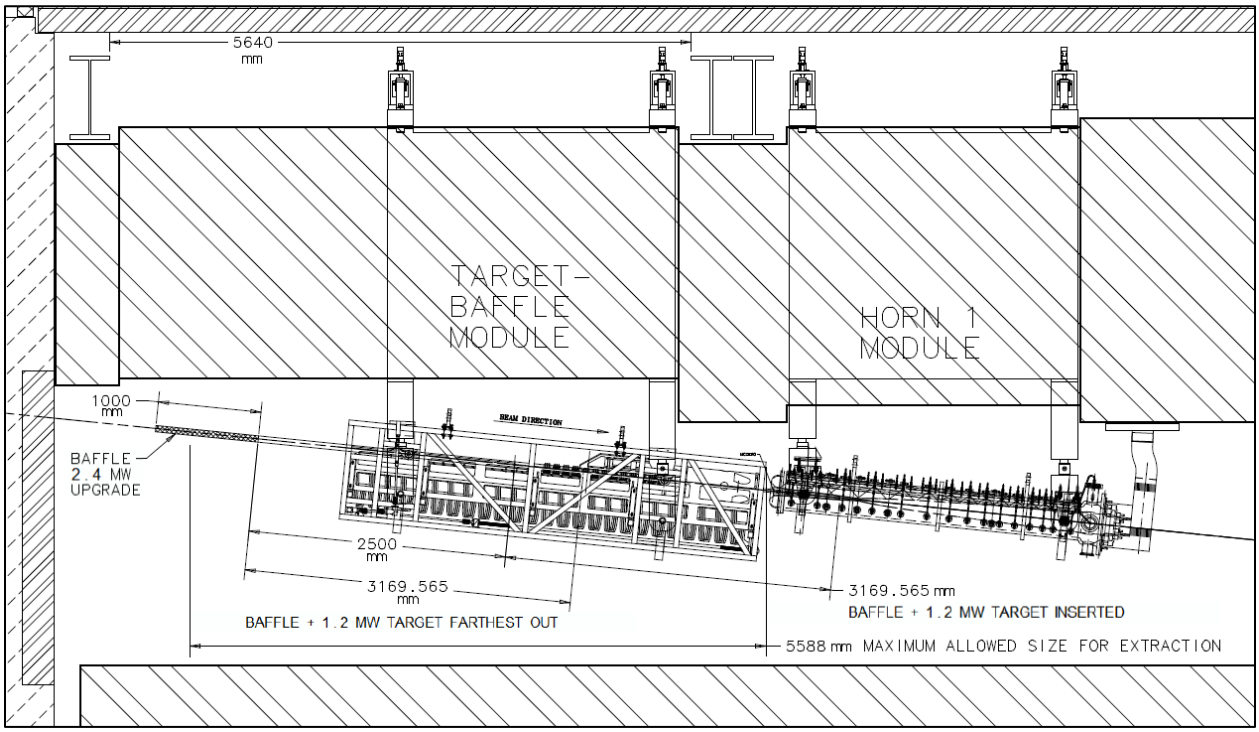

Figure 4-13: Target Carrier in Target Pile Shielding. The length of the baffle plus target assembly is shown in the fully inserted downstream position, and also in the furthest out position 2.5 m upstream of that. 5588 mm is taken as the maximum reasonable carrier length to extract between the carriage cross beams that are 5640 mm apart. The extra 1000 mm length of a baffle for 2.4 MW operation is also sketched in, showing that the usable range of target motion may be modestly reduced by that upgrade.

Horns (WBS 130.02.03.04)

The horns are focusing devices for secondary particles produced by the interaction of the primary proton beam on the target; they act as magnetic lenses that focus these particles, primarily charged pions and kaons, toward the decay pipe. This focusing of particles is achieved through a pulsed toroidal magnetic field, which is present in the inert gas volume between the co-axial inner and outer conductors that form the horn structure. LBNF will have two horns in series; the first of which partially surrounds the target, then extending more than 2 m further downstream in a parabolic shape, as can be seen in Figure 3-9. The second horn, shown in Figure 3-10 is located 6.6 m downstream from reference point MCZERO (defined in Figure 3-9), and also utilizes a double paraboloid inner conductor profile.

Conductor designs used are identical to those being manufactured for the NOvA experiment, which were developed from the NuMI neutrino beam. The horns are designed to operate with a beam power up to 1.2 MW. The inner conductor profiles are designed to produce a neutrino beam with an energy spectrum appropriate for the primary physics goals of LBNF [21], subject to engineering and material constraints. The horn systems will be supported and positioned by support modules, described in Section 3.4.3, which hang from carriage rails in the target hall chase. Electrical current supplied to the horns is transported via an aluminum stripline to the downstream end faces where connections to the horn conductors are made.

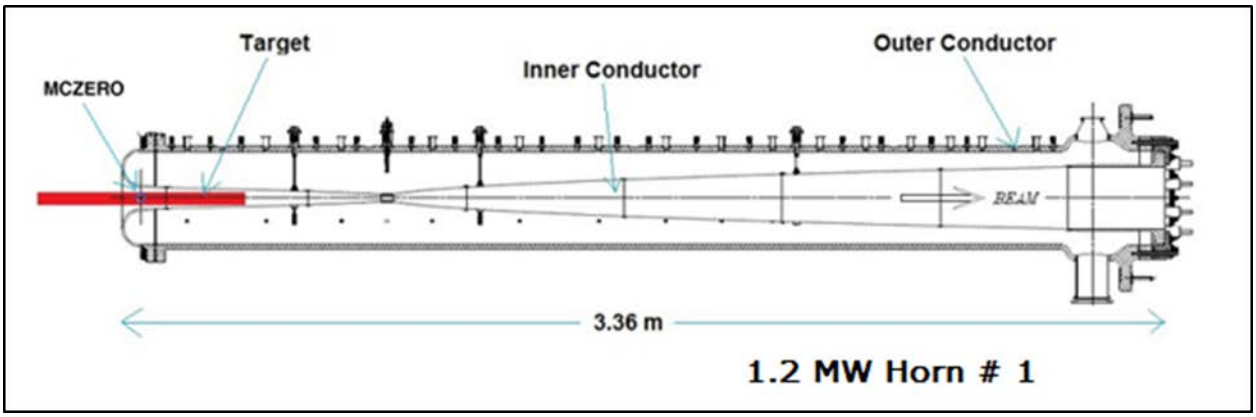

Figure 4-14: Horn 1 Section. The Reference "MCZERO" is the Point along the Beam that Sets the Coordinate System origin for Monte Carlo Simulations. Horn 1 Specifications are Listed in Table –3-2.

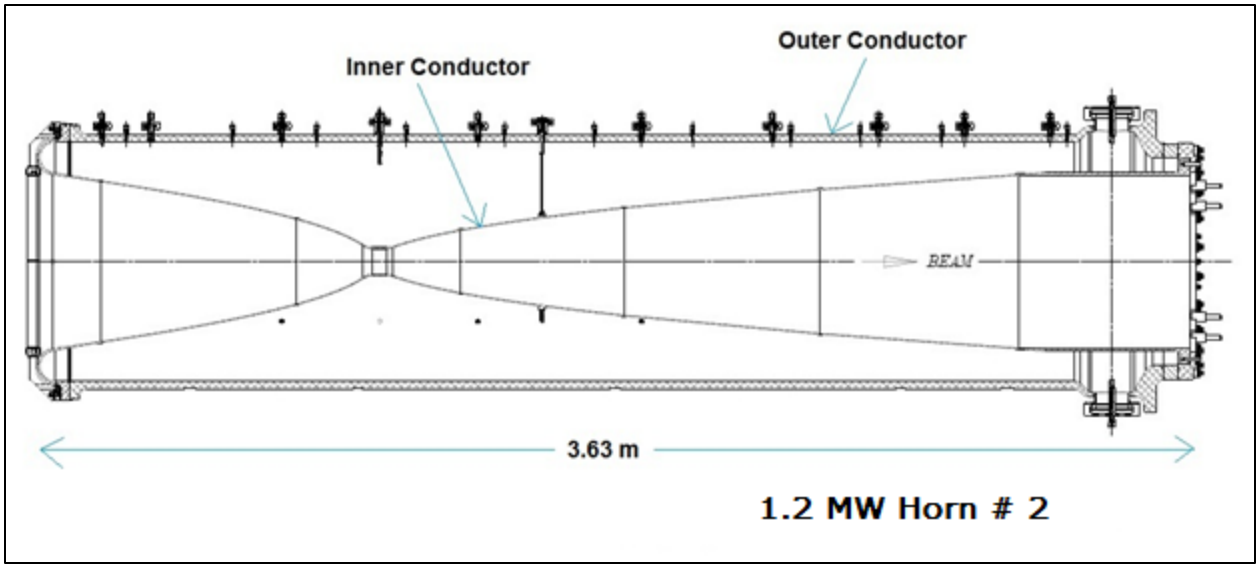

Figure 4-15: Horn 2 Section. Horn 2 Specifications are Listed in Table 3-2

4.4.1 Design Considerations

The horns (i.e., the conductors) must be able to endure the combined heat load from the secondary particle interactions in the horn material and resistive heating by the current flowing through them. To address the former, the thickness of the inner conductor should be minimized to reduce absorption and scattering of secondary particles in the conductor material. Resistive heating can be minimized by keeping the pulse length short, while water-spray cooling is used to keep the conductors at an acceptable operating temperature. Given careful design of the stripline, air cooling is sufficient for the majority of the component, with specific portions possibly requiring water cooling. In addition to the cooling requirements, the inner conductor must withstand repetitive thermal and magnetic stresses over tens of millions of current pulses.

Lifetime expectations for horns are typically described in millions of pulses, with a safety factor associated with that rating. Stress results from finite element analysis can be used to determine the fatigue life of various components, and thus estimate horn lifespan. The component most subject to lifespan limitations is the Horn 1 inner conductor. It is important to demonstrate with analytical simulations that a horn will not fail after a minimum of $1X10^8$ cycles due to fatigue in the inner conductor. The design will be simulated and possibly adjusted to achieve this lifetime with a minimum safety factor of 2. For this conceptual design, both horns are assumed to be replaced every two years.

Cooling considerations must also extend to the module mainframe and drive components, as dimensional stability while in operation is critical. Additionally, the weight of the horn, its support module and stripline block together must not exceed 50 tons, the Target Hall crane capacity. The horn systems assembly must be removable and transferable to the target hall work cell for initial installation, end of life removal, and potential repair activities. Horns are expected to be replaced every few years, while modules are considered permanent and will be designed as such.

4.4.2 Reference Design

The focusing system will be a two-horn design, with the upstream end of the second horn (Horn 2) located 6.6 m from the reference point MCZERO (near the upstream end of Horn 1). Both horns consist of an inner conductor, an outer conductor, a current-supply stripline, a cooling system and a support structure. The inner conductor of Horn 1 has a parabolic upstream section that surrounds the target tube up to the neck of the horn. This neck is followed by a parabolic downstream profile [21] that ends at the downstream face where the stripline is mounted. Horn 2 follows this layout, although varies in parabolic lengths, placement, and wall thicknesses [22]. Both Horn 1 and Horn 2 inner and outer conductors are of aluminum 6061-T6 construction. The inner conductor shapes are generated from the parameterization shown in Figs. 3-11 and 3-12.

Table 4-2: Horn Parameters. The Inner and Outer Conductor Parameters are Abbreviated by IC and OC, Respectively.

	Horn 1	Horn 2
Material	Al 6061-T6	
Peak Current	230 kA	
Min. aperture "neck" radius	9 mm	39 mm
IC Thickness	2 mm	3 mm
Length	3.36 m	3.63 m
OC radius (outer)	165 mm	395 mm
OC Thickness	16 mm	25 mm

The outer surfaces of the inner conductor will be cooled by water spray nozzles distributed along the beam axis and 120° azimuthally. Nozzles at the top of the outer-conductor cylinder will spray water to form a film running down from both sides, illustrated in Figure 3-13. The radioactive cooling water will be collected at the bottom of the horn and will return to an external heat exchanger through a closed circuit. The external surfaces of the horn will be exposed to the target chase airflow. To resist water erosion, the surface of inner conductors will be coated with electroless nickel.

Horn 1 (700 kW version)	Upstream	transition	Neck	transition	Downstream	Equalization section
Z (cm)	0 to 44.047	44.047 to 80	80 to 83.982	83.982 to 95.128	95.128 to 300	300 to 331.437
I.C. R_{in} (cm)	$\sqrt{\frac{92.8454-Z}{7.0483}}-0.2$	$\sqrt{\frac{85.7091-Z}{7.0483}}$	0.9	$\sqrt{\frac{Z-82.2123}{2.1850}}$	$\sqrt{\frac{Z-80}{2.1850}}-0.2$	9.843
I.C. R_{out} (cm)	$\sqrt{\frac{92.8454-Z}{7.0483}}$		1.35	$\sqrt{\frac{Z-80}{2.1850}}$		10.795
O.C.R_{in} (cm)	14.92					Varies, > 14.92
O.C. R_{out} (cm)	16.51					Varies, > 16.51

Figure 4-16: Idealized Shape of the Horn 1 Inner and Outer Conductors. z=0 is the Beamsheet Location MCZERO

Horn 2	Upstream	Neck	Downstream	Equalization section
Z (cm)	0 to 97.617	97.617 to 104.803	104.803 to 300	300 to 353.515
I.C. R_{in} (cm)	$\sqrt{\frac{100-Z}{0.1351}}-0.3$	3.90	$\sqrt{\frac{Z-100}{0.2723}}-0.3$	26.801
I.C. R_{out} (cm)	$\sqrt{\frac{100-Z}{0.1351}}$	4.40	$\sqrt{\frac{Z-100}{0.2723}}$	27.753
O.C.R_{in} (cm)	37.00			varies
O.C. R_{out} (cm)	39.54			varies

Figure 4-17: Idealized Shape of Horn 2 Inner and Outer Conductors. z=0 is the insertion Point of Horn 2, which is 6.6 m Downstream of MCZERO, the z=0 Point of Horn 1.

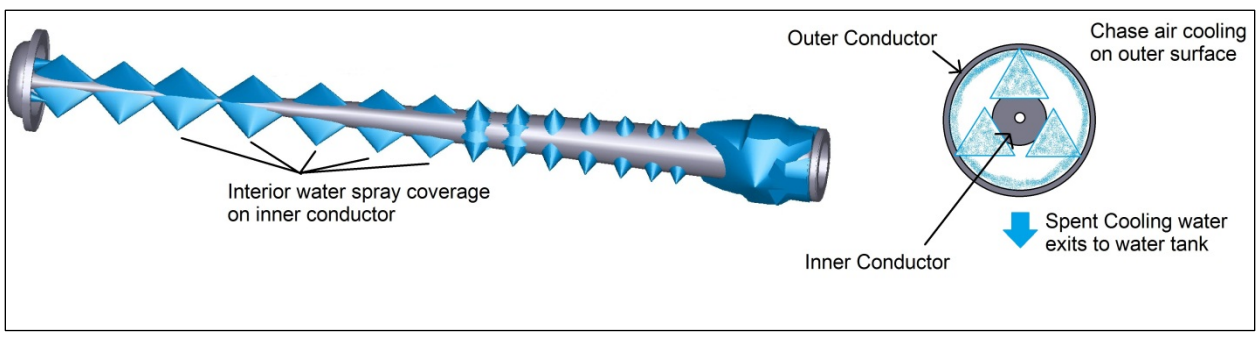

Figure 4-18: Horn 1 Inner Conductor Water Spray Coverage

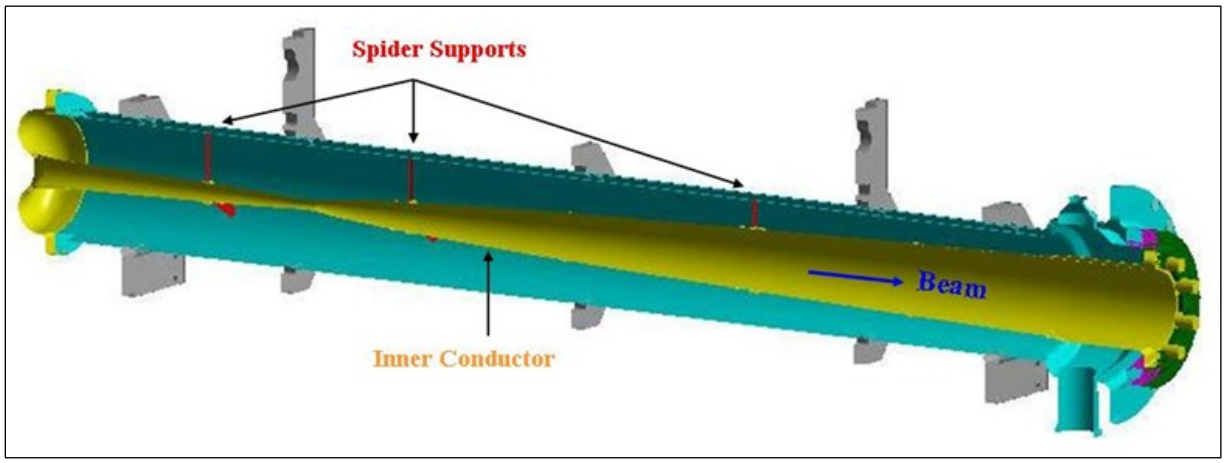

Figure 4-19: Additional Support and Stability for the Thin Inner Conductor are Provided by Welded Struts or Spider" (web) Supports (Thin Red Pieces)

The inner conductor will consist of seven segments welded together with a CNC TIG welding machine. Welds will be completed with a thicker wall at the joints, located away from the high-stress areas to compensate for the reduced strength in the heat-affected zone. Single pass, full-penetration welding will minimize the conductor distortion. Cosmetic passes will be applied if needed to achieve an overall straightness of ±0.020 in. A few sets of spider supports, illustrated in Figure 3-14 will provide the position adjustment of the inner-conductor center line and meanwhile allow free thermal expansion of the conductors along the beam direction.

The electrical connection between the power supply and the horn is provided by a planar-design stripline, which has minimal inductance and resistance, and allows thermal expansion/contraction of the horns and transmission lines. The stripline between the horns consists of eight layers of aluminum 6101-T61 bus bars that are spaced by zirconia ceramic insulators, as shown in Figure 3-15. The stripline is flared out to connect to the horn inner and outer conductors at the downstream end and is insulated by an alumina ceramic ring. The upper portion is connected to the transmission line via a remotely controlled stainless-steel clamp assembly. The horn current pulse is a half-sine wave with a peak current of 230 kA, pulse width of 0.8 ms and a repetition rate of 1.20 s.

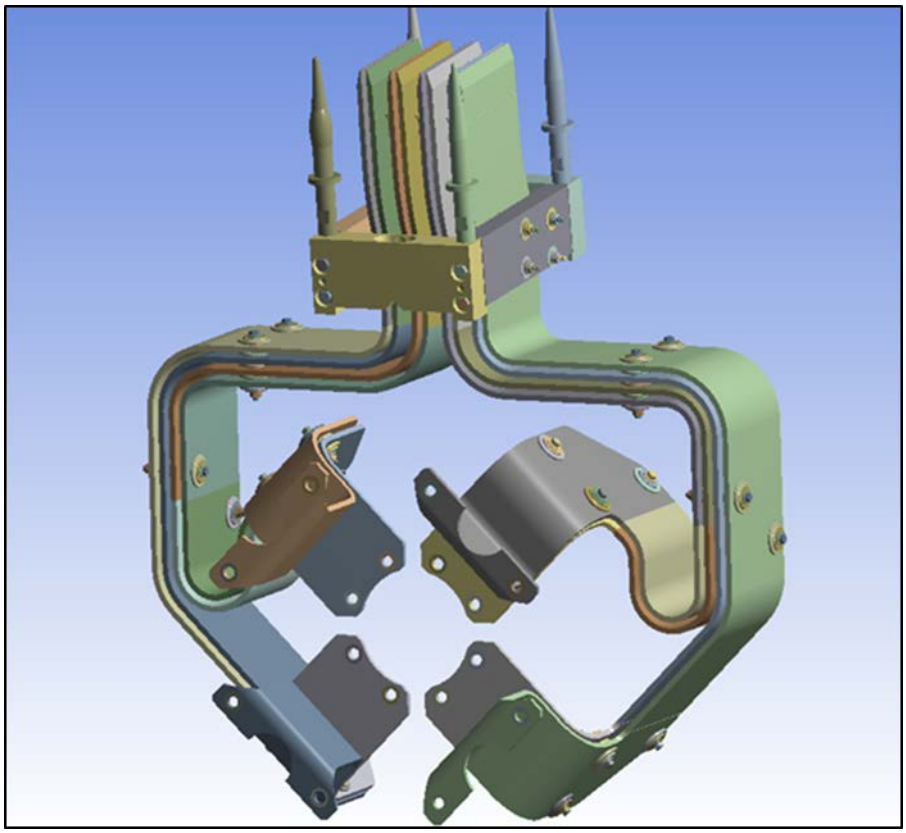

Figure 4-20: Horn 1 Stripline Connection at the Downstream End

The horn striplines must be matched in length for pulse uniformity, and must be profile-matched to lessen the effects of magnetic loading. This profile-matching also helps to eliminate stray magnetic fields during the beam pulse that can adversely affect the beam optics. Ring-down times for the Horn striplines must be analyzed to ensure disruptive vibrations completely dissipate in the 1.2 second cycle time. Any vibration condition left past the 1.2 second period must not have the potential to develop a resonant response and decrease the service life of the horn.

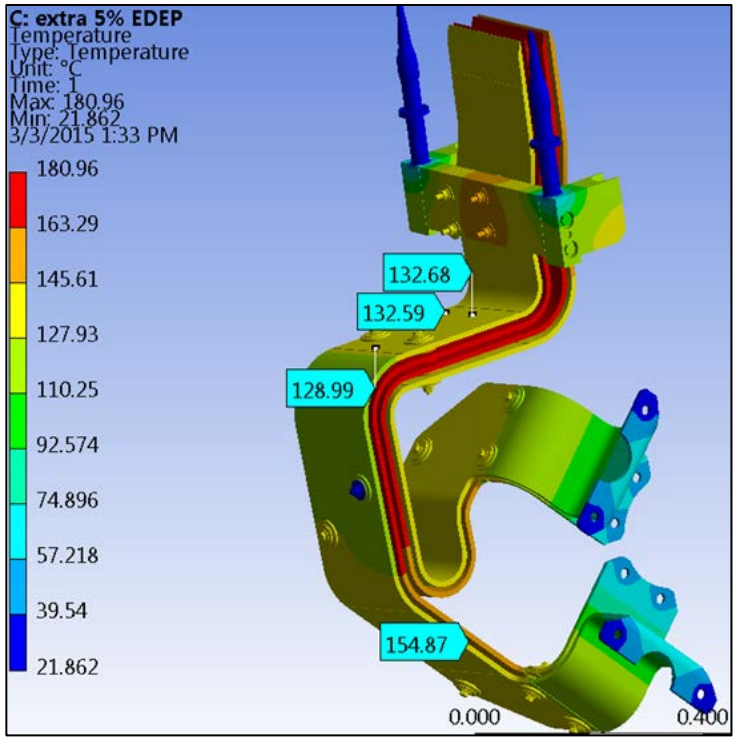

Figure 4-21: NOvA Horn 1 Stripline Analysis at 1.2 MW/120 GeV Operation

Current analysis results of the NOvA stripline design, shown in Figure 3-19, illustrate the high temperatures present at the interior layers where air cooling is currently not sufficient. Efforts are underway to increase air cooling in the inner layers, by means of roughly doubling the gap between segments, and adding forced air cooling through the top of the stripline block. Preliminary results shown in Figure 3-20 indicate much more acceptable temperature ranges, however further refinement and redesign is required to attain an acceptable solution for the anticipated lifetime and operational requirements of a 1.2 MW horn system.

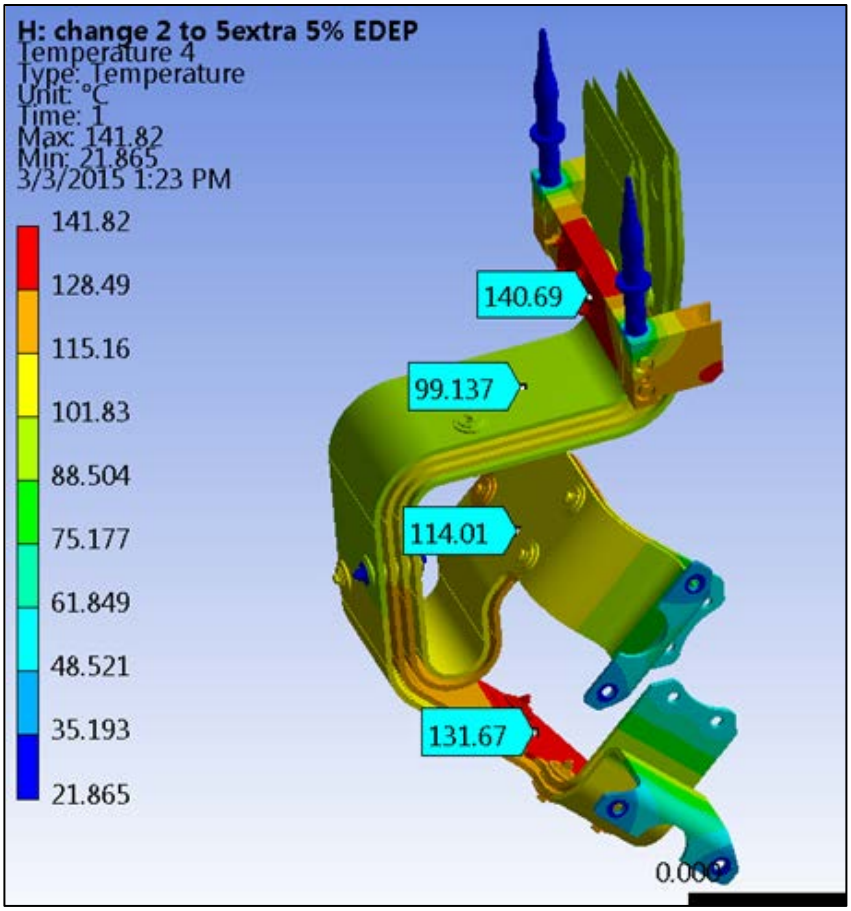

Figure 4-22: NOvA Horn 1 Stripline Analysis at 1.2 MW/120 GeV Operation with Increased Cooling

Table 4-3: Summary of Heating Loads on the Horns. The Results are Separate for the Inner Conductor (IC) and the Outer Conductor (OC).

LBNF	Horn1		Horn2	
	IC	OC	IC	OC
Beam Heating Loads	15.2 kW	24.3 kW	2.5 kW	12.9 kW
Resistive Heating Loads	2.9 kW		0.8 kW	

The heating sources on the horn conductors include electrical-resistive heating by current and instantaneous beam heating due to secondary particle interactions in the material. The beam energy deposition rates in materials are calculated with MARS, a Monte Carlo code [23]. Because of its smaller radius and proximity to the target, the heating loads on Horn 1's inner conductor are much higher than those on Horn 2's inner conductor. Horn 1's maximum heating-load density occurs on the neck immediately upstream of the transition to parabola. See Figures 3-21 and 3-22 and Table 3-3.

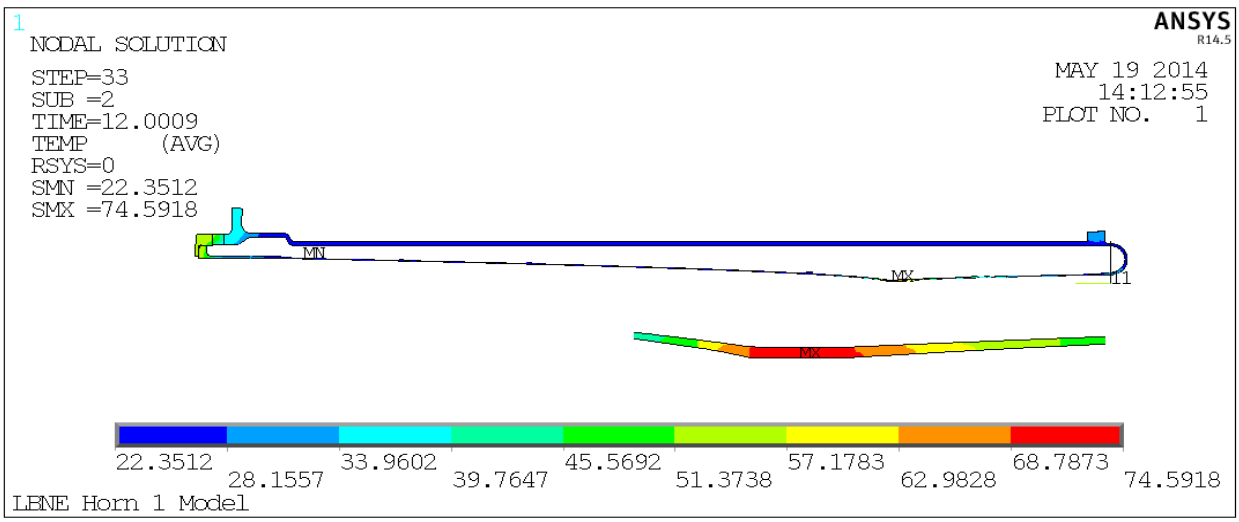

Figure 4-23: Half-symmetry, Axial Cross Sectional View, of Horn 1 Conductor Temperature after Beam Pulse

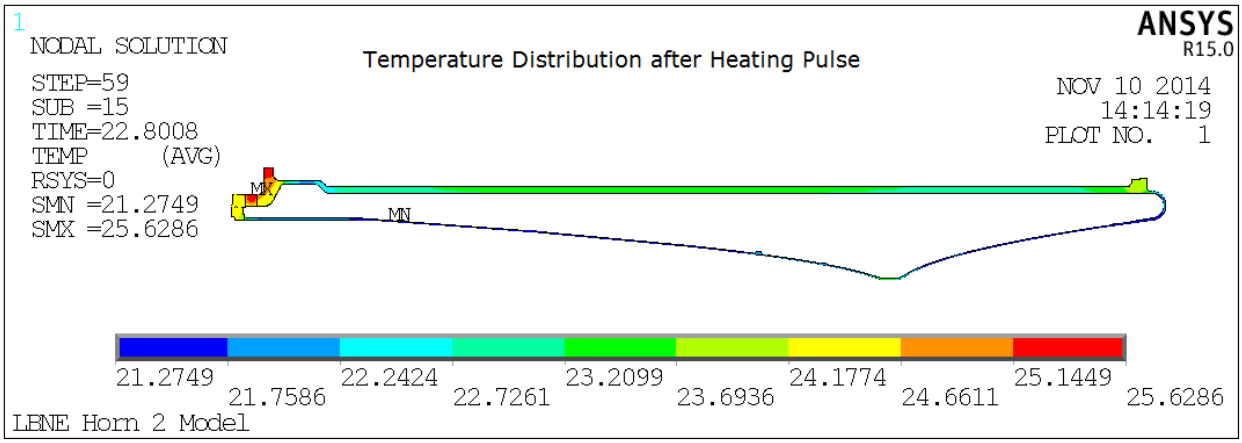

Figure 4-24: Half-symmetry, Axial Cross Sectional View, of Horn 2 Conductor Temperature after Beam Pulse

Heating of the conductors produces thermal stresses, and electromagnetic forces generate magnetic stresses on the inner conductor during current pulsing. Thermal and structural finite element analysis (FEA) have been completed to verify the design and study the fatigue strength of the inner conductors, the alignment stability of the horns, and the temperature profile of the striplines. Modal and buckling analysis will be performed to study the vibration and buckling characteristics of the horns. A detailed temperature and stress history represented in Figure 3-23 for the conductors, has been developed for all operating & loading conditions to ensure a sufficient safety factor. Loading points of concern are: (1) Lower bound pre-pulse, (2) Start of beam pulse, (3) End of beam pulse, and (4) Upper bound post pulse.

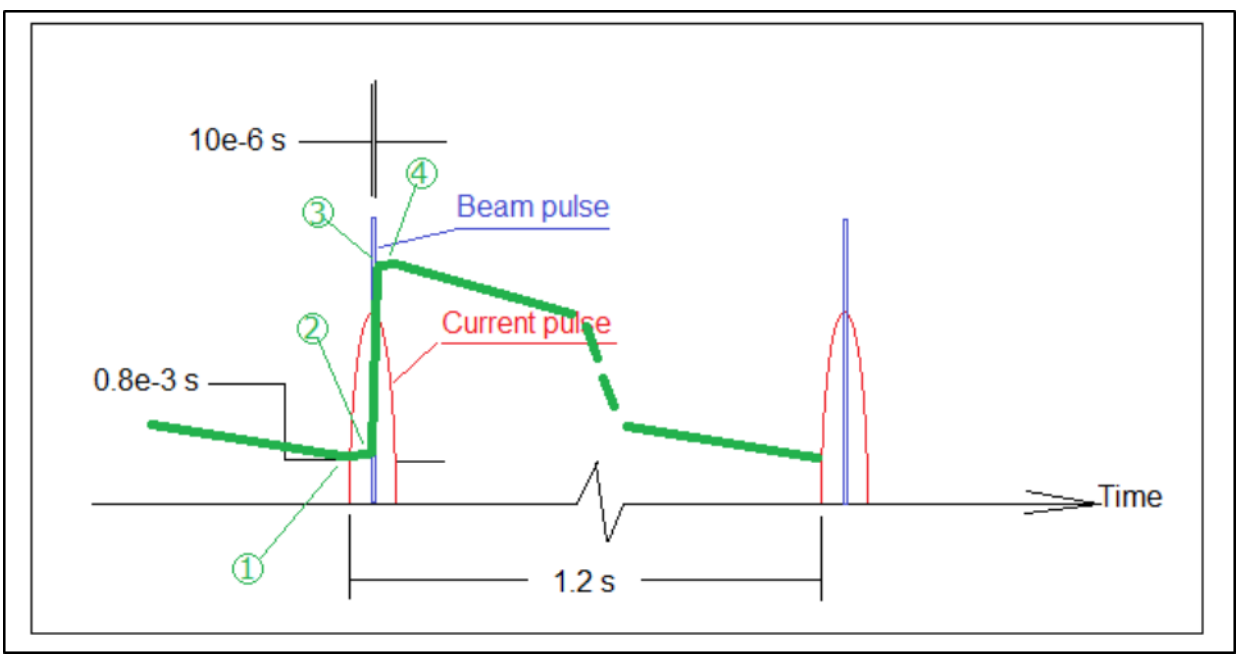

Figure 4-25: Detailed load points for conductor analysis. 1: Start of current Pulse, 2: Start of beam pulse, 3: End of beam pulse, 4: End of current pulse. Temperature profile of the horn neck is represented by the green line.

Completed FEA simulations indicate that with the current design and a convective heat transfer coefficient of 7,500 W-°C/m^2, the horn 1 neck reaches an equilibrium temperature of 58 °C after five beam pulses. After reaching equilibrium, during each pulse at full beam power the neck's maximum temperature would reach 75 °C at the end of current pulse (end-pulse) as shown in Figure 3-21.

Horn 2 temperatures are much lower due to the increased cooling area of the conductor surfaces and a lower current density. Utilizing a 4,000 W-°C/m^2 convective heat transfer coefficient, the horn 2 neck reaches an equilibrium temperature of 23 °C after several hundred beam pulses. After reaching equilibrium, during each pulse at full beam power the neck's maximum temperature only reaches 24 °C at the end of the current pulse as shown in Figure 3-22. These results are consistent with those expected for a horn of this size and position in the beamline.

Based on the obtained results, it was confirmed that Horn 1 is the critical focusing horn with regards to operational stresses and expected service life. From prior research and experience, Horn conductor and critical component temperatures must be engineered to remain below 100 °C, as the fatigue strength (the stress level a material can endure for millions of cycles) begins to drop as operating temperatures pass this limit. The analysis results indicate that this limit will not be reached under all operating conditions for 1.2 MW, and therefore both horns should reach there expected service life.

While the neck gets hot during current/beam pulsing, both end caps of the inner conductor remain relatively cool. Thermal gradients produce compressive stress on the inner conductor, and electromagnetic forces generate compressive circumferential/radial stresses and tensile axial stress. The combination of thermal and magnetic loading results in a range of stress magnitudes and types of stress at different locations and times on the inner conductor. Stress calculations were performed to study the scenarios of steady-state, mid-pulse and end-pulse for the normal beam operation at full power of 1.2 MW for both horn 1 and horn 2. See Figures 3-24, 3-25, 3-26, & 3-27.

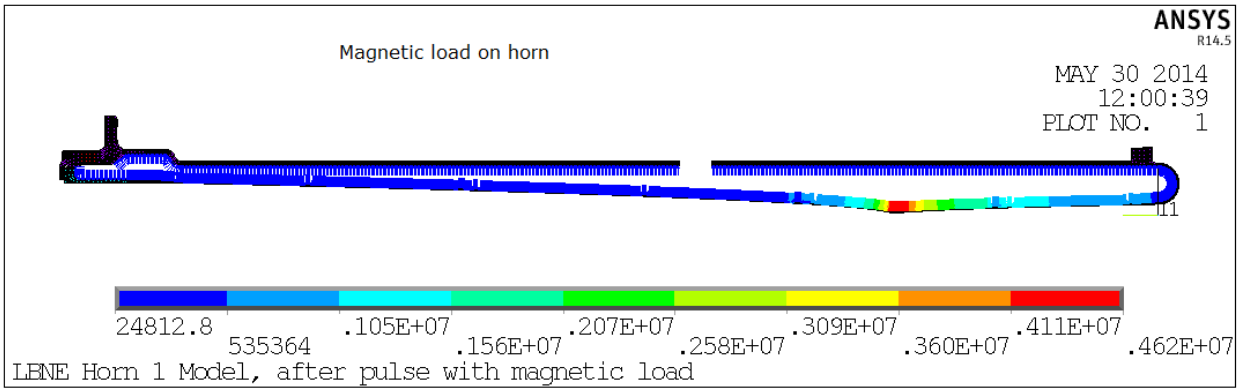

Figure 4-26: Half Symmetry, Axial Cross Sectional View, of Horn 1 Magnetic Pressure Loading

Magnetic pressure loads are applied to the interior volumes of the inner conductors as a normal force to the surface. This pressure creates compressive hoop stress on the inner conductor as well as tensile axial stress due to the force pushing on the transition endcaps. The magnitude of these magnetic loads scales with the current pulse half sine wave which creates complex loading conditions when combined with the temperature profiles caused by beam and joule heating. These loading conditions produce stresses that vary widely depending upon conductor location and timing within the pulse width.

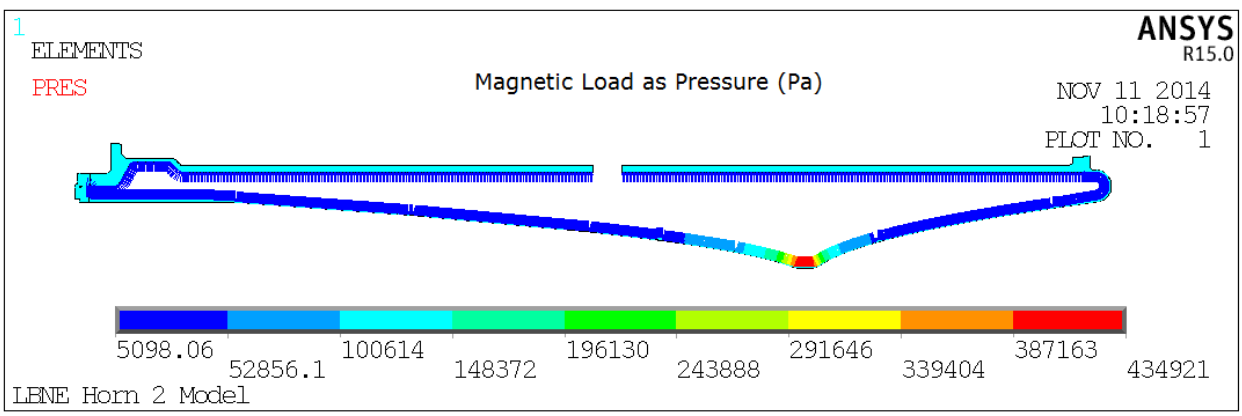

Figure 4-27: Half Symmetry, Axial Cross Sectional View, of Horn 2 Magnetic Pressure Loading

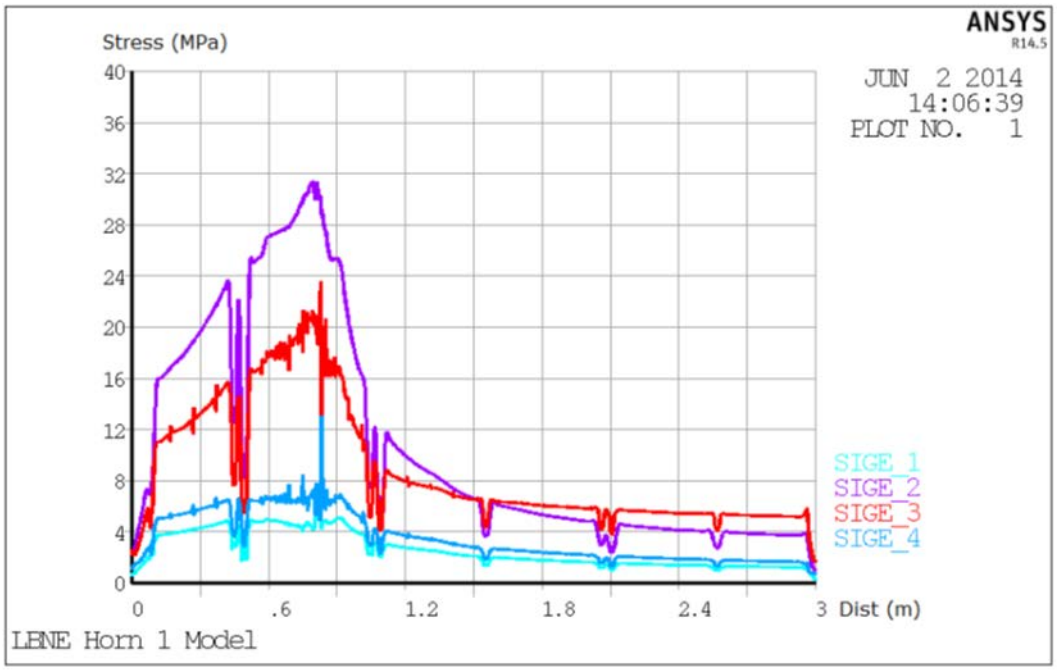

Figure 4-28: Horn 1 Conductor Stresses

Stress profiles are shown representing the load cases for varying operations of Horn 1 and Horn 2. All results are equivalent stresses (Von Mises), obtained from component stresses. Peaks and valleys of the plots correspond to wall thickness differences in the conductor profiles, as well as weld bead and stiffening rib locations.

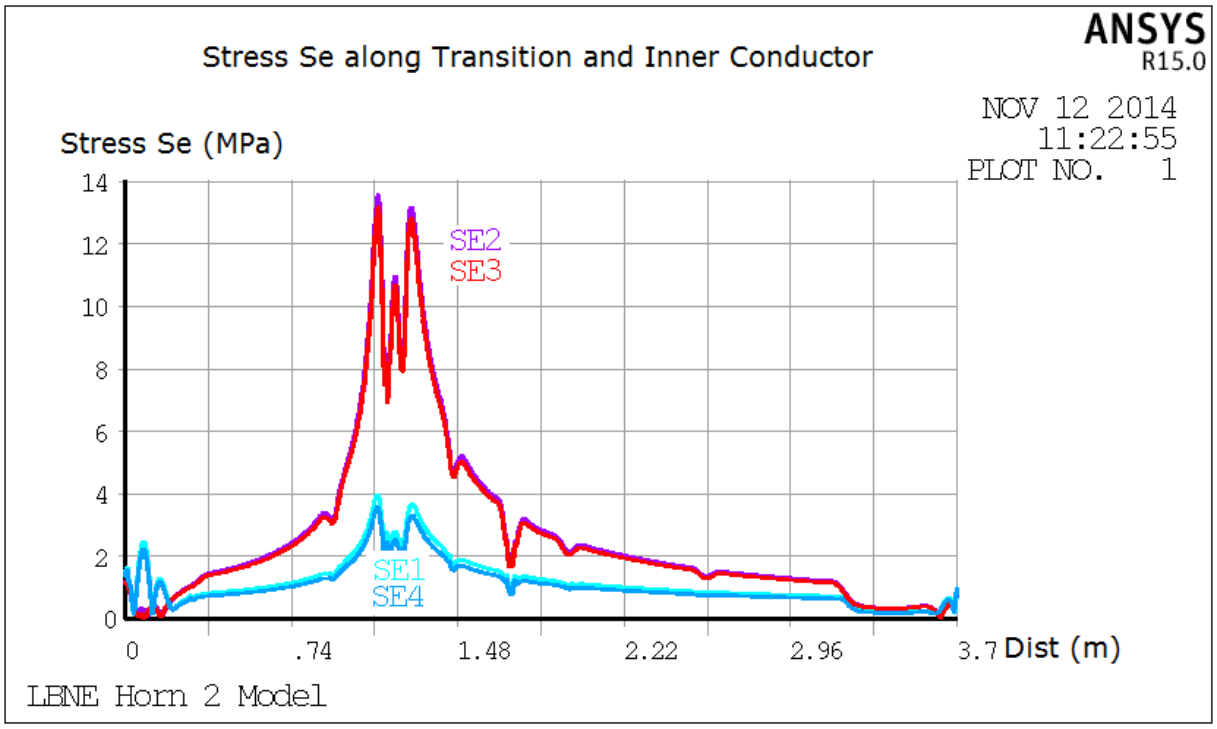

Figure 4-29: Horn 2 Conductor Stresses

Table 4-4: Horn 1 Operational Safety Factors at Critical Conductor Locations

Up-stream Weld	Neck	Down-stream Weld	Transition
2.5	3.5	4.5	9.2

Table 3-5: Horn 2 Operational Safety Factors

Up-stream Weld	Neck	Down-stream Weld
13.1	7.5	8.2

The final safety factors shown in tables 3-4 & 3-5 are calculated using the Goodman Equation:

$$\frac{S_a}{S_f} + \frac{S_m}{S_u} = \frac{1}{SF}$$

Where Sa and Sm are alternate stress and mean stress defined by the following equation:

$$S_a = \frac{S_{Max} - S_{\min}}{2}, \quad S_m = \frac{S_{Max} + S_{\min}}{2}$$

The resultant safety factor (SF), was then modified by an environmental correction factor (.75), to account for corrosion on the interior of the horn volume, as well as a strength reduction factor (.5), to account for the halving of aluminum 6061-T6's strength at the weld locations. Final safety factors for conductor construction, including all correction factors, were found to be sufficient to meet the expected horn lifetime of 3 years or $1X10^8$ pulses, whichever is greater.

4.4.2.1 Ancillary Components

Outside of inner and outer conductors, several other ancillary systems exist to support the horn during operation. These components include the water manifolds and collection tank, upstream and downstream support hangers, as well as "crosshair" assemblies (for beam-aided alignment) and instrumentation.

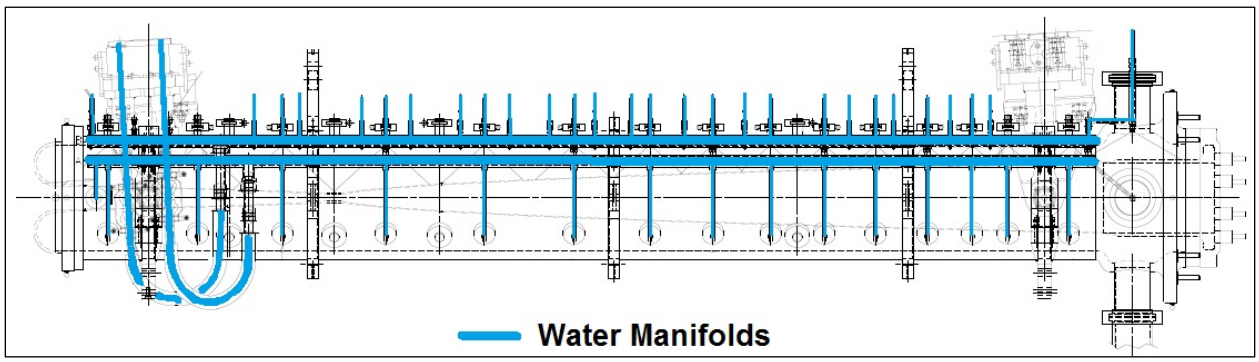

Figure 4-30: Horn Cooling Water Manifolds

The water manifolds run the length of the horn outer conductors and provide cooling water to the spray nozzles. All water manifolds must be electrically isolated by an alumina ceramic assembly that prevents horn current from traveling back to RAW systems and instrumentation. These manifolds and water cooling passages can be seen in Figure 3-28.

The upstream and downstream support hangers hold the horns in position, while providing a degree of freedom for vertical adjustment. Internal hanger bushings are constructed of metalized graphite, as to avoid corrosion problems experienced with other bushing materials. The metalized graphite is also radiation hard and has proven to be a very successful material in hazardous environments. Water line connections, as well as all instrumentation lines run through the hangers, which demand a well-designed layout and specialized fittings for rad-hard, leak free service. A structural analysis has been performed on hangers to ensure material scalloping for weight reduction does not affect overall dimensional stability. This analysis will undergo several iterations as loading conditions for the horns become more defined. An example of this can be seen in Figure 3-29.

A Horn crosshair engineering analysis must also be performed to determine maximum operating temperatures. An aluminum crosshair design has been used successfully in the past, and beryllium has been specified for the NOvA Horn 1 crosshair due to the large amount of beam energy deposition.

Beryllium is the most logical choice for the LBNF Horn 1, as it can withstand high temperatures with little deformation. Dimensional stability of the crosshair is the main consideration however, and additional cooling contacts or geometrical changes from their operation in the NOvA experiment might be needed. These changes would allow for a sufficiently low operating temperature, providing low thermal expansion and resistance to material creep.

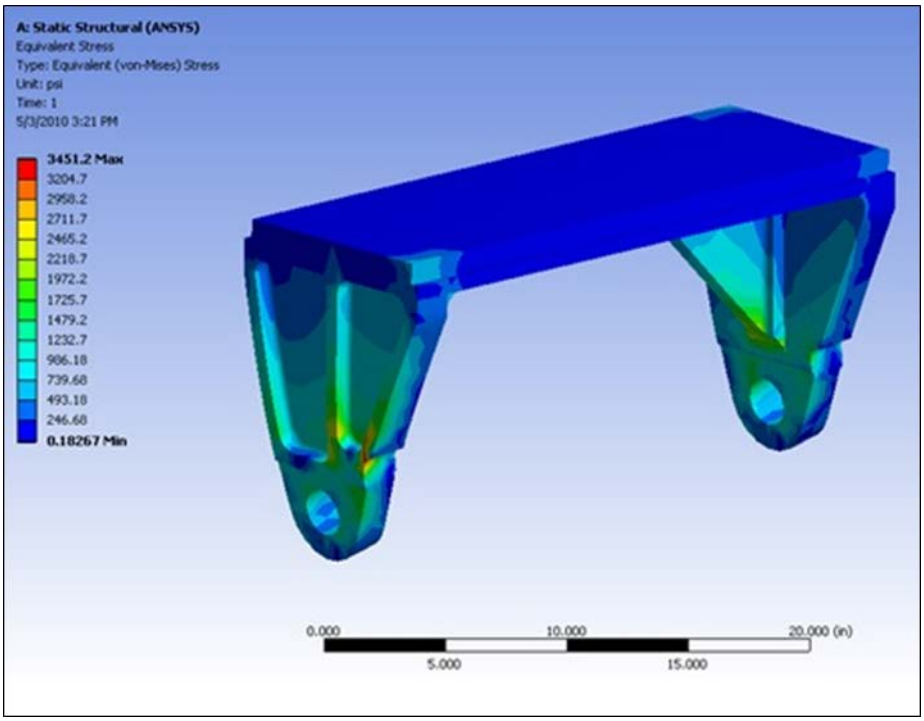

Figure 4-31: Horn Hanger Structural Analysis with Tri-axial Loading

4.4.3 Horn Support Modules

Horns will be supported and positioned by support modules. The intensely radioactive environment of the target chase requires that the horn-support module be adjustable and serviceable by remote control. The horn-support modules provide radiation shielding, and allow the mounting and dismounting of feed-through connections for the stripline, cooling water and instrumentation cabling from the top of the module mainframe, away from the most highly activated areas.

The horn module support concept is shown in Figure 3-30.

Horn-support modules are rectangular boxes open at the top for shielding block insertion, and are constructed from plate steel. The walls perpendicular to the beam at the upstream and downstream ends of the box will be up to 10-in thick. The side walls oriented parallel to the beam line will be up to 2-in thick with two plates welded together to form overhangs that create a labyrinth to shield radiation. A bottom plate will be welded to provide a heat shield for the horn, protecting it from the radiated heat of the non-cooled shielding block components inserted into the module interior.

The modules fix the horn with respect to the module in the horizontal degrees of freedom, but not in the vertical. The module is adjusted with respect to the beam for transverse horizontal position and yaw. The horn is adjusted with respect to the module for vertical and pitch alignment. This is accomplished by two separate motorized systems shown schematically in Figure 3-31.

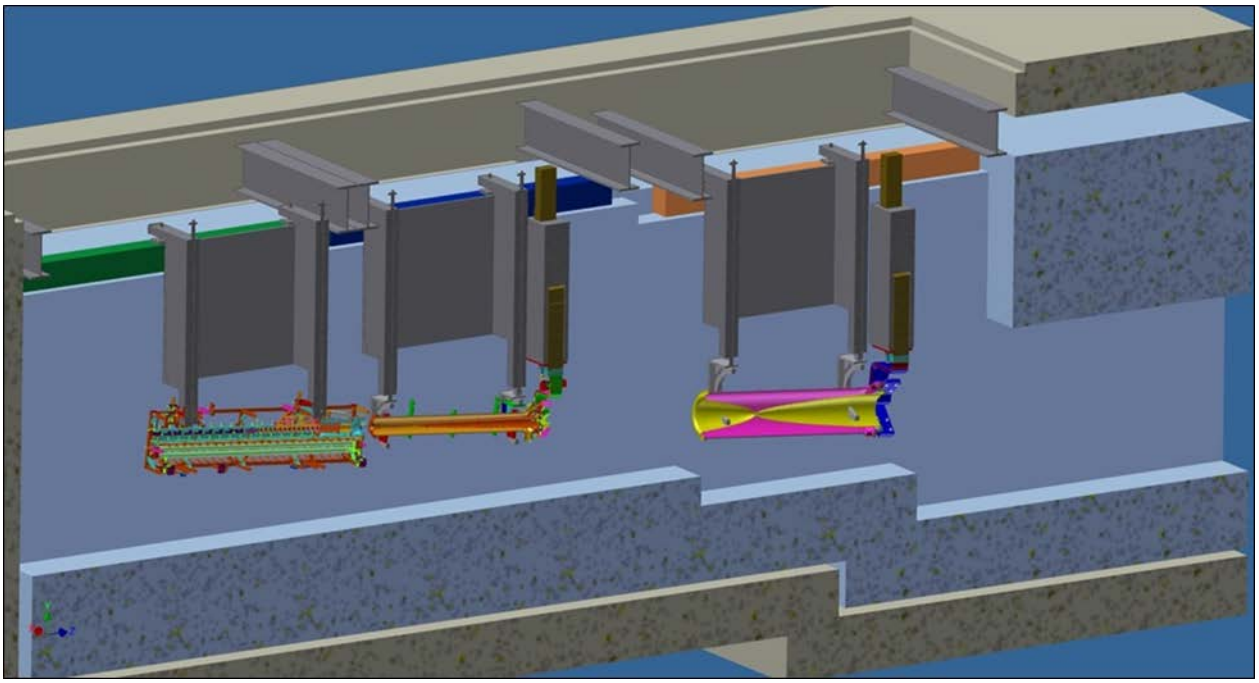

Figure 4-32: Horn Support Module Concept. The Beam comes from the Left, through the Target Carrier Assembly, Followed by the Horn 1 and Horn 2 Module Assemblies

The horizontal system is mounted to the carriage rails to allow the module to be pushed or pulled horizontally perpendicular to the beam with two independent five-ton screw jacks. The screw jack is powered by a radiation-hard stepper motor. The design is based on the existing hardware for the Booster Collimators installed at Fermilab. By differentially driving the horizontal motors at each end of the module, yaw is controlled. The vertical adjustment system is a simple screw-jack-gear-box-motor configuration conceptually similar to the horizontal mechanism. To allow the horn to be crane-lifted out of the beamline for repairs and then replaced without changing its position in the beam line, the module adjustment mechanism includes a kinematic mount. A standard kinematic mount is a three-point support with the third support point sitting on a flat plate to allow free horizontal motion. The modules are on four point supports, so both of the beam left support points are simple flat plates. Once the modules have been surveyed into place the first time, the motorized adjustment mechanisms can be used to scan the horn across the beam for final alignment. High-strength steels – alloys whose yield strength is above 87 ksi – have been found to be a problem in high-radiation areas because of “stress corrosion cracking”. This class of materials will not be used on any component of the modules or their adjustment systems.

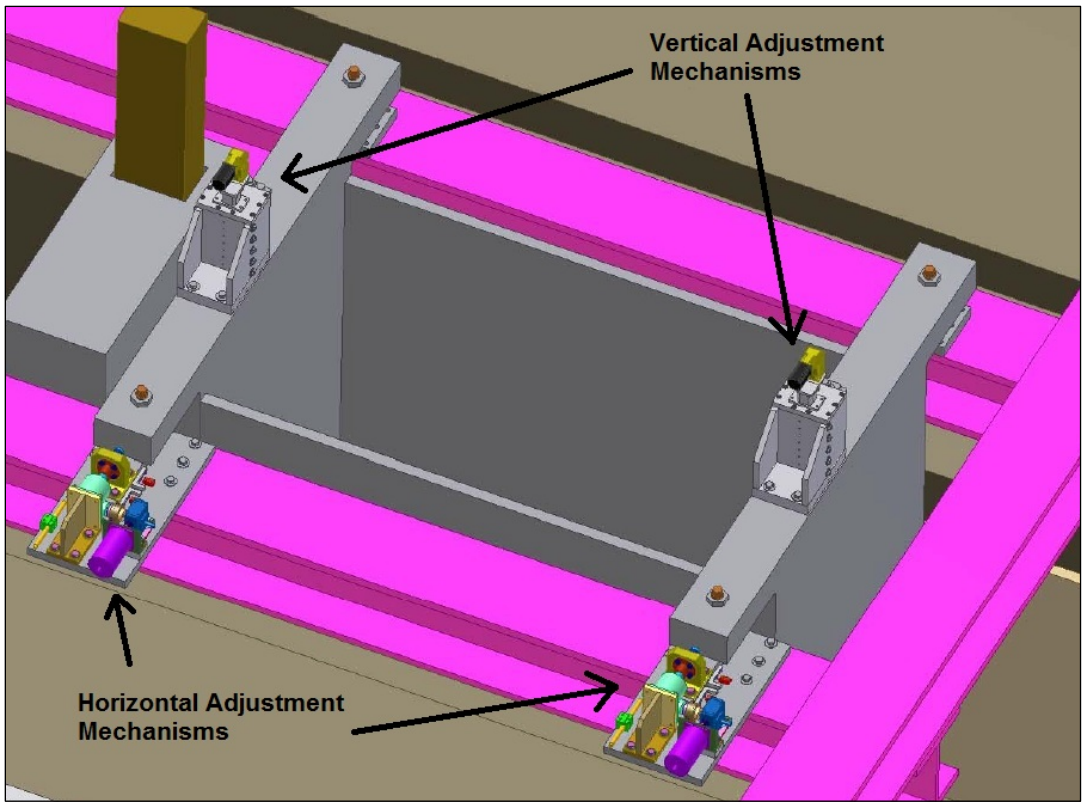

Figure 4-33: Adjustment Fixtures for the Horn-support Module Concept. The Modules are Fixed only Horizontally along the Beam Direction

Effects of module heating due to beam energy deposition will impact the dimensional stability during operation. The resultant temperatures and deformations must be well understood, so as the impacts can be accounted for in the design. A preliminary thermal analysis has been completed on the module mainframe using the conceptual cooling layout as can be seen in Figure 3-32, and efforts are ongoing to increase cooling to specific regions where temperatures are still problematic.

Heat will be primarily removed by cooling water running back to a RAW system heat exchanger, with small contributions on the module exterior by the chase air flow. Cooling water will be delivered by means of 4” diameter cartridge cooling elements that are placed on either side of the vertical position screws on the U.S. and D.S. end-walls (locations 1, 2, 3, & 4). Cooling at the bottom of the module, where the horn hangers will be attached, will be achieved through the use of cooling plates, bolted directly to the sides of the end walls (locations 5, 6, 7, & 8).

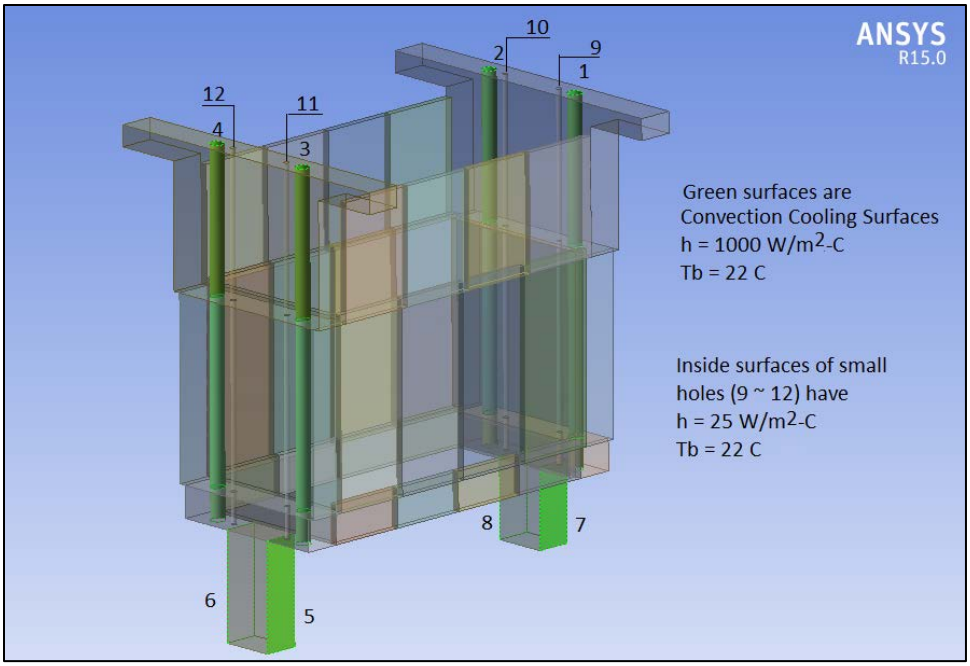

Figure 4-34: Cooling Passage Layout and Module Subsections for Analysis

Initial deformation results of the module horn supports can be seen in Figure 3-33. Continuing efforts are being made to reduce deformation, with the final goal being to remain well within the displacement limitations of the carriage rails when fully loaded. Movement at the upper end of the module and its surrounding shielding blocks is higher than cooled regions, but of no concern as it plays no part in dimensional stability of the horns.

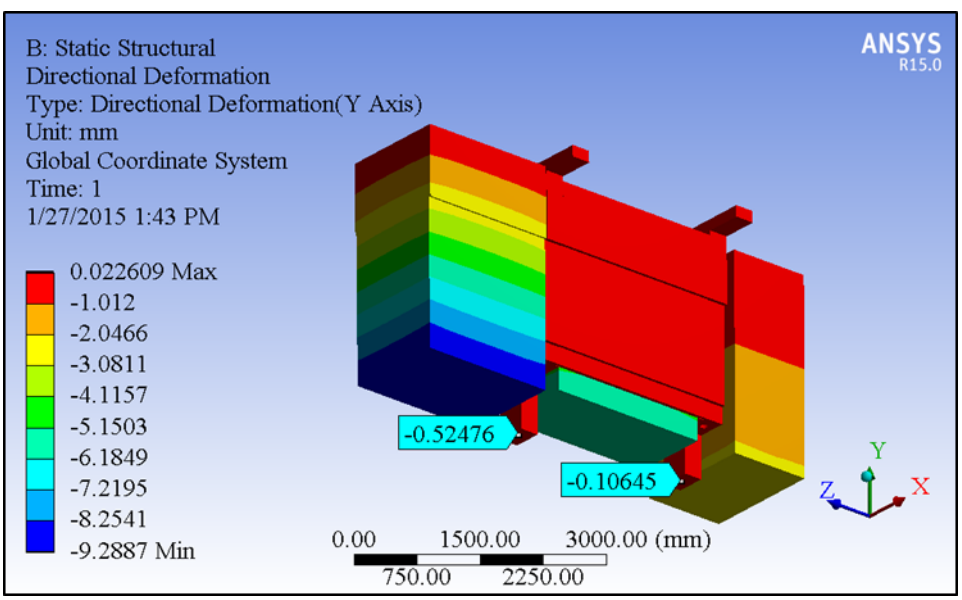

Figure 4-35: Preliminary Thermal Expansion Results for Horn 1 Module Mainframe

4.4.4 Support Module Stripline Blocks

Attached to each horn and supported by the module mainframe, the stripline block provides radiation shielding, as well as a containment structure for the striplines that supply current to the horn conductors. The blocks must have an integral labyrinth for these aluminum layers due to radiation shielding concerns, and also must remotely attach and un-attach from the horn stripline through use of a remote clamp which is mounted to the lower end of the block. The conceptual stripline block assembly can be seen in Figure 3-34. This allows a complete horn system assembly to be assembled and unassembled through remote handing, providing minimal exposure to technicians during horn change-outs.

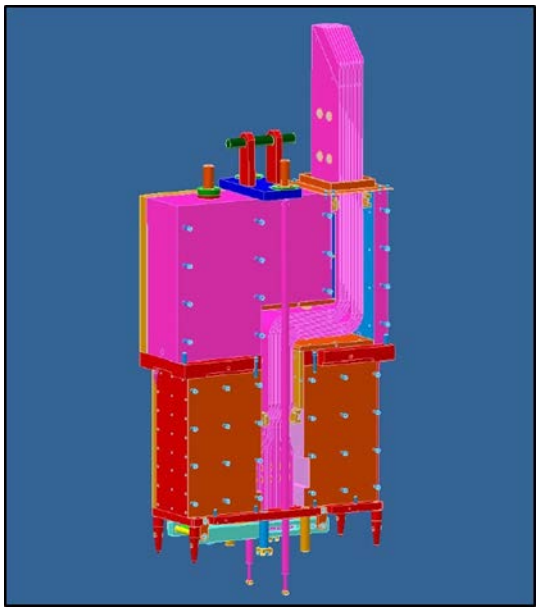

Figure 4-36: Conceptual Horn Stripline Block

The stripline block will primarily consist of steel construction, having a stainless steel outer casing to provide corrosion resistance and containment for any internal components. The remote clamp assembly will be manufactured from 316 stainless steel to resist corrosion, as it must be able to disengage the horn stripline upon release. The remote clamp can be seen in Figure 3-35.

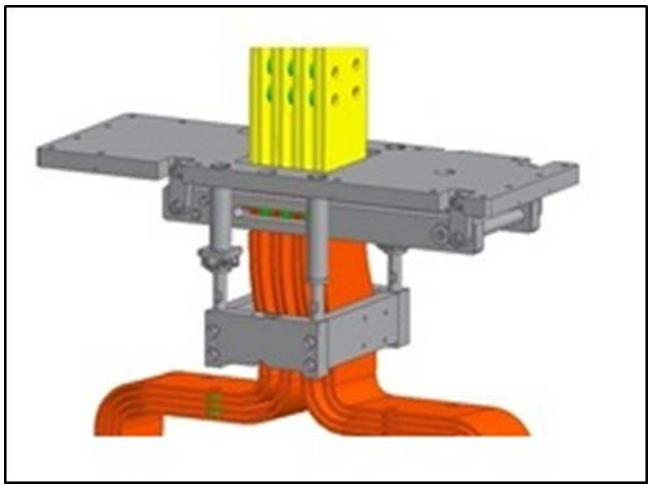

Figure 4-37: Stripline Block Remote Clamp Assembly

4.5 Horn Power Supplies (WBS 130.02.03.05)

4.5.1 Design Considerations

The horn power supply will be designed to supply two horns with a maximum of a 300-kA sine-wave peak, within tolerances set for a minimum beam pulse of 10 microseconds.

A damped LC discharge circuit (as shown in Figure 3–XXX32) will achieve the peak current when the silicon controlled rectifier (SCR) switch releases stored energy from the capacitor bank to the horns via a planar transmission line ("stripline"). The estimated circuit parameters are as listed in Table 3–6.

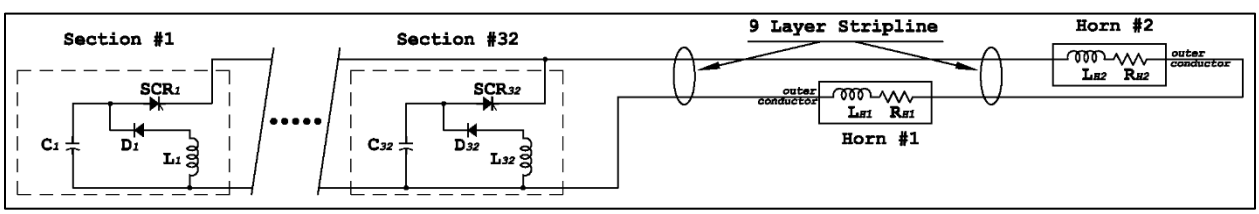

Figure 4-38: LBNF Horn PS Simplified Circuit Diagram

Table 4-5: LBNF Horn PS Circuit Parameters

	Inductance	Resistance
	(Henries)	(Ohms)
Horn_1	1.43E-06	3.20E-04
Horn_2	6.36E-07	8.50E-05
Stripline (45 meters)	4.50E-07	3.80E-04
PS (10 meters stripline)	1.00E-07	8.44E-05
System Total	2.616E-06	8.694E-04
	Farads	**Seconds**
Storage C	2.2910E-02	
Base Width		8.00E-04
Rep Rate		1.20E+00

4.5.1.1 Charging Source

The capacitor bank will be charged during the quiescent period between discharge cycles by a phase controlled, made-to-order unit specified to an outside vendor via bids. Operating voltage for the capacitor bank will be nominally 3.5 kV. Calculated DC-power consumption during operation of the focusing horns is 60 kW.

4.5.1.2 Capacitor Bank

Based on the inductance and resistance value estimates, the capacitance required for the bank is 23 mF. This will be made up of an array of individual capacitors connected in parallel, but electrically separated into 32 cells. The number of capacitors in each cell will be chosen to limit the amount of energy per cell to a value that can be safely contained within an individual capacitor case in the event of an internal fault.

4.5.1.3 Discharge Resistors and Safety System

A safety system will be included to continuously monitor operating parameters during the charge and discharge portions of the cycle, safely shutting down the system if out-of-tolerance conditions are detected. Parameters to be monitored include personnel entry, charging source over-current, over-voltage, over-current on any one cell, total load over current, out of balance conditions between cells, ground fault currents, and excessive temperatures. The loss of cooling to the charging source power supply capacitor bank, transmission line and the horns will also be monitored. When fault conditions are detected, the charging source will be shut down and the capacitor bank immediately discharged via a redundant array of dump resistors and electronic and mechanical switching devices to dissipate all stored energy.

A slow-start controller, regulating output current from zero to full over a time period of 30 s, will be included to allow the system to trip at low-level conditions during initial turn-on in the event the load has been compromised by any form of fault.

4.5.1.4 Switching Elements

The SCR switch proposed for the LBNF Horn Power Supply is a proven design used in systems MP0x supplies and the MiniBooNE Horn. This switch is built around the IXYS UK WESTCODE – Distributed Gate Thyristor Type R1275NC18J. This 'Base Design' will be built around a 10k Amp limit for each switch.

The recovery diode for the LBNF Horn Power Supply by necessity will be different than the recovery diode used in MP0x supplies and the MiniBooNE Horn. This diode must support a much larger current due to the smaller recovery choke inductance. After a search the IXYS UK WESTCODE – Fast Recovery Diode Type M1502NC220 was chosen for the 'Base Design'.

4.5.1.5 Recovery Chokes

The recovery choke design to reverse the capacitor voltage with minimal losses will be a copy of the MiniBooNE Horn PS. As with the MiniBooNE Horn the recovery will be on an individual cell basis.

The fundamental recovery current frequency is about 200 Hz. This is a factor of 3 less than the original MiniBooNE design. Recovery losses are expected to be manageable with this implementation of the existing design.

4.5.1.6 Current Transducers

Passive current transformers installed within each capacitor bank cell monitor the cell performance to 0.4% accuracy. These 12 signals are also summed to provide individual stripline currents plus total load current for over-current monitoring and readout display.

4.5.1.7 Transmission Line

A stripline consisting of a nine-layer assembly of parallel aluminum electrical bus conductors will connect the capacitor bank to the two series connected horns. The aluminum alloy of choice is 6101-T61, having nearly the conductivity of pure Al but with enhanced mechanical properties. Of the successful designs presently in service for the NuMI and MiniBooNE horn systems, the MiniBooNE design is best scaled to the higher LBNE peak current. Its balanced configuration offers much reduced electromagnetic, vibration and mechanical stress. Its cross section is shown in Figure 3–XXX33.

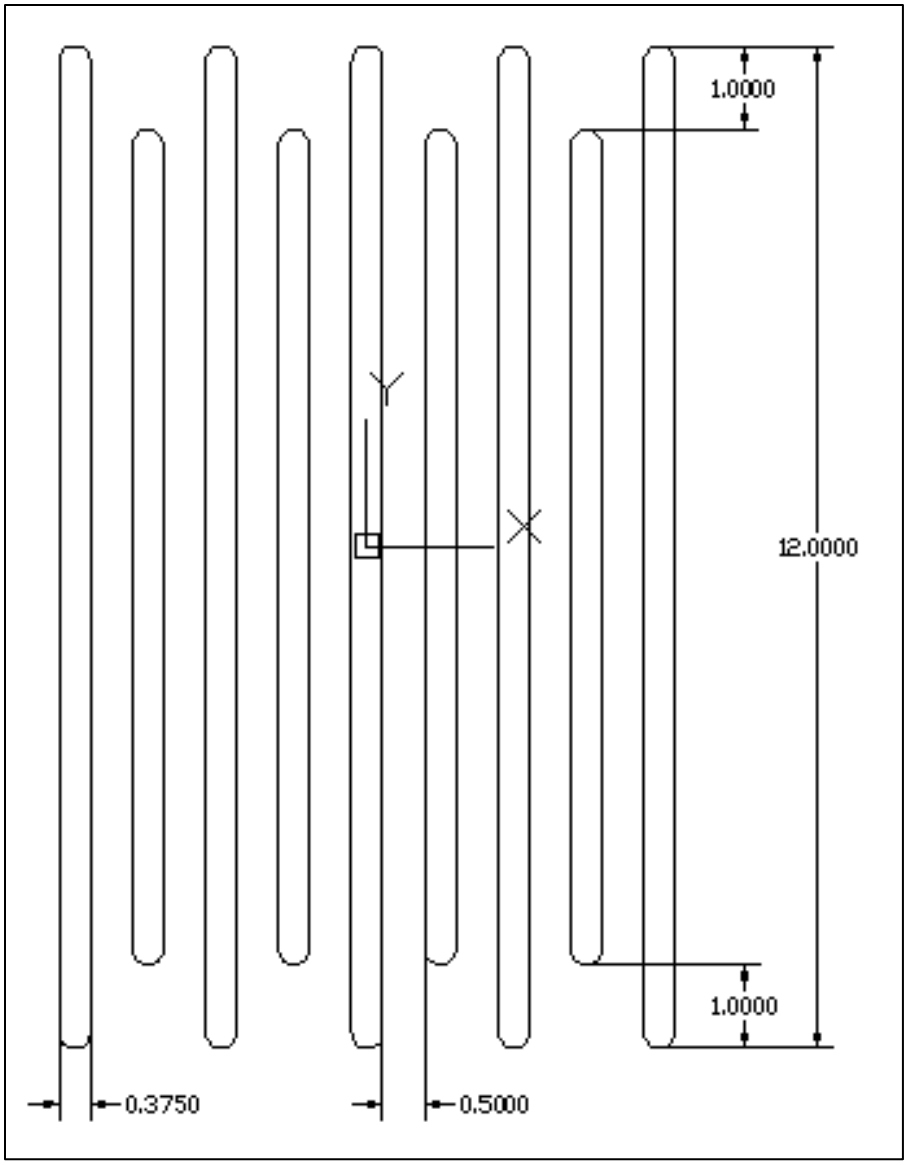

Figure 4-39: Layer Stripline

Additionally, the stripline design must have minimal inductance and resistance, allow for thermal expansion and contraction at horn and capacitor bank connections, and allow rapid reliable connection and disconnection at each horn location. In high-radiation-field portions of stripline, the conductors are spaced with alumina ceramic insulators. In minimal radiation portions, lower-cost inorganic materials will be sought. Lengths between spacers are separated by an air gap. The assembly will be held in compression by overall steel bar-clamps at each spacer location. Vertical floor-mounted stanchions will support the completed structure. Power loss in the transmission line is 422 W/m, 19 kW total, based on an estimated stripline length of 45 m. Overall ducting and filtered forced-air cooling will protect personnel and control temperatures. It will be sized to carry the normal 7,100 Arms operating current. The connection to the horn is shown in Figure 3–XXX34.

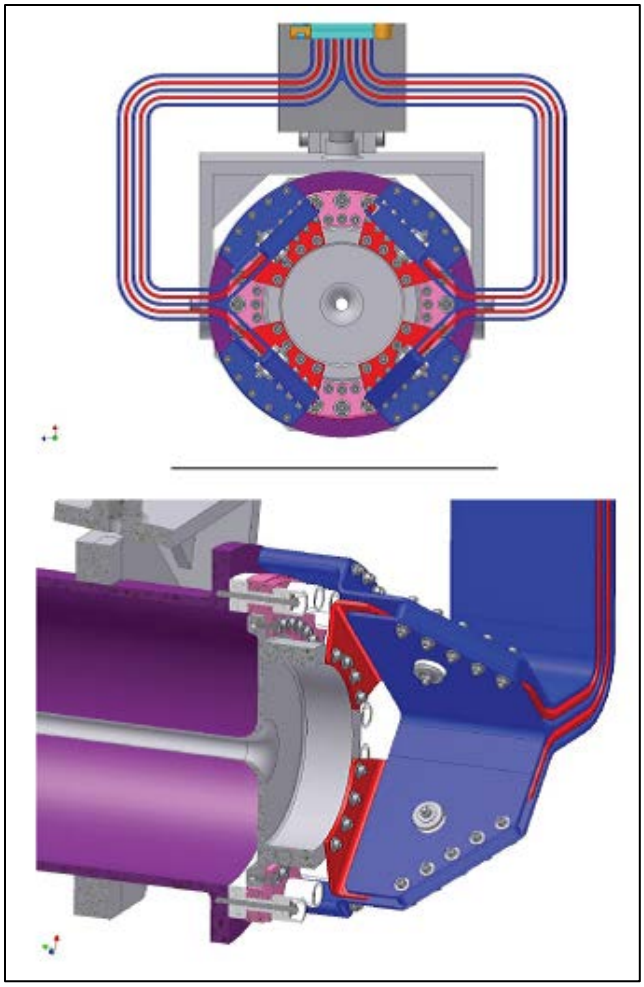

Figure 4-40: Upper: Connection to Horn-1, End View Looking DS; Lower: Vertical Section, Horn/Stripline Interface

4.5.1.8 Ground Fault Protection

To protect other beamline instrumentation equipment from the possibility of Horn Power Supply high current ground faults, its energy storage capacitor bank, D.C. charging source, stripline and horn loads are, by design, isolated from earth ground. To prevent these components from floating to potentials above ground, the common terminal of all capacitors within the system is connected via a suitably rated low value power resistor of < 1000 to Earth-ground. The chosen resistance value shall limit any such fault currents to 20 Amperes or less. Additionally, the resistor serves as a shunt that is continuously monitored by the local controls for ground fault current detection. Detected faults initiate immediate termination of system operation and via electronic crowbar redirect of all remaining stored energy to an internal dump.

Most importantly, all high-voltage equipment enclosures will be connected directly to an Earth ground utilizing low-impedance techniques. This protects personnel making incidental contact with the exterior of any of the system enclosures from transient “ground bounce” should such faults occur during routine operation or maintenance activities.

4.5.1.9 Water Cooling

The SCRs and series charging source inductors will require low-conductivity water (LCW) cooling at a combined total flow rate of 15 gpm. Water flow rates for the charging source supplies will be determined and specified by the vendor. Dump resistors are sized to absorb the maximum stored energy of the capacitor bank by a safety margin of two and can be convection cooled as a consequence of their infrequent operation.

4.5.1.10 Enclosure

The enclosure design, as used by both the NuMI and MiniBooNE experiments, is well suited for LBNE. The heavy steel design provides additional safety for energy containment in the event of internal faults. Its pan-style base serves also for capacitor oil containment in the event of impregnant leakage and allows access to internal components on all four sides.

Target Hall Shielding (WBS 130.02.03.08)

4.6 Introduction

4.6.1 Target Hall shielding (also called the target pile) is designed to (1) keep the accumulated radionuclide concentration levels in the surrounding soil below standard detectable limits; (2) keep prompt radiation levels low enough for electronics in the Target Hall to have adequate lifetimes; and (3) keep residual radiation rates on top of the shield pile low enough to allow personnel to access the top of the steel shielding pile for maintenance with beam off.

4.6.2 Design Considerations

Target pile size cannot be modified or upgraded after completion. Therefore, this part of the neutrino beam has been designed for 2.4 -MW beam-power operation, corresponding to the maximum anticipated power.

4.6.3 Reference Design

4.6.3.1 Target Hall Shield Pile

The Target Hall shield pile refers to the steel shielding surrounding the beamline components (baffle, target, Horn 1, Horn 2, and the decay pipe upstream window) installed in the target chase. The target chase is the central rectangular open volume that runs the entire length of the steel shield pile. The chase extends from the primary-beam window down to the decay pipe. The chase is 54-inches wide at the water-cooling panels in the region of the horns and 64-inches wide elsewhere. Its height varies along the length of the shield pile; the chase floor has one vertical step. The beamline in the Target Hall region slopes downward at 0.101033 radians (5.78876°) from upstream to downstream, as illustrated in Figure 3-44.

The chase acts as a collimator for pions from the target and horns that are not well-focused. This collimation reduces the beam power deposited in the decay pipe.

The shield will consist of two main layers. An inner, steel layer will absorb all of the stray particles from interactions of the primary beam, except neutrons below a few MeV energy. The outer layers are used to moderate and absorb most of the neutrons that escape from the steel layer. These outer layers consist of concrete, marble, or borated polyethylene plates, depending on location.

The shielding is divided into two sections: (1) the bottom and side shielding which must appropriately shield the surrounding earth and ground water from tritium activation; and (2) the top shielding which must shield the upper Target Hall. The shielding is illustrated in Figure 3-45, which is the lateral cross section of the target pile at MC-ZERO.

The LBNF steel, concrete, marble, and borated polyethylene shielding requirements are given in Tables 3-7 and 3-8. Additionally, there is a 120-in-thick concrete wall and 9-inch thick steel slab at the upstream end to separate the target pile from the pre-target tunnel. For comparison, NuMI has 1 m of concrete and 52 in of steel shielding on the bottom and sides and 73 to 82 inches of steel and 18 in of concrete on the top.

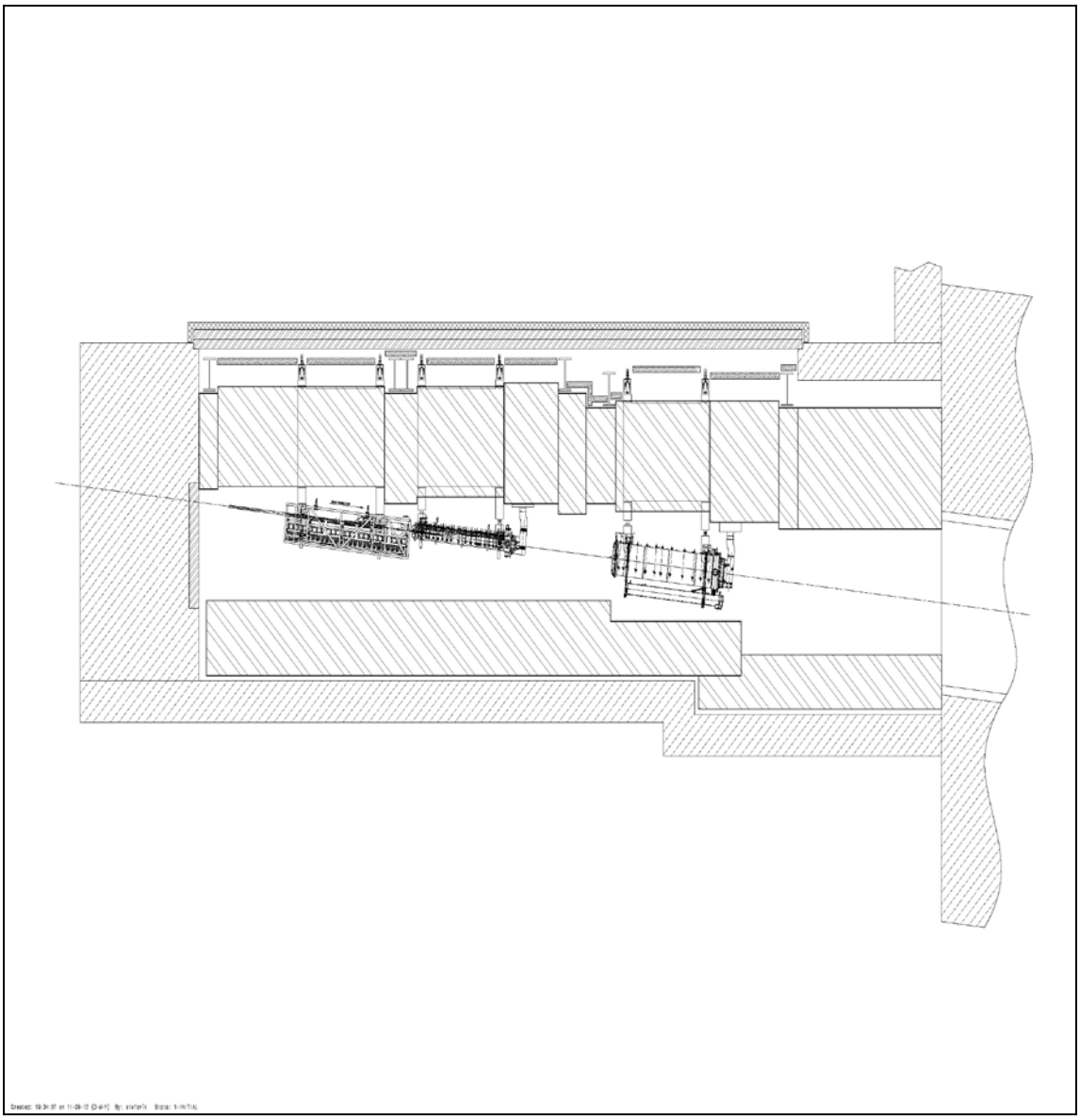

Figure 4-41: Beamline Elevation View – Beam direction is Left to Right

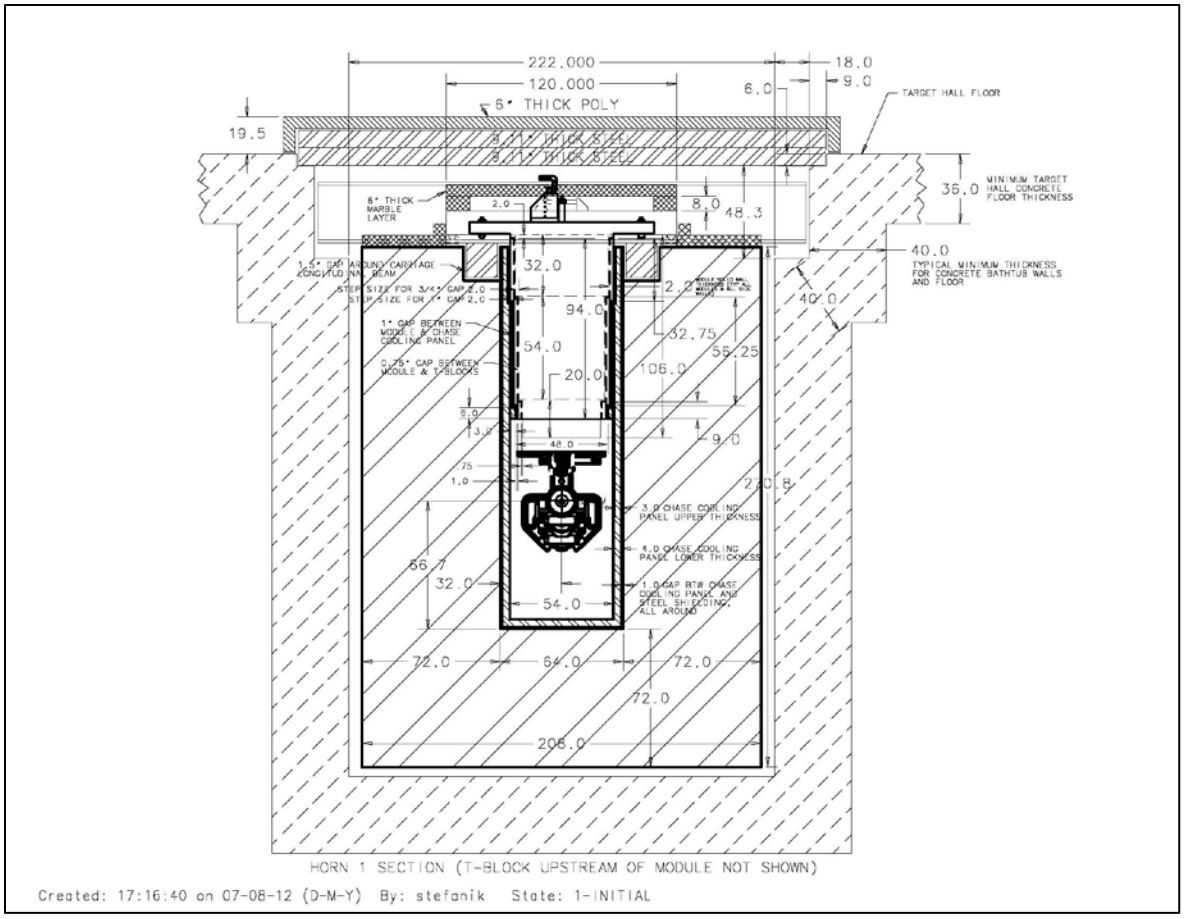

Figure 4-42: Cross Section of Target Chase Steel Shielding (Cross-hatched Areas). The Secondary Beam is Confined to the Rectangular Opening in the Center.

Table 4-6: Shielding Requirements for the Top of the Target Chase

	Iron (in)	Marble+ Borated Poly (in)	Concrete (in)
Top of chase- All regions	18	0	0
Baffle	92	6	0
Horn 1	106	6	0
Between horns Sec. 1	116	6	0
Between horns Sec. 2	92	6	0
Horn 2	106	6	0
Downstream Horn 2	116	0	36

Table 4-7: Shielding Requirements for the Walls and the Floor of the Target Chase

	Iron (in)	Concrete (in)
Upstream wall	12	140
Baffle floor	72	40
Baffle right wall	72	96
Baffle left wall	72	40
H1 floor	72	40
H1 right wall	72	85
H1 left wall	72	112
Between Horns floor Sec.1	72	40
Between Horns right wall Sec.1	52	112
Between Horns left wall Sec.1	52	112
Between Horns floor Sec. 2	72	40
Between Horns right wall Sec.2	52	112
Between Horns left wall Sec .2	52	112
H2 floor	52	40
H2 right wall	52	85
H2 left wall	52	40
DS of H2 floor	52	40
DS of H2 right wall	52	85
DS of H2 left wall	52	40

The open space between the steel shielding and the floor and walls of the Target Hall concrete pit form air cooling channels for the exterior surface of the steel pile. The channels are named “bottom” for the floor and “side” for the walls. The space between the top of the steel shielding pile and the poly layer is called the “top” channel. The poly layer is the cover over the Target Hall pit. The cooling airflow, discussed below, flows through these channels to enter the chase.

Shielding steel is stacked in a staggered and interlocking fashion so there are no line of-sight cracks through the steel shielding pile. Vertical gaps between pieces are filled with steel shim stock to the required maximum gap size. Two methods are used to close the top of chase. Removable, specially made steel blocks called “T-blocks” are used where beamline components are installed. Steel blocks and slabs are used in the other areas.

A view of the bulk steel shielding after roughly two-thirds of it has been installed is shown in Figure 3-46.

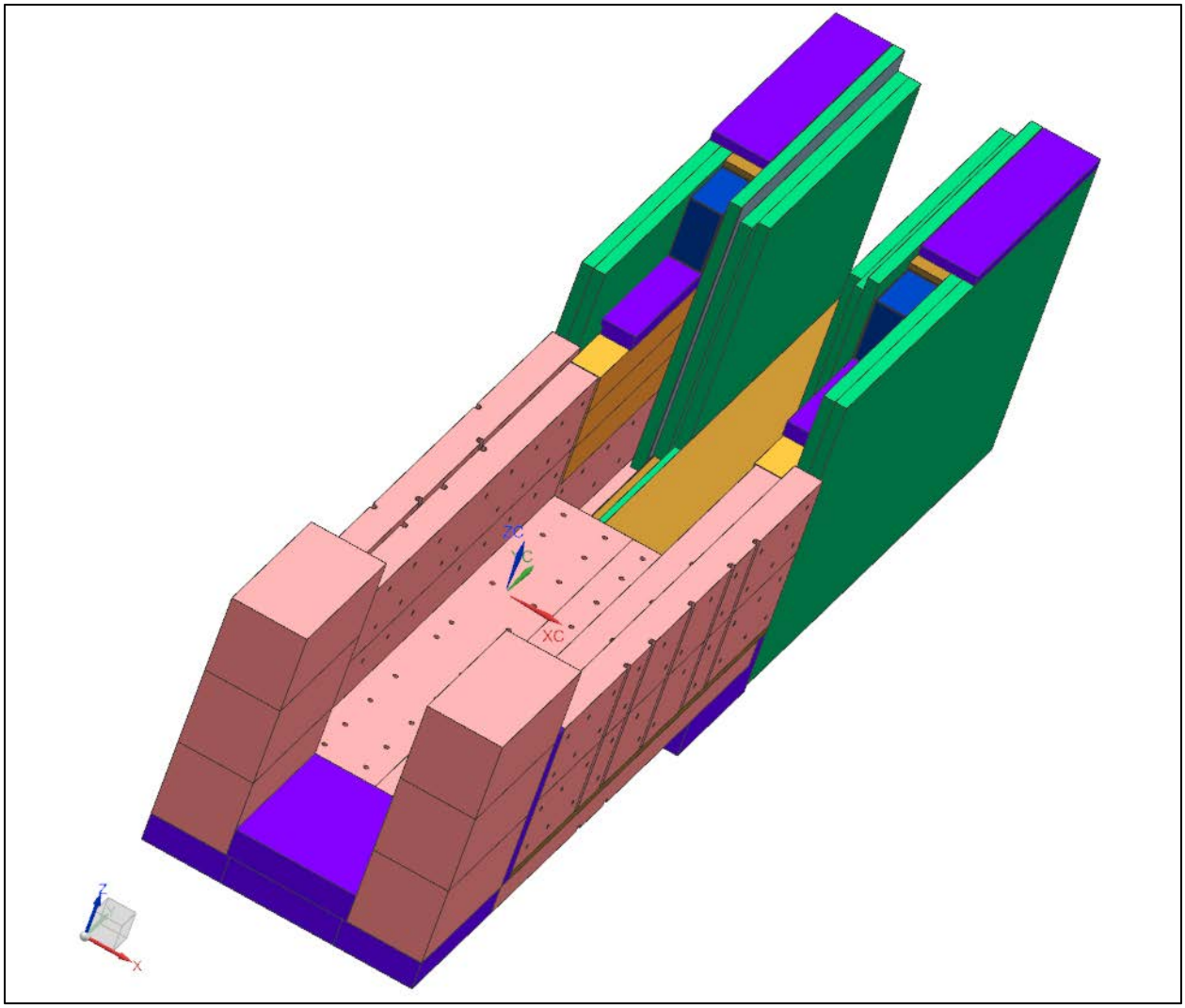

Figure 4-43: View of the Bulk Steel Shielding after the Large Steel Pieces have been Installed and Installation of the Downstream end has Started

4.6.3.2 Target Hall Air-Cooling

Energy deposited in the shielding pile and the beamline components by the 2.4-MW beam or the 1.2 MW beam is removed by water-cooled shielding, an air-cooling system and cooling systems on the beamline components. The water-cooled shielding, i.e., carbon steel chase panels, T-blocks and module bottoms, intercept approximately half of the beam energy leaving the chase. The air-cooling system and cooling systems on the beamline components remove the balance of the deposited beam energy. The air cooling flow rate is 35, 000 scfm. The airflow rate is obtained by scaling the 25,000 scfm airflow rate for the 46-inch NuMI chase to the 64 to 54-inch LBNF chase using the cross sectional chase flow areas.

The discussion below describes the air-cooling system. The equipment needed for air cooling is provided by Conventional Facilities at the Near Site, and discussed in Volume 5 of this CDR. The flow schematic for the target pile air cooling system is illustrated in Figure 3-47.

A single air handler, located in the Air Handling Room, provides 35,000 scfm of cooled and dehumidified air to help cool the shielding pile. Starting at the "Target pile air handler" box in Figure 3-47, the cooling airflow enters the target pile at the downstream end above the steel shielding and flows upstream in the top, bottom and side channels. All of the air exits the bottom and side channels at the upstream end of the pile, turns 180 degrees, and enters the chase. All of the air flowing in the top channel flows vertically downward through clearances between the T-blocks and into the chase. The 35,000 scfm cooling airflow exits the chase at the downstream end and enters the air return duct back to the air handler to be cooled and dehumidified. Approximately 20,000 scfm flows in the top channel, 5,000 scfm flows in each of the two side channels, and 5,000 scfm flows in the bottom channel. A welded, stainless steel duct is embedded in the steel shielding, called the "air block", to separate the supply and return air flows in the target pile. The supply and return ducts have labyrinths and steel shielding where the ducts enter or leave the shield pile to attenuate radiation leakage out through the ducts.

There are two studies in progress that could eventually affect which gas is selected for use in the target pile cooling system: (1) LBNF Corrosion Task Force, and (2) LBNF Air Releases to the Atmosphere. The conclusion from either one or both of these studies could require that the oxygen concentration in the target pile cooling system be minimized to mitigate the possible problems of (1) corrosion of the steel shielding, destruction of the primer coating, and corrosion of the stainless steel air block due to ozone production, and/or (2) radionuclide emission to the atmosphere. Compliance with a requirement to minimize the oxygen concentration will be accomplished by changing the cooling gas from air to nitrogen gas. Using nitrogen gas instead of air as one of the target pile coolants will impact the target pile fluid handler and the room it is in. The impacts are the fluid handler must be sealed very well to minimize nitrogen gas leaks and the room might need to be classified as an ODH, Oxygen Deficiency Hazard, area.

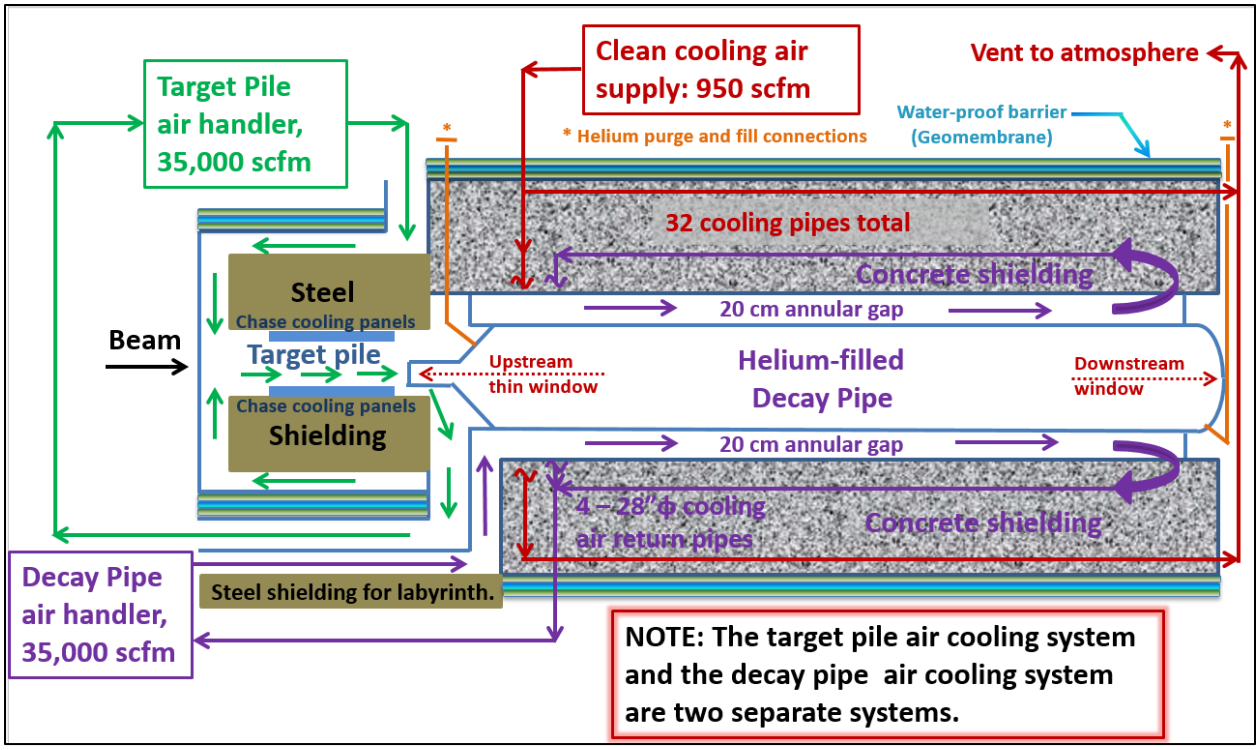

Figure 4-44: The Flows for the Target Pile and Decay Pipe Air-cooling Concept are Shown Schematically

Supply and return air ducts connected to the target pile are shown in Figure 3-48. The ducts are provided by Conventional Facilities at the Near Site and are discussed in Volume 5 of the CDR.

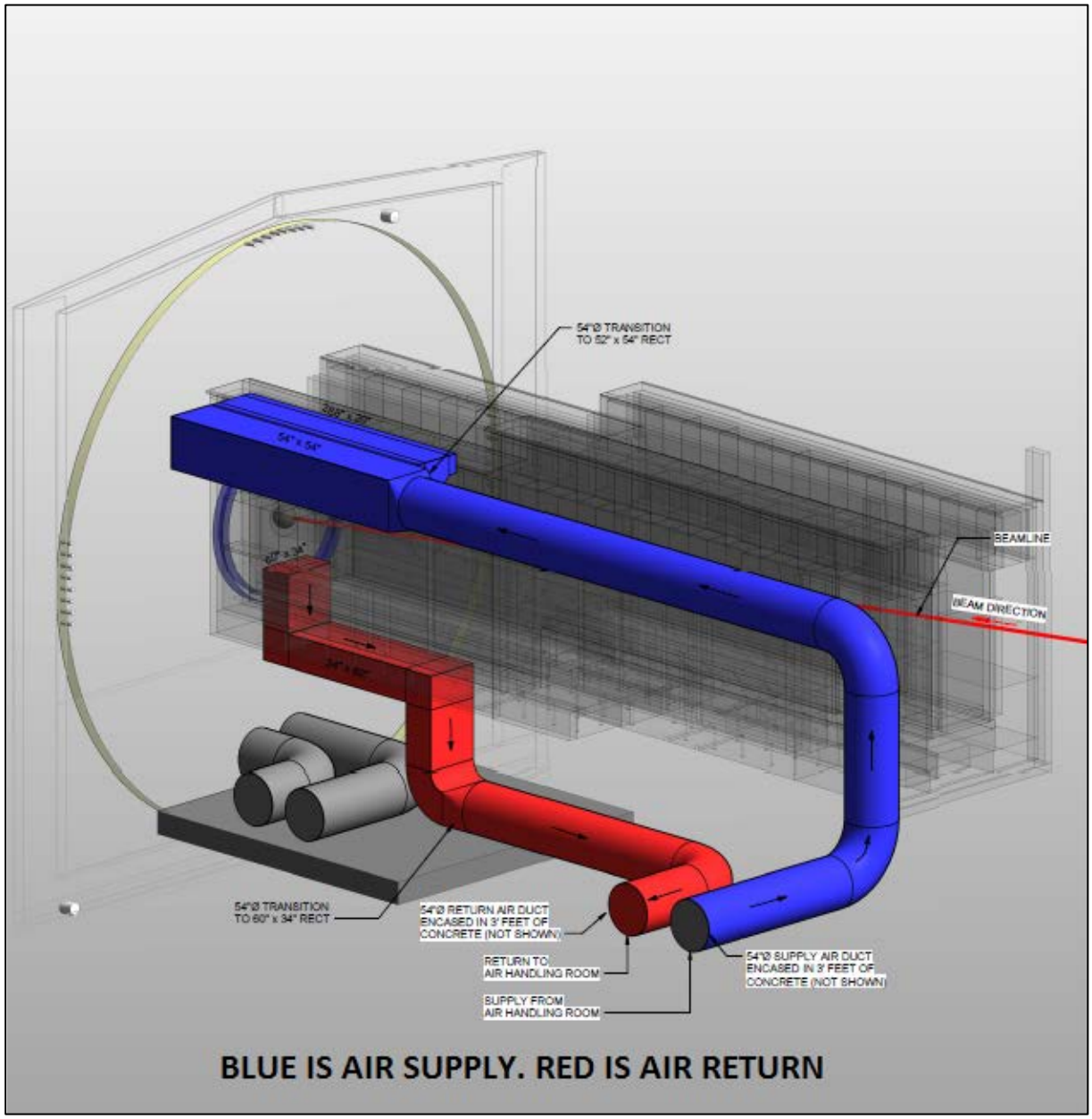

4.7

Figure 4-45: Supply and Return Air Ducts for the Target Pile

4.7.1

Helium-filled Concentric Decay Pipe (WBS 130.02.03.06)

Introduction

The helium-filled decay pipe is the region where the pions and kaons generated from the target decay into neutrinos. The length is determined by the distance at which most of the pions decay, producing neutrinos near the maximum energy required by the physics goals of LBNE. The pipe must be of sufficient diameter to allow for decay of the lowest-energy pions required by the experiment. The decay-pipe reference-design length is 203.7 meters and the diameter of the inner pipe is 4 meters.

Concrete radiation shielding surrounds the decay pipe to minimize activation of surrounding ground water. Heat generated in materials due to beam reactions will be removed by airflow through an annular duct surrounding the decay pipe. A geomembrane system surrounds the decay-pipe concrete to act as a barrier for minimizing ground-water inflow. Any ground water that penetrates the barrier system will be collected in pipes and conveyed to sumps located in the Absorber Hall, described in Section 21. A second set of air-cooling pipes just inboard of the geosynthetic system keeps the geosynthetic at low temperature to extend its lifetime.

The scope of work described in this section includes specifying (1) the length, material, diameters and wall thicknesses for the concentric decay pipe, (2) specifying the cooling parameters, and (3) designing and providing the downstream window. Conventional Facilities at the Near Site (see Volume 5 of this CDR) designs and provides the corrosion-protected concentric decay pipe, shielding concrete and the geomembrane ground-water barrier and drainage system.

Design Considerations

4.7.2 The decay pipe and its shielding are built underground and their size cannot be modified or upgraded after completion. Therefore, this part of the neutrino beam is being designed for 2.4-MW beam-power operation, corresponding to the maximum anticipated power. The concentric decay pipe and shielding concrete are illustrated in Figure 3-XXX35, which shows the system designed by Conventional Facilities at the Near Site to satisfy the Beamline requirements. The CF design is described in detail in Volume 5 of this CDR.

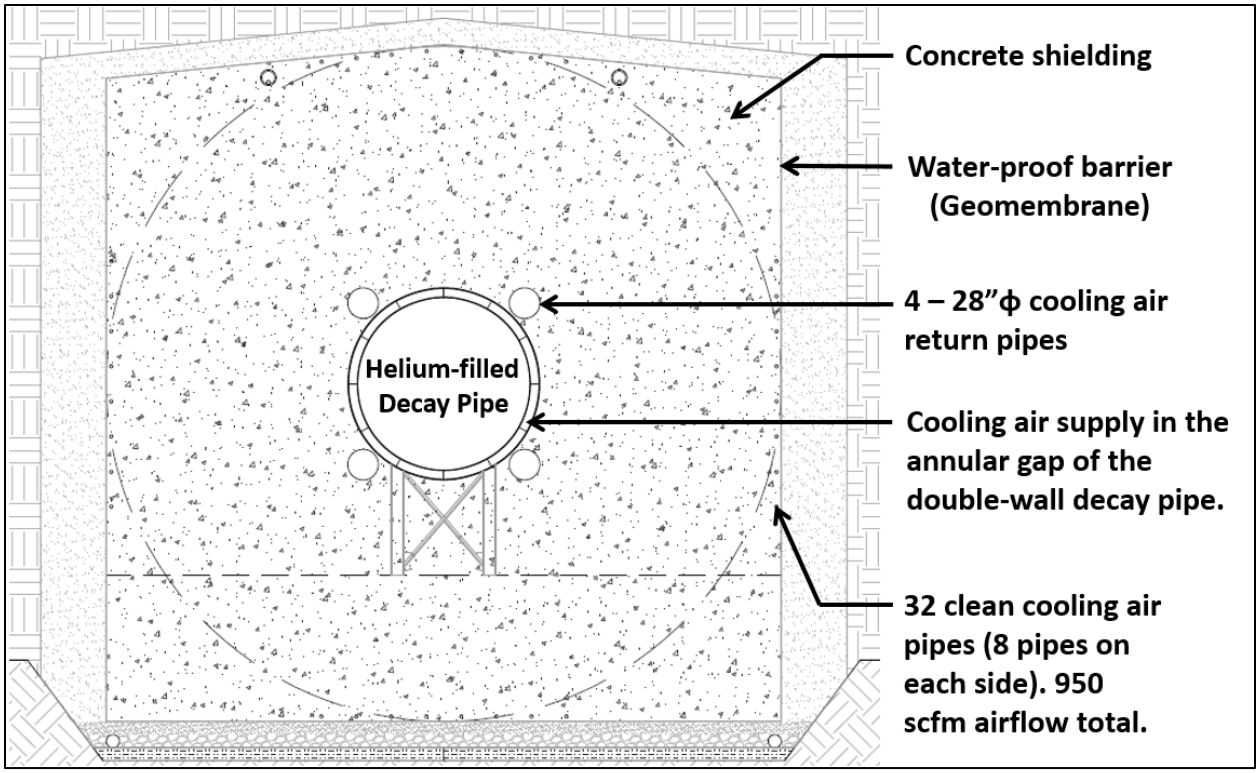

Figure 4-46: Typical Cross section of Concentric Decay Pipe and Shielding Concrete

The decay pipe must be built to meet these requirements:

- 203.7-m length
- 4-m inside-diameter steel pipe installed concentrically in a 4.43-m inside diameter steel pipe; the radial annular gap between the pipes is 0.2 m
- commercial-grade pipe with thickness of 12.5 mm
- spacers welded between the two pipes to maintain concentricity and to not interfere with the airflow
- a geomembrane ground-water barrier system to drain water away from the decay pipe as part of the overall tritium-mitigation strategy, discussed in Section 24
- alignment accuracy maintained at 20 mm
- external and internal corrosion protection
- concrete radiation-shielding thickness of 5.5 m

3.5.3 Reference Design

The decay-pipe region begins 17.3 m downstream of the beamsheet coordinate MC-ZERO which defines horn 1 position. A standard pressure vessel head is welded to the upstream end of the inner decay pipe. The head has a 1.5-meter diameter opening at its center. A 1.5-meter diameter pipe is welded at the center of the head to cover the opening. The pipe extends 2 meters into the target pile chase and is referred to as the decay pipe snout. The decay pipe upstream window is installed on the upstream end of the snout. The upstream decay pipe window is discussed in Section 3.2. The snout is open to the inner

decay pipe and is filled with helium. The snout is shown in Figure 3-XXX36 using target pile layout drawing 487105.

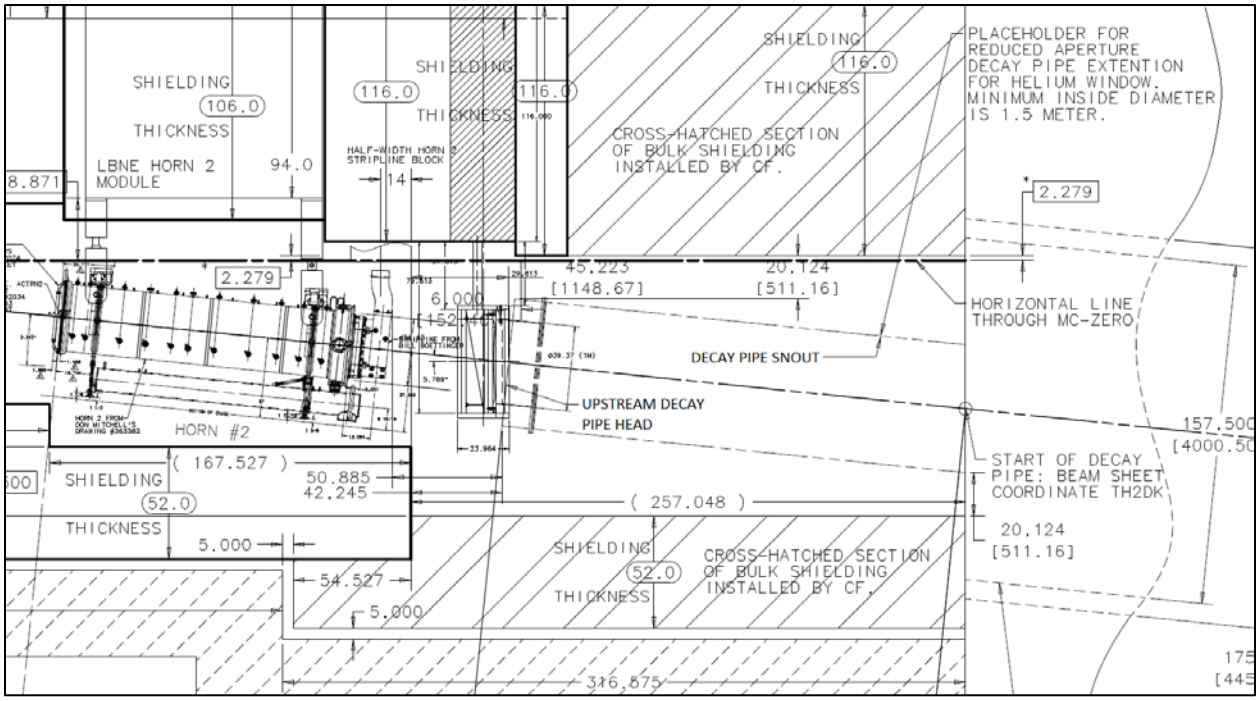

Figure 4-47: Concentric Decay Pipe Snout and Upstream Window

Heat generated by beam interaction has been calculated to be 834 kW, distributed non-uniformly along the length of the decay pipe. Approximately half of this heat is generated in the inner steel pipe, with the remainder generated in the outer steel pipe and concrete. An air cooling system is employed to cool the decay pipe. The cooling airflow schematic is shown in Figure 3-XXX37.

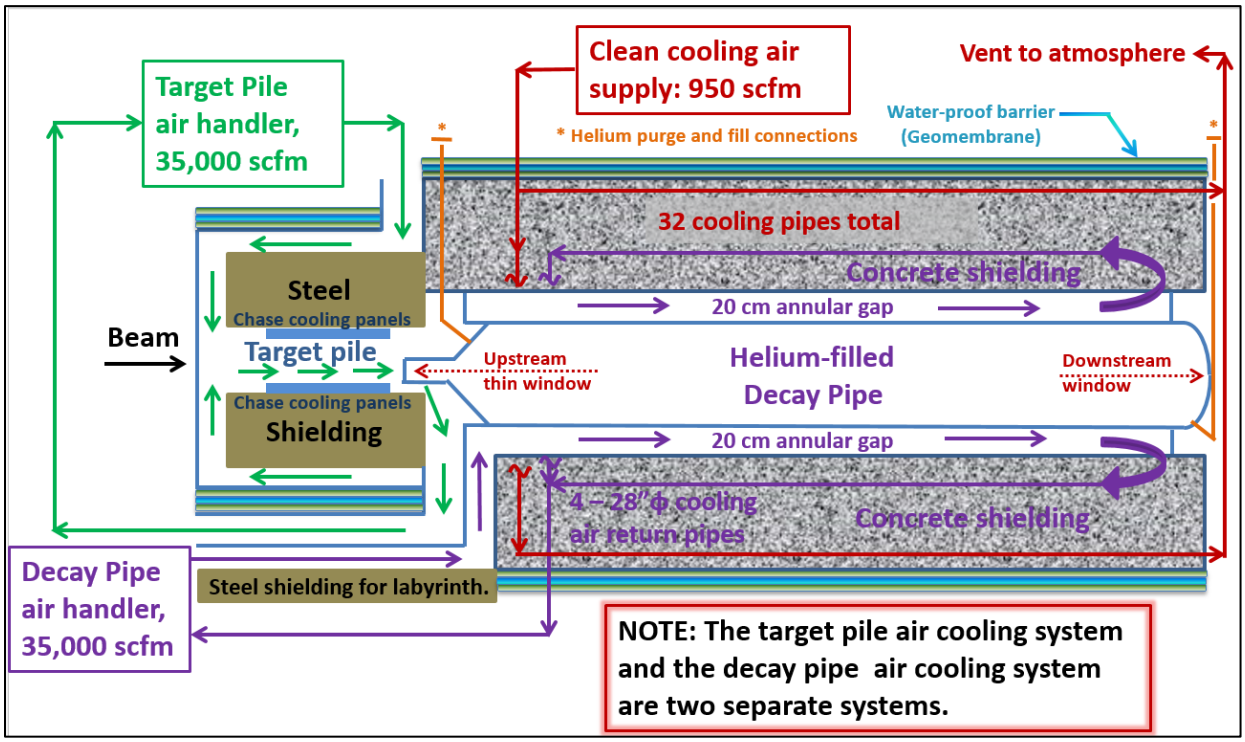

Figure 4-48: Cooling Airflow Schematic for the Concentric Decay Pipe and Shielding Concrete

The following discussion describes the air-cooling system. The equipment needed for air cooling are provided by Conventional Facilities at the Near Site and are discussed in Volume 5 of the CDR.

A single air handler, located in the Air Handling Room, provides 35,000 scfm of cooled and dehumidified air to cool the steel decay pipes and the shielding concrete. Starting at the "Decay pipe air handler" box in Figure 3-XXX37, the cooling airflow enters the annular gap of the concentric decay pipe at its upstream end and flows downstream. At the downstream end the air flows out of the annular gap into the four 28" diameter return pipes, after turning 180 degrees, and flows upstream. At the upstream end the 35,000 scfm enters the air return duct back to the air handler to be cooled and dehumidified. The supply and return ducts have labyrinths and steel shielding where the ducts enter or leave the shield pile to attenuate radiation leakage out through the ducts. For the cooling airflow of 35,000 scfm and an air supply temperature of 15 °C, maximum temperatures at the point of peak energy deposition are estimated to be 90 °C for the steel pipes, 95 °C for the shielding concrete, and 42 °C for the geomembrane water-proof barrier. Air return temperature to the "Decay pipe air handler" is 57 °C. The upstream and downstream ends of the decay pipe must be closed as part of the air cooling system of the pipe.

There are two studies in progress that could eventually affect which gas is selected for use in the decay pipe cooling system: (1) LBNF Corrosion Task Force, and (2) LBNF Air Releases to the Atmosphere. The conclusion from either one or both of these studies could require that the oxygen concentration in the

decay pipe cooling system be minimized to mitigate the possible problems of (1) corrosion of the thin-walled decay pipe base metal and welds, and destruction of the primer coating due to ozone production, and/or (2) radionuclide emission to the atmosphere. Compliance with a requirement to minimize the oxygen concentration will be accomplished by changing the cooling gas from air to nitrogen gas. Using nitrogen gas instead of air as the decay pipe coolant will impact the decay pipe handler and the room it is in. The impacts are the air handler must be sealed very well to minimize nitrogen gas leaks and the room might need to be classified as an ODH, Oxygen Deficiency Hazard, area.

The decay pipe ends in the upstream wall of the Absorber Hall. The Beamline L2 Project will design and provide the window at the downstream end of the decay pipe. The downstream window is a 6-mm thick aluminum, dished cylindrical plate, 1-meter in diameter. It is centrally set in a hot-rolled steel pressure vessel head. The head is welded to the inner pipe of the concentric decay pipe. The head and aluminum window are cooled by natural convection with air on the exterior, and by natural convection with helium on the interior. The downstream window is not replaceable. The downstream decay pipe steel head and aluminum window are shown in Figure 3-XXX38. Three energy deposition cases are considered for the heat transfer and stress analyses: normal operation, on-axis accident, and off-axis accident; these cases are illustrated in Figure 3-XXX39. For normal operation, the maximum steel temperature is 67°C, the maximum aluminum temperature is 56°C, and the maximum stress is 52 MPa; the maximum stress occurs in the aluminum. The highest temperature and stress for the accident cases are 120 °C and 110 MPa; both maxima occur in the aluminum. The following beam energies and powers were analyzed for each energy deposition case: 120 GeV @ 2.4 MW, 80 GeV @ 2.13 MW, 60 GeV @ 2.06 MW, 120 GeV @ 1.2 MW, 80 GeV @ 1.065 MW, and 60 GeV @ 1.03 MW. For all of the cases, the temperatures and stresses are below the allowable values. All of the temperatures vary little per pulse so fatigue can be neglected. All of the temperatures are also below the creep temperature limit so creep can be neglected.

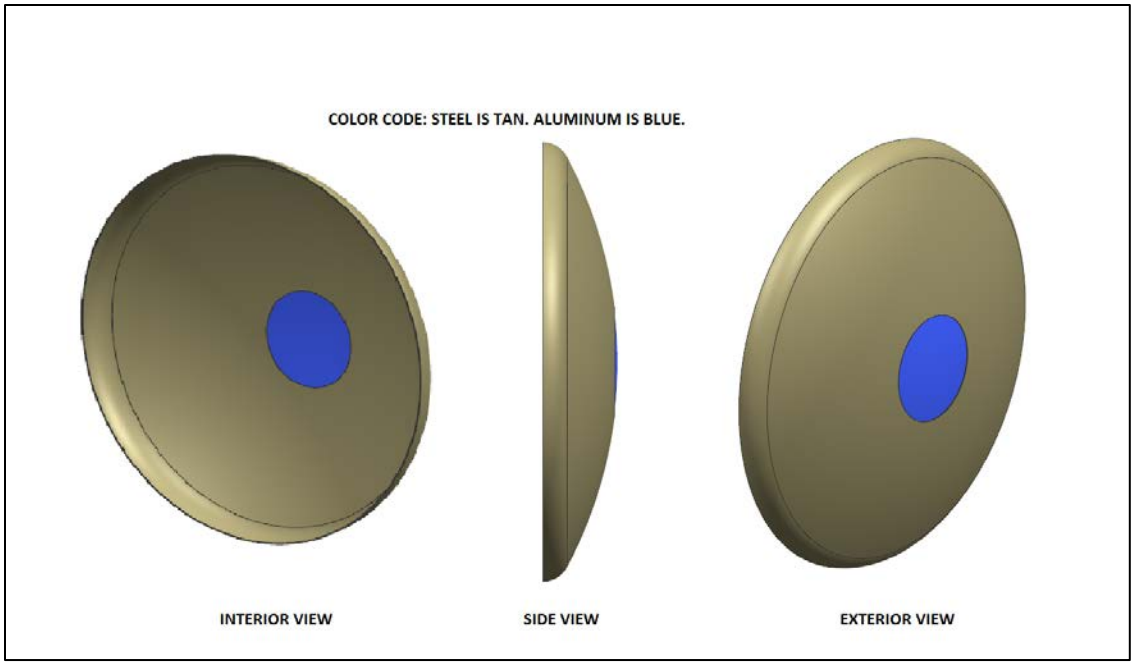

Figure 4-49: Downstream Decay Pipe Steel Head and Aluminum Window

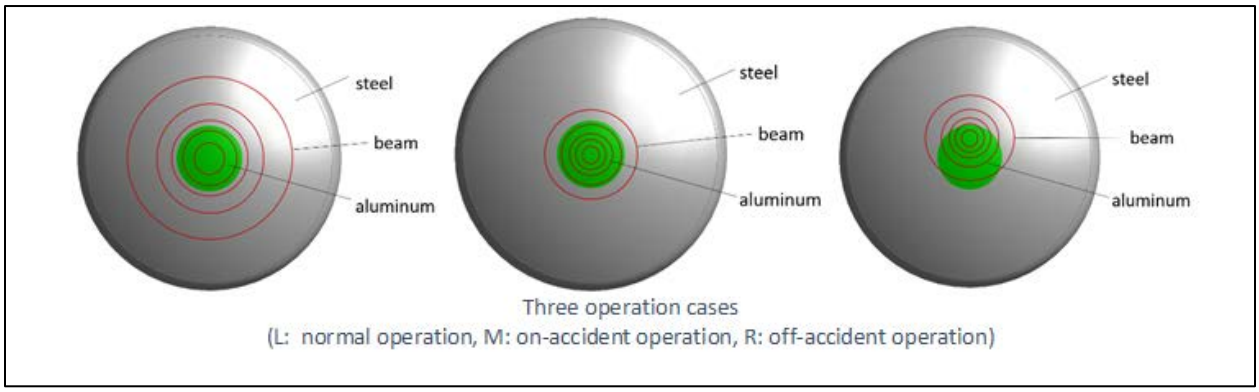

Figure 4-50: Downstream Decay Pipe: The Three Energy Deposition Cases for Heat Transfer and Stress Analyses

The concentric decay pipe has a design pressure of 5 psig as required by the helium system to purge, fill and operate the decay pipe. The helium system is discussed in Section 3.2.

Supply and return air ducts connected to the concentric decay pipe are shown in Figure 3-XXX40. The ducts are provided by Conventional Facilities at the Near Site and are discussed in Volume 5 of the CDR.

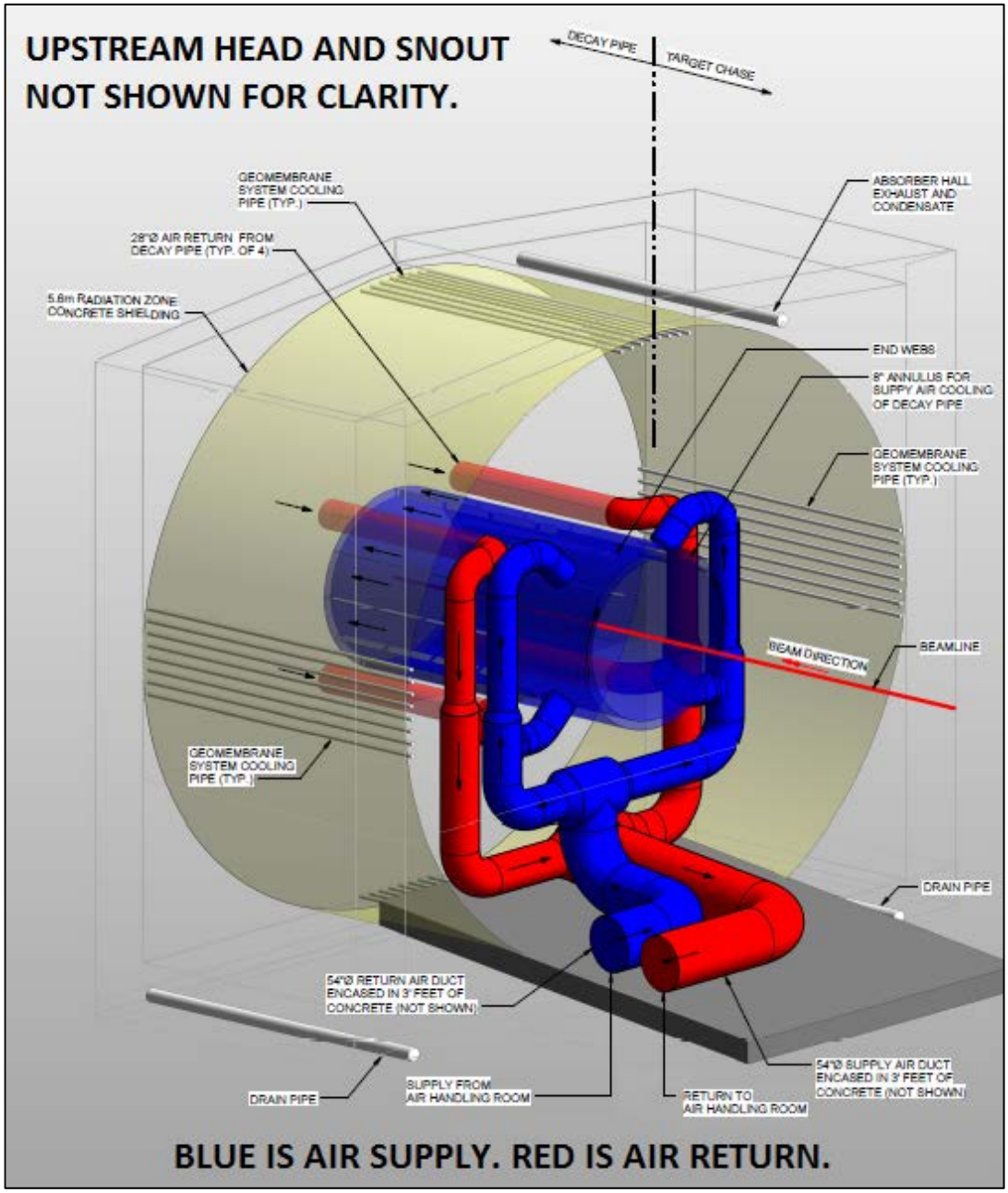

Figure 4-51: Supply and Return Air Ducts for the Concentric Decay Pipe

Beam Windows (WBS 130.02.03.02)

Introduction

4.8 This WBS includes two objects; the primary beam window (the window through which the primary proton beam exits the vacuum beam pipe before hitting the target) and the decay pipe upstream window (the large diameter window that the secondary beam passed through after the second horn and before entering the decay pipe).

4.8.1

Both windows will be exposed to very high levels of beam power and are expected to have lifetimes significantly shorter than the anticipated operational lifetime of the facility. Therefore, both windows will need to be replaceable. Because both windows will become significantly activated as a result of beam operation, means to replace the windows with minimal human exposure to activated components is part of this design effort.

Design Considerations

4.8.2 Design inputs for both windows are for a primary proton beam of energies 60, 80 and 120 GeV with beam power levels of 1.2 megawatts and 2.4 megawatts (at 120 GeV). Preliminary primary proton beam spot sizes at the primary beam window are beam spot size of 1.7 mm sigma in both x and y directions for 1.2 MW and normal condition; 1.3 mm sigma for an accident condition at 1.2 MW and larger spot sizes for the 2.4 MW beam power. Cases to consider for both the primary beam window and the decay pipe upstream window include:

- 120 GeV beam with 1.2 and 2.4 MW power levels
- 80 GeV beam with 1.07 and 2.14 MW power levels
- 60 GeV beam with 1.03 and 2.06 MW power levels
- All cases run for:
  - Beam centered on window (hitting target for the decay pipe window)
  - Beam missing target, centered on target (an accident condition only applicable to the decay pipe window, the primary beam window always has un-interacted protons on it)
  - Beam hitting window off centered (an accident condition) with the beam missing the target for the decay pipe window.

Design lifetime for the both windows should exceed 1 year of operation. Obviously longer lifetimes are advantageous.

The upstream beamline enclosures are separated from the target chase by a 3.9-m-thick concrete shielding wall to isolate the upstream beamline components from high radiation dose rates. The primary protons enter the target chase through a window in the wall; it is a beryllium foil that seals the evacuated primary beam pipe.

Experience from NuMI shows that the primary-beam window has an estimated lifetime limit of three years at 708 kW. The 708-kW primary-beam window design validated by NOvA considers an air cooled, 0.25-mm-thick, 25.4-mm-diameter beryllium grade PF-60 foil.

Lastly, the window itself (also referred to as the beryllium foil) may require active cooling at the 2.4-MW value.

Reference Design

4.8.3.1 Primary Beam Window Assembly:

4.8.3 The embedded 273-mm O.D., 6.4-mm-thick, stainless-steel stepped liner pipe implemented during the civil construction is shown in Figure –3-XXX48(a). The primary beam pipe cartridge consists of an internal 76-mm O.D., 1.5-mm-thick beam pipe suspended within an outer 260 mm O.D. stepped pipe housing, both constructed from stainless steel as shown in Figure –3-XXX48(b). Spider collars at each end provide adjustment between the cartridge housing and internal beam pipe. These collars will lock following pre-alignment and the annular void between cartridge inner housing and outer beam pipe surfaces is filled with shielding material to prevent up stream (US) radiation back-scatter. Silver plating the exterior cartridge surface and implementing a 550-mm O.D., 25-mm-thick, stainless-steel cartridge extraction flange eases removal. This extraction flange also provides indexing of the cartridge to establish longitudinal position and fixed rotation.

A conceptual section view of a 50-mm diameter, 0.2-mm-thick, partial-hemispherical beryllium window whose periphery is water-cooled given the 2.4-MW (1.5 to 3.0 mm spot size) case, is shown in Figure –3-XXX50. The primary beam window design is constructed from a 117.5 mm O.D., 19.1 mm thick 316 stainless-steel vacuum flange. This flange is a bolted connection which attaches to the primary beam pipe mating vacuum flange with a knife edge seal. The window construction and knife edge seal must be shown to have no detectable leak to achieve primary beam pipe design pressure.

Alignment of the primary beam pipe is a multi-step process. First, the embedded liner is measured and mapped from the upstream (US) beamline enclosure prior to beamline commissioning. Remote pre-alignment of the cartridge is necessary relative to the mapped liner. Then, after securing the primary beam pipe position within the cartridge (locking end collars and filling void with shielding material), a cart and cable system transports the assembly to the US beamline enclosure for installation. Insertion of the cartridge involves a combination of support from the cart and overhead rigging operation while moving axially.

Initial alignment of the beam pipe cartridge and attached window is obtained by using a DS docking feature shown in Figure –3-XXX49 and attachment at the upstream (US) extraction flange. This support-alignment system provides repeatable positional alignment within a final alignment resolution of approximately 0.5 mm. There is a provision for the insertion of an US and downstream (DS) aperture shielding plug used for protection during primary beam pipe cartridge replacement. These aperture shielding plugs would be constructed from steel and moved into the US beamline and target chase only during periods of cartridge replacement. DS remote handling of the aperture shielding plug within the

target chase is possible through a rail/cable system, which attaches to an embedded stainless-steel plate within the concrete wall at the target chase US face.

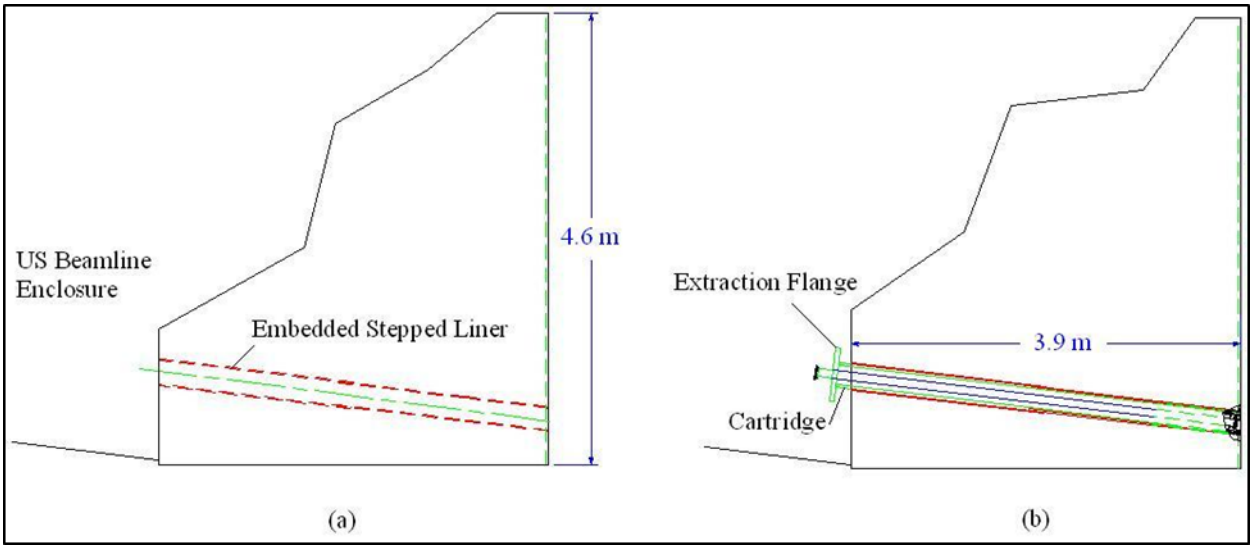

Figure 4-52: (a) Shielding Wall with Embedded Stepped Liner. (b): After Cartridge Insertion

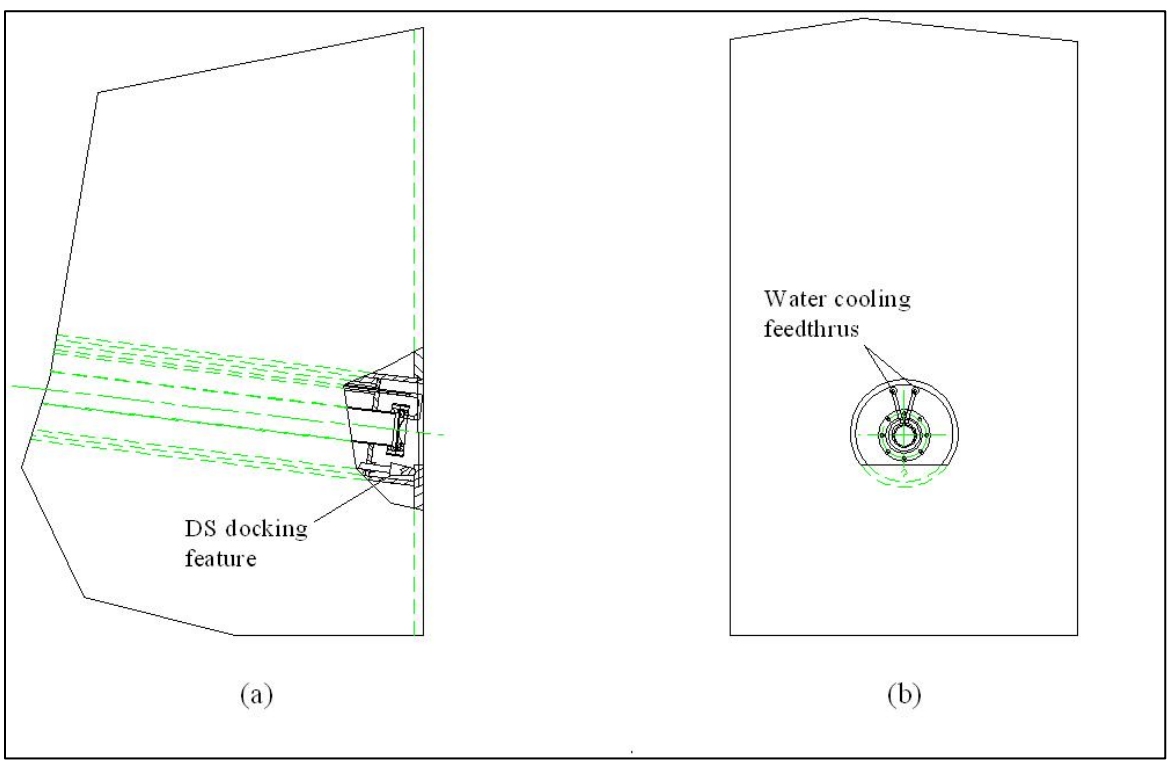

Figure 4-53: (a) Section View of Replacement Window Assembly. (b): End View of Window Assembly

The 1.2 MW primary beam beryllium thin window design is able to withstand the stress waves and also pressure and thermal loading given a 1.3-mm spot size while periphery air-cooled. At 2.4-MW beam energy, a 50-mm diameter partial hemispherical beryllium window with a 3.5-mm spot size and natural convective cooling also is sufficient. A 1.3-mm spot size at 2.4 MW is not acceptable since the combined maximum shock stress, transient stress and transient temperature induced within the window are above the ultimate tensile stress for beryllium. Optimization of a periphery air-cooled, hemispherical tapered beryllium window shape with a thin center and gradually thicker outer crown which allows greater conduction is worthy of further investigation.

We disregard the fine structure inside the beam pulse. Hence for time distribution the beam pulses are square pulses of length 10 microseconds, one pulse every 1.2 second.

Beam energy deposition in window material is provided by MARS simulation. We can fit the energy deposition data by exponential function

$$E = E_0 \exp\left(-\frac{r^2}{2\sigma^2}\right)$$

For E_0 = 9.3e-3 GeV/g, and σ= 1.8 mm, it is very close to MARS data, as shown in Figure 3-XXX2.

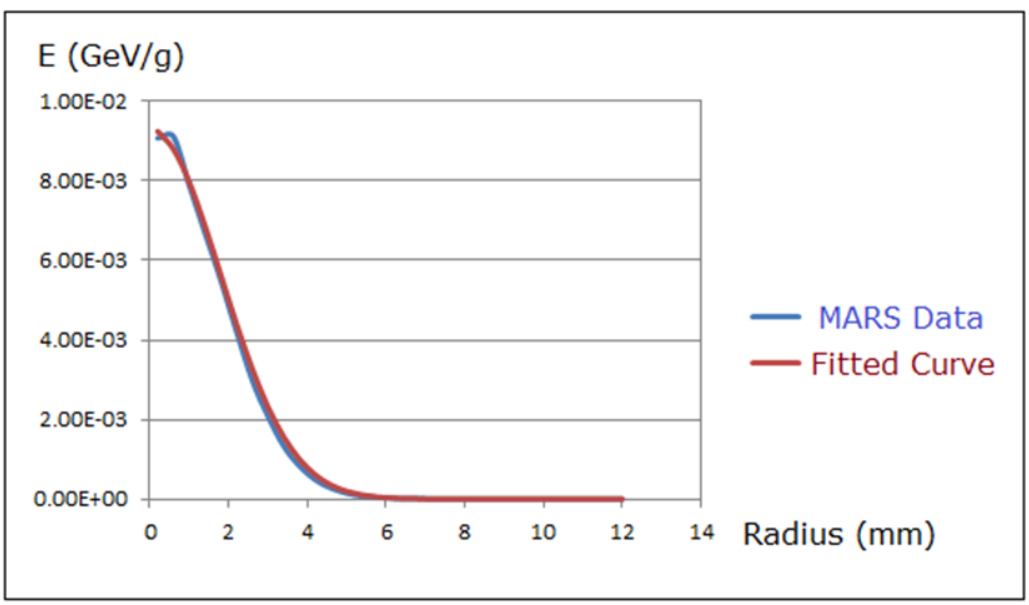

Figure 4-54: Spatial Distribution of Beam Energy Deposition

If we consider the 1.2 MW case, there are 7.5×10^{13} protons in one pulse. The maximum energy deposition is (9.3e-3)*(7.5e13) = 69.75e10 GeV/g = 111.6 J/g. Divided by the specific heat of beryllium, we have maximum temperature increase during the beam pulse 111.6/1.829 = 61 C.

4.8.3.1.1 The Thermal Cycles

An axial symmetric finite element model is built. Beam heating is applied to get the temperature distribution and its change with time. Figure 3-XXX3 shows the temperature history at the center of the window. Figure 3-XXX4 shows temperature distributions at valley and peak when temperature cycles are stabilized.

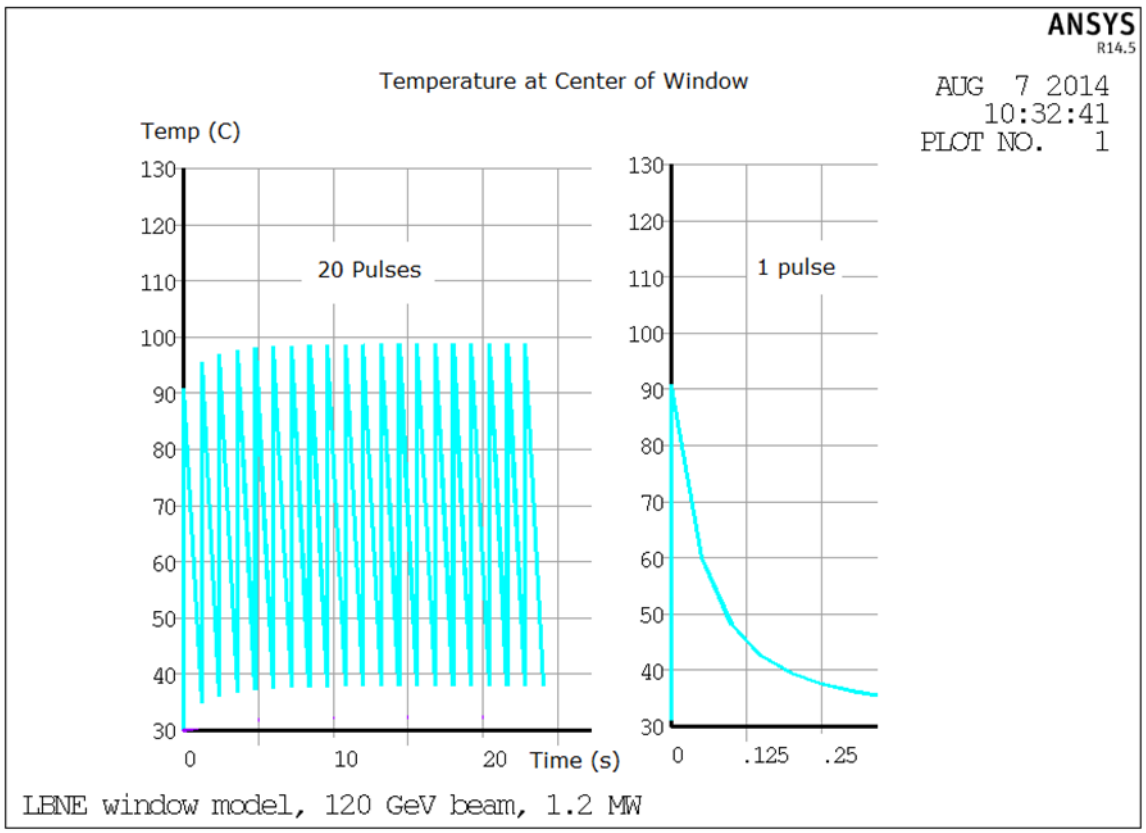

Figure 4-55: Temperature History at the Center of Beam Window

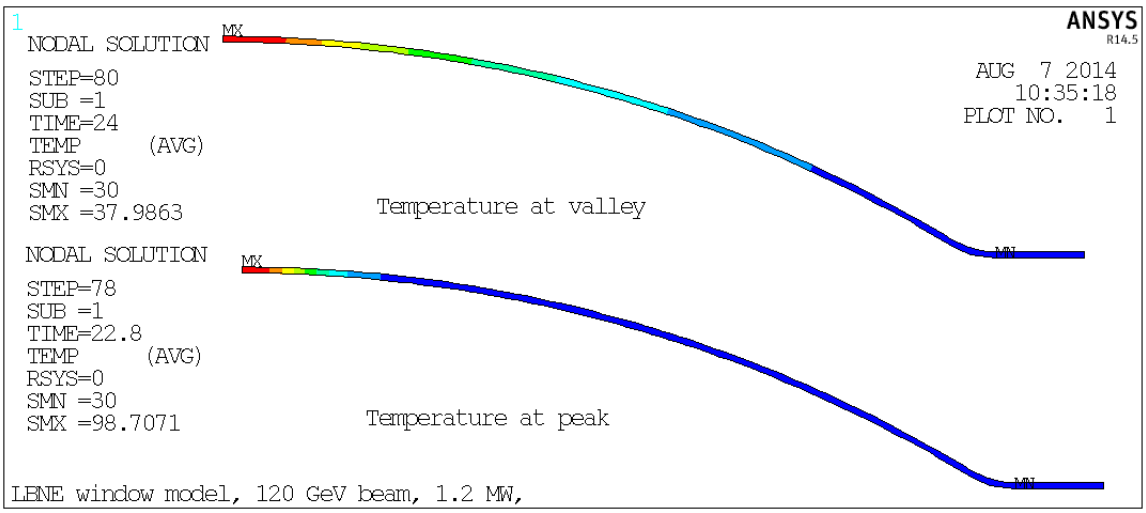

Figure 4-56: Temperature Distributions at Valley and Peak

Dynamic behavior of the primary beam window when one beam pulse passes through the window is shown at: https://lbne2-docdb.fnal.gov:440/cgi-bin/RetrieveFile?docid=9612&filename=model-2-mech_uy.avi&version=2

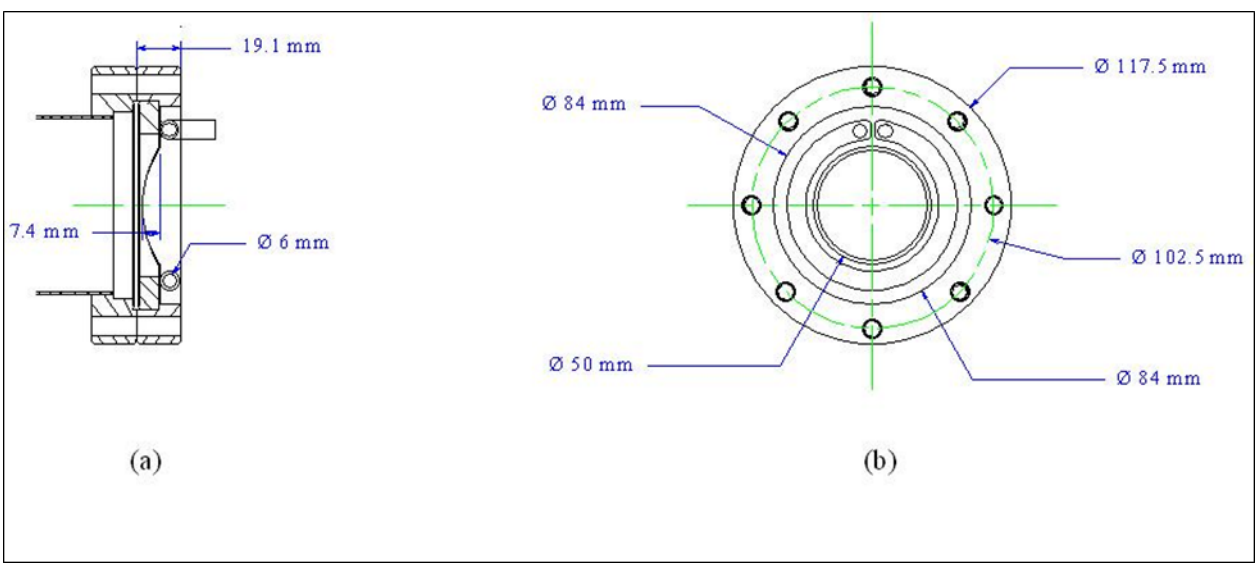

Figure 4-57: (a) Section View of 2.4-MW-Capable Beryllium Window. (b): End View of Window Assembly

4.8.3.2 Upstream Decay Pipe Window

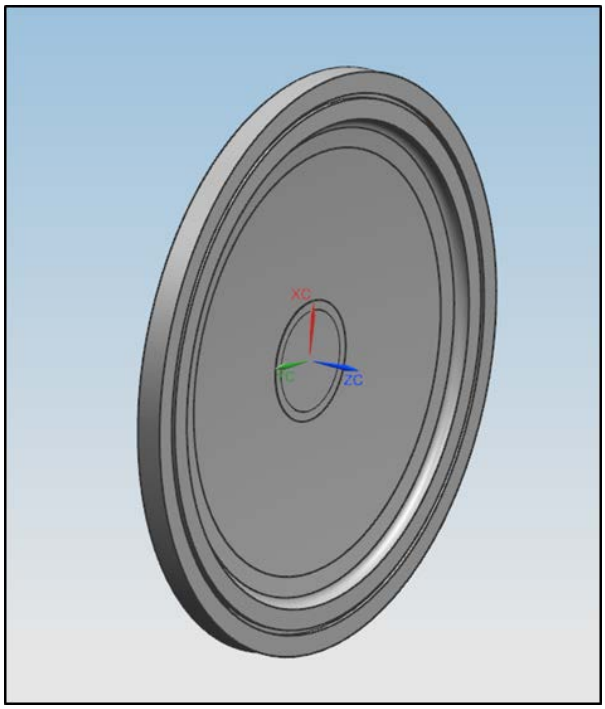

Figure 4-58: Upstream Decay Pipe Window from NX Solid Model

The upstream decay pipe window (see Figure 3-XXX51) is comprised of a beryllium or a beryllium - aluminum alloy foil welded to a heavier aluminum ring. This heavier ring includes a seal groove for an all metal seal. The center portion of the decay pipe window through which the proton beam will pass will be made of either beryllium or a beryllium - aluminum alloy. The annular disc outside of the center region will be made of a beryllium - aluminum alloy or aluminum.

It is likely that the material selections will be different for the 1.2 MW beam compared to the 2.4 MW beam. The lower power beam may alloy use of more beryllium-aluminum alloys while the higher power beam may require beryllium in the center section. Requirements based on MARS energy deposition and thermal stress analysis have been completed and the minimum material property requirements are known. What remains to be completed in the advanced conceptual design effort is to understand the cost implications.

The metal seal will be a commercially produced metal seal available from at least two suppliers and is used because elastomer seals are understood to be sufficiently degraded due to radiation exposure that the seal would leak before the window foil requires replacement.

Seal requirements include:

1) 5 psig (0.3 bar) maximum internal decay pipe helium pressure,
2) 1.5 psig normal working internal decay pipe pressure,
3) survive a high radiation and a corrosive atmosphere,
4) remote actuation (area will become too radioactive for a person to access)

5) An allowable leak rate of approximately 10 cubic centimeters per minute.

The foil will be held in a frame which will be removable from above, consistent with the other target pile components. This frame will include provisions for applying the load on the seal. One feature of the all metal seals is that they require significantly higher forces applied to attain a leak tight seal. The goal seal leak rate is approximately 10 cubic centimeters per minute. This is equivalent to 200 cubic feet per year, about one standard gas cylinder.

Several mechanisms are candidate designs for applying the seal load and include a wedge system, a four-bar mechanism, and a compressed gas system. Evaluation of the candidate seal loading designs and selection of an optimal design are part of the advanced conceptual design phase.

Removal of heat deposited by the beam in the window has been considered in the completed work. Convection heat transfer has been applied to both surfaces using forced convection values. Actively cooling the heavier outer ring which houses the seal has considered and will likely be incorporated into the final design. The provisions for this cooling will be included in the advanced conceptual design.

Results from temperature calculations for normal running conditions for different primary proton energies and beam powers are shown in Table 3-XXX1. Resulting stresses are shown in Table 3-XXX2.

Table 3-XXX1: Temperature Result for 120 GeV, 80 GeV and 60 GeV on the Decay Pipe Upstream Window with no cooling on the flange and convection cooling on both surfaces of the window foil. Normal beam (not accident) conditions.

Table 4-8: Temperature Result for 120 GeV, 80 GeV and 60 GeV on the Decay Pipe Upstream Window with no cooling on the flange and convection cooling on both surfaces of the window foil. Normal beam (not accident) conditions.

Be (s-65)	Cycle time	The Center of the Window Be Section				Flange Aluminum T6061	
		T average (Steady state)_C	T maximum ©	Tmin_C	ΔT _C	Tmax_C	ΔT _C
120 Gev- 2.4 MW	1.2 sec	68.46	71	67.77	3.24	87.4	0
120 Gev- 1.2 MW	1.2 sec	53.4	54.74	53.07	1.66	61.9	0
80-Gev 2.14 MW	0.9 sec	64.48	65.72	63.97	1.75	80.92	0
80-Gev 1.07 MW	0.9 sec	51.44	52.08	51.19	0.894	58.67	0
60-Gev 2.06 MW	0.7 sec	62.99	63.76	62.60	1.15	77.32	0
60-Gev 1.03 MW	0.7sec	50.71	51.1	50.51	0.59	56.87	0

Accident conditions for the decay pipe upstream window have been considered for the primary beam missing the target but being centered on the window and for the primary beam missing the target and being miss-steered so as to hit the decay pipe window off center.

4.8.3.3 Helium Decay Pipe Purge and Helium Recovery:

The decay pipe will be filled with normal air during construction and at the completion of the construction activities. Design prohibits evacuation and backfilling with helium gas. Therefore, a method of purging the air out of the vessel with inexpensive, relatively heavy, carbon dioxide and then

displacing the carbon dioxide with helium has been developed. This system will allow 99% helium concentration to be achieved and offers the possibility of increasing the helium purity by absorbing the carbon dioxide.

When the decay pipe upstream window is changed, the default solution will be to reverse the helium fill process; that is recover the helium, replace the decay pipe gas with carbon dioxide, and then purge the carbon dioxide with air (so as to avoid and oxygen deficient hazard condition) prior to removing the upstream window. Alternative methods of installing a temporary seal to isolate the window from the decay pipe during window replacement activities will be considered during advanced conceptual design.

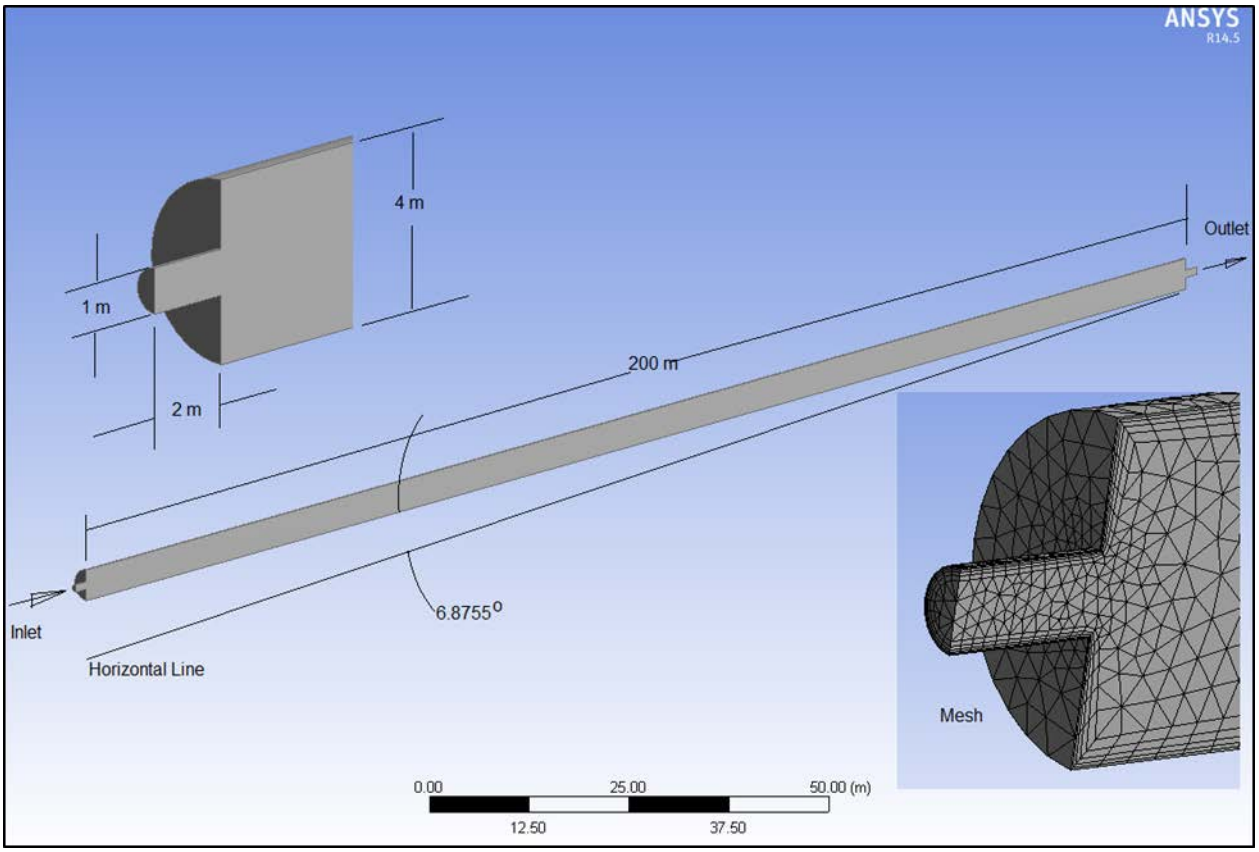

Figure 4-59: Finite Element Model to Simulate the Helium Fill of Decay Pipe

A finite element model is built as shown in **Figure 4-59**. Using symmetry, only half of the decay pipe is modeled. At the two ends, we have a cylinder of 1 meter diameter and 2 meters length for inlet and outlet. The model is initially filled with CO_2. Helium is pumped in from the inlet at the speed of 0.444 m/s (except for the first 800 seconds, the speed is 0.111 m/s). The carbon dioxide content is calculated and plotted in **Figure 4-60** and **Figure 4-61.**

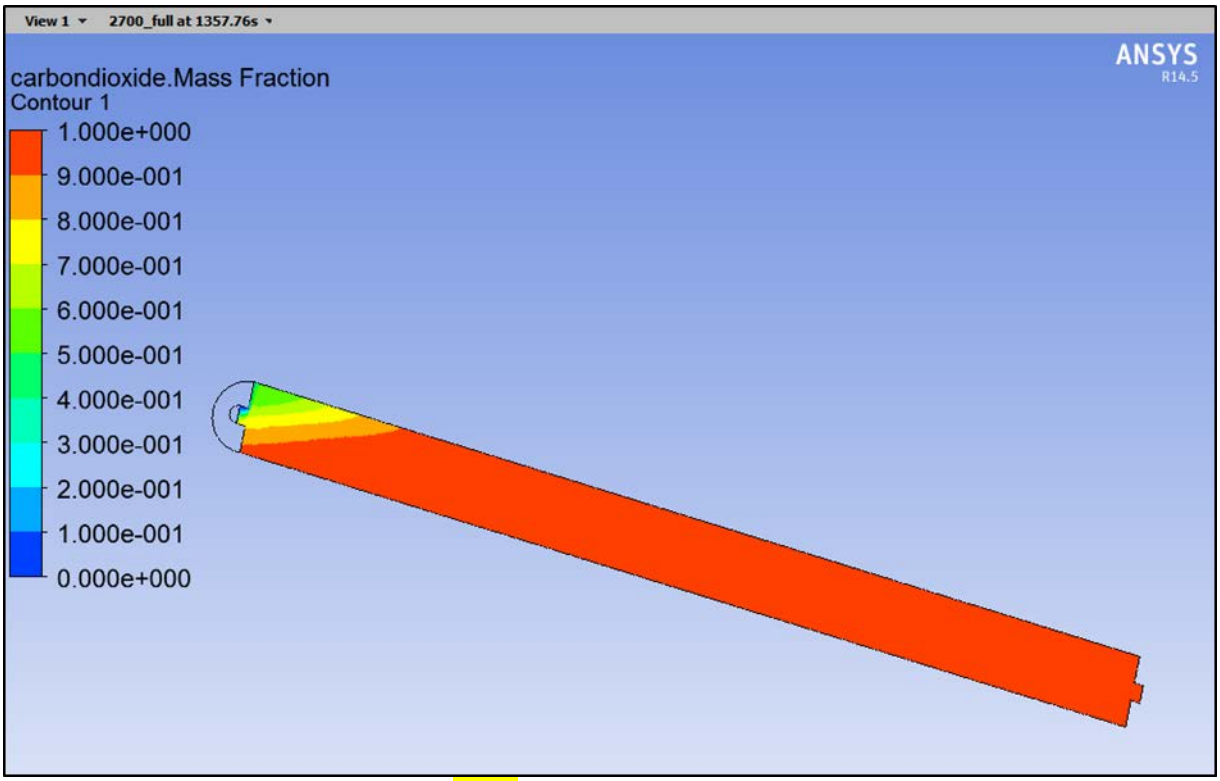

Figure 4-60: CO2 Mass Fraction at 1358

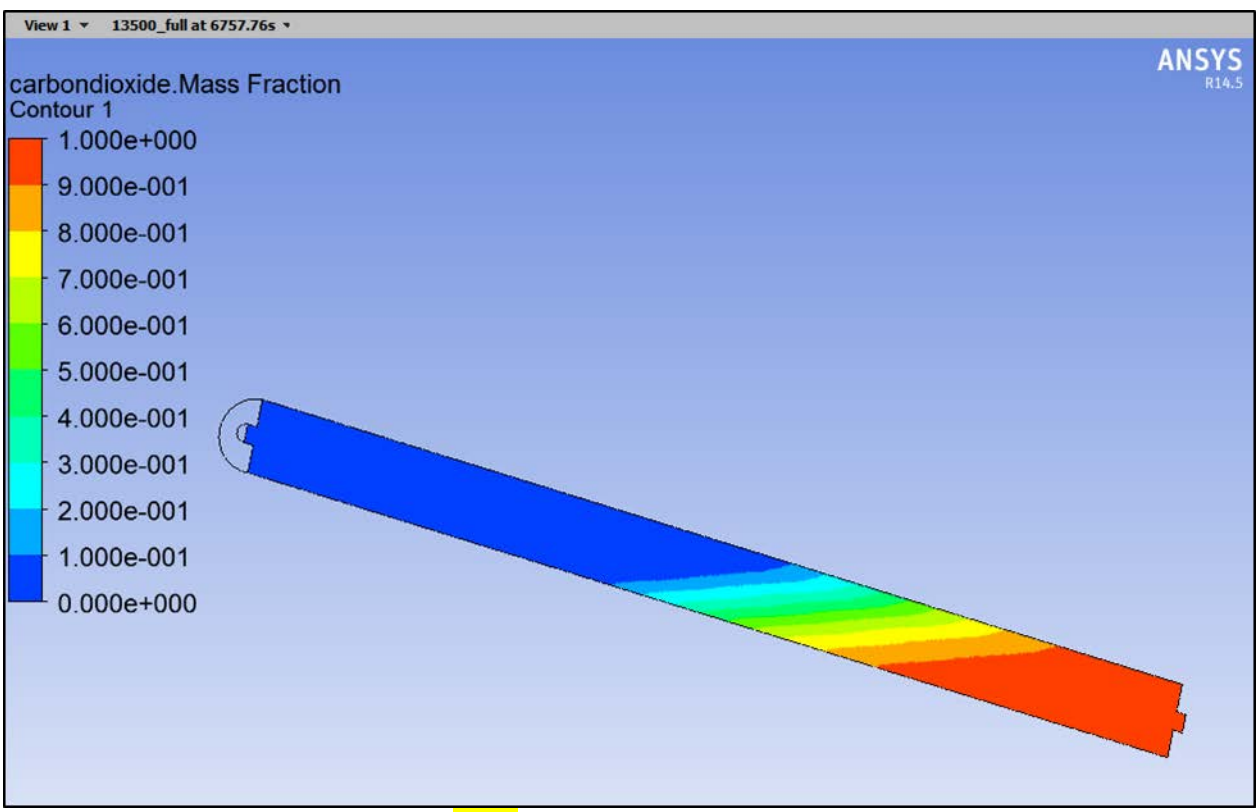

Figure 4-61: CO2 Mass Fraction at 6758

The cross sectional area of the inlet is 1/16 of the decay pipe. The average velocity in the inlet is 0.444 m/s, so the average velocity in the decay pipe is 0.02775 m/s. To fill the 200 m decay pipe, we need 7207 seconds.

After 12355 seconds, the CO2 content is only in the lower corner. Its maximum value changes with time as shown in **Figure 4-62**.

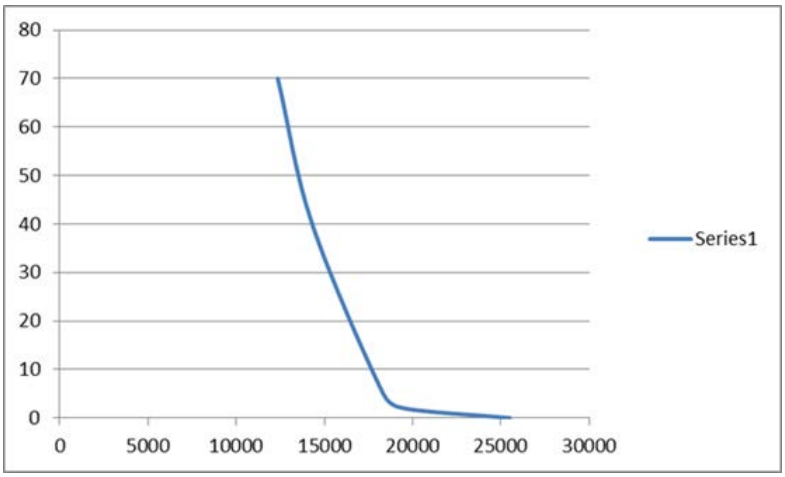

Time (s)	CO2 (%)
12355	70
14300	40
18332	5
19538	2
25510	0

Figure 4-62: Maximum CO_2 content during the Decay Pipe Purging Process as a Function of Time in Seconds

From our simulation, at the end of 25510 s there is no detectable content of CO2.

If we move the outlet to the lower corner of the end of the decay pipe, we may accelerate the purge process.

4.9

4.9.1 Hadron Absorber (WBS 130.02.03.07)

Introduction

The hadron-absorber structure (also called simply the "absorber") is located directly downstream of the decay pipe. The absorber, a pile of aluminum (Al), steel, and concrete is designed to absorb the residual energy from protons and the secondary particles (hadrons) which have not decayed. Approximately 750kW of the 2.4MW beam power is deposited into the absorber and must be properly contained to prevent activation of soil and groundwater. The absorber is designed for the worst case condition at 2.4MW operation: shortest helium-filled decay pipe (204m long) and the shortest target envisioned at 2 interaction lengths.

The absorber consists of two major sections, as shown in the left image of **Figure 4-63**. The core, a section consisting of replaceable water-cooled blocks, is shown inside the green box. It is enlarged in the right image of **Figure 4-63**. The core consists of an aluminum spoiler block to initiate the particle shower, aluminum mask blocks with air space in the center to allow the shower to spread, a sculpted aluminum region of reduced central density to further distribute the heat load, solid aluminum blocks, and solid steel blocks. The beam power deposited into the core is 519kW, which is the majority of the

incoming beam power into the absorber. Outside of the core is forced-air cooled steel and concrete shielding.

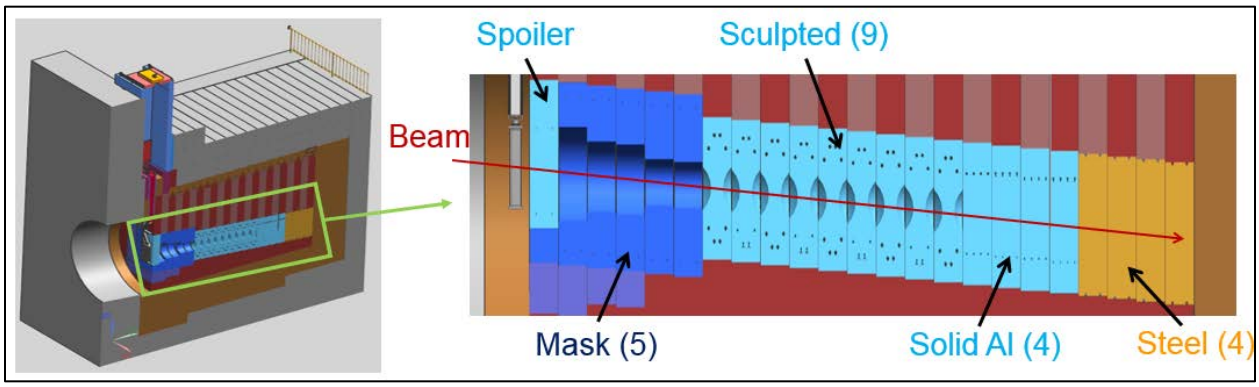

Figure 4-63: Left, cross section of absorber through beam axis. Right, cross section of absorber core.

4.9.1.1 Requirements

The absorber must provide radiation protection to people and groundwater for the life of the experiment with minimal maintenance. However, the water-cooled core blocks must be replaceable to handle any unforeseen circumstances. The absorber will have the ability to handle two accident pulses without damage or loss of function. An accident scenario is where the beam is mis-steered or the target is removed from the beam, resulting in the full proton beam traveling down the decay pipe and into the absorber. An interlock system shall be designed to pull the beam permit after no more than two accident pulses (see target hall instrumentation section). Additional requirements can be found at LBNE DocDB #10148.

4.9.2 Energy Deposition Calculations

The energy deposition calculations were performed using a unified computer model that includes the target hall, target chase and absorber hall. The incoming beam for the absorber was calculated with the MARS15 code in the exclusive mode using the LAQGSM hadron generator. Interactions in both the target and decay channel were taken into account, so that one studied the effect due to replacement of the air with helium in the decay pipe. In the current model, the sculpted aluminum blocks shown in **Figure 4-63** are described using a rectangular approximation. The studied cases—normal operation, accident with a mis-steered beam, and no-target on-axis accident are described in the following subsections. In all cases, the calculated three-dimensional distributions of deposited energy were provided as input for subsequent analysis with ANSYS code.

4.9.2.1 Normal Operation

The calculated distributions of the incoming particle flux over the entire decay pipe cross section at the downstream end of the decay pipe are shown in **Figure 4-64**, while the data for the central region is shown in **Figure 4-65**. In order to properly describe the distribution of deposited energy, a double grid shown in **Figure 4-66** was employed in transverse direction for the energy deposition calculations in the aluminum core blocks. For the steel core blocks in the downstream part, a simple uniform grid was used

due to substantial shower spreading in the transverse direction. In the longitudinal direction, each studied core block was divided into four parts. The calculated three-dimensional distributions of the deposited energy in the most important core blocks were represented as distributions over the corresponding set of small volumes defined by the used grid. A distribution of total power deposited in elements of the central region of the absorber is shown in **Figure 4-67** and a detailed two-dimensional distribution of power density over the absorber is shown in **Figure 4-68**.

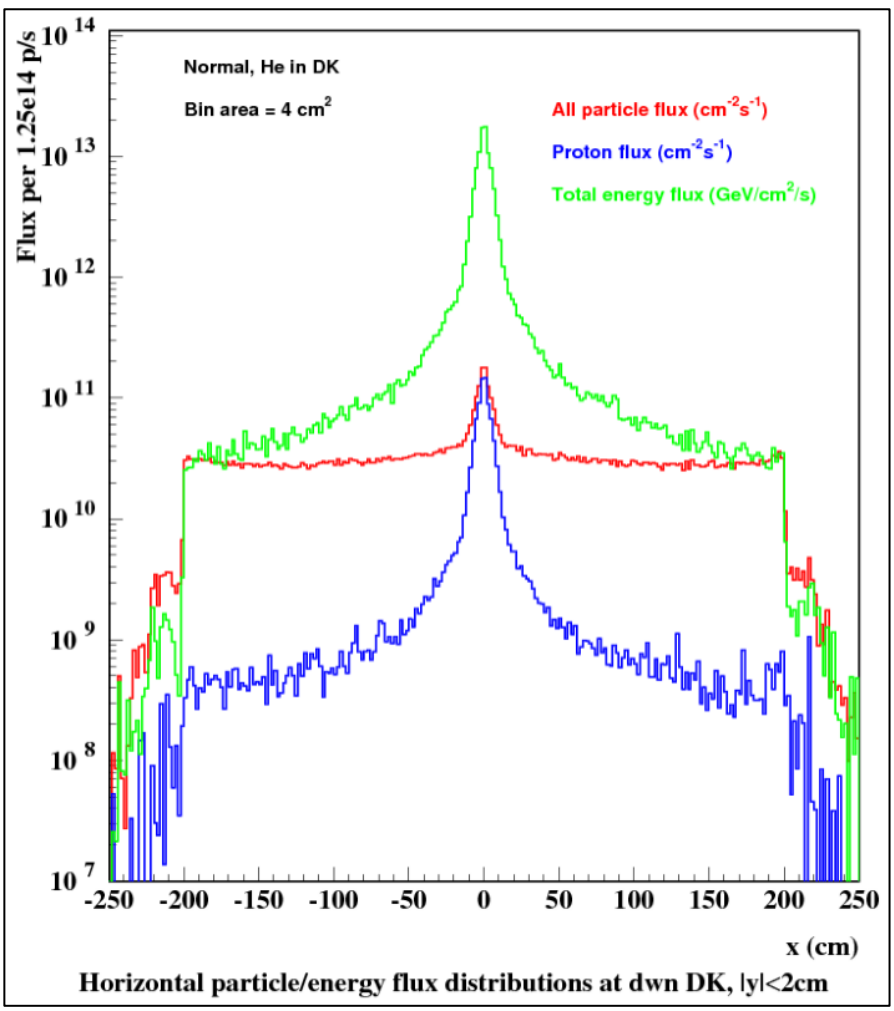

Figure 4-64: The Distribution of the Incoming Flux at the Downstream End of the Decay Pipe

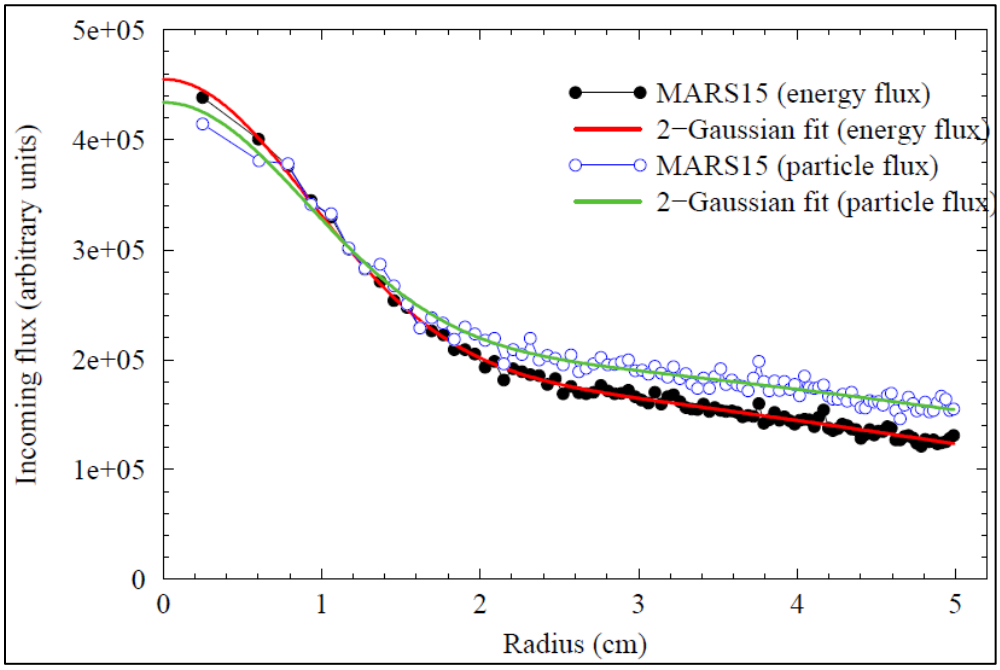

Figure 4-65: The calculated incoming flux at the downstream end of the decay pipe in the central region in radius, and the results of fitting with two Gaussians (σ_1=0.9 cm and σ_2=5.3 cm).

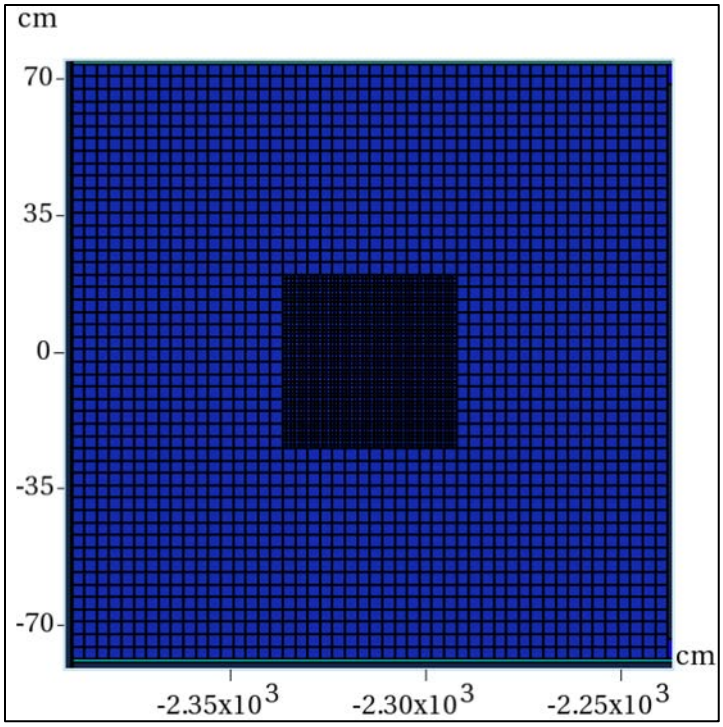

Figure 4-66: The double grid employed in transverse direction for MARS15 energy deposition calculations in the sculpted core aluminum blocks. In the outer grid, the bin size is 2cmX2cm, and this linear bin size is three times as large as that in the inner grid.

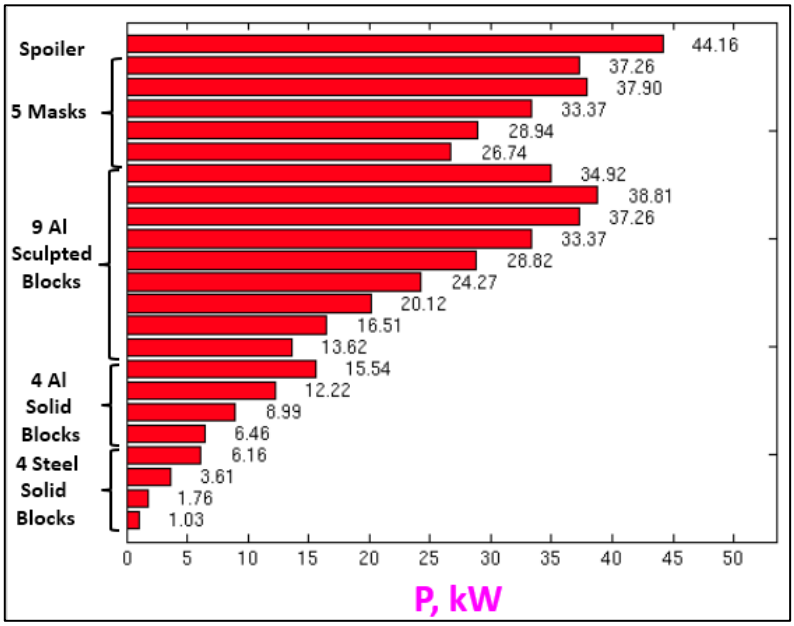

Figure 4-67: Distribution of Total Power Deposited in the Central Part of the Absorber (see Figure 1).

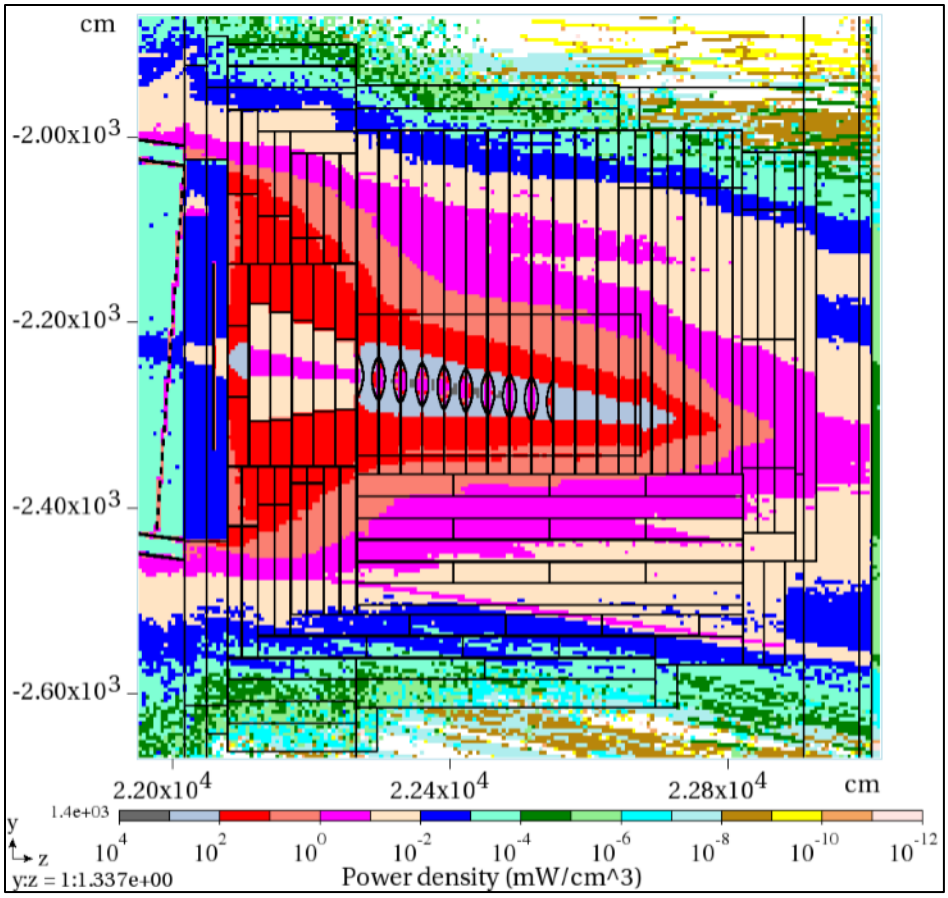

Figure 4-68: Calculated Two-dimensional Distribution of Power Density over the Absorber at 120 GeV

4.9.2.2 Accident with a mis-steered beam

In a scenario with a mis-steered beam, the region with the highest energy deposition is expected to be right above the sculpted regions in the aluminum core blocks. In order to correctly describe this case, another transverse and longitudinal grid was used as shown in **Figure 4-69**.

4.9.2.3 No-target on-axis Accident

In a scenario "target disappears," the beam hits the absorber core on-axis, so that for energy deposition calculations one used the same grid developed for normal operations with the only modification: for the inner grid the bin size in transverse direction was 0.5cm X 0.5cm. A detailed calculated two-dimensional distribution of deposited energy for this case is shown in **Figure 4-70**.

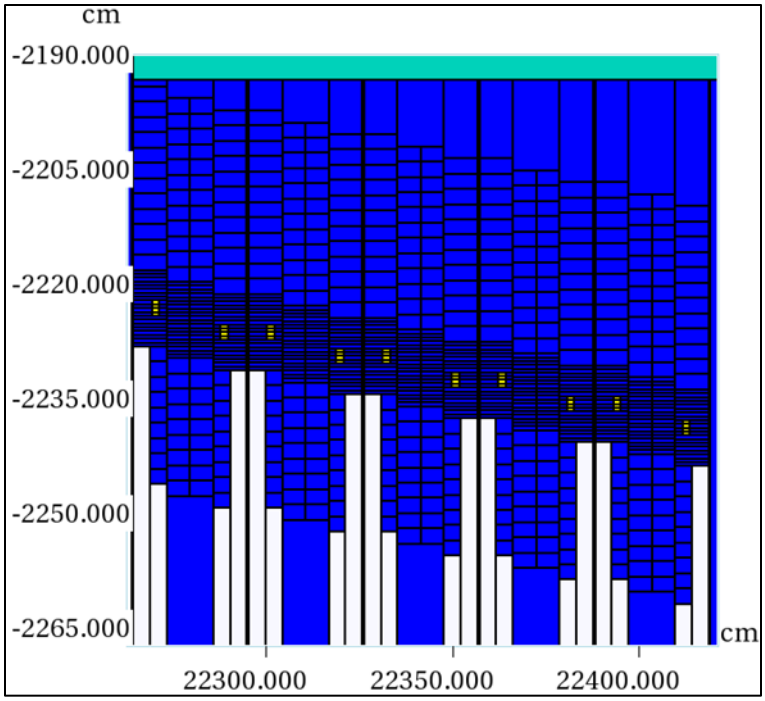

Figure 4-69: A longitudinal view of the grid employed for MARS15 energy deposition accident calculations in the core aluminum blocks. The yellow regions show the water-cooling channels.

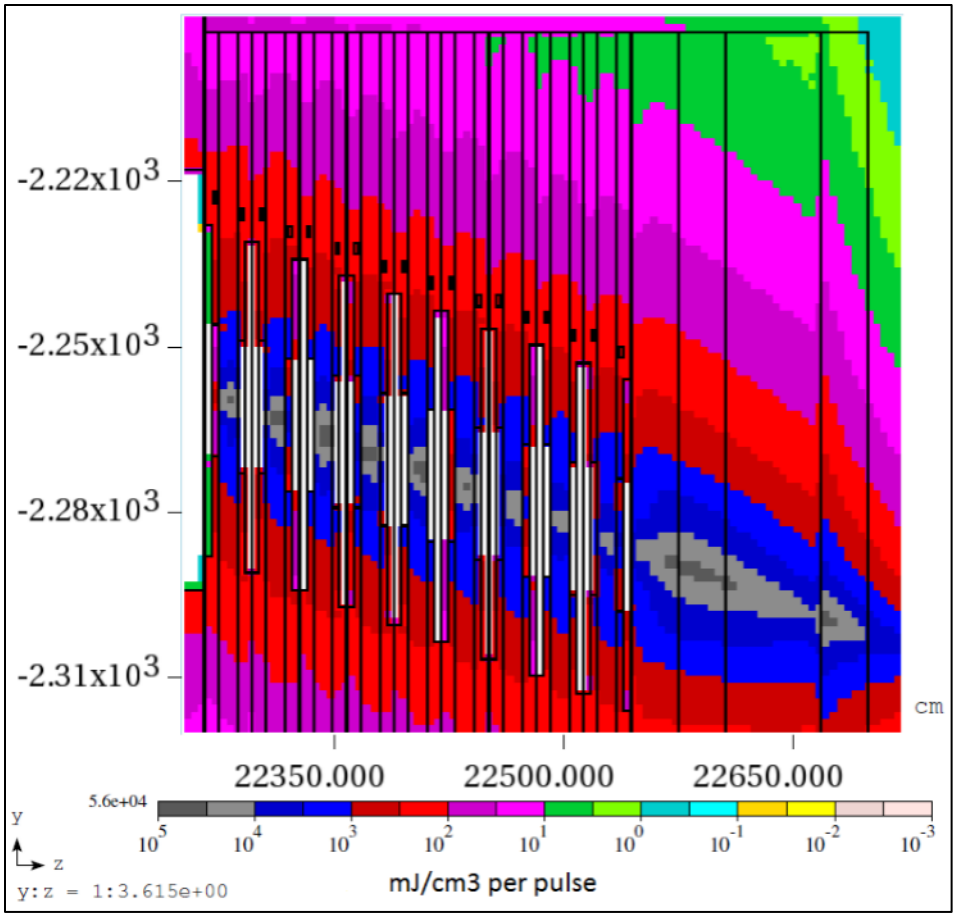

Figure 4-70: Calculated two-Dimensional Distribution of Deposited Energy over the Absorber for the Case of "No-target on-axis" Accident at 120 GeV.

4.9.3

FEA and Analysis

Using the MARS energy deposition results as a basis for heat load on the absorber and its core blocks, many iterative simulations between MARS and ANSYS have been carried out to determine the final configuration of the absorber. The main driver of this optimization is reduction of temperature and stress to acceptable levels for the materials in both normal operation and accident scenarios. Creep and fatigue effects have been considered when applicable.

Aluminum core blocks are all water cooled via four 1" diameter gun-drilled channels in the aluminum with 20 gallons per minute (gpm) volumetric flow rate through each channel. The water will be cooled to 10°C. Steel blocks are cooled via two 1" diameter stainless steel lines along the perimeter of the block with 20 gpm flow rate each. A full set of absorber operating parameters can be found at LBNE DocDB #10095.

4.9.3.1 Steady State Normal Operation – Core Analysis

A number of requirements were kept in mind during the analysis of the steady state operating condition. The material must survive fatigue conditions from beam off/on cycles. Creep criteria for

aluminum 6061-T6 must be considered due to elevated temperature and stress. The block must also be temporarily operable with a malfunctioning water line.

Steady state temperatures and stresses were evaluated at the locations shown in **Table 4-9** for both 120 and 60 GeV operation. The blocks shown in the table are the worst case conditions for each area: spoiler, mask, sculpted block, full Al blocks and full steel blocks. The most challenging locations at 120 GeV are the 3rd sculpted Al block and the 1st steel block. 120 GeV operation is by far the worst case due to the lower amount of beam scattering and higher overall beam power compared to 60 GeV operation. Stresses were not evaluated for 60 GeV operation for this reason.

Table 4-9: Steady State Operating Temperatures and Stresses for 120 GeV and 60 GeV.

	Steady State Maximums - 120 GeV		60 GeV
	Max Temp (°C)	Max VM Stress (MPa)	Max Temp (°C)
Spoiler	60	34	39
1st Mask	25		
3rd Sculpted Al - Center	88	103	44
3rd Sculpted Al - Water Line	25	74	18
2nd Solid Al	84	48	39
1st Steel	225	199	104

Contour plots of temperature and Von-Mises stress for the 3rd sculpted block are shown in **Figure 4-71**. Maximum temperature occurs in the center of the block, where the beam interacts directly with the aluminum. Compressive stress is also concentrated in this area due to the arch shape provided by the sculpting cut, with a maximum of 103 MPa. Stress at the water line also needs to be considered. This location is in tension, with a maximum Von-Mises stress of 74 MPa at roughly room temperature.

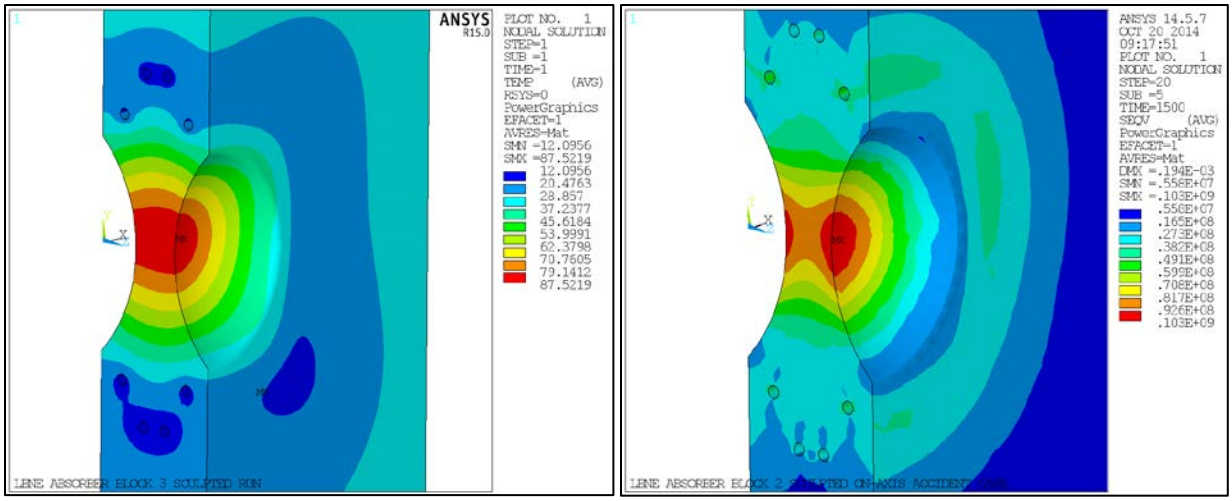

Figure 4-71: Temperature (°C) and Von-Mises stress (Pa) for 3rd Sculpted Block

Since this block has the largest stress and highest temperature, it will be used as a basis for fatigue and creep calculations. The temperature rise per pulse in this block is about 0.8°C, so the effects of each beam pulse on fatigue life can be ignored. Assuming a conservative 5 cooldowns per day during the life of the experiment, results in 36,500 cycles (3.6e4). Referring to fatigue tables for both room temperature and elevated temperature testing at 150°C (Kaufman, 1999), safety factors can be computed at both the water line and maximum stress locations and are shown in **Table 4-10 .**

Creep must also be considered since the aluminum is being held at an elevated temperature under stress – 103 MPa at 88°C in the worst case. Creep data for 6061-T6 aluminum bus conductors (Kirkpatrick, 1989) shows an average stress required to produce 1% creep at 100°C for 10 years to be 172 MPa. Other data (Kaufman, 1999) indicates the stress values are well below the 250 MPa needed to produce even 0.1% creep at 100°C, although this data only extends to 1000 hours.

Another possible concern is losing the T6 temper of the material due to elevated temperature. After 100,000 hours (11.2 years) at 100°C, there is no change to tensile strength, yield strength, elastic modulus, or elongation (Kaufman, 1999).

Another consideration is the effect of a down water line. In the case of the 3rd sculpted aluminum block, the downstream end of the block has a larger energy deposition than the upstream side. For this analysis, convection in the downstream inner water line is removed and the analysis is re-run. **Figure 4-72** shows contour plots of temperature and Von-Mises stress, with maximums of 109°C and 174 MPa respectively. At these temperatures and stresses, the block would be at least temporarily operable while a replacement is fabricated, and could possibly be run longer if necessary.

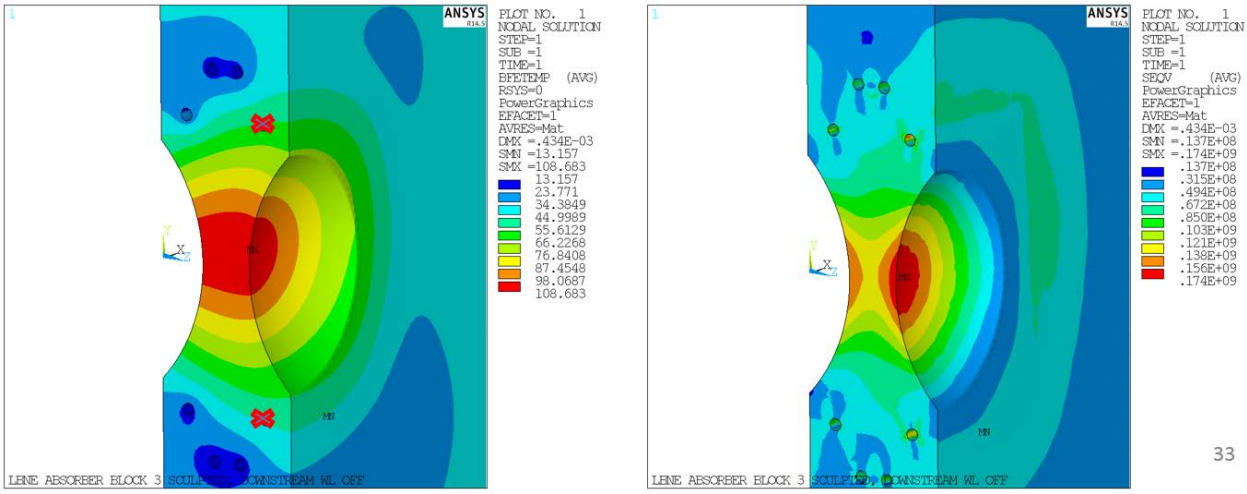

Figure 4-72: Effect of a Down Water Line on Sculpted Block 3. Left: Temperature (°C). Right: Von-Mises Stress (Pa).

Using the previously presented stress values, safety factors can be calculated for each location. These values are shown in **Table 4-10,** and are not compensated for any additional load or uncertainties. The lowest safety factors are for fatigue to the center of the sculpted block, and to yield for the steel block. The fatigue limit set for the center of the sculpted block is very conservative from the actual case. It uses nearly 3 times the number of cycles to failure (1e5) and the test temperature is 60°C higher (150°C). Also, this area is in compression, so concerns about opening a crack are small. The steel block does have a low safety factor to yield, although yielding the material does not necessarily indicate failure. Many design options have been presented to increase this safety factor including alternate materials, alternate cooling line routing, and design changes.

Table 4-10: Steady State Normal Operation Safety Factors

	Steady State Maximum		Safety Factor to Yield	Safety Factor to Fatigue	Satisfies Creep Criteria?
	Temp (°C)	Stress (MPa)			
Spoiler	60	34	6.8	7.6	Y
Sculpted, Center	88	103	2.3	1.6	Y
Sculpted, Water Line	25	74	3.7	3.5	Y
Solid Al	84	48	4.8	3.4	Y
Steel	225	199	1.4	-	-

4.9.3.2 Accident Conditions

The absorber must be able to handle, without loss of function or damage, an accident condition where two pulses of the full proton beam do not hit the baffle or target and travels down the decay pipe. Two accident scenarios were considered. First, an on-axis accident, in which the beam travels down the center of the absorber and strikes the region that already has the highest temperature and largest stress from normal operation. Second, an off-axis accident where the beam strikes the absorber offset from the on-axis accident and passes directly through the water lines, where the water-line geometry might

induce stress-risers and where one does not have the shower-spreading advantage of the central sculpting region. These two accident scenarios are shown visually in **Figure 4-73.**

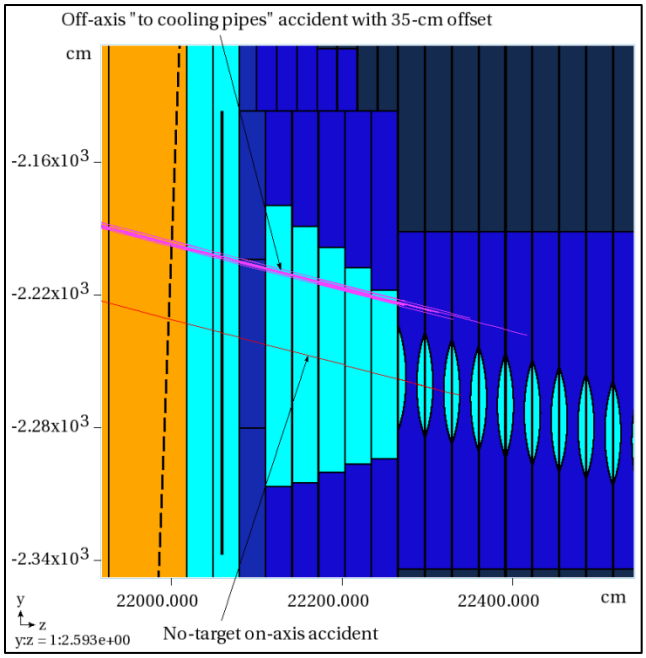

Figure 4-73: Locations of Absorber Accident Conditions

For the on-axis accident case, temperatures and stresses were simulated for the spoiler, 2nd sculpted Al block, 2nd solid Al block, and 1st steel block. Results from these simulations are summarized in **Table 4-11**. For a point of reference, the yield strength of 6061-T6 aluminum at 150°C is 190 MPa. All of the stress values shown are under this yield strength. The thermal portion of the model was also run out to 10 pulses to determine if any melting would occur. Maximum temperature after 10 pulses occurred in the spoiler. It reaches about 270°C, which is well below the melting point of 660°C.

Table 4-11: On-axis Accident Temperature and Stress Results

	Temperature after 2 accident pulses (°C)	Von-Mises Stress after 2 accident pulses (MPa)	Temperature rise per accident pulse (°C)
Spoiler	146	121	50
2nd Sculpted Al	140	148	38
2nd Full Al	120	63	18
1st Steel	242	199	10

The off-axis accident case was modeled for sculpted Al block 2, where the peak energy deposition occurs. Water in the line and the energy deposition into it are included in this model. After two pulses, the maximum temperature reaches 170°C as shown in the left image **Figure 4-74**. At this temperature, a possible concern is a localized loss of the T6 temper. Tensile data at elevated temperature (Kaufman, 1999) shows no change in 6061-T6 mechanical properties after 0.5 hours at 177°C.

The induced stress exceeds the yield point of 6061-T6 aluminum after a single pulse, and a temperature dependent bilinear kinematic plasticity model was introduced to model plastic strain. A plot of plastic strain after two pulses is shown in the right image of **Figure 4-74**. The maximum plastic strain achieved is 0.7% while the plastic strain to failure for 6061-T6 aluminum is 16%.

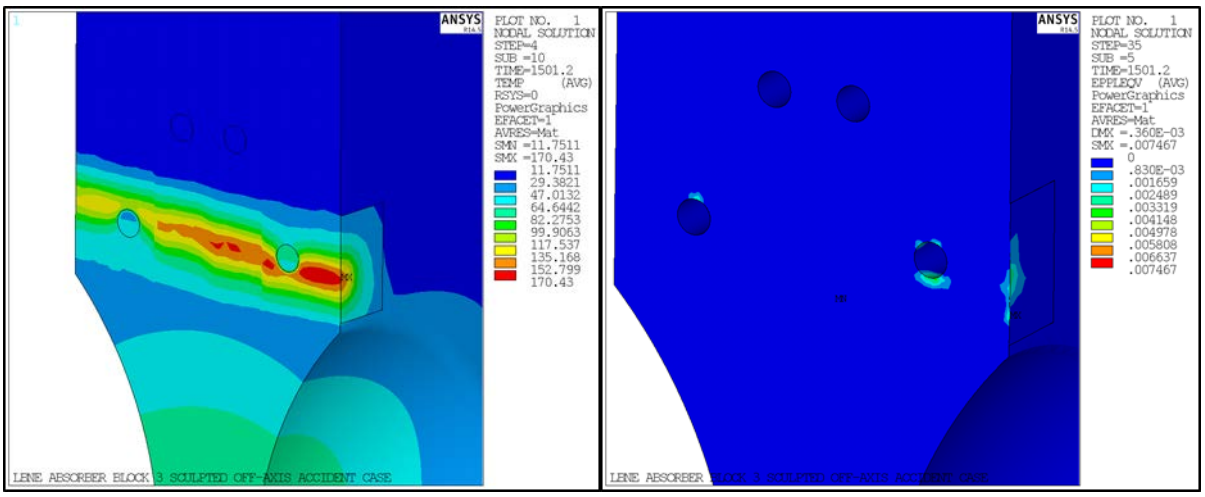

Figure 4-74: Contour Plots after Two off-axis Accident Condition Pulses. Left, Temperature (°C). Right, Plastic Strain

When beam strikes a water line, the induced water pressure spike from the thermal expansion of water must be considered. A simplified model was constructed to examine this effect. The maximum pressure achieved is 1.7 MPa (246 psi), shown in **Figure 4-75**. This pressure spike would most likely be attenuated by any gas in the system and the 90 degree bends formed by the gun drilled cooling channels, but still must be considered when constructing the water piping system and its joints.

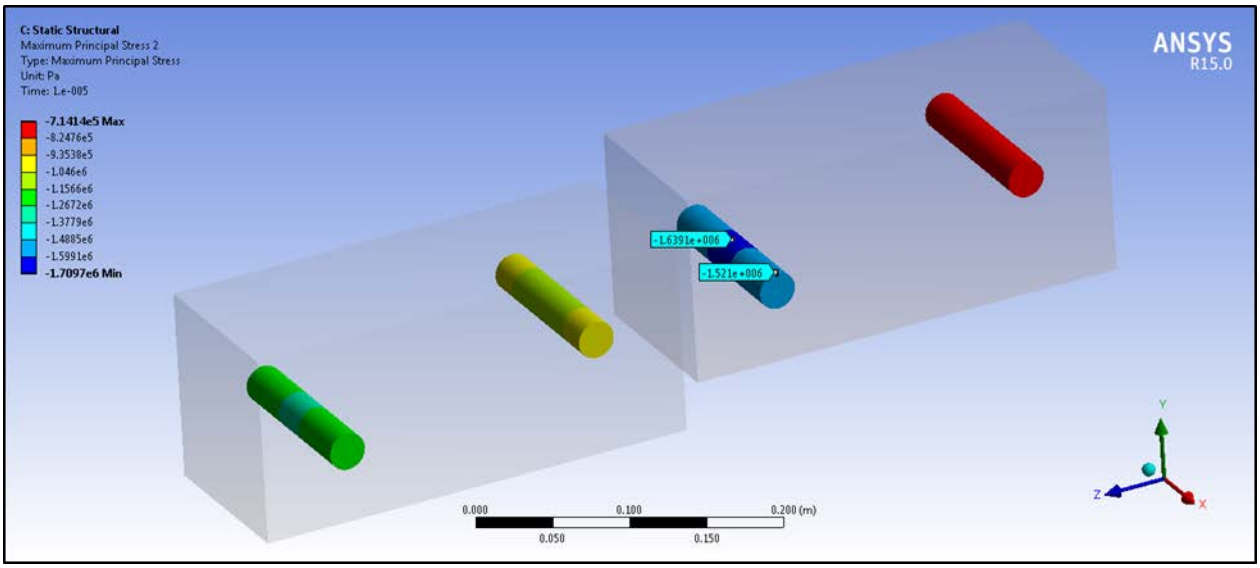

Figure 4-75: Water Pressure (Pa) in Cooling Channels of Sculpted Al Blocks Right: 2 and Left: 3 During off-axis Accident

4.9.3.3 Steel Shielding Air Cooling

While the bulk of the beam energy reaching the absorber is deposited in the core, the outer steel shielding still receives a significant portion of the energy deposition at 223kW. However, this energy deposition is not as concentrated as the core, and lends itself well to air cooling. The proposed routing method for the cooling air is shown in **Figure 4-76**. Air from the air handling room flows over the top of the absorber, then flows downward through 5mm gaps in the steel shielding. After passing through the 5mm gaps, the air flows through a duct on the bottom of the absorber formed by a gap in the shielding and then is fed back to the air handling room.

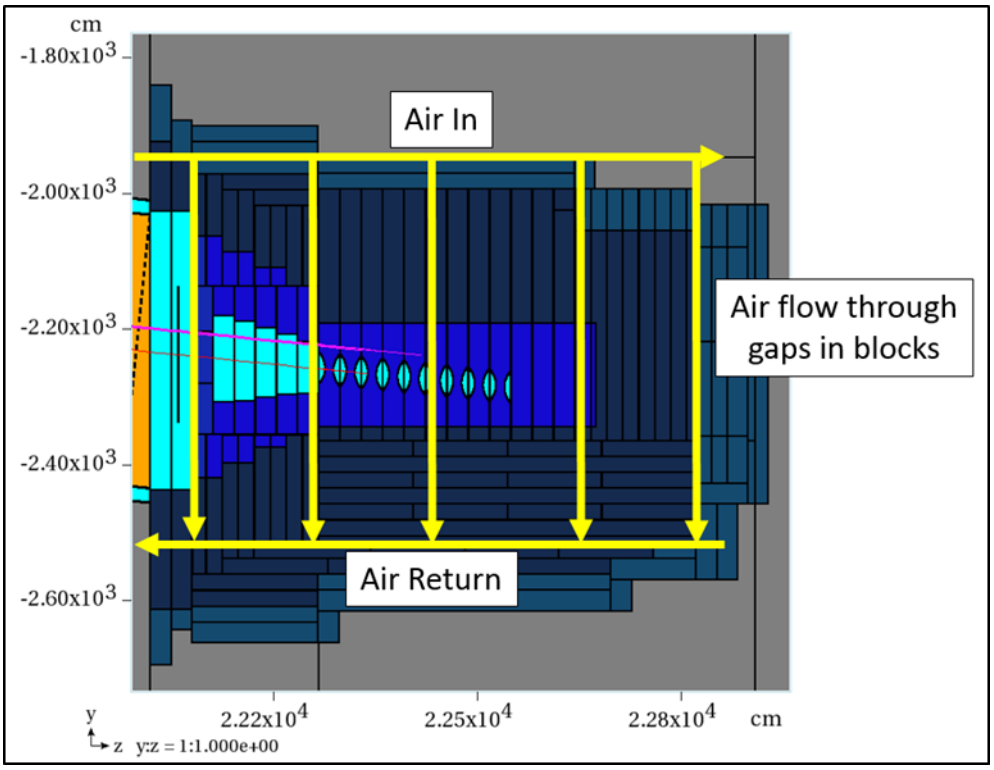

Figure 4-76: Routing Method for Air Cooling of Outer Steel Shielding

The NuMI target chase air cooling system operates at 25,000 cfm and removes approximately the same heat load, so this flow rate was selected for calculations in the absorber air cooling model. A simplified model of the absorber is constructed using 34 CCSS blocks at 9.11" thick each, with dimensions of 6m wide and 6m tall. The blocks are spaced 5mm apart, and the air passes through these gaps. This simplified model is represented in **Figure 4-77**. With these parameters, the pressure drop through the 5mm gaps is 10" water gauge (approximately 2490 Pa gauge).

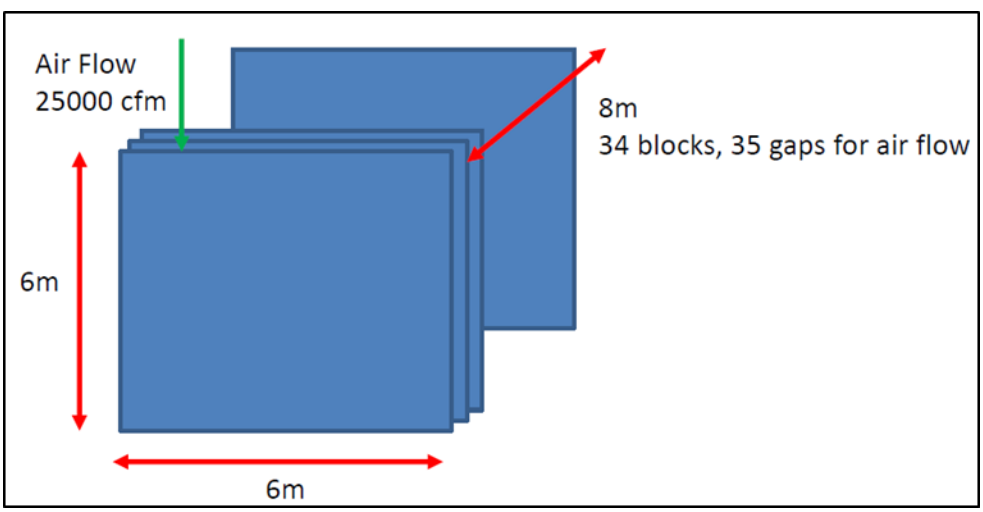

Figure 4-77: Simplified Model of Absorber Steel Shielding for Air Cooling Calculations

To model temperatures, an axisymmetric version of this model is implemented in ANSYS. This method slightly overestimates heat generation in the shielding at 240kW. Air cooling in the gaps is modeled as convection with an applied convection coefficient of 55 W/(m^2-K) using 25°C air, and the blocks are assumed to be independent of each other. The resulting maximum temperature is 63°C as shown in **Figure 4-78**, occurring in the shielding near the first sculpted Al block.

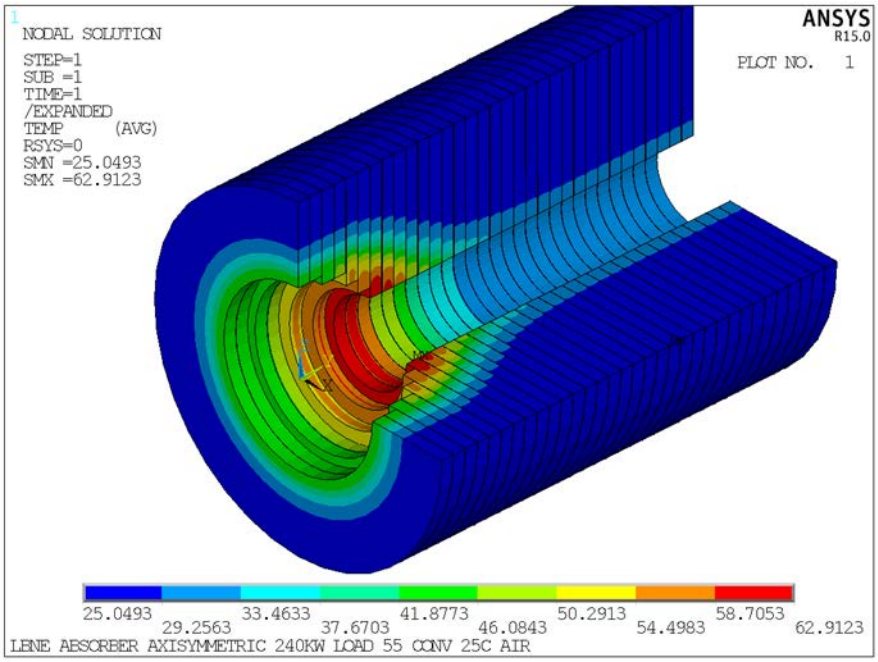

Figure 4-78: Absorber Shielding Temperatures (°C) with Air Cooling

This model does not account for the temperature rise of air through the absorber. Bulk temperature rise of the air through the absorber is 16°C. For air going through the hottest gap between the last core block and the first sculpted Al block, the temperature rise is 66°C. Taking a simple sum of maximum temperature in the core and temperature rise of the air flowing through the hottest gap, 130°C is the maximum temperature the steel could achieve. This is well within limits for steel and the paint applied to it (see LBNE DocDB #10264).

4.9.4

Mechanical Design and Remote Handling

The mechanical design of the absorber is based off the proven design of the NuMI target hall shown in , utilizing remotely handled T-blocks to support the core. These T-blocks are supported by the steel shielding, and are fully encapsulated by steel and concrete shielding for radiation protection. The T-Blocks are removable via an overhead crane with a lifting fixture attached.

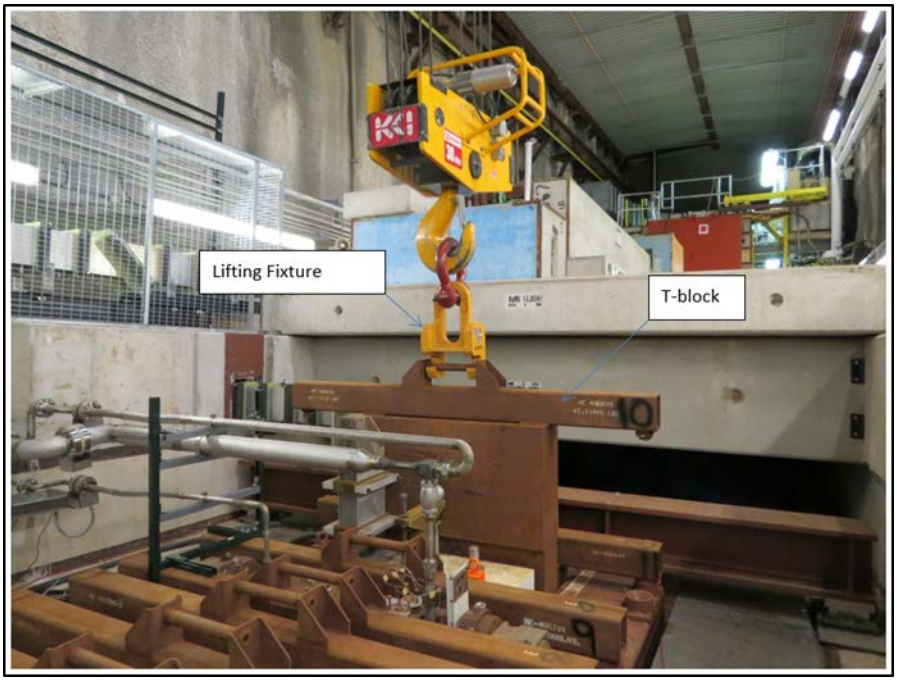

Figure 4-79: NuMI Target Hall Chase with T-block and Lifting Fixture

Water cooling of the aluminum core blocks is achieved by gun-drilling intersecting holes for water to flow through and plugging the remainder of the hole that is not needed, as shown in the left image of **Figure 4-80**. Aluminum pipes are then welded to the entry and exit ports of the gun-drilled water channel and routed up the T-Block to make connections with a manifold, shown in in the right-hand images of Figure 3-YYY20. The final T-block assembly in the absorber is shown in the top image **of Figure** 4-81, including a cover for the pipes coming into the core block to prevent any straight line paths. The bottom image of **Figure** 4-81 shows the water line connections for each T-block to the 10" manifold to the RAW room.

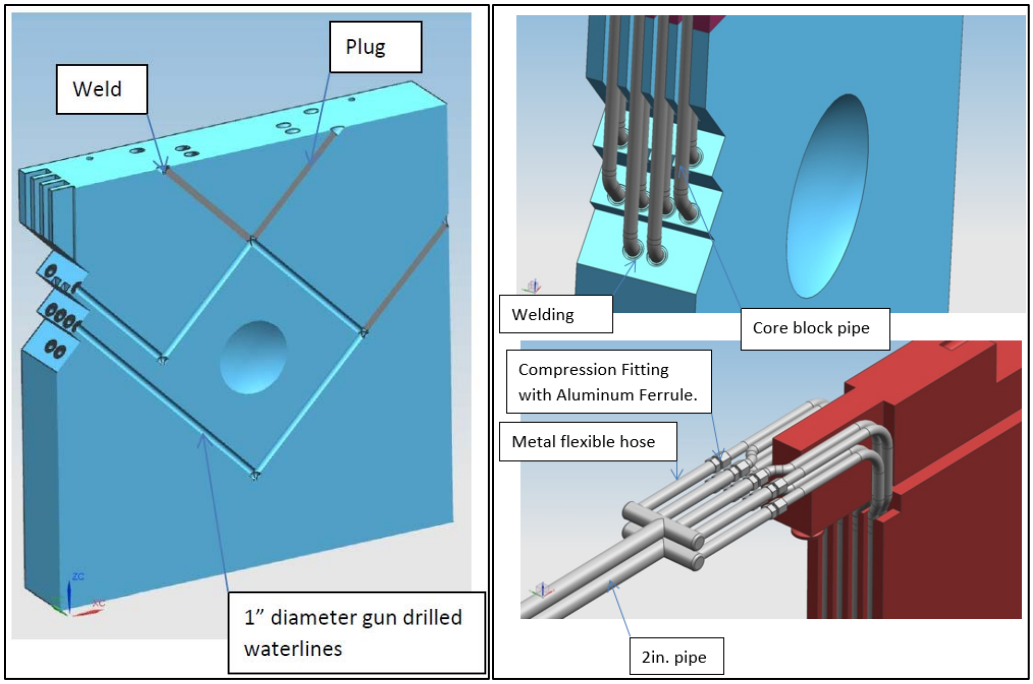

Figure 4-80: Left: Cut-away Cross Section through a Water Line in a Sculpted Absorber Core Bock. Upper Right: Connections to the Aluminum Tubes. Lower Right: Connections to the Manifold

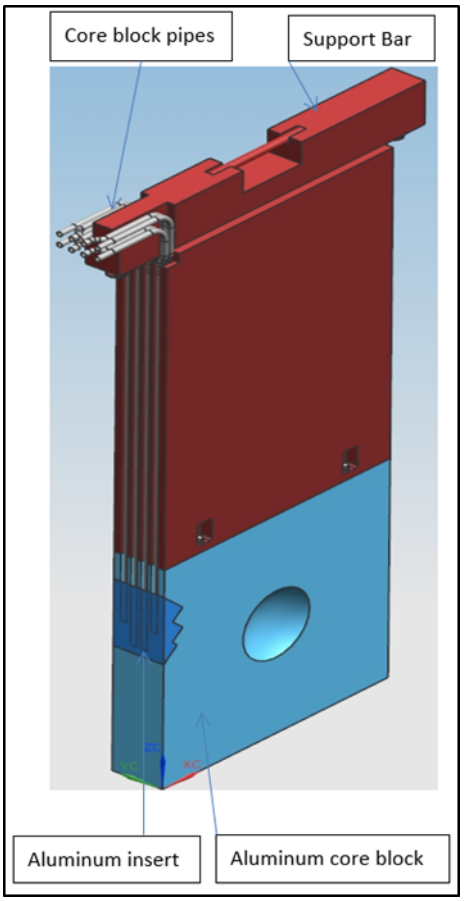

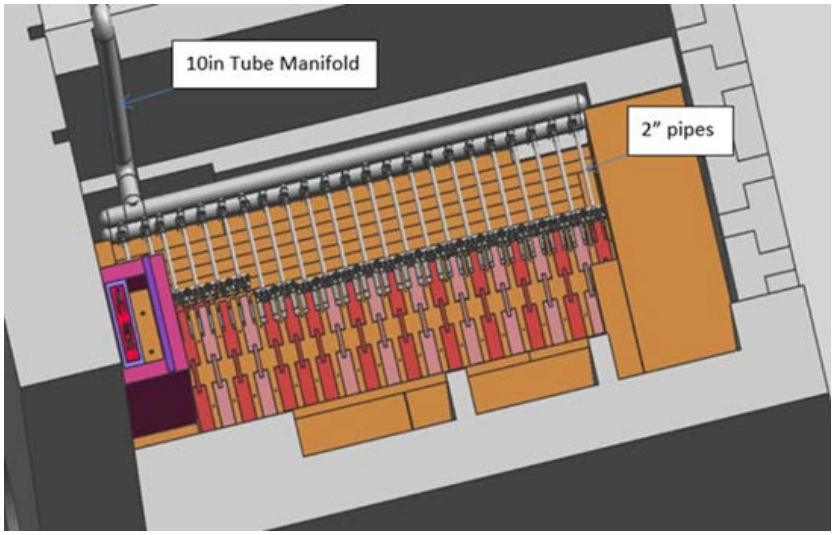

Figure 4-81: Top, Core Block Assembly with T-block. Bottom, T-blocks Assembled into Absorber Showing Water Line Connections

There are 23 core blocks that require water cooling, with each of the aluminum blocks requiring 80 gpm of total flow. The steel core blocks require 40 gpm each. With the addition of 80 gpm for filtration

purposes, the total system flow rate is estimated to be 1760 gpm with a total volume of 1810 gallons. Additional optimizations to the core are planned to reduce this required system flow rate.

Active temperature monitoring of select core blocks will be necessary to determine if any accident pulses arrive at the absorber and to aid in beam and target diagnostics. A design for a thermocouple array in a solid Al block is shown in **Figure 4-82**, with thermocouples spaced to allow the detection of an accident pulse. These thermocouples fit in removable bars that slide in T-slots to allow easy access for replacement as necessary. Jack screws are implemented on both sides of the bar to facilitate removal.

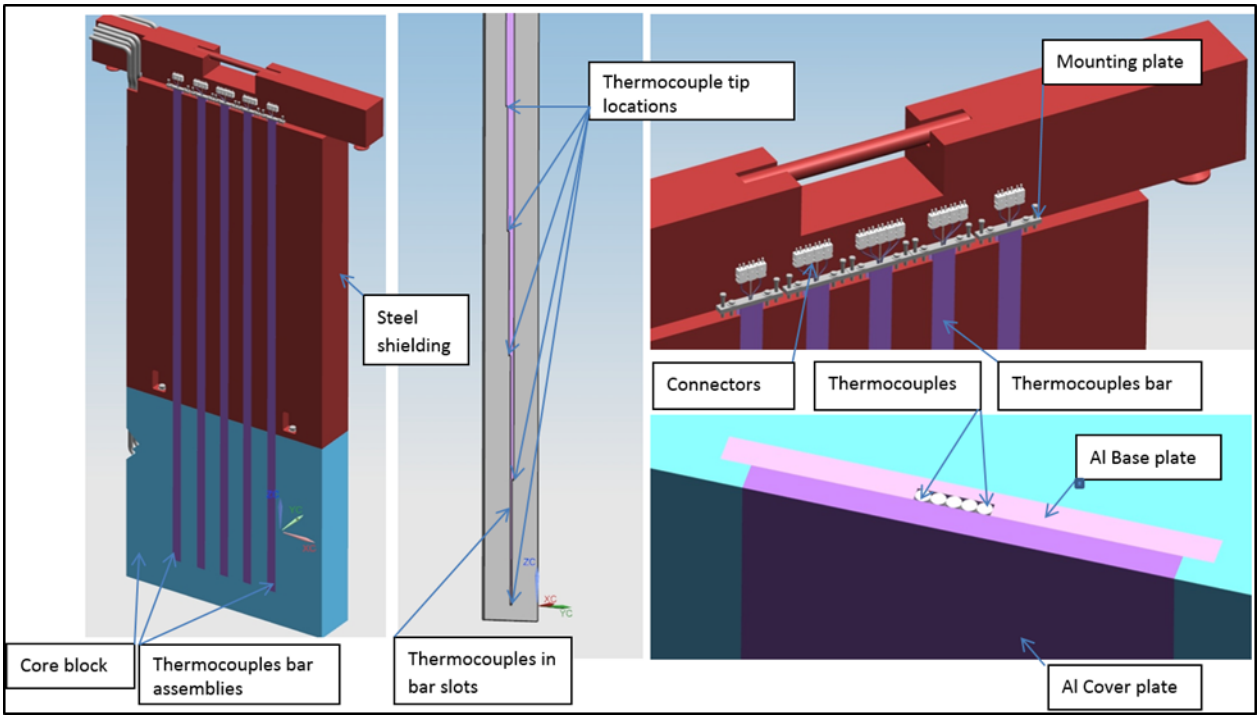

Figure 4-82: Left, thermocouple assembly in T-block. Center, thermocouple tip locations. Right, thermocouple mounting and routing

The absorber design incorporates three different sized morgues to accommodate failed radioactive core blocks and hadron monitors, shown in Figure 4-83. The most upstream is the mask morgue and can accept a total of two mask or spoiler blocks. Next is the core block morgue and it can accept a total of two sculpted Al blocks, full Al blocks, or steel blocks. The hadron monitor morgue is sized for three hadron monitors. All morgues are covered with concrete shielding blocks.

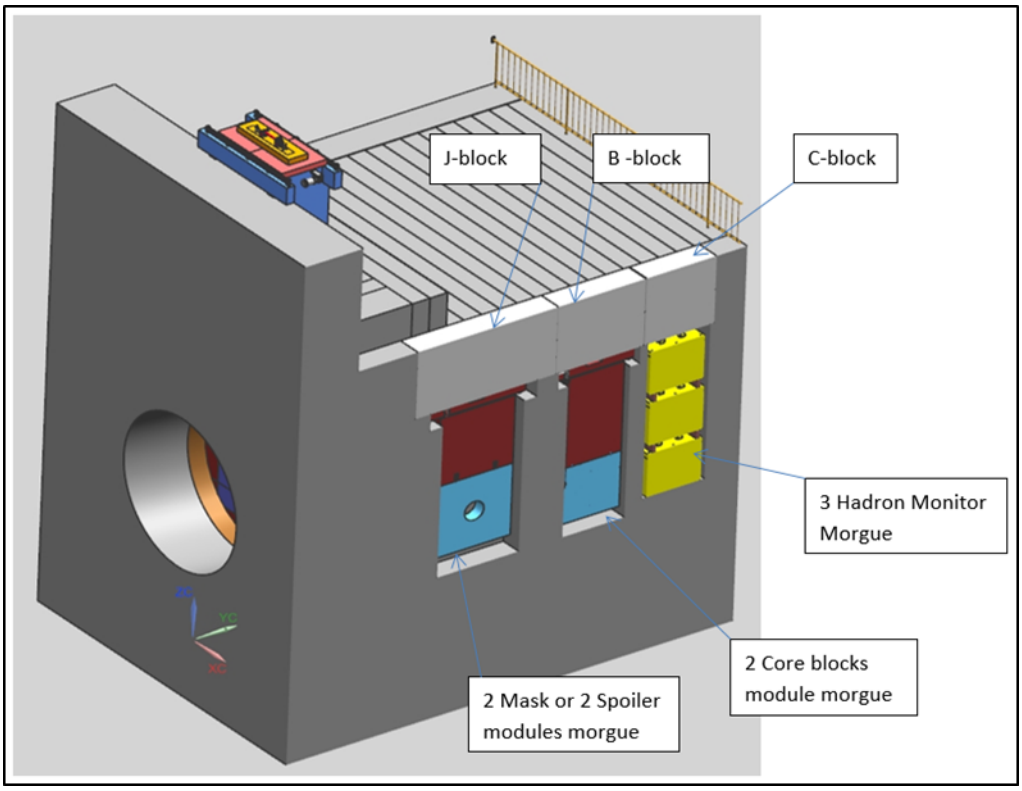

Figure 4-83: Cross Section of the Absorber Showing Morgues

4.10 Remote Handling Equipment (WBS 130.02.03.11)

4.10.1 Introduction

Technical components installed in the Target Hall enclosure are subjected to intense radiation from the primary or secondary beam. The level of irradiation in some LBNF environments will reach levels that are unprecedented at Fermilab. These radiation levels will be too high for workers near such components. The failure of some of the technical components (such as target or horns) is likely over the lifetime of the LBNF experiment. Therefore remotely operated removal and handling systems are an integral part of the Target complex design. Because the remote handling systems are integrated into the infrastructure of the Target complex and cannot be upgraded after irradiating the Target complex areas, they must be designed to be sufficient for 2.4-MW beam power.

4.10.2 Design Considerations

Components to be handled, serviced and/or stored range in size (from 0.20 m^3 to 26 m^3), range in weight (from 10 kg to 30,000 kg) and range in estimated dose rate (from 5 R/hr to 8,000 R/hr on contact), as described in the Remote Handling Component Lists [?]. Shielding requirements for work cells and storage areas have been determined to be 48 inches of concrete or 12 inches of steel to reduce dose rates to workers to below 5 mrem/hr at 1 ft (from the shielding surface). Storage and work cell areas must have redundant sump systems with emergency back-up power systems to mitigate contamination of in-flow water by radioactive particulate from serviced and/or stored components. Steel casks used to transport radioactive components will be sized to reduce dose rates to workers to

below 5 mrem/hr at 1 ft where possible (limited by the crane capacity of 50 tons). Where not possible, it is expected that casks should be of sufficient thickness to allow brief hands-on access by radiation workers, if absolutely needed (300-500 mrem/hr at 1 ft maximum).

The design is based upon a conceptual design study performed by the Remote Systems Group at Oak Ridge National Laboratory. Since the study was performed, remote handling plans were revised significantly resulting in reduced scope and reduced cost. The final report of this study is available [?], and the applicable portions of that study are reflected in the following sections.

4.10.3 Reference Design

The LBNF remote-systems reference design includes equipment and systems in two functional locations. These are the surface Target complex (Target Hall enclosure and neighboring service areas) and the underground Absorber Hall. Along with shielded, remote-capable work areas, each of these locations will have the variety of equipment, lifting fixtures and vision systems required to carry out needed operations.

4.10.3.1 Target Complex Remote-Handling Facilities

The Target Hall enclosure contains the components for generating neutrinos and focusing them toward the near and far detectors. The beamline component arrangement is shown in **Figure 4-84.** The remote handling of components in the Target Hall enclosure chase will be accomplished with long-reach tools, a bridge crane and a shielded work cell. The high levels of radioactivity within the Target Hall while running beam restricts access to facility shut downs after a short cool-down period. The conceptual design closely resembles the layout for the NuMI Target Hall. Since this layout eliminates the possibility for personnel to access any portion of the Target Hall during facility operation, it will require a separate beam-on accessible service area for temporary storage of radioactive components and staging area for remote handling activities.

The main hallway for transport of equipment shielding, and components is located at the upstream portion of the Target Hall enclosure and connects to the Morgue/Maintenance areas (floors of both Target Hall and Morgue/Maintenance areas are at the same elevation). It is through this hallway that radioactive components must pass to get from the Target Hall to the maintenance and morgue (short-term storage) areas. Since most of the service areas are planned to be occupiable with beam on, a shield door must be provided to shield the service areas from the Target Hall. In addition, the air volume of the Target Hall enclosure and the air volume of the neighboring service areas must be separated to avoid radioactive-air contamination of the service areas. The shield door will incorporate an air seal to achieve this air-volume separation. This Target Hall shield door is included in the scope of the remote systems WBS. The layout of the Target Complex is shown in **Figure 4-85** with an expanded view in **Figure 4-86.**

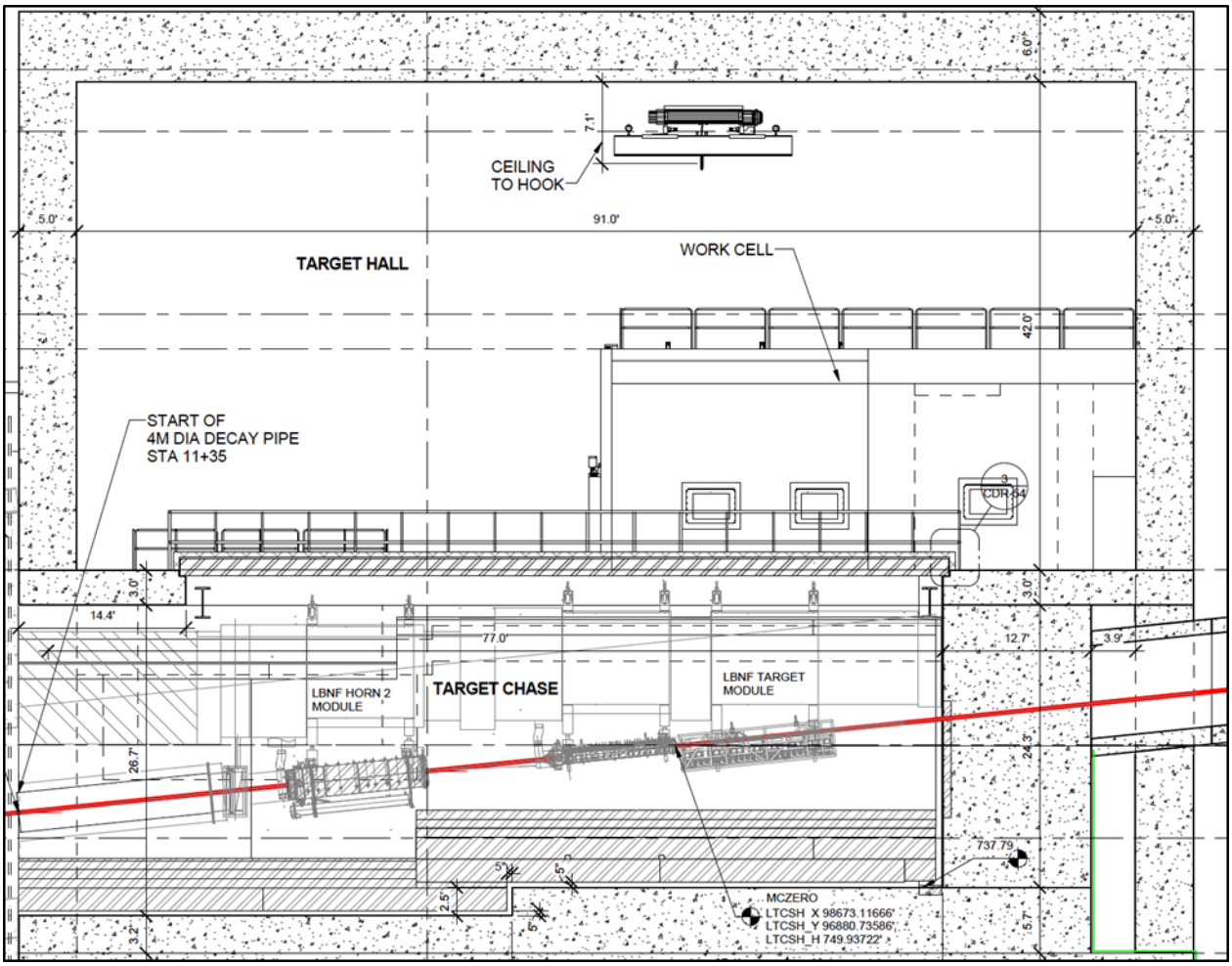

Figure 4-84: LBNF Target Hall Enclosure Beamline Elevation Section

The Target Complex remote operations plan incorporates one hot storage rack in the Target Hall enclosure, designed to provide short- or long-term storage for Horn Module "T-blocks" during component replacement activities. The hot storage can also provide temporary storage of other components that the Morgue cannot accept at the time of removal from the chase. The T-block storage rack is configured as a pit with T-block mounts similar to the carriage mounts that exist in the chase. It is located in the Target Hall floor next to the chase with removable shielding covers.

The work cell is located at the upstream end and the hot-storage rack is located at the downstream end of the Target Hall enclosure on the beam-right side of the chase. The work cell is primarily used to remotely remove a horn, target/baffle, or decay pipe window that has reached its end of life from an activated module and attach a new replacement component. Other remote handling activities such as emergency repairs will have to use the work cell in an ad-hoc way as current operations in NuMI target hall are conducted, or repair operations can use the remote handling facility at C-0 if over-road transport is available. See **Figure 4-85** and **Figure 4-86**.

The chase is covered with shielding composed of steel, marble and borated polyethylene. The borated polyethylene functions as a neutron shield. The marble functions as a residual radiation shield to help reduce the dose to workers during beam-off access. These chase shield covers shall be designed to be stackable such that, when accessing the target chase, the removed covers can be temporarily stored on an un-accessed section of the chase. The replacement of a horn or target is likely to require the greatest number of shield blocks to be removed. One should note that at this point in the conceptual design, Horn 1 with the module attached is the tallest item moved during operation. The shield blocks cannot be stacked so high as to block access of the horn to the work cell. It is not expected that shield blocks from the chase will be occupying the needed set-down space in front of the work cell, but if this situation arises, additional set-down space is available at the US end of the enclosure.

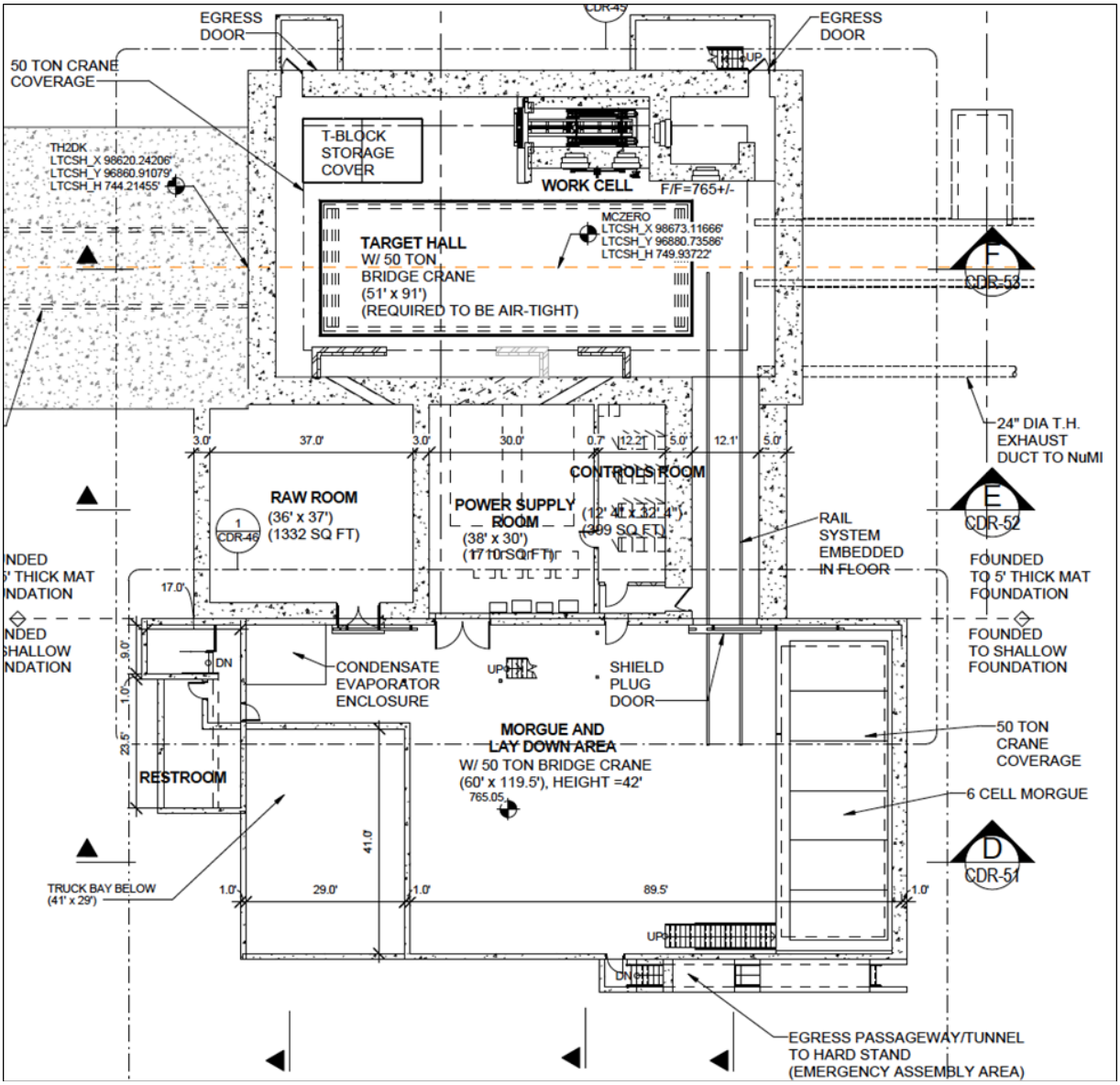

Figure 4-85: Target Complex Plan View

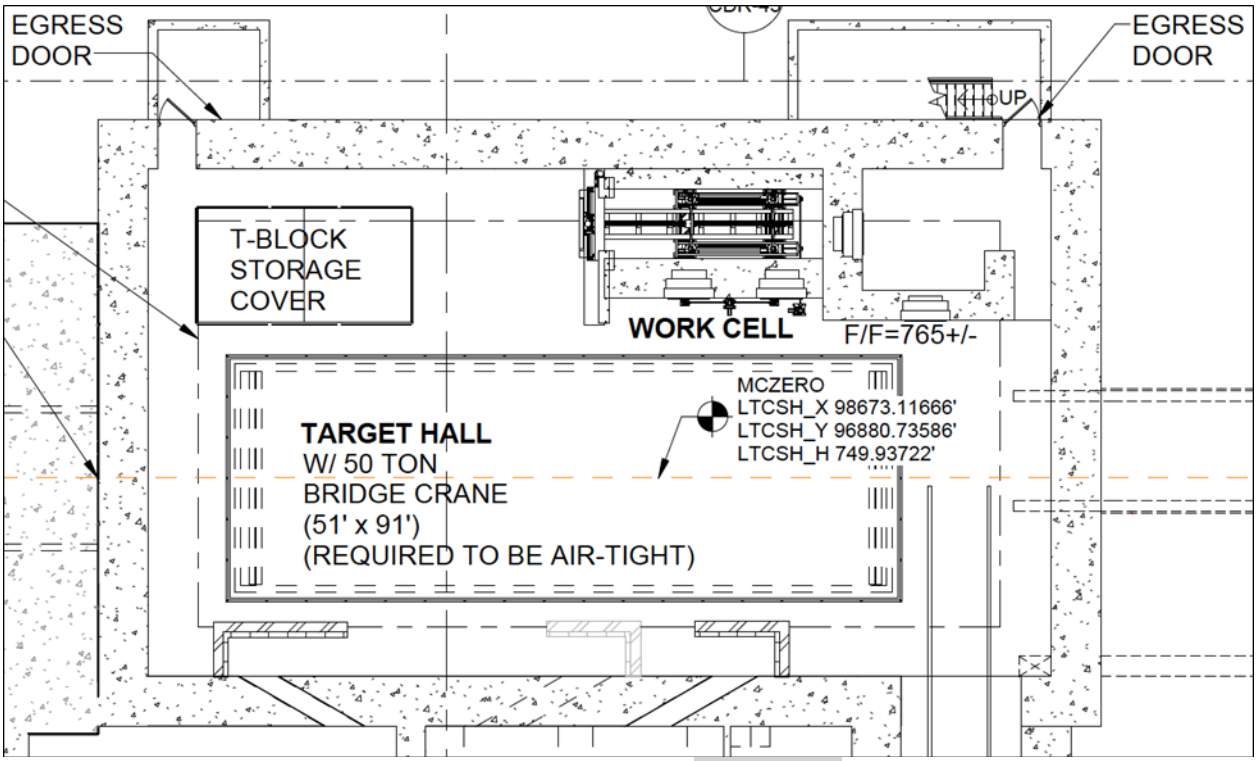

Figure 4-86: Target Complex Plan: Expanded View of Figure 4-85

Similar to the NuMI work cell design, the Target Hall work cell conceptual design uses three shield walls fit together into a "U-shape" with a sliding shield door on the side facing the downstream end of the Target Hall. One of the side walls is incorporated into the Target Hall enclosure side wall to save on space and shielding. The door allows a horn module with horn attached to enter into the cell. The sliding shield door is fabricated from steel with a thickness of 12 in. The door translates using a v-groove track and multiple v-groove rollers along with an additional set of rollers at the top of the door to prevent door tipping. The shield door is moved by a power screw driven by an electric motor located outside the cell, which is similar to what has proven successful with NuMI. The large work cell shield door is fitted with a smaller shield door that allows removal and insertion of a horn or target assembly into the work cell without having to remove the hot module from the work cell. This allows for a much shorter horn/target replacement time as it alleviates the need to temporarily place the hot module back into the chase and replace chase shielding mid-way through the change-out procedure. Proper controls will be added to allow the shield door to be remotely operated via the control area. The control area is in a shielded concrete "cave" built into the US end of the work cell. The control cave will allow operators to remotely view and operate activities in the target facility and work cell. The control cave has a secondary means of egress out of the target facility so that workers can exit without entering the target chase area when radioactive activities are being performed. The top of the work cell is covered with removable shield blocks that fit around the top of the module. The design of this cell minimizes construction cost while maintaining all required capability for completing a horn or target/baffle replacement operation. This cell is approximately 25-ft long, 12-ft wide and 19-ft tall (excluding the personnel safety railing). On the bottom of the cell is a lift table to accept failed components and mount replacement components to their mating modules.

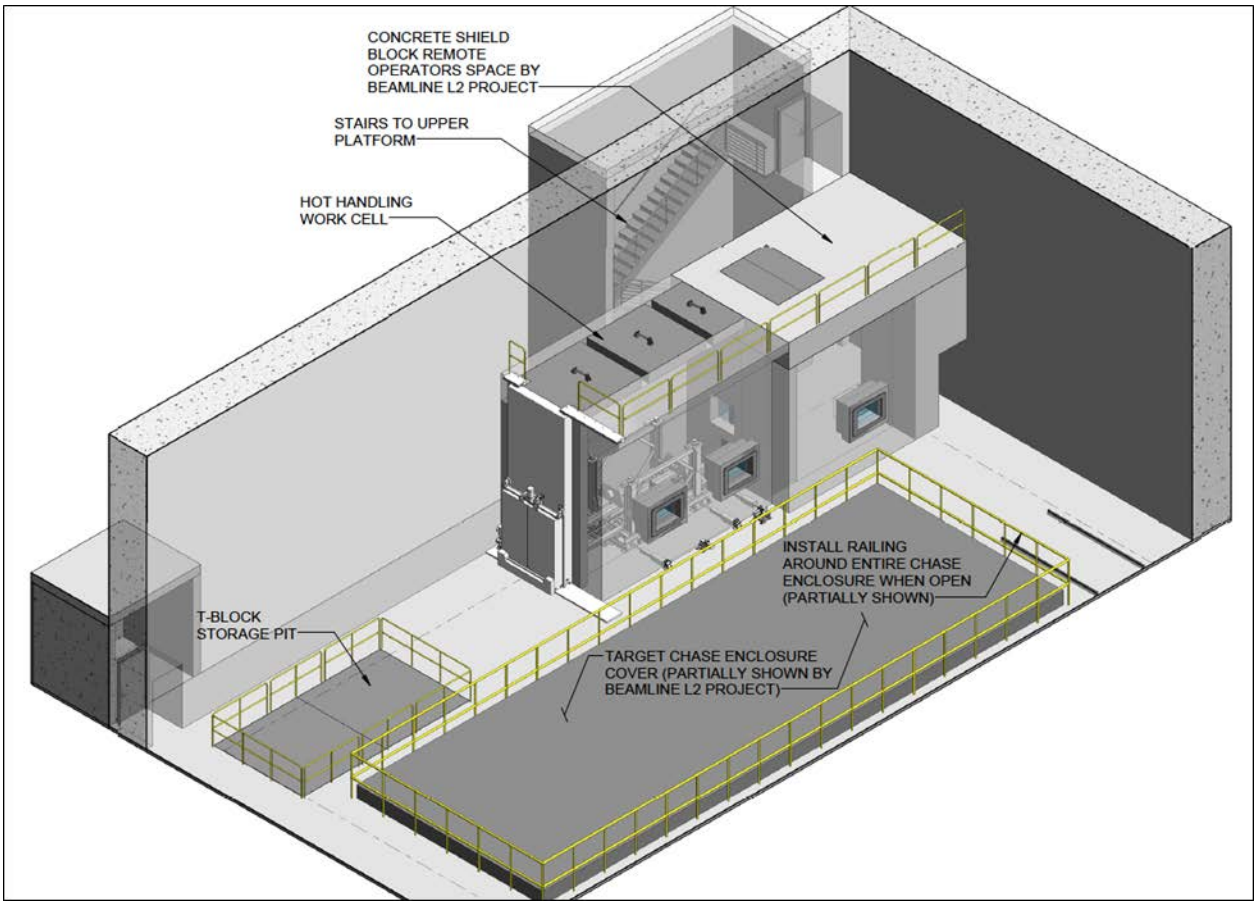

Figure 4-87: Target Hall Work Cell Concept

Lead glass windows will be utilized in the upstream and beam left walls to allow remote viewing and alignment activities (similar to NuMI) as needed. Two additional window openings will be provided (one in the work cell beam left wall and one in the control cave beam left wall), filled with concrete plugs, that offer the opportunity to add lead glass windows in the future.

Before the horn/target replacement operation begins, the shield cask must be placed in the Target Hall, at the upstream end of the enclosure. The shield cask is designed to provide maximum shielding while maintaining a total loaded weight under 50 tons, the capacity of the service areas and Target Hall bridge cranes. The shield cask comprises a shield container, and an end load shield door (shutter type). The cask includes a drive system to push/pull a failed component into and out of the cask on a cart system.

With the cell and cask prepared, the module with failed horn attached can be removed from the chase. The steel and borated polyethylene shielding about the failed horn is removed. The utilities connected to the failed horn are disconnected by hand or using long-reach tools. The marble and steel module shielding (T-blocks) are remotely removed from the module, placed in the T-block storage pit, and covered with the T-block storage pit shield covers. Multiple top shield blocks are removed from the cell using the bridge crane. Then the sliding shield door is remotely opened from the control room. The bridge crane remotely lifts the module and horn and transports them to the cell, placing the module on

alignment feet located on corbels inside the cell. The work cell top shielding can be placed around the module, the shield door is closed and the shielding above the chase is returned.

After all the shielding is properly returned, personnel access to the Target Hall enclosure can be granted, and the failed component can be removed from the module. This is accomplished by locating the lifting table under the failed horn in the cell and then elevating the platform until the horn's weight is fully supported. Using a long-reach tool through openings in the shielding, the connections between the failed horn and module are released, similar to what has proven successful with NuMI. With the component disconnected from the module, the elevating platform is lowered. Now, the shield cask is positioned in front of the small work cell shield door using the crane and the end shutter cask door is removed. The small work cell shield door is opened remotely and the cask cart system is used to pull the horn out of the work cell and directly into the waiting cask. The cask cart systems utilizes a flexible push/pull mechanism called a serapid chain which enables remote motion of the cart. Shield doors are closed on both the work cell and the cask and the cask can now be moved by crane to the motorized cart on rails system for exit to the service building morgue. In the service building, the cask is positioned in front of an open morgue bay, the cask shutter door is removed and the hot horn can be pushed into the morgue again using the serapid chain and cart mechanism. Shield doors are replaced and the cask is moved to the service building main area to be loaded with the replacement horn.

The replacement horn in the cask is transported into the Target hall and positioned in front of the small work cell shield door. The cask shutter door and the small work cell shield door are opened and the serapid chain and cart system are used to push the replacement horn onto the lift table in the work cell. The work cell door is closed and the cask is removed using the crane. Now, personnel can safely access the top of the work cell and use long-reach tools to connect the replacement component to the module. The module and replacement component are now ready to be returned to the chase and personnel must leave the Target Hall enclosure. The shielding above the chase and work cell are removed along with the marble and steel (T-block) shielding in the module. Then the sliding shield door is opened. The bridge crane transports the module with replacement horn to the chase, and the marble and steel shielding can be returned.

The cell's removable shield blocks are then returned, and the shield door is shut. With all the shielding in place, personnel access is allowed. The technicians can enter the Target Hall enclosure and connect the component utilities by hand or using a long-reach tool. Once the utilities are connected, the component's alignment can be checked and adjusted if needed. Then the steel and borated polyethylene shielding above the chase can be returned and air seal established. With all the shielding in place and the component functioning properly, the facility can return to operation.

The work cell conceptual design provides a basic method for horn replacement while also providing a work area for ad-hoc repairs. This concept is not capable of quickly replacing the horn or target if the situation arises. However, this concept's minimal size and limited use of expensive equipment results in a very cost-effective solution.

The specifications for a remotely operated crane can be driven by either regulatory requirements or operational or mission requirements. Facility safety assessments will determine issues such as whether airborne contaminants are a concern if a crane failure were to occur, or whether significant radiation exposures to personnel or the public could result. These types of situations might cause the crane to be considered to be a Credited Engineered Control, which would impose higher design and operational standards. If that type of environment or risk is not applicable, then operational or mission requirements could also impose these higher crane standards. This would be the case if the risk to the Project were such that if a load was dropped or a crane failure occurred with a suspended radioactive load, then the consequences would be extremely severe in terms of personnel safety or recovery time and expense.

In general, cranes used in radiation environments have features that are driven by requirements in one or more of these areas:

- Being able to support and hold a load during and after a defined seismic event
- Having dual load paths and redundant mechanisms to ensure loads cannot fall
- Having features that allow recovery from a crane failure by being able to manually lower a load and move the crane to a safe area for repair

For LBNFLBNF, the use of the crane to lift a radioactive load will occur only after facility start-up has begun. After that point, crane usage will be intermittent, with potentially weeks or months between uses. With that type of usage, the probability of a seismic event occurring while holding a load becomes extremely small, so from this standpoint a fail-proof (ASME NOG-1) crane is not considered necessary. However, when dealing with unshielded radioactive loads, the incorporation of redundant emergency drive systems is desired to enable putting unshielded radioactive loads in a safe condition in the case of a crane drive failure. In addition, some custom provisions to prevent “two-blocking” and removing the crane electronics from the Target Hall enclosure (to avoid exposure to beam-on conditions) are recommended. These features and other crane specifications are listed in **Table 4-12**.

Table 4-12: Target Hall Crane Characteristics

Feature	Value or Description
Capacity	50 tons in a true vertical lift configuration
Lift	50 ft
Speed	Creep modes for all axes of travel
Reeving	Double reeved, single-failure-proof with provisions to prevent "two-blocking"
Radiation Environment	Total Absorbed Dose: 1 x 10^4 rads - Maximum Dose Rate: 1 x 10^2 rads/hr
Hook Rotate Capability	Continuous
Hook	Supported by two independent drive systems
Auxiliary Hoist	5T capacity, 50ft lift, no powered hook rotate
Brakes	Shall restrain all loads without slip or overtravel
Electronics	All electronics, including axis drive amplifiers, control circuits, and memory devices shall be located outside

Feature	Value or Description
	the Target Hall
Load Sensing with Overload Alarm/Interlock	Capability required
Cable Slack Detector	Capability required
Video Cameras (by Others)	Mounts and cable accommodation required
Lights (by Crane Vendor)	Mounted on bridges
Variable-speed Control	Local pendant and wired remote from control room
Recoverability Features	Custom redundant drives and/or manual winch for bridge recovery

With no personnel allowed in the Target Hall enclosure during many maintenance operations, a remote viewing system is essential. Similar to current NuMI operations, the Target Hall viewing system will consist of several cameras on PZT mounts that can be placed in multiple locations (including on the crane bridge). The system includes transceivers for signal and control communications and a portable control station consisting of video monitors and camera controls

CCD cameras have a limited radiation tolerance, approximately 10^3 rads total integrated energy, and if it weren't for the neutron radiation could potentially be left in the Target Hall during beam-on. However, the neutron exposure would render the cameras inoperable, so during remote operation, the cameras will be removed from the Target Hall and placed in a protected area. Given the relatively low background radiation levels expected in the Target Hall during maintenance operations, the high cost (>$60,000 each) of radiation hardened tube cameras is not justified, so the CCD cameras will be considered disposable.

The Morgue and Maintenance area of the Target Complex is an area for short-term storage of spent components. In addition, it will serve as a maintenance area for in-beam components. These facilities are described in this section from the perspective of remote handling activities and equipment that will occupy this area. The building, including the cast-in-place concrete shielding for the morgue, will be provided by Conventional Facilities (see Volume 5 of this CDR for construction details).

The services areas of the Target Complex will be constructed with thick concrete walls sized to reduce the dose rate external to the building (i.e., the residual dose rate from radioactive components being serviced/stored inside) to acceptable limits. Some pertinent characteristics of this facility include:

- Integrated truck bay for surface-level loading/unloading
- Overhead bridge crane accessing both a truck bay and Morgue/Maintenance areas
- Shielded storage and repair areas for activated components, referred to as the morgue

Figure 4-85 provides a plan view of the services areas of the Target Complex. It is a dual-level facility with a ground-level truck bay of approximately 1,200 ft^2 and an elevated morgue maintenance level of approximately 7,200 ft^2. From a radiation protection perspective, the truck bay is expected to be open access for personnel, while the morgue will be limited access. Each level is covered with the same 50-ton overhead bridge crane. The Target Hall enclosure is connected through a large hallway at the

upstream end. As the Target Hall enclosure ventilation system must be separated from the neighboring service areas, a sealed shield door in this connection hallway is required during beam-on operations.

It is assumed that the Morgue will be a radiation buffer area, which requires that radiation levels in personnel-accessible areas are less than 5 mR/hr. A calculation was made to determine the thickness required to reduce the radiation from an assumed unshielded dose rate of 1,100 R/hr to a shielded rate of 5 mR/hr. The result showed that 4 ft of concrete or 12 in of steel is needed between the component and personnel in the facility or to the exterior of the building. All transport activities of radioactive components in the Morgue area will be shielded to the extent possible with the crane capacity of 50 tons.

Groundwater activation is not a concern for components being handled at the Morgue because they will not have enough energy to activate the water. However, surface water contamination due to collection of activated dust and loose particles in a flood scenario will be a concern, and the morgue level will require a redundant sump system and back-up power generator.

The LBNFLBNF Target Hall Complex is configured to provide short-term storage space of spent components in a 6-cell morgue for about 2 years of 1,200 kW operation, with the expectation that, after 2 years of decay time, radioactive components could be moved to a long-term storage location. If the morgue storage requirements increase (due to shorter than assumed component lifetimes), the morgue could be expanded by storing components, shielded with concrete blocks, on top of the existing morgue. The expected storage requirements for the morgue are shown in **Table 4-13** for both the 1,200 kW and 2.4 MW cases. Because the horns are the largest components (with Horn 2 being somewhat larger than Horn 1), storage cells are designed to accommodate one Horn 2. For the 1,200 kW 2 year storage space requirement, a total of six cells are allocated to the facility concept.

The longer-term storage location is assumed by LBNFLBNF to be provided by Fermilab. This facility is required to be available to accept LBNFLBNF components after the LBNF Beamline has been running for about 2 years, presently scheduled to be approximately 2027. At the present time, the Fermilab Directorate has approved the construction of a long-term radioactive storage area located at the C-0 Remote Handling Facility. The new storage area began construction in 2014 and is anticipated to be ready to accept radioactive components starting in 2018.

Table 4-13: Morgue Storage Requirements

Component	Replacement Frequency at 1,200 kW, #/yr	Storage Quantity at 1,200 kW, 2 yrs	Replacement Frequency at 2.4 MW, #/yr	Storage Quantity at 2.4 MW, 2 yrs
Target/Baffle carrier	2.5	5	5	10
Horn 1	0.33	.67	0.3	.67
Horn 2	0.33	.67	0.3	.67

Spent components would be transported from the Target Hall enclosure to the Morgue/ Maintenance area of the Target Complex in a shielded steel transport cask. The cask thickness would be determined

by crane capacity in the Target Complex (50 ton) rather than the thickness required to reduce dose rates to a level that allows long-term direct human contact with the container. For horns, an estimated cask thickness is 4 in. Because hands-on contact may be limited, the casks must be able to be remotely loaded and unloaded. The casks and morgue cells will be side loaded, enabling the radioactive component to be transferred from one to the other largely under shielding. For NuMI and NOvA components, a system that achieves this has been already designed and used in operation.

Figure 4-88 shows a picture of the morgue/cask transfer system in place at C-0 Remote Handling Facility. The component in the cask is supported by a rolling cart and pushed/pulled by a serapid chain mechanism mounted to the back of the cask. Temporary shielding is set around the gap between the cask and the morgue when the morgue and cask doors are removed.

Figure 4-88: Photo of Cask-to-Morgue Cell Transfer System Used at C-0 Remote Handling Facility

The cask and morgue doors are designed to be remotely operated using the building crane, as is the temporary shielding. The area above the morgue cells may be used for storage or for storage cell upgrade (to provide an additional 6 cells in a second layer). The above floor design reduces the possibility of water contamination issues due to flooding.

To separate the air volumes of the Target Hall enclosure and the service areas of the Target Complex, a Target Hall-connecting hallway shield door and air seal must be constructed. The door is expected to consist of 6 inches of steel and 1 inch of borated polyethylene mounted on rails to allow motorized

movement. The exterior side of the door will be lined with galvanized steel sheet to form the air barrier. The air seal at the edges of this barrier is conceived to be either double O-rings with toggle clamps or a double inflatable air diaphragm with passive clamps. An air monitoring station, located in the Power Supply Room, to monitor the air activation on the Target Hall side of the door will provide information needed prior to granting removal of the cover.

4.10.3.2 Absorber Hall Remote Handling Facilities

The Absorber Hall remote handling facilities are similar in concept to those for the Target Hall in that they will include a bridge crane, cask system and long-reach tools to enable the replacement of the hadron monitor upstream of the hadron absorber. However, unlike in the Target Hall, replacement of components will not require a work cell and all hadron monitor replacement crane operations are planned to incorporate shielding that allows for some minimal hands-on access. In addition to hadron monitors, water-cooled absorber modules and steel shielding may fail, and some provisions must be made to allow replacement. Although the absorber components are designed to last the lifetime of the facility and will include redundant water-cooling lines, the consequences of complete failure are significant. Therefore, provisions will be made in the design of the Absorber Hall components and shielding to allow future replacement. However, because of the low probability of complete failure, final design and construction of remote handling equipment for absorber modules and water-cooled shielding will not be included in the LBNF project. If complete failure occurs during operation, a long downtime (6 months to 1 year) would then be required to final design, build, develop procedures and safely replace the failed component(s).

The conceptual design of the Absorber Hall is shown in **Figure 4-89** and **Figure 4-90**. The hadron monitor and the absorber modules are located under steel and concrete shielding blocks. The hadron monitor is the furthest upstream component in the absorber assembly. Directly to the beam-right of the absorber assembly is an empty, shielded pit volume called the morgue (see **Figure 4-91**). This morgue has been designed to accept three hadron monitors and two absorber core (or mask) modules. In order to replace a hadron monitor, first, with shielding in place, utilities to the component must be disconnected by hand at the top of the absorber pile. After disconnecting utilities, the top cover plate of a shielding tower (called a “castle”) is opened allowing the crane to lift the hadron monitor and module into the castle. On the side of the castle, a special cask and monitor exchange system is installed on a horizontally moving platform for removing the spent hadron monitor (see **Figure 4-92**). The platform and extraction cask are then remotely moved into the castle and under the hadron monitor. The hadron monitor and module are lowered so the hadron monitor is within the extraction cask. Now working from above, workers can disconnect the instrumentation and gas lines from the hadron monitor and the hadron monitor is disconnected from the module. The module is lifted back up within the castle and the platform can be moved carrying the cask with hadron monitor within it out the side of the castle. Working remotely with the crane, the top of the extraction cask can be installed. With all shielding back in place, the cask containing the spent hadron monitor can be moved to a storage location (the side morgue) or out of the Absorber Hall as appropriate. The new monitor is installed in the reverse order and all shielding is replaced. Finally, after a system check-out procedure, utilities can be re-connected and operation can be resumed.

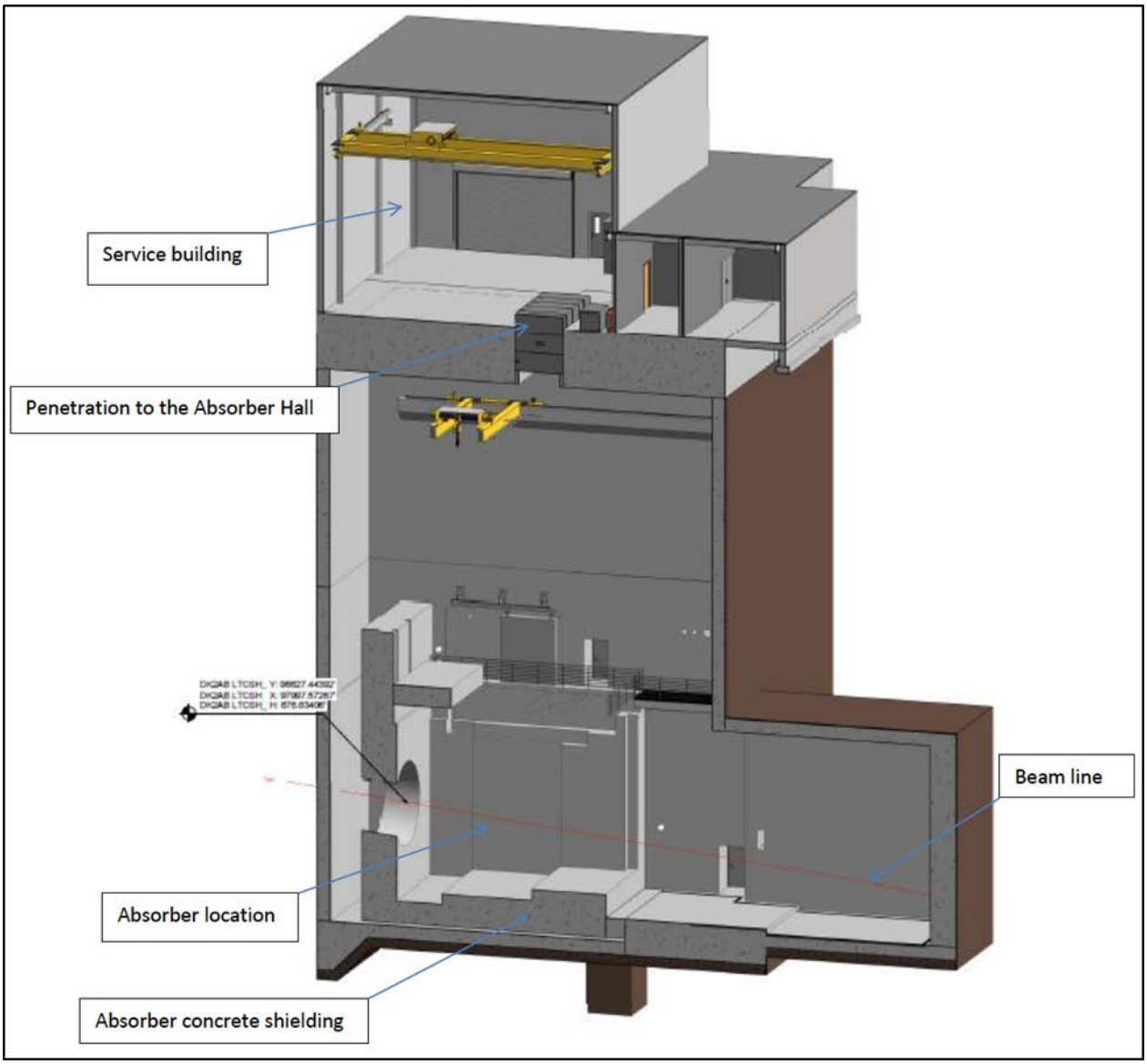

Figure 4-89: Absorber Hall Section

The beam comes from the left. The downstream end of the decay pipe is bottom left. Absorber is not shown in this figure.

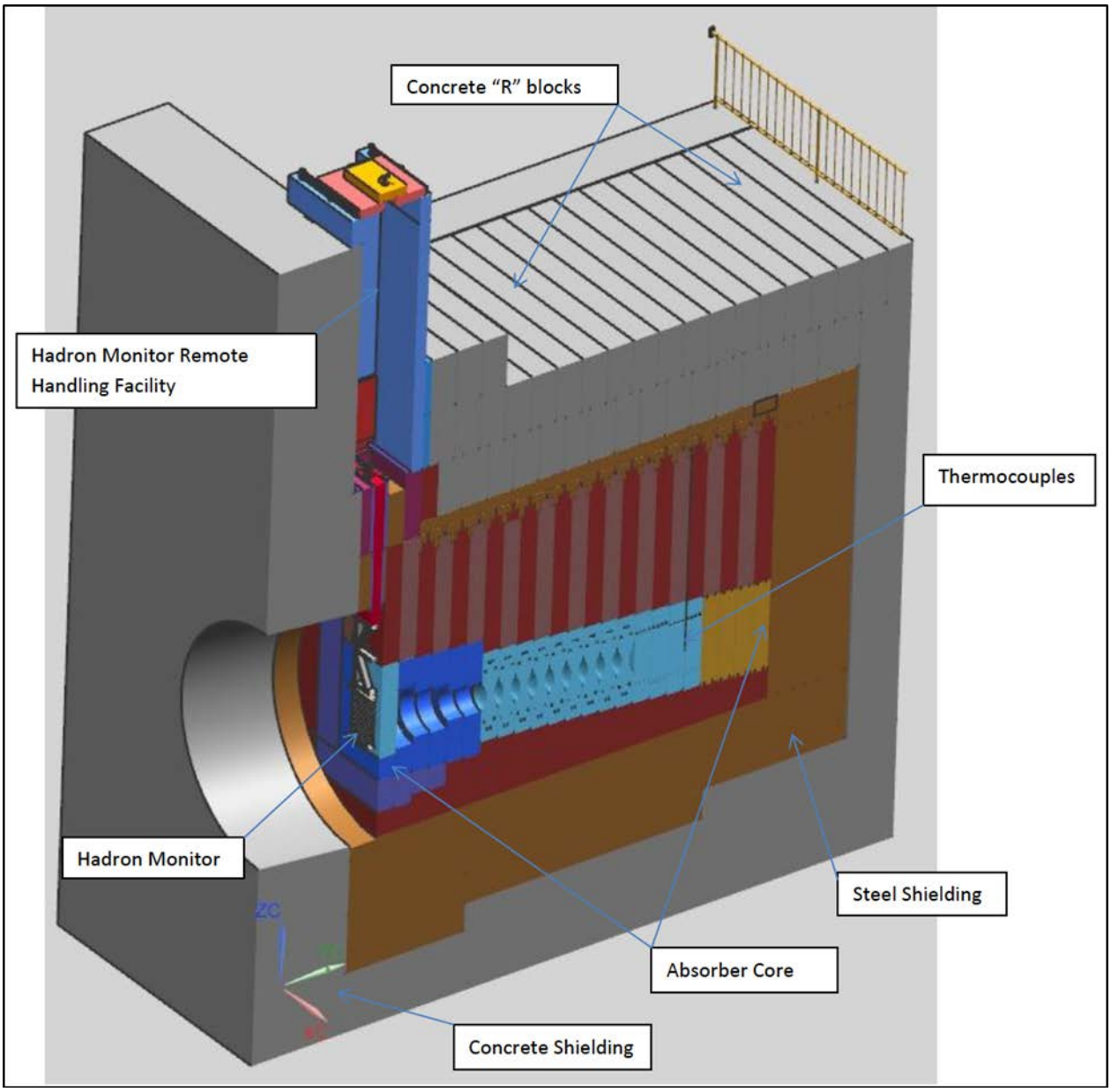

Figure 4-90: Absorber Hall Section Showing Details of the Absorber Core and Shielding Arrangement

There are no plans within the Project to provide support for removal of radioactive items from the Absorber Hall morgue to the surface. However, nothing in the Project plan precludes doing so in the future should it be necessary. Shielded casks could be built to shield radioactive components during transport, and the Absorber Hall bridge crane could be used to load and unload those casks.

The Absorber Hall bridge crane has a very similar function as the Target Hall bridge crane. LBNF. The use of the 30 ton crane to lift a radioactive load will occur only after facility start-up has begun. After that point, crane usage will be intermittent, with potentially weeks or months between uses. With that type of usage, the probability of a seismic event occurring while holding a load becomes extremely small, so from this standpoint a NOG-1 crane is not considered necessary. In addition, because the hadron

monitor exchange system incorporates shielding casks (castle) at every step, recovery systems in case of crane failure are not necessary. A standard, industrial 30 ton bridge crane (with provisions to remove electronics from the Absorber Hall during beam operation, if deemed necessary) is sufficient. In addition, since true remote operations using the crane are not planned for hadron monitor exchange, a control room for the Absorber Hall is not required.

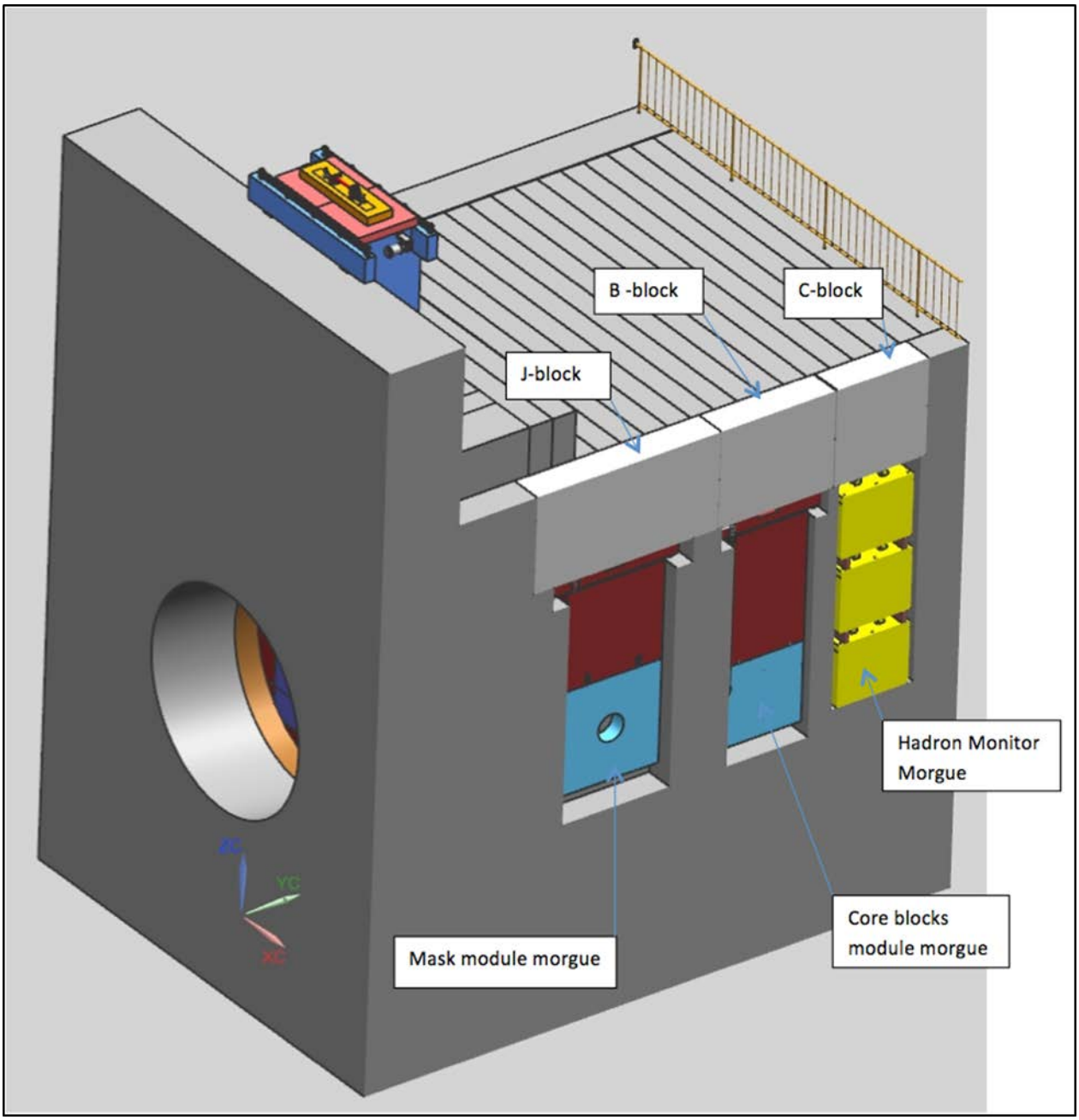

Figure 4-91: Cross Section of Absorber Hall Beam View Showing Morgue Storage Area

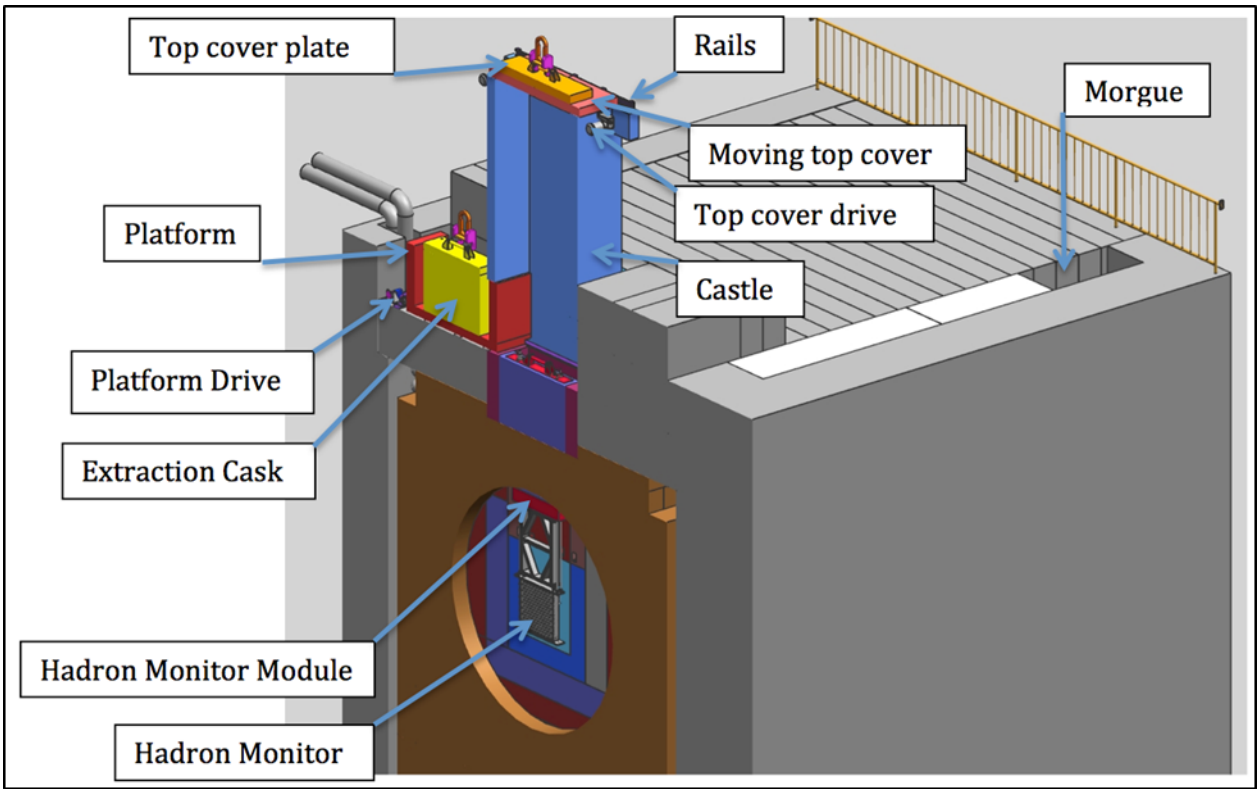

Figure 4-92: Cross Section of Absorber Hall Beam View Showing Hadron-monitor Replacement Concept

4.11

4.11.1 RAW Water Systems (WBS 130.02.03.09)

Introduction

Many components in Target Hall as well as the core of the absorber are water-cooled. Since these elements are operated in an environment with a high flux of energetic particles from the beam interacting with the target, the cooling water itself will be activated and cannot be allowed to mix with unactivated water. Therefore, these components are cooled using a closed-circuit water system; the heat being moved by conduction and convection to secondary water heat-exchanger/chiller system connected to the outside world. The closed-loop Radioactive Water Systems (RAW systems) are used extensively at Fermilab in removing heat from high-flux particle environments. They are generally of modular design with integral secondary containment systems, and easily transportable into their final location.

Design Considerations

In general, all NB RAW systems will follow layouts similar to those used and proven with NuMI / NOvA experience. These will benefit from maturity of design from lessons learned during years of operational support and maintenance.

4.11.2

All RAW equipment skids will have suitable containment for RAW leakage and tritium capture, and all should be designed with an intermediate loop between the RAW system and exposure to systems outside of the enclosures. All the RAW systems will require radiographic inspection of welds. Both piping and vessels will adhere to FESHM Chapter5031, as well as the Fermilab Engineering Manual. Piping will be designed and installed in accordance with ASME B31.3 Code for Process Piping. Pressure vessels shall be designed in accordance with ASME Boiler and Pressure Vessel Code Section VIII Division 1.

Most RAW system volumes are expected to fall into the range of 100 to 200 gal each, except for the Chase Shielding, which will be around 600 gallons, and the Absorber Pile, which will be around 1200 gallons. RAW skids will have sufficient containment to capture these volumes. (System design of both the Chase Shielding and Absorber Systems leave most of the RAW contained in the component in the event of a system leak on the skid.) Also, Fermilab's guideline is to limit RAW activity to 670,000 pCi/ml; LBNF will design the system to operate around an activity level of 500,000 pCi/ml. The activation limit is expected to be reached on a monthly basis for the target and horn systems, and biannually or so for the remainder of the systems. Because of this, the addition of RAW capture and drainage systems are included. Their purpose is to help with the capture of RAW waters from each of the skids in such a way as to limit manpower exposure and frequency of water change-out. Similarly, the Target Hall and Absorber Hall will have adequate space for the local storage of hot de-ionization (DI) bottles and components.

The RAW systems must be capable of removing heat at the original design loads for 1.2MW beam, and easily upgradable for sufficient heat removal for a 2.4MW beam. In addressing system heat loads versus design parameters, the following strategy is used:

Heat exchange through a component or within a heat exchanger is proportional to both flow and the change in fluid temperature. For our RAW and LCW systems, desired ranges for flow velocity (v) in the system piping is in the range of 7 to 10 feet per second (fps), and for temperature change (delta-T or dT) of 10F to 15F. Using these preferred limits, we can design RAW systems using target values of v = 7fps and dT = 10F for 1.2MW beam. Then, when upgraded to a 2.4MW beam, 10fps and 15F is used. This would mean the vast majority of the system would meet the needs of either beam power, and upgrading for future higher beam power would mainly be an issue of increasing pump size and heat exchanger capacity. The same strategy is used for the Intermediate Systems. The RAW Exchange Systems remain unchanged, as they are unaffected by heat load.

Reference Design

4.11.3.1 Target Hall Systems

4.11.3 Located outside the Target Hall will be a RAW equipment room, which will hold the majority of the equipment for RAW skids, for cooling of the Target, Horns 1 and 2, and the Target Chase Shielding Panels.

The estimated overall heat load due to components is around 475kW (at 1.2MW-beam power). Due to the distance from the Central Utility Building (CUB), a local system will prove advantageous. Local chillers were selected for the reference design and the load is included in the CF Target Complex design.

The reference-design Target Hall RAW systems are as follows:

- Target and Baffle RAW System
- Horn 1 RAW System
- Horn 2 RAW System
- Target Chase Shielding & US Decay Pipe Window RAW System
- RAW Exchange and Fill System
- Intermediate Cooling system

Anticipated heat loads for the various systems are as shown in the chart below, and include added heat from pumps, and heat exchanger efficiencies:
Insert new table:

System	Heat Load kW @ 1.2MW	Heat Load kW @ 2.4MW
Target and Baffle RAW skid	28	56
Horn 1 RAW Skid	64	128
Horn 2 RAW Skid	49	98
Target Chase Shielding / Window Skid	332	664
RAW Exchange System	none	none
Intermediate Cooling System (RAW total + 10%)	592	1080

4.11.3.2 Absorber Hall Systems

Located outside the main Absorber Hall will be a RAW equipment room, which will hold the majority of the equipment for RAW skids for cooling of the absorber.

The estimated total heat load for the Absorber Hall RAW systems is approximately 260 kW (at 1.2MW beam power). The most likely source of outside cooling water would be for a chiller system at ground

level and a recirculation and cooling system to supply the enclosure. While possible, a local pond water-cooling system would most likely prove too expensive for consideration.

There is a possibility that further design work could point to greater utility of space and efficiency being achieved by breaking this system into two or three smaller systems. This is left for further study at this time. It is felt that the current estimate should be sufficient to cover this case, should it arise.

The reference-design Absorber Hall RAW systems are as follows:

- Absorber RAW System
- RAW Exchange and Fill System
- Intermediate Cooling system

Anticipated heat loads for the absorber systems are as shown in the chart below, and include added heat from pumps, and heat exchanger efficiencies:

Insert new table:

System	Heat Load kW @ 1.2MW	Heat Load kW @ 2.4MW
Absorber RAW System	375	660
RAW Exchange System	none	none
Intermediate Cooling System (RAW total + 10%)	425	740

4.11.3.3 RAW Exchange Systems

Most of the systems are closed-loop high-purity radio-activated water systems. IE, the Target, Horns, Shielding, and Absorber skids. A “lessons learned” from the NuMI operation and maintenance of these systems is that the handling of the RAW was problematic under 2 recurring conditions: First, that of regular skid maintenance, requiring draining of a percentage of the system, from a few gallons to nearly the full volume. Second, the RAW is constantly flowing through components and conditions that raise its activation levels. In order to maintain reasonable levels, a portion of each RAW system was drained off on occasion, and replaced with fresh LCW, thereby diluting the activation concentration.

Both of these conditions had techs exposed to radiation and hazards more than desirable, crawling around systems and handling RAW, all in hot areas. These procedures also required down time for access to the RAW rooms. As a way to reduce this exposure, and make the entire procedures less bothersome, easier to perform, easier to do safely, and better from a containment viewpoint, RAW exchange & fill systems were devised. Since their installation with NOvA upgrades, they have proven quite useful in both the TH and AH. Therefore, similar systems will be designed for use in the LBNF RAW areas.

4.11.3.4 Recent Additions, Modifications

In late 2013, due to feedback from the ANU Lessons Learned panel, it was found that instrumentation had been inadequately estimated for NOvA RAW and LCW Systems. Therefore, a thorough study was completed for all of LBNF LCW and RAW instrumentation. The information was presented to project leadership, and suggested to be implemented as a Change Request. Although agreed upon to do this, timing left it out of project action until now. It is hereby included as part of the CD1 Refresh estimate.

Not included in the original CD1 was the Target Chase Shielding & US Decay Pipe Window RAW skid. As a recent addition to the scope of TH RAW Systems, the estimates for it are very preliminary. All of the associated design issues are not fully understood. This is a relatively large RAW system, and more than triples the total heat load to be removed from the Target Hall RAW systems, and has repercussions for the Intermediate Cooling System, which has chillers outside of the LBNF-5 service building. It also influences the design of the RAW Exchange System, as requiring a much larger capture tank for disposal of RAW, and a much larger fill/expansion tank to supply make-up water to the RAW skids.

A change in the Absorber Hall systems is that the flow desired for the heat load for the Absorber Pile is over double what was originally estimated. This translates into larger piping, heat exchangers, pumps, and overall system volume. Chillers for that system are located outside of LBNF-20. Similar to the Chase /Window system in the Target Hall, this increase in system size has influence on the intermediate and RAW Exchange Systems as well. In addition, at this time the Absorber RAW system is over-designed for worst-case scenario. Optimization of the system may lead to separation into two or three smaller systems, for better temp control while increasing overall efficiency.

All of these changes have been incorporated into the latest Cost and Effort Spreadsheet. There are significant increases due to larger heat exchangers and pumps as required. Some of this work has large 60% contingencies, as thorough design work has not yet been accomplished, and more confident numbers are not available. However, where greater design maturity, better quotes, and/or estimates allowed, contingencies were adjusted downward, as low as 20% for some items.

RADIOLOGICAL CONSIDERATIONS (WBS 130.02.01)

Overview

In the 2012 version of this CDR, it was envisioned that the beam line will start operating with a 700 kW beam and after the accelerators upgrades were completed, about five years later, the beam line will be running a 2.3 MW proton beam. Since then the accelerator upgrade plan has changed. Currently, it is planned to start the operation of the beam line at 1.2 MW for five years followed by fifteen years at 2.4 MW, when the accelerators upgrade is ready. It is expected that this 20 years of running beam to be accomplished over the span of thirty years of accelerators operations. Change in radiological quantities, in going from 2.3 MW to 2.4 MW, is only a few percent. In this section (3.10), some of the radiological calculations presented have not yet been updated to the 2.4 MW. This actual beam power used will be noted where needed.

Only radiological issues for operation of the LBNF beam line with 2.4 MW beam power are considered, since retrofitting the LBNF facility for 2.4 MW after years of operation at 1.2 MW is very costly and not practical. The scope of radiological issues includes the primary transport line, target hall, decay pipe and the absorber hall. The analyses contained in this section are based on current requirements of the Fermilab Radiological Controls Manual, FRCM [29]. Other measurements and verification data available are also used where applicable.

The posting and entry control requirements for access to areas outside of beam enclosures where prompt radiation exposure may exist for normal and accident conditions are given in the Fermilab Radiological Controls Manual. All results presented in the following subsections are based on the MARS modeling of the LBNF facility (See Section 3.12).

In the NuMI (700kW) primary beam line, fractional beam losses are controlled to better than 10^{-5}. To maintain the same radiation level when scaling to 2.4 MW (desirable to keep residual radiation at a level where maintenance is not hindered), corresponds to controlling the losses at 3×10^{-6} for LBNF. Control of the LBNF beam average operational losses is assumed to be 10^{-5} for shielding purposes, which gives a sensitivity/safety factor of more than 3 larger. While accidental beam losses are difficult to estimate from first principles, again the NuMI beam can be used as the analog to LBNF for this estimation. During the six years of NuMI primary beam operation, more than 50 million beam pulses were transported to the NuMI target with a total of more than 1.2×10^{21} protons on target at 120 GeV. A total of 6 beam pulses have experienced primary beam loss at the 1% level, all due to Main Injector RF problems. Since 2005 only one full intensity pulse has been lost. Therefore, it is assumed that control of LBNF primary beam losses to less than 2 pulses/week is possible by using a control system similar to that developed for the NuMI beam.

A computer model for the entire beamline has been built in the framework of the MARS15 Monte-Carlo code [NM1]. This model includes all the essential components of the target chase, decay channel, hadron absorber and the steel and concrete shielding in the present design. The MARS simulations are used specifically in the calculation of: (1) beam-induced energy deposition in components for engineering design, (2) prompt dose rates in halls and outside shielding, (3) residual dose rates from

activated components, (4) radionuclide production in components, shield and rock, (5) horn focusing design and optimization of neutrino flux.

The radiological requirements outlined in this section are applied to the designs of the technical systems and equipment for the Beam line discussed in this volume, as well as to the conventional facilities discussed in Volume 5 of this CDR.

5.2 Shielding

5.2.1 Primary Beamline

The Conceptual Design for the LBNF facility has been developed with external primary beam soil shielding of 25 feet (7.6 m). This provides an additional safety factor beyond the calculated LBNF required shielding for both the normal and accidental losses. The calculated soil shielding required for 2.4 MW beam, for unlimited occupancy classification, is 22.5 feet (6.9 m) for continuous fractional beam loss of 10^{-5} level and 25 feet (7.6 m) for 2 localized full beam pulses lost per hour.

To reduce the contribution of accidental dose from muons at the site boundary to less than 1 mrem, MARS simulations show that an additional 54 feet (16.5 m) of soil in the path of the muons, downstream of the target hall, is required to shield against losses at the apex of the embankment. The width of the embankment should be no less than 6.5 ft beam-left and 10.5 ft beam-right. It is also possible to accidentally lose the beam on one of the beam line elements, on the uphill side of the embankment. The worst case is when the beam is lost near the top. In this case the upward going muon plume will have the minimal soil shielding in its path, before exiting the transport-line shielding. MARS simulation show a maximum dose rate of about 35 mrem on a small area on the embankment is possible. Based on the transverse dimension of the plume a fenced area is designated that encloses the area such that the accidental dose at the fence boundary will be less than 1 mrem.

5.2.1.1 Target Hall/Target Pile

The target hall and target pile shielding is designed to contain prompt radiation, residual radiation, activated air, accidental spills of radioactivated water, and to control a thirty-year buildup of the radionuclides in the soil outside the shielding to below requirements. Another goal of the design is to have an average dose rate of less than 100 mrem/hr in the target hall above the target pile during the normal beam operations, to minimize radiation damage to lights, crane, etc. A combination of steel, marble and borated polyethylene is used for shielding on top of the target pile. Because of sky shine considerations, the walls and the ceiling of the target hall are required to be 5 feet (1.5 m) and 7 feet (2.1 m) of concrete, respectively. For the sides and the bottom of the target pile, combinations of steel and concrete shielding are used. Details of the target hall and the target pile shielding are given in Section 22.

5.2.1.2 Decay Pipe

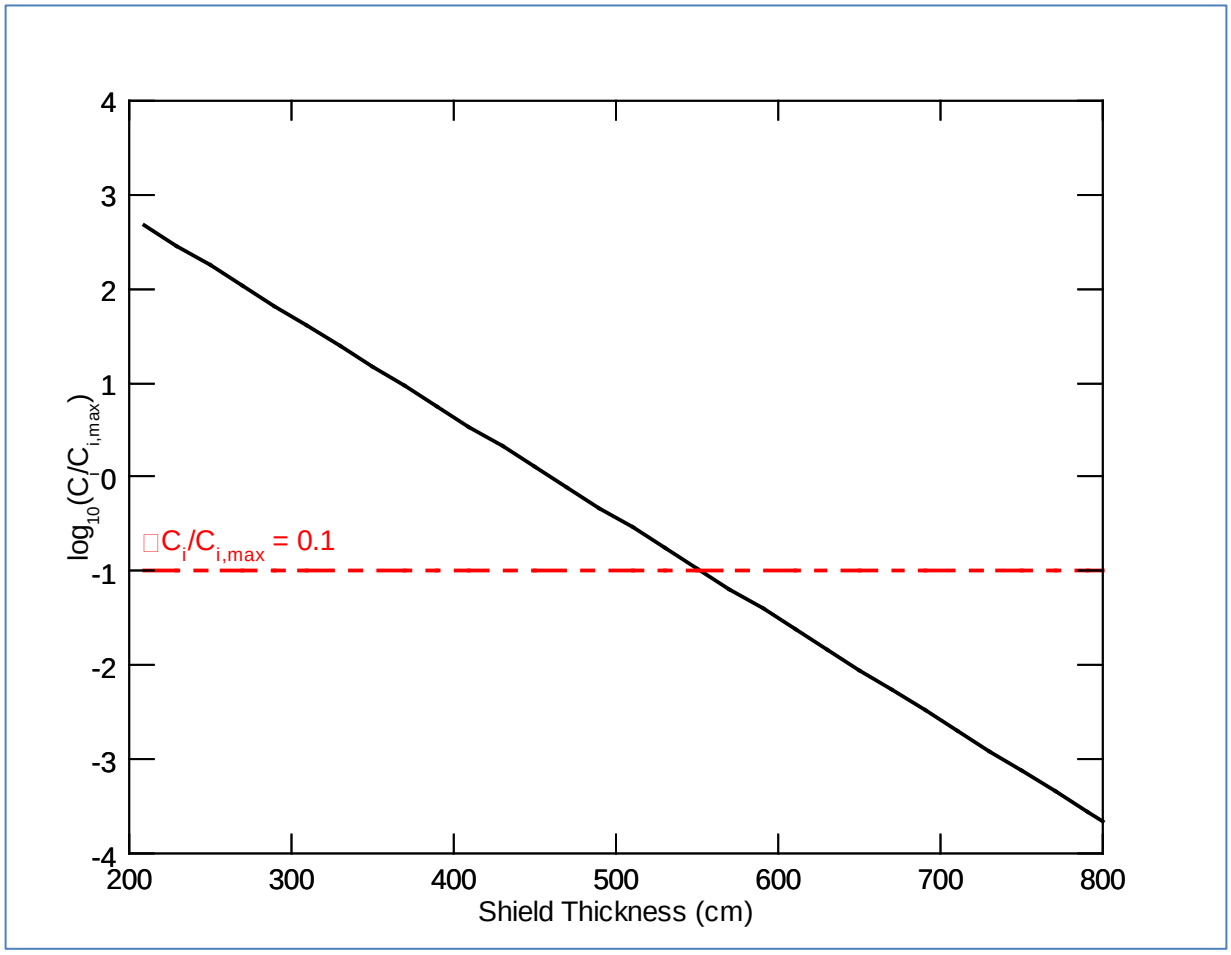

Figure 5-1: Sum of the ratio of radionuclide concentrations (Ci) over the Federal drinking water limits (Ci,max) for tritium and 22Na as a function of decay pipe shield thickness. The dashed red line shows the self-imposed limit on the ratio sum which will result in the radionuclide concentrations in the ground water to be below the detection limits

Given the geology in the region near the Main Injector, if the Decay Pipe was constructed horizontally at the elevation of the Main Injector with enough shielding such that the production of radionuclides in the soil will have concentrations below surface water limits, so no additional mitigation would have been required. However, the Decay Pipe will be partly underground with the downstream end close to the aquifer. Under these conditions, it is prudent (ALARA) to reduce the radionuclide concentrations by two orders of magnitude; e.g. tritium concentration to be 0.3 pCi/ml, which is below the standard level of detection. Based on the requirement set by the project [?], the decay pipe will use 5.6 m of concrete shielding. **Figure 5-1** shows the sum of the ratio of radionuclide concentration in ground water over the Federal drinking water limit as a function of decay pipe shield thickness. To achieve undetectable levels of tritium and ^{22}Na, the sum of concentration ratio should be 0.1 or less. Additionally, to protect against tritium leaking out of the shielding and being released to the environment, the concrete is surrounded by multiple protective outer layers of water impermeable material. For water drainage, the decay pipe shielding will be surrounded by a large volume of sand, with a sump pump at the downstream end. This

sand layer will also be incased in a system of water impermeable layers to further isolate the decay pipe form water from the outside. (see Section 20).

5.2.1.3 Absorber Hall Complex

As by-product of neutrino production, a flux of primary protons non-interacted in the target and non-decayed secondary hadrons (mostly and K-mesons) and leptons must be absorbed to prevent them from entering the surrounding rock of the excavation and inducing radioactivity. This is accomplished with a specially absorber structure which is located directly after the ~ 204 m long decay pipe (DP). It is a pile of aluminum (Al), steel and concrete blocks, water- and air-cooled, which must contain the energy of the particles after the DP. The vast majority of these secondary hadrons and primary protons, essentially, all of them are stopped in the absorber. The fluxes of secondary particles (mainly neutrons) escaping the system must be attenuated by the absorber and shielding to the tolerable levels. According to the MARS15 simulation, in total, 31% of the total beam power is deposited in the absorber. The shielding configuration, composition and dimensions have been thoroughly optimized in massive MARS15 simulations [N. Mokhov, LBNE-doc-10198] to keep the calculated radiation quantities safely below the regulatory limits in the following four areas:

1. Prompt dose (beam-on): Service Building, elevators: < 0.25 mrem/hr for unlimited access of radiation workers, and < 0.05 mrem/hr for general public outside.

2. Residual dose (beam off) in Absorber Hall, Raw and Sump Rooms: < 5 mrem/hr.

3. Groundwater activation in soil/rock immediately outside the concrete shielding: below the limit for H^3 and Na^{22} with a safety factor of ten that corresponds to the hadron flux of 400 cm^{-2} s^{-1} with energy > 30 MeV.

4. The hadron fluxes with energy > 30 MeV in air pockets inside the absorber and in various regions of the Absorber Hall and Muon Alcove below the air release limits (see below).

The unique feature of the design for such a high-power high-energy beam is groundwater activation in deep-inelastic muon interactions in the rock downstream of the Absorber Hall. The sophisticated MARS15 calculations have shown that a muon plume 170-m long and ~10 m in diameter is steadily generated in the rock with a central region (80-m long and up to 7 m in diameter) where hadron fluxes exceed the above-mentioned limit of 400 cm^{-2} s^{-1} for groundwater activation. It means that such a regions needs to be protected from groundwater penetration through it that is nontrivial and expensive from the civil construction point of view. It has been found in optimization MARS15 studies [N. Mokhov, LBNE-doc-10198] that the dimensions and cost of such a construction can be substantially reduced by using a steel conical kern 30-m long (7-m maximal and 3-m minimal diameters) immediately downstream the Absorber Hall concrete wall with the excessive hadron fluxes contained in the kern (see **Figure 5-2** and **Figure 5-3).**

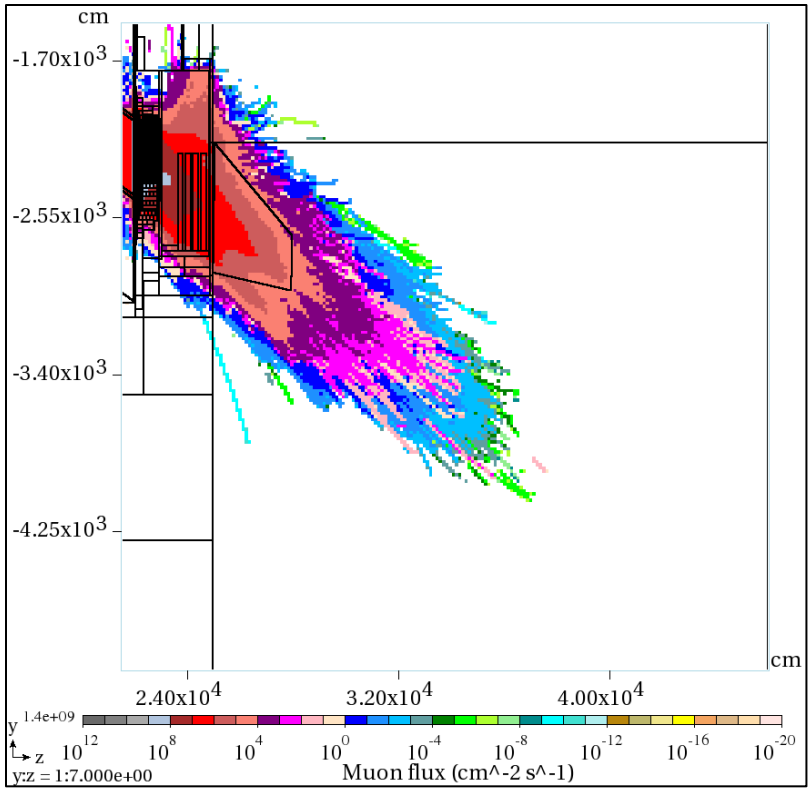

Figure 5-2: Muon isoflux contours (cm-2 s-1) in the rock and steel kern downstream the Absorber Hall; muon plume length is reduced from 170 m in pure rock to 113 m

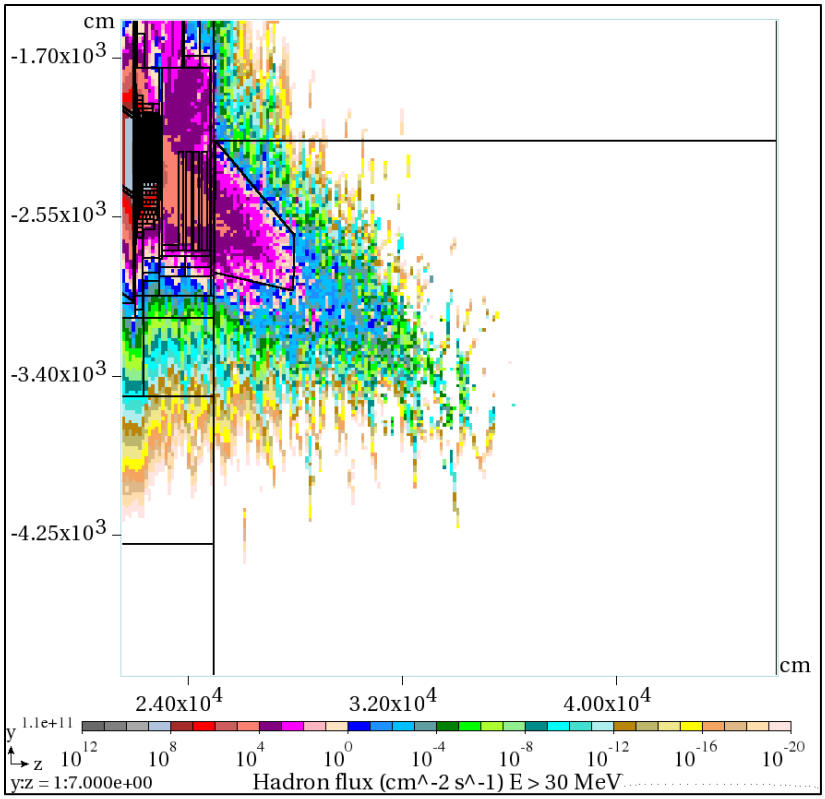

Figure 5-3: Hadron (E > 30 MeV) isoflux contours (cm-2 s-1) in the rock and steel kern downstream the Absorber; hadron fluxes outside the steel kern are below the accepted limit of 400 cm-2 s-1 for groundwater activation

The absorber (Section 21) and the Absorber Hall Complex shielding is based on the ground water management requirement [?] set by the project using the latest MARS model[?]. The shielding is designed to keep a thirty-year buildup of the radionuclides in the soil outside the shielding to below the standard detection levels. Another goal is to reduce the residual dose rates outside the absorber block to well below 100 mrem/hr to allow for maintenance activities, and to preclude significant activation of the equipment in the absorber RAW room. During proton beam operations, the following areas will be designated as "limited occupancy" for the radiation worker: the service building, personnel elevator and stairway shaft, elevator lobbies at the three stops, the three sump pump rooms and the Instrumentation room. The rest of the complex (Absorber hall, muon monitor area, RAW room, air handling room) is considered a high-radiation area and will not be accessible during beam-on periods.

5.2.2

Other Radiological Design Issues

5.2.2.1 Groundwater and Surface Water Protection

The production of potentially mobile isotopes such as tritium (^{3}H) and sodium-22 (^{22}Na) is an unavoidable consequence of high-energy particle collisions with nuclei. Since the primary transport line is located in the glacial till, with no direct connection to the aquifer, all radionuclides produced in the soil surrounding the enclosure will have to migrate down through the soil layers to reach the aquifer.

These seepage velocities, for the layers in the glacial till, are very small and the concentrations of the radionuclides are reduced by 5 to 7 orders of magnitude, well below detectable values.

The target hall and the target chase are also at grade level, located in the glacial till. The shielding of the target hall and the target chase is designed such that a 20-year accumulation of radionuclides in the soil immediately outside the shielding, assuming no dispersion, would result in maximum concentrations of 27% of the surface waters limits. Additionally, the target chase and the target hall will have a geo-membrane barrier system, preventing water from coming in contact with the shielding. For the rest of the beam line, from the decay pipe to the end of absorber hall, there will be sufficient shielding and water impermeable layers to render the concentration of the radionuclides of interest, accumulated in the soil over 20 years, to be less than the current standard detection limits [30]. The current accepted detection limits are 1 pCi/ml for tritium and 0.04 pCi/ml for sodium-22.

5.2.2.2 Tritium Mitigation

Tritiated water molecules (e.g. HTO) are highly mobile, especially in humid air, and can create significant concentrations in drain waters that are then collected in the pumping processes that keep the beam line areas dry. These basic processes, namely tritium production and migration, show that strategies to avoid unnecessary effluent will rely on isolating the materials in which the tritium is produced from water, and in the dehumidification of air in contact with these materials, together with subsequent collection and evaporation of the tritiated condensate. Additionally,

- There will be a geomembrane barrier system installed between the decay pipe concrete and the soil that is largely impervious to water. In this way the decay pipe concrete (in which tritium is created during operations) will be held at a low saturation. Numerical studies using the NuMI system indicate that if shielding concrete is unsaturated, the mobility of created tritium is low[32].

- The operational design of a sampling and monitoring program is straightforward, and allows for maintenance of the drainage system.

5.2.2.3 RAW Systems

The cooling water for the baffle, target, horns and the absorber will be highly activated after a short time of operation. The prompt dose rates from the RAW (RadioActive Water) skids belonging to these devices will be high and in addition to the short lived radionuclides, large concentrations of the tritium will build up in these systems. Shielding and cool-down times will be used to reduce the dose from these systems. Remotely controlled drainage and top up with fresh water will be used to keep the tritium concentrations at manageable levels. Alarms and containment systems will be used to prevent spills and contamination of the soil and surface waters. Water from these systems will be disposed of as low level radioactive waste.

5.2.2.4 Activated Air

High levels of radioactive air will be produced in the target chase (at the center of the target pile), in the decay pipe air cooling system, and in the absorber hall. The air to the chase and decay pipe cooling are

closed, isolated loops, that however are expected to leak at some level. The most significant leaks will be at the air handing systems in the air handling room, with smaller leak expected through seals on the covers of the target pile in the target hall. Additionally, the air from the absorber hall is sent to the air handling room, where it combines with the target chase and decay pipe air leaks. The air handling systems filter, chill and dehumidify the air in the cooling loops. The air handling room structure and the doors are designed to be fairly air-tight, and the air-handling room and target hall are maintained at lower pressure than the outside of the structures by pulling air to the NuMI target hall through a buried pipe, and through the NuMI pre-target volume and then exhausted. The transit time from the LBNF target hall to the NuMI exhaust is a sufficient to allow the airborne radionuclides to decay by orders of magnitude. The current Fermilab radioactive air emissions permit allows the annual exposure of a member of public offsite to the radioactive air emissions, from all sources to be less than 0.1 mrem. It is the goal of the LBNF design is to have the air emissions contribute less than 30% of this limit which allows for the emissions from other accelerators and beam lines at Fermilab.

5.2.2.5 Outside Prompt Dose

There are two ways where the prompt dose rates may reach outside the facility: (1) direct attenuated radiation outside the shielding and (2) sky shine, which is radiation, primarily neutrons, due to back scattering from air. FRCM Article 1104 [29] describes the regulatory requirements/limits regarding the maximum annual allowable dose to the public. The LBNF primary beam transport line, target hall and the decay pipe and the absorber service building can contribute to outdoor doses. Based on the latest MARS calculations [33,34] both the annual direct and sky shine doses are calculated for both offsite and onsite locations. Direct accidental muon dose at the apex of the transport line is also included in the offsite dose.

5.2.2.6 Offsite Dose

To allow operations of other experiments, beam-lines and accelerators, the offsite goal for LBNF is set at 1±1 mrem in a year, from all radiation sources generated by this beam-line. The total offsite dose, at the nearest site boundary, due to both direct and skyshine is estimated to be 1.32 mrem in a year.

5.2.2.7 Onsite Dose

Wilson Hall is the nearest publically occupied building to the LBNE beam line. Both the maximum direct and skyshine annual dose to the occupants of the Wilson Hall has been calculated. The total annual dose, at Wilson Hall, due to both direct and skyshine is estimated to be 0.06 mrem. Doses for other locations onsite, further away, will be less.

5.2.2.8 Residual Radiation

Based on the past experience and the difficulty of component replacement with the steep grades (~10%) of the LBNF primary beam enclosures, the beam loss and beam control devices would be employed to keep the residual radiation inside the beam line to no more than 50 mrem/hr on contact. This allows for repair or replacement of the beam line elements with little programmatic impact and keeping the dose to the workers ALARA.

There are other beam line devices, such as targets/horns and their mounting modules, target pile cooling panels and absorber core modules that are exposed to high levels of beam spray and are

expected to become highly radioactive. These devices may need to be repaired or replaced. The LBNF design provides for remote handling and shielded storage of these devices. The shielding of the work/repair cell used for targets/horns and modules is designed such that for a 20 kR/hr object, the dose rate outside the cell is less than 1 mrem/hr. The shielding of the containers used for the over the road transport of such devices will be such that the dose rate outside the containers is less than 100 mrem/hr at one foot.

6 SYSTEM INTEGRATION (WBS 130.02.04)

6.1 Introduction

This chapter covers the System Integration activity of the LBNF Beamline L2 Project. The System Integration team's responsibilities can be broken into two major areas: first, the oversight of systems for Controls, Alignment and Interlocks, and Installation Coordination. Second, there is the task of ensuring that the interfaces between each of the subsystems of the Beamline L2 Project are complete. The Controls, Alignment, Interlocks and Installation Coordination span the entire Beamline project and must therefore be properly supported by all the interfaces in addition to the relevant components. Interface coordination involves both achieving consensus as to the location and nature of each interface and the party responsible for it. The coordination activity must also ensure proper distribution of requirements and specifications so that all the needed components are accounted for, and that they will be constructed such that they will fit together properly during installation and operate successfully.

System Integration thus has the primary responsibility of facilitating good communication throughout the L2 project in order to prevent deficiencies and scope-related problems, and for any that are introduced, to spot them early on and make sure they get corrected.

6.2 Controls (WBS 130.02.04.02)

6.2.1 Introduction

Any high-energy external beamline requires a robust control system to ensure proper operation. The control issues for a beamline like LBNF's are well understood. The control system must be able to perform as follows:

- Reliably log data for every beam pulse (this implies a digitization with appropriate throughput).
- Plot both real-time and logged data in strip-chart form and capture all operational information for the beamline devices in a database.
- Issue alarms for off-nominal conditions and provide power-supply controllers with ramping capability.
- Handle the so-called slow-control subsystems: water, vacuum and temperature.
- Provide environmental monitoring.
- Display information from the position and loss monitors along the beamline and provide an auto-tuning facility to keep the beam centered over its length without significant human intervention.

The LBNF beamline consists of a large number of components, and the control system must have sufficient bandwidth to collect the necessary information from each component for each beam pulse.

The Accelerator Controls Network (ACNET) provides services for process control, monitoring, timing, save-and-restore and data logging for the Fermilab accelerator complex. Since the LBNF beamline is an extension of the accelerator complex, its control requirements will be supported via ACNET.

Given LBNF's very high beam power, 1.2 MW with a possible upgrade to 2.4 MW, the beam energy delivered per pulse, if misdirected, is sufficient to damage beamline components. This necessitates the use of a beam-permit system to verify a host of parameters about each beam pulse before it is extracted and to issue a "permit" if everything is in order. The beam-permit system must also be able to determine when a single bad pulse has been extracted and ensure that no further pulses are extracted until the problem is resolved. LBNF will use a system developed for NuMI that has also been used for several other Fermilab beamlines.

Reference Design

6.2.2.1 ACNET Controls

Controls for LBNF will be made up of standard Fermilab accelerator-control system interface and networking components. These include VME, HRM and PLC hardware with appropriate modules to provide control and monitoring of technical equipment along with commercial Ethernet switches and hubs for the networks. It should be noted that there are no plans to support the older CAMAC systems in the new LBNF areas. However, since it is unlikely that CAMAC will have been fully replaced in the MI by then, any LBNF equipment that might be installed in the MI-10 service building may be connected to ACNET via CAMAC.

ACNET services for LBNF will include connections to existing accelerator-timing systems (TCLK and MIBS from MI-8) and to the LBNF Beam-Permit System via single mode fiber cables.

ACNET consoles provide the ability to monitor and control accelerator operations throughout the complex. This will include the LBNF beamline and technical components. While operations are typically directed via consoles in the Main Control Room remote consoles are available at a number of locations around the complex.

New controls for LBNF will be installed in five locations (Primary Beam Service Building (LBNF 5) Controls Room, Target Hall (LBNF 20) Controls Room, Target Hall Power Supply Room, Absorber Service Building (LBNF 30) Controls Room and Absorber Hall Instrumentation Room). LBNF user-interface displays will be configured to show the LBNF beamline as a single entity from the extraction kicker (described in Section 9.3.6) to LBNF target (described in Section 17).

6.2.2.2 Beam-Permit System

The LBNF Beam-Permit System works in two modes to prevent extraction of errant pulses that could cause damage: current-pulse mode to inhibit a faulty pulse from being extracted and next-pulse mode to prevent extraction of subsequent pulses in case of a problem.

In current-pulse mode, the beam permit system examines a few hundred parameters in the last few milliseconds before beam delivery to ensure everything is ready for the beam. All magnet power

supplies are examined, and ramping to the flat-top level is checked. Beam positions of the circulating MI beam near the LBNF kicker will be examined to test the real-time orbit in the accelerator. Kicker charge level will also be checked to ensure that the desired extraction angle will be achieved. In addition, the beam-permit system will examine parameters of the MI radio frequency (RF) system to assure that the accelerating voltage is correct for nominal extraction. If anything wrong is sensed in any of the data, the kicker will be inhibited and the beam will be sent to the MI Beam Abort.

In next-pulse mode, the beam-permit system takes many measurements after a pulse has been delivered to ensure that it was delivered properly. Chief among these are measurements from the total and local loss monitors distributed along the beamline. These monitors are sensitive to losses on the order of one part in 10^4 and can sense an errant beam pulse immediately after its delivery.

Other measurements are taken from the beam-position monitors near the target, which indicate the proper delivery of beam and from an array of sensors reading out target data. In the case of an errant beam pulse, subsequent pulses are inhibited.

When the system is tripped in either mode, further delivery of the beam is inhibited until a control-room operator provides a manual reset. Repeated permit-system trips caused by beam losses escalate the authority level required to restart the beam; authority moves to beamline experts or safety personnel, depending on the circumstances.

The permit system has proven to be an excellent diagnostic for beamline and MI operations. If trips are kept at a low value, on the order of 5 to 10 per day, one can be reasonably sure that the beamline integrity is intact. After a down period, the permit system is used to check that the beamline is ready for re-establishment, and a single pulse is generally all that is required for start-up.

6.3 Radiation-Safety Interlock Systems (WBS 130.02.04.03)

6.3.1 Introduction

This section describes the philosophy, policies, procedures, design, fabrication, installation, checkout and commissioning for the Electrical Safety interlock System (ESS), Radiation Safety Interlock Systems (RSS), Radiation Monitors, Radiation Air Monitors, and Radiation Frisker Stations. Underlying all safety-system designs is a commitment to providing the necessary hardware, procedures, and knowledge to personnel to ensure their well-being. Inherent in each of these systems is the concept of redundancy.

The RSS systems are designed to protect personnel from exposure to particle beams. They are intended to prevent injury, serious overexposure or death from beam-on radiation and X-Rays. The ESS systems are designed to protect personnel from exposure to high-voltage/high-current power supplies and X-Ray producing devices. This includes the enclosure access-control interlocks, exclusion-area boundary gates, access keys and cores, emergency stop system, audio warning system, electrical-safety system, electrical-safety system interface units, critical-device controllers, the beamline critical-device-control contactors (removes 480V AC input power from critical device magnet power supplies), and associated interconnect cabling.

The Radiation Monitors are used to detect stray radiation during beamline operations. This includes Fermilab's "Chipmunk" radiation monitors (so-called because they emit an audible "chip" sound), and "Total Loss Monitor" (TLM) system, multiplexing (mux) monitoring network, and safety-system radiation-monitor interlock components.

The Airborne Radiation Monitors are used to monitor the amount of radionuclides that are released to the environment during beam operations. This system includes the airborne-radiation monitors and the associated enclosure to house the components.

The Radiation Frisker Stations are used to survey personnel and materials being removed from the beamline, Target Hall and absorber enclosures. These include the portable and wall-mounted laboratory frisker and "wallflower" detectors and installation at the enclosure entry points.

6.3.2 Methods

The principal method employed by the interlock systems is to establish and maintain exclusion areas surrounding active accelerator areas, maintaining sufficient distance between beamline operating components and the closest point of approach. When potential exists for personnel to be within the defined exclusion area, the Radiation Safety Interlock System disables all operations that may create hazardous conditions.

Electrical-safety systems, a subset of the Radiation Safety Interlock System, have been developed to provide protection from high voltage, high current, and x-ray producing devices.

Another method is redundancy. All hardware is designed such that no single failure will result in the loss of protection. To accomplish this, two separate circuits are used to detect a given condition. For example, two separate switches monitor each door to detect its status. Each of these switches in turn is connected to a separate control circuit. Thus if one switch were to fail, the other would still operate, providing the necessary protection. An extension of the redundancy concept is used in the control of radiation-safety-system critical devices, i.e., one that prevents beam from entering an area. Two critical devices will be controlled by a single radiation-safety system. When a possibility exists for personnel to be in an area, two devices are used to provide protection.

Another key principle used in designing all safety systems, is the idea of "fail-safe" circuits. All circuits are designed in such a way that if a circuit fails, the failure would initiate a system shutdown, resulting in a safe condition. For example, if the cable that controls a device were cut, the device could not be enabled. In this way personnel are still safe. Since not all component failures can be detected by the interlock systems, functional testing in accordance with the Fermilab Radiological Control Manual (FRCM) needs to be performed at periodic intervals and test results documented to ensure reliable operations.

"Search and secure," a walkthrough of an area in a predefined sequence by at least two qualified persons to ensure that the area is unoccupied, is perhaps the most important method to ensure radiation and electrical safety system's integrity is maintained. This is required each time before beam or power supplies are enabled. The search sequence will be programmed into a Programmable Logic

Controller (PLC) for the LBNF Radiation and Electrical-Safety systems. The order in which the interlocks are reset will be designed so as to ensure that no personnel are missed by the search team.

Once an area has been searched and secured, status displays on the outside of each access door and each section gate indicate to individuals that the area is interlocked and that access is forbidden to unauthorized personnel. Immediately before beam is brought into an area or power supplies are enabled, a prerecorded message consisting of a siren and verbal announcement will be played to allow personnel, which in the unlikely event of being missed on a search, have time to safely exit the area. Audio warning speakers will be located at approximately 125-foot increments. All doors to an area are locked and the keys to open these doors are interlocked and guarded in the Main Control Room.

Distribution of these keys is not taken lightly. Only authorized personnel are allowed access. The type of access determines the authorization level required for the individual.

6.3.3 Reference Design

The Radiation Safety Interlock Systems (RSS) for LBNF extends throughout the underground enclosures with the exception of the following areas, which are to remain accessible during LBNF beamline operations.

- LBNF Target Hall Power Supply and Utility Rooms, Controls Room, Morgue service area and truck bay
- LBNF Absorber Hall access shaft
- LBNF Below-Ground Absorber Hall elevator landing area
- LBNF Absorber Sump and Pump Room and Instrumentation Room

Areas of exclusion during LBNF beam operations are divided into three separate areas. The primary beam enclosure is interlocked to the Booster RSS (not under LBNF control). The remaining exclusion areas, the Target Hall and absorber are interlocked to the LBNF RSS. The primary beam enclosure and Target Hall are contiguous with the decay-pipe region separating the Target Hall and absorber.

The LBNF RSS must be cleared for beam to be transmitted down the beamline. The state of the RSS is also an input to the LBNF Beam-Permit System. While not integral to the LBNF RSS, radiation “stack” monitors sample and record levels of activated air from the Pre-Target, Target Hall and absorber areas.

6.3.3.1 Critical-Device Controller

In support of LBNF operations, two critical devices will be utilized and controlled by the LBNF Critical Device Controller (CDC). This controller will be permitted when it is safe to extract MI beam into the LBNF beamline. The controller will be connected to the power supplies feeding two separate bend magnet strings, both of which are required for beam to be transported to the LBNF beamline. Should the controller detect a failure of either power supply not turning off, the controller will send a failure mode signal to the Booster RSS disabling any further beam to the MI.

6.3.3.2 Exclusion Areas

A new extraction pipe will be installed inside the MI enclosure connecting to the primary beam enclosure. The upstream section of the LBNF beamline, the beamline service building access point, LBNF 5, and the enclosure down to the upstream end of the Target Hall will be interlocked to the Booster CDC.

The Target Hall Complex will be interlocked as a separate enclosure allowing for work in the Target Hall while the upstream LBNF enclosure is interlocked in support of MI area operations.

The LBNF absorber is accessible from the LBNF 30 Service Building through the access shaft. The absorber will be interlocked as a separate enclosure.

It is expected that no more than two personnel will be required to satisfactorily search and secure areas in the domain of the LBNF RSS.

6.3.3.3 Electrical-Safety System

Electrical hazards from exposed conductors and connections will inevitably exist in the LBNF beamline from the point of extraction to the magnetic focusing horns. These hazards are typically associated with the beamline magnetic elements, introduced in Section 5, such as the extraction kickers, the Lambertsons, the dipole and quadrupole magnets and the focusing horns. The Electrical Safety System (ESS) extensions of the MI and LBNF RSS provide permitting inputs to associated power supplies in order to partially mitigate the hazard of exposed and otherwise unguarded conductors. The ESS connections to permit magnet power supplies will be available at the MI-10, LBNF 5 and Target Hall areas. Trim and correction-element power conductors and connections are guarded and connection of their associated power supplies to an ESS is not necessary.

Prior to access into the MI and LBNF tunnel areas pulsed power feeder 96/97 is de-energized. This feeder provides the input pulsed power for MI and LBNF magnet power supplies which do have exposed bus in the tunnel areas.

6.3.3.4 Radiation-Loss Monitoring

Fermilab has several radiation-monitoring devices available to detect beam losses. Although the radiation-shielding assessment has not been completed, some areas of concern have been identified. Given the shape of the beamline, one area is just downstream of the apex of the embankment. Excessive beam losses in this region could potentially lead to muons directed off-site. One of two types of the radiation-monitoring devices, called a “Scarecrow,” or “TLM” will be placed here. If excessive beam losses are detected, the system will trip the LBNF Critical Device Controller (CDC) preventing further beam transport.

Non-interlocked Chipmunk monitors will be placed at various locations around the Target Hall and absorber areas to monitor for excessive radiation rates. Fermilab’s MUX monitoring network will be extended into the LBNF area for recording of both interlocked and non-interlocked radiation-monitoring instruments.

6.3.3.5 Airborne-Radioactivity Monitors

Airborne Radiation Monitors are used to monitor the amount of radionuclides released to the environment during beam operations. Airborne activation results primarily from the direct interaction of primary and secondary particles with the air (or other gaseous medium). Dust, from natural erosion, wear or work on radioactive accelerator components is a secondary source, as is third source of airborne radioactivity results from the emission of gaseous radioactivity from “hot” liquids in the radiation environment produced by the accelerator. Since the vast majority of the radioactive atoms produced are short-lived, delayed ventilation, with a delay time of one hour from production to exhaust, is used to reduce the radioactivity by roughly one order of magnitude at the air exhaust stack. Activation from the downstream LBNF primary beam, the Target Hall and the absorber areas will be monitored.

6.3.3.6 Enclosure Radiation Monitors

Radiation frisker stations are used to survey personnel and materials being removed from the primary beam, Target Hall and absorber enclosures. Fermilab has a standardized pair of instruments for frisking and determining a material’s radioactive class. The laboratory standard frisker and wallflower detectors will be installed at each enclosure entry point. Emergency-exit locations will not be outfitted with frisker stations.

6.4 Alignment (WBS 130.02.04.04)

6.4.1 Overview

This section summarizes the concepts, methodology, implementation and commissioning of the geodetic surveying (global positioning) efforts for determining the absolute positions of the LBNF beamline components at Fermilab and the location for the Far Detector at SURF. This information is critical to achieving proper aim of the neutrino beam. From this information, the beam orientation parameters are computed, as well as the alignment of the LBNF beamline.

6.4.2 Design Considerations

Clearly, directing the neutrino beam to intersect the Far Detector located 1,300 km distant from the source, is of paramount importance. Physics requirements will drive the absolute and relative alignment tolerances.

The divergence (spatial spread orthogonal to the line of travel) of the neutrino beam at this distance is on the order of kilometers. The spectrum of neutrino energies varies with their offset from the beam’s center line, higher-energy neutrinos are closer to the center, lower-energy ones are farther out. Based on NuMI’s requirement for the energy spread, LBNF will require that the combined effect of all alignment errors must cause less than 2% change in any 1-GeV energy interval in predicting the Far Detector energy spectrum.

To accomplish this, and prorate from NuMI to SURF, the neutrino-beam center must be within ±133 m from its ideal position at the far detector, corresponding to an angular error of $\pm 10^{-4}$ radians. Achieving this tolerance requires precise knowledge of the geometry of the neutrino beam. Table 4-1 lists alignment tolerance requirements for the low-energy beam for NuMI, which will also be established for

LBNF, with the exception of the Far Detector which was prorated to SURF. A Monte Carlo (PBEAM_WMC) was used to calculate the effect of misalignments of each beamline element for the determination of the Far Detector spectrum (without oscillations) from the NuMI's measured near-detector spectrum.

The requirement on the relative alignments of the beamline components and the target-station components (target and horns) is that they be within ±0.35 mm (requirement based on NuMI). To accomplish this, high-accuracy local geodetic and underground networks will be established to support the installation and alignment of the primary-beam components, neutrino-beam devices and the near detector.

Table 6-1: Alignment Tolerance Requirements (1σ)

Position	Tolerance
Beam position at target	±0.45 mm
Target position - each end	±0.5 mm
Horn 1 position - each end	±0.5 mm
Horn 2 position - each end	±0.5 mm
Decay pipe position	±20 mm
Downstream Hadron monitor	±25 mm
Muon monitors	±25 mm
Far Detectors	±21 m

6.4.3 Reference Design

6.4.3.1 Geodetic Determination of the Global Positions

The computation of the geometric parameters of the beam trajectory, expressed in terms of the azimuth and the slope of the vector joining the two sites, requires precise knowledge of the absolute positions of the two ends of the vector, at the near and far sites.

The geodetic orientation parameters of the beam, based on the absolute and relative positions of the target at Fermilab and the far detector at SURF, will be determined with GPS to a high level of accuracy in conjunction with the national Continuously Observed Reference Station (CORS) network. All other geodetic aspects related to the project, i.e. local geoid modeling, deflection from the vertical, differential tidal variations, plate tectonics, point velocities and precise azimuth determination, will be resolved and confirmed for quality assurance.

The development in the past decade of the CORS System led us to conclude that direct GPS observations of long baselines between monuments located at Fermilab and the SURF site, combined with CORS data, would provide the most precise and reliable results. Connections derived from two or more CORS stations will ensure unprecedented positional integrity without the expense of sending additional receivers and personnel into the field.

As a result of the ongoing collaboration, a Cooperative Agreement with the National Geodetic Survey (NGS) will be established for determining the coordinates of several points belonging to the Fermilab and SURF networks in conjunction with the CORS system. In addition to the data analyzed at Fermilab,

NGS will compute an independent solution and provide geodetic coordinates for the two sites using the adjacent CORS network.

The GPS observation campaign will follow the NGS specifications. Except for station occupation time, the specifications are similar to the High Accuracy Reference Network procedures regarding equipment setup, GPS-receiver controls, weather-data collection, and documentation. During three days of observations and using four dual-frequency receivers, three sessions of 9-10 hours of data at each site will be collected, staggering the observation start times in order to observe the complete satellite constellation orbital period of 12 hours.

The network for determining accurately the coordinates for the Fermilab-SURF baseline is formed by four CORS stations and the two primary LBNF monuments: 66589 at Fermilab, the closest to the designed LBNF Target Hall, and a new monument near SURF's Yates access shaft, for which the most GPS observation data will be collected. From the CORS stations adjacent to the main Fermilab-SURF baseline four were selected, two on each side of the vector in a balanced manner. **Figure 6-1** shows a map of the Midwest CORS stations with the proposed network superimposed.

The vector solutions for the network will be processed by combining the GPS data collected by Fermilab with the data collected by the CORS stations that are made available for retrieval via the Internet. To improve the accuracy of the baseline GPS-vector computations, the satellites' precise orbits, made available by NGS, will be used. Observed meteorological data will also be used for modeling the tropospheric effect on the GPS signal propagation.

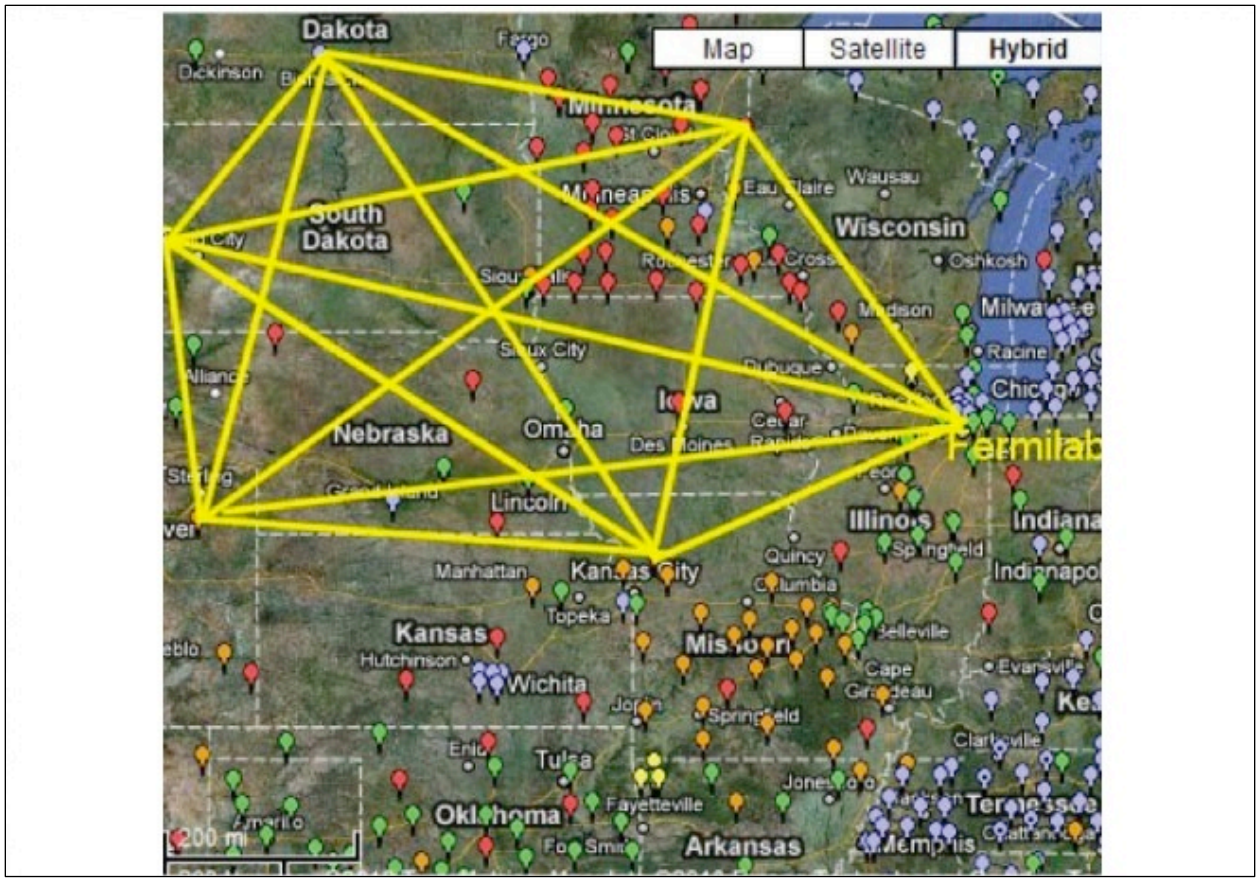

Figure 6-1: GPS Network Tying Fermilab and SURF to the CORS System

A minimal-constraint, least-squares adjustment consisting of 72 observations (24 vectors) will be performed. Simulations and past experience form NuMI show the standard deviations of the adjusted coordinates to be in the millimeters range in all three coordinates (longitude/latitude 1–3 mm, ellipsoid height 7–10 mm) at 95% confidence level. As a measure of internal consistency, the rms of the residuals of the adjustment were 2 mm in both latitude and longitude and 6 mm in height as shown in Figure 4-2.

The high quality of this network will be further confirmed by computing standard deviations for the spatial distances and height differences for all adjusted vectors using variance-covariance propagation.

Past experience from NuMI shows that standard deviations for the spatial distances are less than 5 mm (this includes lines across the network). The height differences have standard deviations of 10–15 mm.

Past experience from NuMI shows that a comparison between the two sets of results, computed independently by Fermilab and NGS, indicated differences on the mm level for the longitude and latitude and amounting up to 10 mm in height. These differences can be explained by the fact that the computations were performed independently in two reference frames: (International Terrestrial Reference Frame (ITRF96) and North American Datum (NAD 83) and that temporal tidal variations were not accounted for in the computations. The NAD 83 reference frame is defined such that the North American tectonic plate does not move as a whole relative to it. On the other hand, relative to the ITRF,

even points located on the rigid part of the North American tectonic plate move continuously at rates ranging from 9 to 21 mm/year in the United States.

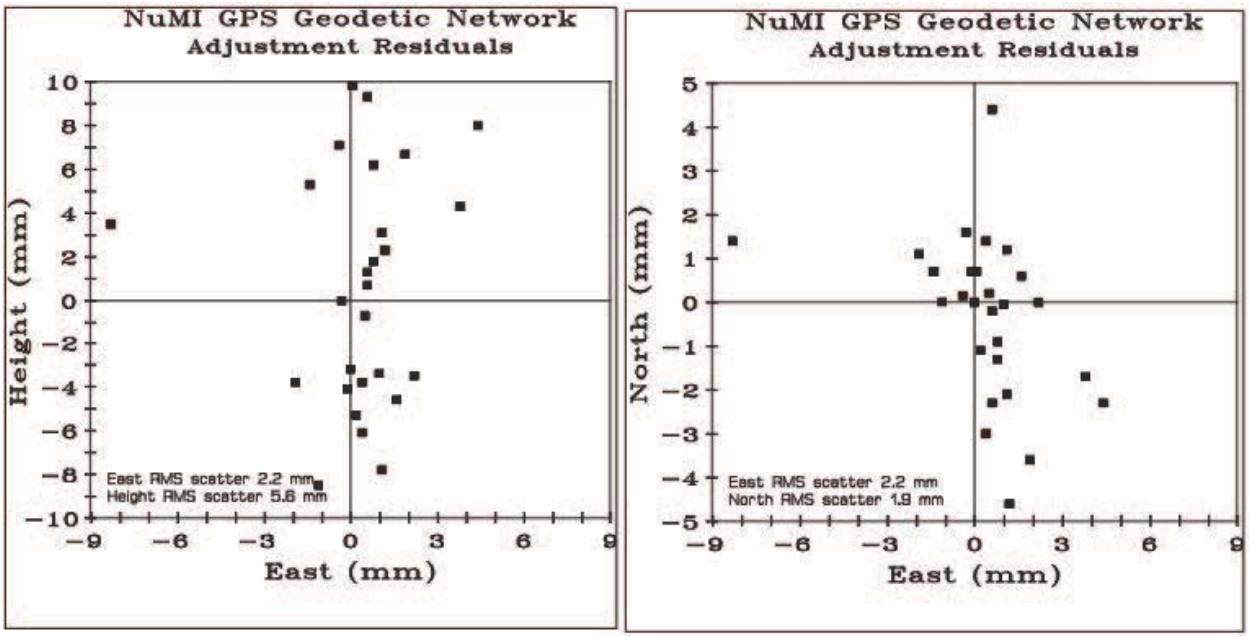

Figure 6-2: Residuals in Latitude/Longitude and Residuals in Height

6.4.3.2 Coordinate Transfer at the Homestake Mine from Surface to 4850 Level

The proposed method for determining the location at the 4850 level of the Homestake mine with respect to the geodetic coordinates system established at the surface is through inertial measurements techniques. Based on past experience from NuMI, we will contract The Department of Geomatics Engineering from the University of Calgary to perform a survey through the Yates and Ross deep mine shafts using a HG Honeywell 2001 Inertial Navigation System (INS) unit. Considering that errors in the meter range would not be significant with respect to the large divergence of the neutrino beam, we require that the rms be below 1 meter.

The inertial survey technique makes use of an Inertial Measuring Unit (IMU) composed of three accelerometers and three gyroscopes to output specific forces and respective angular velocities from the orthogonal sensor triads. The outputs are used in a dead-reckoning method which after initialization provides three dimensional geodetic coordinates at a high data rate. The accuracy of the results depends, besides the quality of the hardware, on the method used to estimate systematic errors inherently present in the sensors. Table 4-2 presents the HG Honeywell 2001 sensors performance specifications.

Table 6-2: HG Honeywell 2001 INS Sensor Performance Specifications

Performance Parameter	Class II 1.0 nmi./h
gyro bias uncertainty (deg/h)	0.003
gyro random noise (deg/ sqrt(h))	0.001
gyro scale-factor uncertainty (ppm)	1
gyro alignment uncertainty (arc sec)	?
accelerometer bias uncertainty (mGal)	10-25

Performance Parameter	Class II 1.0 nmi./h
accel. scale-factor uncertainty (ppm)	50
accelerometer alignment uncertainty (sec)	5
accelerometer bias trending (mGal/sec)	?
σ_{pos}	0.5 m at ZUPTs every 3 min
$\sigma_{acceleration}$	net bias < 50 mGal short term bias < 3 mGal

After the calibration of the inertial system, multiple determinations will be performed by running the unit, which will be rigidly attached in the center of the elevator car, through the access shafts between the surface and the 4850 level of the mine. For NuMI, the comparison between the runs showed an agreement of 0.040 m in height and longitude and about 1 m in latitude. Although it met the given requirements, the latitude discrepancy was most likely caused by an initial azimuth misalignment between the IMU system and the surface geodetic control system, which will be corrected by additional observations.

By setting the inertial system data collecting rate to 1 second during the elevator runs we will also obtain a fairly precise mapping of the 4850 feet deep access shafts. Moreover, the inertial system will be used as a redundant method to check the orientation of the 4850 level local reference system with respect to North. The results obtained for NuMI indicate an agreement with our 1998 Gyro determinations to 2 arc seconds (0.01 mrad).

For the final computation of the geometric parameters of the beam trajectory we will use the geodetic coordinates provided by the tie to the CORS national network and the updated location of the 4850 level of the Homestake mine provided by the inertial system survey.

6.4.3.3 Primary Surface Geodetic Network at Fermilab

The geodetic reference for supporting the construction and positioning of the LBNF project is derived from a high-accuracy local surface network. The existing Fermilab/MI master control network, which has a relative positional accuracy better than 2 mm, includes the monuments surveyed during the CORS tie campaign, and will be supplemented with six geodetic monuments, providing densification around the access points. Figure 4-3 shows a simplified version of the network geometry.

The LBNF absolute-positioning-tolerance requirements call for extensive combined GPS, terrestrial and astronomic surveys. The computations will be performed in the NAD 83 system, which uses the Geodetic Reference System (GRS 80), which consists of a global reference ellipsoid. Simulations and past experience from NuMI show that minimal-constraint least-squares adjustment consisting of more than 410 observations will yield absolute error ellipses in the mm range at the 95% confidence level.

Precise astronomical azimuth determinations will be performed on two MI geodetic monuments surveyed during the CORS campaign. Those monuments, with wide visibility over the LBNF upstream area covering the entire beamline, will be used extensively during the project as reference for transferring absolute coordinates from the surface into the underground tunnels and halls. They will also serve as a calibration baseline for the surveying tool, a DMT-brand Gyromat 2000 precision

gyroscope. Based on experience from NuMI, the standard deviation of the azimuth over three nights of observations was 0.66 arc seconds (0.003 mrad).

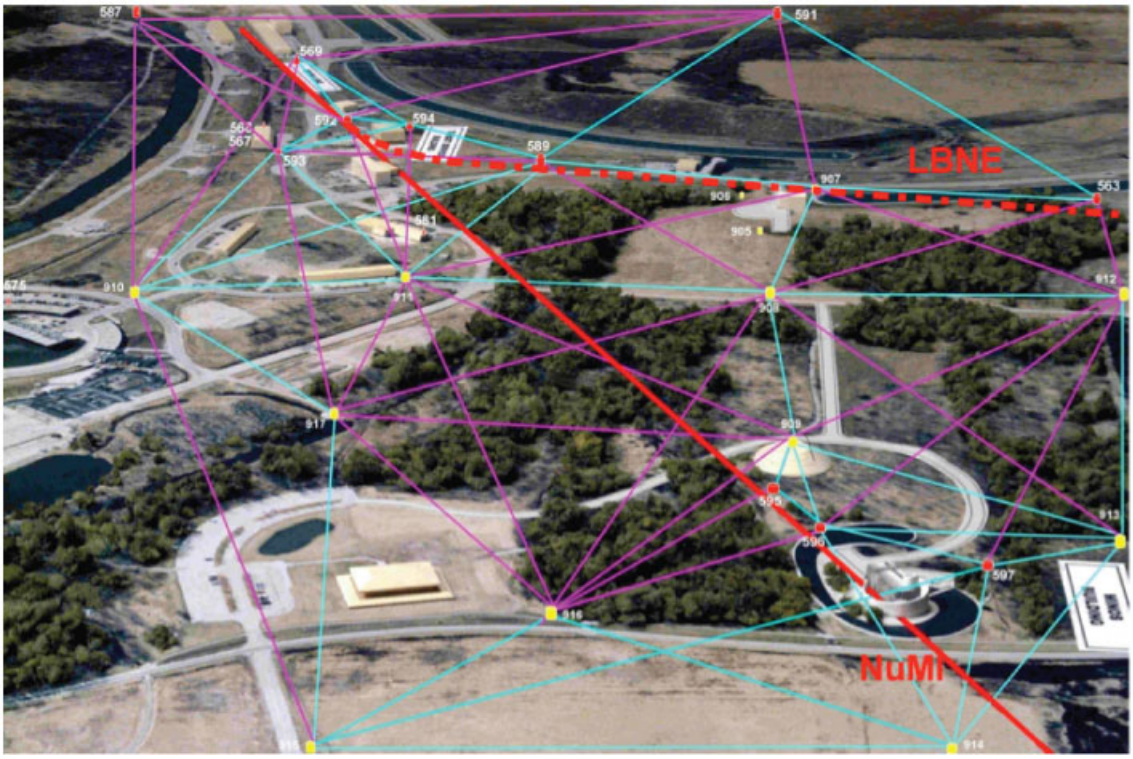

Figure 6-3: Fermilab LBNF Surface Geodetic Network

The vertical alignment of the beamline components along the vector joining the two sites relies on leveling measurements, which use as a reference surface the geoid, defined as the equipotential surface of the Earth's gravity field at mean sea level. The general shape of the geoid over a large area, in other words, is determined by gravitational parameters.

The non-homogeneity of the earth and the surrounding Fermilab topography may not change dramatically enough to raise major concerns for distortions of the gravity equipotential surfaces. However, for the purpose of aiming the neutrino beam correctly, it is important to consider local variations in the gravity field in order to precisely determine the gravity vector at the origin. This information also allows precise determination of the magnitude of corrections that will compensate for deflections from the vertical.

Since the LBNF beamline originates from the MI, the study of the local geoid model covering the Fermilab area developed in the mid-1990s was used to help determine the exact spatial geometric relationship between the Tevatron and the new MI. With both high-precision GPS and geodetic leveling measurements available for a rather large number of monuments covering the site, the geoid height at those points was calculated differentiating between GPS ellipsoidal height and the orthometric height from geodetic leveling. The local geoid model then used a best-fitting surface employing a second-order polynomial and a spline function to interpolate heights at other points where surveying data was not

available. The results show that the accuracy for computing relative geoid heights and the two components of the deflection of the vertical were in the range of ±3 mm and respectively ±0.1- 0.2 arc seconds with respect to the local origin.

The local geoid model was compared with the Geoid93 model provided by the National Geodetic Survey (NGS). Based on over 1.8 million terrestrial and ship gravity values, the model uses a Fast Fourier Transform (FFT) method to compute the detailed geoid structure which, combined with an underlying OSU91A geopotential model, produces a geoid height grid with a 3’ x 3’ spacing in latitude and longitude referred to as the Geodetic Reference System 1980 (GRS 80) normal ellipsoid. The values for the intermediary points are then interpolated by using locally a biquadratic fit function. NGS estimates that the comparison of the Geoid93 model with combined GPS and levelling yields roughly a 10-cm accuracy (one sigma) over length scales of 100 km. Better accuracy is expected over shorter lengths.

The comparison between the two models shows differences up to 5 mm, consistent with the expected values. Furthermore, this is also an indication that there are no local gravity anomalies (local variations in the gravity field) not modeled by the national model for this area, at least at this level of sensitivity.

The LBNF beamline falls in the 1.5-mm range of those differences, well within the estimated accuracy for the local or the national geoid models. The national geoid model was considered sufficient to cover the tolerance requirements for the project. As a result, the Geoid93 and Deflec93 provided by NGS were used in the LBNF geodetic computations.

6.4.3.4 High-Accuracy Sub-Surface Control Network

The final primary-beam trajectory is of crucial importance to LBNF. To minimize the relative errors between the beamline components, target and horn alignment and to provide dynamic monitoring of their relative positions, a high-accuracy control network with strict tolerances will be implemented. Relative component positions established to ±0.35 mm (1σ]) are expected throughout the extraction enclosure, transfer tunnels and Target Hall. The residuals from the NuMI Target Hall to the MINOS Near Detector, as shown in **Figure 6-4**, provide an example of the degree of coordinate uncertainty in a measured system like LBNF.

Network simulations of different models have led to an optimized design of the number (six) and locations of vertical sight risers. This is sufficient to provide azimuthal constraints and to control the scale of the network.

The configuration of the control network is limited by the geometry of the tunnels and halls. Studies and past experience with NuMI have led to a configuration based on chains of polygons. In order to improve the isotropy of the network and compensate for the weaknesses caused by the poor ratio between the sides of polygons, additional measurements spanning adjacent polygons are added.

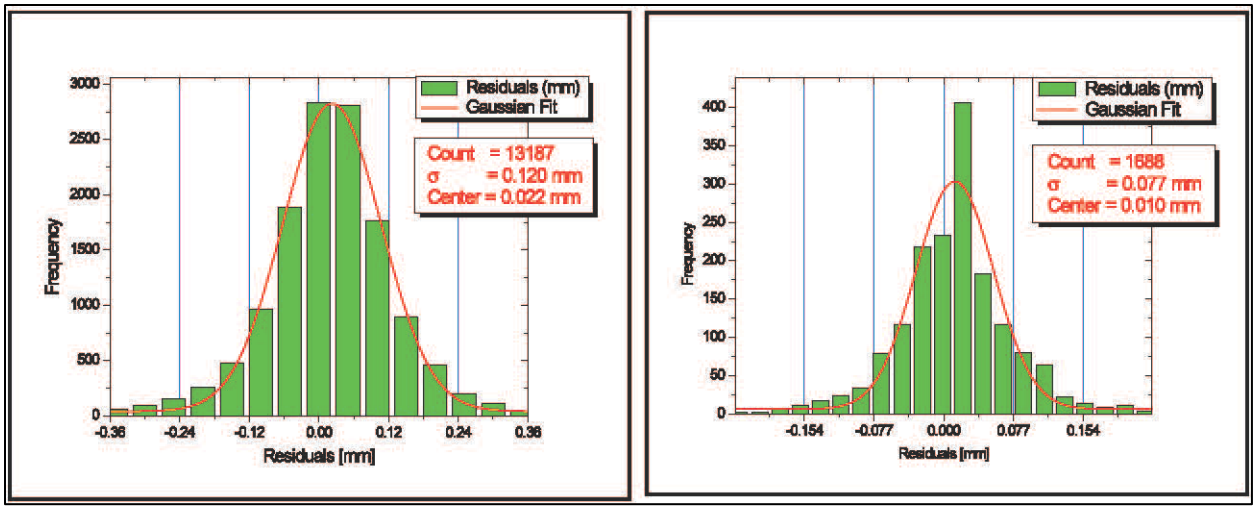

Figure 6-4: Distribution Observation Residuals for the Target and Near Detector Halls in MINOS

6.5 Installation Coordination (WBS 130.02.04.05)

This activity provides the management oversight of the day-to-day activities taking place in the installation areas and the framework for sequencing and scheduling the installation tasks. The scope of this role is driven by the need of balance the resources required in four distinct installation sub-projects. In addition, there is a need to ensure that all activities are conducted with a consistent level of safety and quality assurance throughout the entire project. The role of Installation Coordination is distinct from the actual task of installation. Its role is primarily the coordination of installation activities and will be led by an Installation Coordinator. The responsibility for the design, fabrication and installation of each element of the Beamline L2 Project resides in its appropriate subsystem.

Installation Coordination will draw on the experiences of previous installations such as NuMI, and the lessons learned from more recent installation projects such as ANU. In addition, the team will be organized in a manner that advantageously uses the project management tools being implemented throughout the laboratory. The implementation of Installation Coordination will begin with the managerial role of sequencing and controlling the activities in each of the areas. See **Figure 6-5**. Each area (e.g., Main Injector, Primary Beamline, Target Complex, and Absorber Hall) will be under the supervision of either an Operations Specialist or a Floor Manager whose job it is to oversee the overall installation activity taking place in the area and to supervise the daily activities of task managers who are leading the work crews in each area. Floor Managers will report directly to the Installation Coordinator.

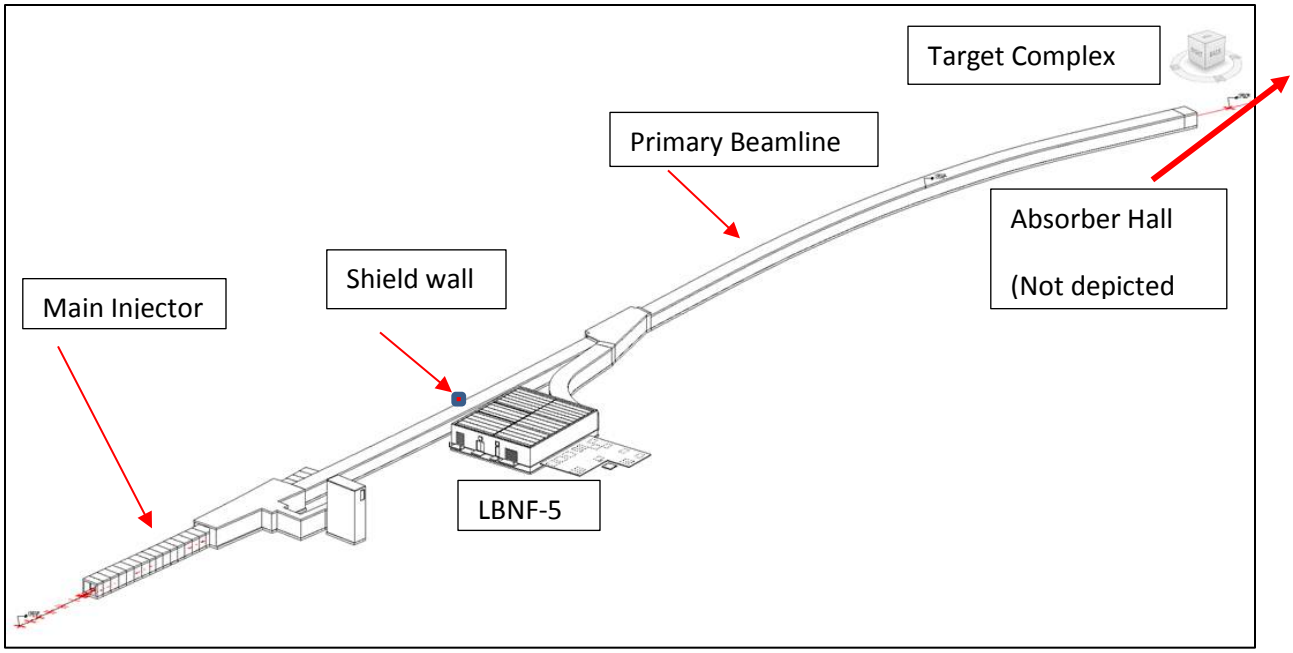

Figure 6-5: Primary Beamline Areas of Installation

The responsibilities of the Floor Manager, which include, directing the day to day activities, are described in detail in the Installation Coordination Plan. During the period of installation, daily "tool box meetings" will be held along with a regular end-of-week installation meeting. The tool box meeting will be led by the Floor Manager and all workers expecting to be conducting activities in the work area will be present. The content of this briefing will include a task list, significant work activities, potential interferences to be avoided, changes in priorities, etc. The end-of-week meeting will be held with the Installation Coordinator and Deputy, the Floor Managers from all areas, and the ES&H Manager to review the progress of the week and discuss issues that have arisen. This meeting will also be used as a status update in preparation for the Weekly Summary Meeting

The Weekly Summary Meeting will be held at the beginning of the week to review the past week's progress and highlight any issues that have arisen. This meeting will be attended by the Neutrino Beamline Project Management Team, the Level 3 and Level 4 Managers, ES&H team members, and the Floor Managers from all areas. The expectation is that this meeting will be held at the beginning of the week so that any issues that have arisen may be addressed expeditiously. It is expected that as issues arise which impact cost and schedule, they will be discussed if not resolved.

The Installation Coordination Plan offers a more comprehensive description of the responsibilities of each member of the Installation Coordination Team.